Method development for valid high-resolution profiling of mitochondria and Omics investigation of mitochondrial adaptions to excess energy intake and physical exercise

Dissertation

der Mathematisch-Naturwissenschaftlichen Fakultät

der Eberhard Karls Universität Tübingen

zur Erlangung des Grades eines

Doktors der Naturwissenschaften

(Dr. rer. nat.)

vorgelegt von

Lisa Claudia Charlotte Kappler

aus Weingarten

Tübingen

2018

Gedruckt mit Genehmigung der Mathematisch-Naturwissenschaftlichen Fakultät der Eberhard Karls Universität Tübingen.

Tag der mündlichen Qualifikation:	27.03.2018
Dekan:	Prof. Dr. Wolfgang Rosenstiel
1. Berichterstatterin:	Prof. Dr. Carolin Huhn
2. Berichterstatter:	Prof. Dr. Rainer Lehmann

Over the long term,

symbiosis is more useful than parasitism.

More fun, too.

Ask any mitochondria.

-Larry Wall-

Index

1 Scopes and aims of the thesis

The goal of this work was to study mitochondrial adaptions to excess energy intake, insulin resistance and exercise. The role of mitochondrial dysfunction in the etiology of insulin resistance and diabetes was discussed quite controversially up to now. Therefore, this was further investigated in this thesis using a systems biological analysis of isolated mitochondria from cell culture and tissues from mouse models covering not only lipidomics but also protein and functional analyses including respirometry. In contrast to functional assays, which highly depend on mitochondrial integrity and viability, the quality of subcellular "omics" analyses is directly related to sample purity. Thus, one of the main objectives and a prerequisite of this work was to establish and validate novel workflows that enable comprehensive lipidomics analyses, including oxysterols, from highly pure mitochondria isolated from liver, muscle and cultured cells.

The biological questions addressed here are:

It is still unclear whether metabolic overflow leads to disturbances in substrate utilization and, consequently, insulin resistance or if mitochondrial dysfunction is a consequence of impaired insulin signalling. To get deeper insights, the effects of insulin resistance induced by chronic exposure to high concentrations of insulin in combination with substrate overflow through high glucose concentrations on skeletal muscle mitochondria using C2C12 myotubes were investigated in this thesis.

Skeletal muscle insulin resistance is considered the initiating or primary defect that is evident decades before β-cell failure and hyperglycemia develops. Therefore, tissue specificities for murine liver and muscle -as two insulin target organs-, which are responsible for endogenous glucose production and disposal, were investigated to distinguish the tissue-specific mitochondrial function. Thereby, the hypothesised tissue-specific contribution of their (dys)function to e.g. insulin resistance should be clarified. A high-energy diet feeding mouse experiment including treadmill exercise with subsequent lipidomics and functional investigations was employed to gain further and ideally comprehensive understanding of the molecular changes underlying the alterations in mitochondrial function and metabolic control induced by an energy-rich western diet. Additionally this experiment aimed at unravelling the mechanisms by which exercise compensates overnutrition and prevents mitochondrial dysfunction.

Summarizing, the major aims of this dissertation were firstly to establish novel protocols for functional and lipidomics analyses of highly purified mitochondria. Secondly, a causal relationship between insulin resistance and substrate overflow with regard to mitochondrial (dys)function was examined in a murine skeletal muscle cell line. Furthermore, tissue-specific differences between mitochondria derived from mouse liver and muscle were investigated to unravel hypothesised tissue-specific contributions towards disease developments. Additionally, this thesis aimed to unravel tissue-specific mitochondrial adaptions to a high-energy diet causing insulin resistance and the proposed prevention by exercise on a molecular level.

2 Introduction

2.1 Insulin resistance and type 2 diabetes

Type 2 diabetes mellitus (T2Dm) is rapidly developing to one of the greatest global health challenges of this century. According to World Health Organization (WHO), 422 million people over 18 years suffered from diabetes in 2014, i.e. with a fasting plasma glucose ≥ 7.0 mmol/l.[1] Worldwide diabetes prevalence rose from 4.7% in 1980 to 8.5% in 2014. Rare monogenetic forms of diabetes are described,[2] but type 2 diabetes is more prevalent of polygenic nature and therefore often covered in GWAs (genome wide association scans).[3] Although the underlying mechanisms in the pathogenesis of T2Dm are still not elucidated, it was clearly shown that insulin resistance (IR) plays a major role in the development of type 2 diabetes.[4-6] In a state of IR the target organs like liver, white adipose tissue and muscle, show a lower response to insulin and the body fails to increase insulin production accordingly to overcome this resistance. Hallmarks of a lifestyle that can lead to IR and T2Dm are over- and malnutrition, together with physical inactivity.[1] Skeletal muscle and liver are the main insulin targets playing an essential role in glucose homeostasis, with skeletal muscle being responsible for over 80% of the glucose disposal.[7,8] Skeletal muscle insulin resistance is considered to be the initiating or primary defect that is evident decades before β-cell failure and hyperglycemia develops.[4] Different theories about mechanisms underlying peripheral IR development are discussed, which are the keys to elucidate the etiology of type 2 diabetes. There is evidence of ectopic accumulated fatty acid metabolites causing lipotoxicity after elevated secretion of fatty acids by the liver in a state of obesity.[9] Numerous studies reported strong associations between triacylglycerol (TAG) accumulation in skeletal muscle tissue and insulin resistance,[10,11] but lean endurance-trained athletes showed also high levels of accumulated TAGs while being highly insulin sensitive, called the Athlete's paradox.[12,13] This paradox indicates that TAG accumulation *per se* does not lead to insulin resistance, what led to the hypothesis that its more an altered or incomplete lipid metabolism that may be an important factor in the progression of insulin resistance. One discussed mechanism is that increased plasma fatty acid concentrations, initiated by infusion or high-fat feeding, lead to intramyocellular fatty acyl-coenzyme A (CoA) and diacylglycerols (DAG) accumulation, which activates protein kinase C theta (PKC-θ) and thereby increases insulin receptor substrate 1 (IRS-1) serine 307 phosphorylation.[14] This causes a decreased IRS-1 tyrosine phosphorylation and decreased activation of IRS-1-associated PI3-kinase, which results in decreased insulin-stimulated glucose transport activity.[15,16] Additionally, it is discussed that circulating cytokines secreted by white adipose tissue can influence insulin sensitivity of liver and muscle.[17] In recent years, investigations on mechanisms linking mitochondrial function to IR came into focus, due to the central metabolic function of mitochondria, their essential role in the regulation of bioenergetic processes, of cell stress response and epigenetic modulations.[18-20]

2.1.1 Diet and physical activity

Mitochondrial membranes are discussed to adapt to the lipid composition provided by the diet.[21] In turn, these changes in lipid homeostasis are very likely to regulate mitochondrial structure and function.[22,23] Availability of certain fatty acids was speculated to be the limiting factor determining mitochondrial lipid composition depending on the acyl groups dominant in the respective tissue.[24] High-fat feeding experiments were shown to induce insulin resistance whilst mitochondrial mass was increased.[25,26] Eight weeks of overfeeding in healthy humans did not change mitochondrial content or respiration in muscle.[27] This is challenging the proposal of the controversially discussed reduced mitochondrial mass (as described in 2.2.3.1), which was speculated to contribute to the development of insulin resistance. Physical exercise has been frequently promoted to prevent and combat obesity related complications such as insulin resistance, T2Dm and non-alcoholic fatty liver disease. Although the molecular mechanisms have not yet been fully illustrated, the proposed one is likely due to its impact on cellular metabolism and mitochondrial alterations. Physical activity was shown to increase mitochondrial mass and oxidative capacity in skeletal muscle.[28-31] Exercise has not only a strong impact on muscle but also on liver as shown by our group.[32-34] This thesis aimed therefore to unravel mitochondrial adaptions to a high-energy diet causing insulin resistance and the proposed prevention by exercise on a molecular level. Alterations on protein and lipid levels and composition in liver and skeletal muscle were observed after physical exercise, but also by chronic excess energy.[35-37] In particular, the effect of exercise on fatty acid profiles of total lipids was investigated in whole liver[38,39] and muscle tissue.[39,40] However, only little data are available on the effect of exercise on the subcellular level, e.g. on mitochondrial lipid composition in liver or muscle[21,41,42] and even no studies about the response of the liver mitochondrial proteome to exercise.

2.2 Mitochondria, structure and function

2.2.1 Function of mitochondria

Mitochondria are highly dynamic organelles with a double membrane producing energy by oxidative phosphorylation. Four respiratory chain complexes on the inner membrane transport electrons derived from NADH or $FADH_2$, provided by the tricarboxylic acid (TCA) cycle and lipid β-oxidation. They are NADH-ubiquinone (coenzym Q; CoQ) reductase (complex I), succinate-CoQ reductase (complex II), CoQ-cytochrome c reductase (complex III), cytochrome c oxidase (complex IV). Complexes I, III, and IV are reduction- and oxidation-driven proton pumps using the energy to pump protons out of the matrix. Thereby, an electrochemical proton gradient is built up, which is used by the ATP synthase (complex V) to convert ADP to ATP. CoQ and cytochrome c are two freely diffusible molecules that mediate the transfer of electrons between complexes. Besides being the major sites of energy production by ATP generation through oxidative phosphorylation, a great deal of information about mitochondrial metabolism is already available (see Figure 1). Mitochondria are equipped with enzymes needed for free fatty acid metabolism and the TCA cycle, but also major steps of heme synthesis, ketogenesis and hormone synthesis reside within mitochondria.[43-46] Mitochondria are major sources of reactive oxy-

gen species in cells[20,47] and even have their specific scavengers like the mitochondrial superoxide dismutase.[48] Additionally, mitochondria are involved in calcium homeostasis and programmed cell death.[19,49-51] Given their central metabolic role, it is not surprising that mitochondria are widely discussed in context of many diseases such as neurodegenerative disorders, cancer and diabetes.[52-54] The main function of mitochondria, cellular respiration, as established and investigated in this thesis, is central to many processes like electron transport chain complex (ETC) activities, reactive oxygen species (ROS) generation, ATP production and substrate oxidation through TCA cycle and β-oxidation. Mitochondrial function in this thesis -measured mostly as *ex vivo* oxidative phosphorylation (OXPHOS) capacity- therefore covers multiple features.

2.2.1.1 Tissue-specificity of mitochondria

Mitochondria are tailored to the specific needs and demands of different tissues as demonstrated by morphological differences illustrated in electron microscopy studies, but also enzymatic equipment, mtDNA copy numbers, protein abundances and oxidative capacity between cell types.[55-60] Despite this apparent physiological diversity, little data exists combining several approaches to investigate overall molecular mechanisms from mitochondrial lipid and protein composition up to mitochondrial function for these tissue-specific differences. Investigations on mitochondrial specificities of liver and skeletal muscle as two insulin target organs could help to elucidate organ cross-talks and might lead to more target-specific treatments of mitochondrial dysfunctions associated with e.g. insulin resistance and type 2 diabetes. Skeletal muscle and liver fulfill different physiological tasks and vary in the extent of metabolic pathways present in their mitochondria (Figure 1): Under aerobic conditions, glucose and fatty acids are metabolized into acetyl-CoA by glycolysis and β-oxidation and fed into the TCA cycle. Glucose utilization is balanced by the liver with the release of glucose from gluconeogenesis, which contributes to a major extent (64%) to total glucose production even during the first 22 hours of fasting in humans.[61] In such states of fasting or low insulin levels for example due to diabetes, the liver utilizes oxaloacetate for gluconeogenesis, leading to its depletion in the TCA cycle, and to diversion of acetyl-CoA to ketone bodies.[44] This mitochondrial process, called ketogenesis, provides acetoacetate and 3-hydroxybutyrate as substrates for peripheral tissues like skeletal muscle.[44,45] Mitochondria in skeletal muscle are facing large variances of ATP demands upon physical activity by varying its metabolic rate to a greater extent than any other tissue and thereby adapting it to the demands.[62] In postprandial states, muscle energy demands are mainly satisfied by utilizing carbohydrates, mainly glucose. Skeletal muscle is responsible for over 80% of the glucose disposal.[7,8] During states of fasting or in general caloric insufficient supply, muscle relies on TCA-cycle-linked substrates such as fatty acids, acetate, ketone bodies, lactate and amino acids for ATP generation. This ability to switch between carbon sources for ATP production is called metabolic flexibility.[63]

In humans, the liver is the major site of fatty acid production, called *de novo* lipogenesis,[64] while in rodents the adipose tissue is also important.[65] Additionally, fatty acids can also be taken up by the liver either for oxidation, storage or for packaging them into lipoproteins for export and storage in other tissues.[66] Because of its relative size in men and most animals, however, the muscle is considered to be the major organ for fatty acid disposal.[67] Amino acids are catabolized in the liver,

branched-chain amino acids (BCAAs), however, are primarily oxidized in the peripheral tissue, mainly in skeletal muscle.[68,69] Not only metabolic pathways in mitochondria are tissue-specific, but also the morphology of liver versus muscle mitochondria varies distinctly. Skeletal muscle mitochondria are distributed between sarcomeres embedded in the microfilaments and microtubules, while liver mitochondria are more round and show fewer cristae.[55]

Given such widely varying morphologies, metabolic pathways and tissue-specific demands, it is reasonable to expect that the oxidative function, the lipid and the protein composition of these organelles may vary significantly from tissue to tissue. Proteomics approaches showed distinct tissue specific differences between mitochondria from liver and muscle tissue,[70] and since the mitochondrial phospholipid content and composition have been shown to affect electron transport chain activity and respiratory function,[71-73] a lipidomics approach as applied in this thesis combined with functional studies might help understanding mitochondrial organization by identifying common and unique tissue specificities.

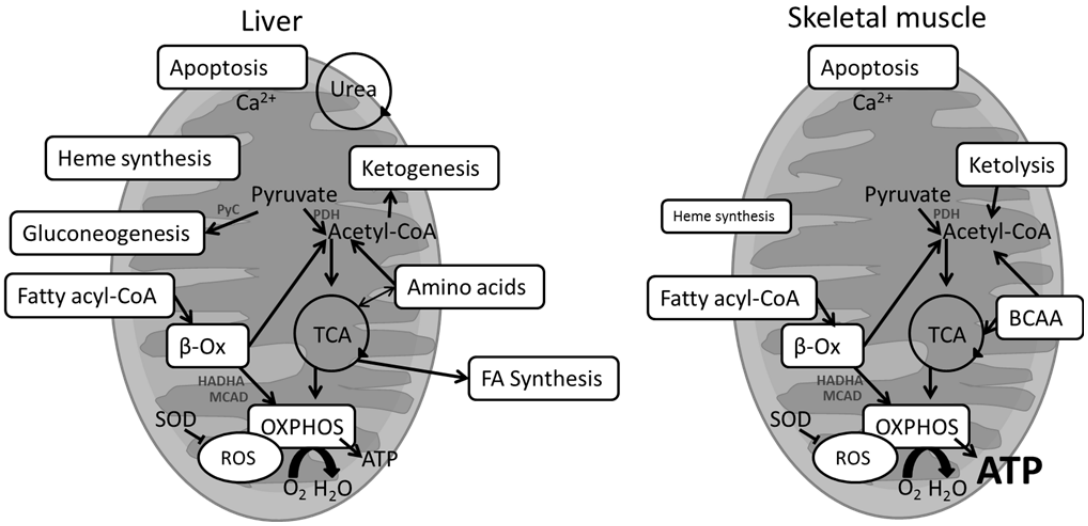

Figure 1: Main functions and metabolic processes in mitochondria in liver and muscle. β-Ox= β-Oxidation, BCAA= Branched-chain amino acids, ROS= reactive oxygen species, TCA cycle= tricarboxylic acid cycle, OXPHOS= oxidative phosphorylation, PyC= pyruvate carboxylase, PDH= pyruvate dehydrogenase complex, HADHA= hydroxylacyl-CoA dehydrogenase, MCAD= medium chain acyl-CoA dehydrogenase, SOD= superoxide dismutase, ATP= adenosine triphosphate, FA= fatty acyl.

2.2.1.2 Oxidative stress

Mitochondria are major sources of ROS in cells. Respiratory complexes I, II and III reduce O_2 to $O_2^{\bullet-}$. The contribution, however, of the complexes to the overall $O_2^{\bullet-}$ production differs depending on the organ, respiratory states and pathological states.[74-78] Potentially, not only the complexes are sources for $O_2^{\bullet-}$, but also several mitochondrial dehydrogenase complexes like the pyruvate dehydrogenase.[79] Approximately 0.01% to 5% of electrons passing down the electron transport chain leak to oxygen during oxidative respiration, which is converted to reactive oxygen species.[47,79] On the other hand, mitochondria have their own antioxidative defence system: superoxide dismutase catalyses dismutation of $O_2^{\bullet-}$ to H_2O_2.[80] This potent source of oxidizing equivalents is utilized in many signalling reac-

tions.[81,82] Increased oxidative stress is associated with damage of cellular organelles and enzymes, increased lipid peroxidation, mitochondrial DNA mutations[83] and development of insulin resistance.[84] It is also suggested that oxidative stress plays a major role in the pathogenesis of T2Dm.[85-90]

2.2.2 Mitochondrial lipids

2.2.2.1 (Patho)physiological role of mitochondrial lipids

Besides β-oxidation, the main pathway for fatty acid oxidation,[91] mitochondria are also sites of lipid synthesis, remodelling and inter-organellar lipid trafficking.[92,93] Thus, changes in lipid homeostasis are very likely to affect mitochondrial membrane composition which, in turn, regulates mitochondrial structure and function.[22,23] Mitochondria synthesise approximately 45% of their own phospholipids,[94] mostly phosphatidylethanolamines (PE), phosphatidylglycerols (PG), phosphatidic acids (PA) and cardiolipins (CL).[92,95] Mitochondrial lipids are not simply membrane constituents, but also involved in physiological processes such as mitochondrial fusion and fission, membrane structure and fluidity, electron transport chain assemblage, protein biogenesis, apoptosis and many more.[23,96-100] The role of lipids in mitochondrial function is exemplified by CL, the mitochondrial signature phospholipid, which has been shown to be a key player in the organization of the general mitochondria membrane structure and in the organization of the essential electron transport chain components into higher order assemblies.[97,99,101,102] Most lipids are not specific for individual organelles and therefore challenging to quantify in a mitochondria-specific fashion. Therefore, an accurate, comprehensive lipid profiling strategy, as established in this thesis, which enriches mitochondria and minimizes contaminations by membranes from other organelles is a prerequisite to investigate the contribution of individual lipids to mitochondrial (dys-)function.

2.2.2.2 Oxysterols, a lipid class of oxidised sterols

Oxysterols, oxygenated derivatives of cholesterol[103] and its precursors,[104] are intermediates in the formation of steroid hormones, 1,25-dihydroxyvitamin D3 and bile acids[105]. They are formed by enzymatic oxidation in the first steps of sterol metabolism,[105-107] autoxidation,[108] and reaction with reactive oxygen species (ROS)[109] or can be derived through diet.[110] The introduction of an oxygen moiety such as a hydroxyl, epoxide, or ketone group into the hydrophobic cholesterol enables oxysterols to pass through cell membranes and equilibrate much quicker throughout the cell than cholesterol itself[111,112]. Featured with diverse biological activities together with a high abundance in some tissues (e.g. 1.0-1.6x10^5 ng/g 24-hydroxycholesterol in brain[113]), oxysterols are evidently implicated in the pathogenesis of several chronic diseases like artherosclerosis[114,115] or neurodegenerative disorders.[116,117] Possible mechanisms, like oxysterol induced apoptosis via the mitochondrial pathway[118-120] and induced ROS production,[121] link the effects of oxysterols to mitochondrial (dys)function as their main target in the cell.[122] Mitochondria even contribute by the mitochondria-specific CYP27A to the enzymatic generation of oxysterols like 27-hydroxycholesterol,[106,123] an oxysterol widely discussed in context with several diseases.[124-127] Mitochondrial oxysterol levels might influence mitochondrial functioning, but so far only very few reports about oxysterol levels in mito-

chondria themselves exist,[128,129] probably due to the challenging isolation procedure of pure mitochondria[130] and the challenging oxysterol analysis.

2.2.3 Dysfunction of mitochondria

Dysfunctional mitochondria (an unspecific term to describe various mitochondrial abnormalities) were widely discussed to be involved in the pathophysiology of human diseases such as neurodegenerative disorders, cancer and diabetes.[52-54]

2.2.3.1 Dysfunction of mitochondria and insulin resistance

In the context of IR mitochondrial dysfunction is discussed as its cause, its consequence but also as an innocent bystander. Although a connection between mitochondrial dysfunction and insulin resistance was first described already more than 40 years ago,[131] the mechanisms are still not clear. The different hypotheses about the causal relationship of mitochondrial dysfunction and insulin resistance are discussed controversially: Mitochondrial oxidative capacity could be impaired by a lower substrate influx in IR.[132] Alternatively, lower rates of substrate oxidation caused by a deficiency in the electron transport chain or even a lower mitochondrial content could lead to inhibited metabolic fluxes and/or accumulation of toxic metabolites from incomplete oxidation of glucose and lipids and thereby to IR.[133,134] This deficiency could either be caused by substrate overflow leading to disturbances in substrate utilization, oxidant production and IR or this mitochondrial dysfunction could be a consequence of impaired insulin signalling. The focus of research over the last years was mainly on alterations in skeletal muscle. In addition to earlier human studies assuming mitochondrial dysfunction to decrease lipid oxidation in muscle in obesity and diabetes (measured across the leg),[135,136] Kelley et al. (2002)[137] eventually observed smaller mitochondria and a decreased ETC activity (measured as NADH:O_2 oxidoreductase) in mitochondria preparations of type 2 diabetics and obese patients compared to lean.

In the last years, various features of mitochondrial dysfunctions were uncovered in muscle of insulin resistant and/or type 2 diabetics compared to healthy subjects. Lowered oxidative capacity in muscle biopsy material from T2Dm patients compared to healthy subjects was observed in several studies.[137-140] Normalisation to mitochondrial content commonly applied did not change the results except in one study.[139] The results were also confirmed in isolated mitochondria.[141] This reduction of oxidative capacity was often associated with a reduced mitochondrial content,[137,142] mostly investigated using electron microscopy[137,142,143] or citrate synthase activity.[137,139,144] Mitochondrial alterations and possible mechanisms for reduced mitochondrial content and oxidative capacity were investigated on mRNA levels of genes responsible for mitochondrial biogenesis like PGC-1α.[144,145] But also decreased mitochondrial enzyme activities[137,139,141,144] or lowered protein abundance[141,144] were observed, in particular of those involved in the ETC.[137,140] A lower mitochondrial content and oxidative capacity was observed in non diabetic individuals with a family history of type 2 diabetes, suggesting that mitochondrial alterations might be the cause and not the consequence of IR.[146] But results of mitochondrial dysfunction and its role in skeletal muscle insulin resistance remain still conflicting. Some research groups did not observe the mitochondrial alterations like the reduced oxidative capacity,[139,147]

or the reduced mitochondrial content[140] between health and insulin resistance. Even some animal studies, mostly high-fat-feeding induced insulin resistance showed an opposite relationship and described an increased fatty acid oxidation capacity, mitochondrial content and increased oxidative protein activities in skeletal muscle as compensatory effect to overcome excess substrate flows at early stages of the disease development.[25,148-152] High-fat-diet was shown to induce insulin resistance in rats although the mitochondrial amount was even increased.[25] An iron-deficient diet leading to a deficient ETC by decreasing the iron-containing ETC proteins even protected rats from insulin resistance by high-fat feeding.[153] Blocking of the entry of fatty acids into mitochondria in malonyl-CoA decarboxylase knockout mice, protected the mice from insulin resistance by high-fat feeding.[134] Given this inconsistency of data, the role of mitochondrial dysfunction in the etiology of muscle insulin resistance remains unclear. To this extent a causal relationship between insulin resistance and substrate overflow with regard to mitochondrial (dys)function was examined in this thesis in a murine skeletal muscle cell line.

The role of liver in context of insulin resistance as also one of the insulin target tissue and the major site for endogenous glucose production is still up for debate. Human studies about mitochondrial alterations in livers of T2Dm patients are quite rare. A higher oxidative capacity of liver mitochondria from biopsies was observed in insulin resistant obese compared to lean patients despite a non-alcoholic fatty liver (NAFL).[154] This was also seen in indirect methods assessing hepatic mitochondria.[155,156] Contrarily, there is also evidence of a normal oxidative phosphorylation in T2Dm compared to lean and obese patients assessed by high resolution respirometry (HRR)[157] and even an impaired hepatic mitochondrial function in T2Dm was described,[158,159] which was also seen in diabetic rats after high-caloric feeding.[160]

2.3 Investigation of mitochondrial composition and function

2.3.1 Mitochondrial purification

Although a causative role for alterations in mitochondrial protein and lipid composition in mediating mitochondrial dysfunction is very likely, the challenge of isolating adequate amounts of sufficiently pure mitochondria has hampered comprehensive studies combining functional and systems biological approaches up to now. The existence of diverse mitochondria isolation procedures with different requirements regarding time and equipment applying different principles of separation makes a decision for the most suitable method quite challenging for a scientist planning to perform mitochondrial analyses. Impurities caused by contaminations with other organelles may not only result in misleading analytical findings, but also hamper the comparability of data from different groups.[99,161] The most common used and simple method is differential centrifugation (DC) [162-166] since it is relatively fast and provides intact, functional mitochondria well suited to investigate mitochondrial physiology.[167,168] Briefly, tissues or cells are minced and homogenised, commonly using a Dounce homogeniser.[169-171] A slow centrifugation step is performed to sediment unbroken cells and cell debris, which is followed by a fast centrifugation step using the supernatant to pellet the mitochondria (further described in

3.2.6.2). A higher purity can be achieved by subsequent high-speed centrifugation on a density gradient.[163,172-175] This additional step can, however, reduce the yield of mitochondrial protein. Furthermore this step requires an ultracentrifuge, which may not be accessible for every scientist. In addition, centrifugation-based methods tend to be time-consuming, particularly when numerous samples are isolated simultaneously. Thus, a more rapid approach to isolate mitochondria has been commercialized that was first described by Hornig-Do et al. (2009)[176] After sample homogenisation, mitochondria are coupled to anti-TOM22-antibodies conjugated to paramagnetic beads. Bead-coupled mitochondria can then be isolated in a magnetic field. This so-called MACS (magnetic cell isolation and separation, here: magnetic bead assisted mitochondria isolation) procedure achieves higher yields of mitochondria.[176] Liver mitochondria isolated by MACS have been shown to exhibit higher oxygen consumption rates than mitochondria isolated by DC.[177]

2.3.2 Mitochondrial respiration: Investigation of OXPHOS capacity

Investigations of mitochondrial oxidative capacity are usually performed with complex 1 and 2 linked substrates.

2.3.2.1 Complex 1 linked substrates- NADH (Pyruvate/Glutamate and Malate)

After crossing the outer mitochondrial membrane via VDAC, externally added pyruvate is electroneutrally exchanged via the mitochondrial pyruvate carrier (MPC) by OH^- (Figure 2). The pyruvate dehydrogenase complex decarboxylates pyruvate to acetyl-CoA, CO_2 and $NADH(H^+)$, which transfers electrons to complex 1.[178-180] Acetyl-CoA condensates with oxaloacetate (which was oxidised from malate by malate dehydrogenase) to citrate, which is further metabolised in the TCA cycle providing reduction equivalents.[181] In gluconeogenic tissues like liver pyruvate is carboxylated to oxaloacetate by pyruvate carboxylase (PyC).[61] Glutamate is transported into the mitochondrial matrix by the glutamate-aspartate carrier or the glutamate-/OH^- exchanger and oxidized by glutamate dehydrogenase to 2-oxoglutarate and $NADH(H^+)$.[182-184] Malate cannot permeate the membrane and requires a carrier (dicarboxylate carrier, tricarboxylate carrier and 2-oxoglutarate carrier).[185,186]

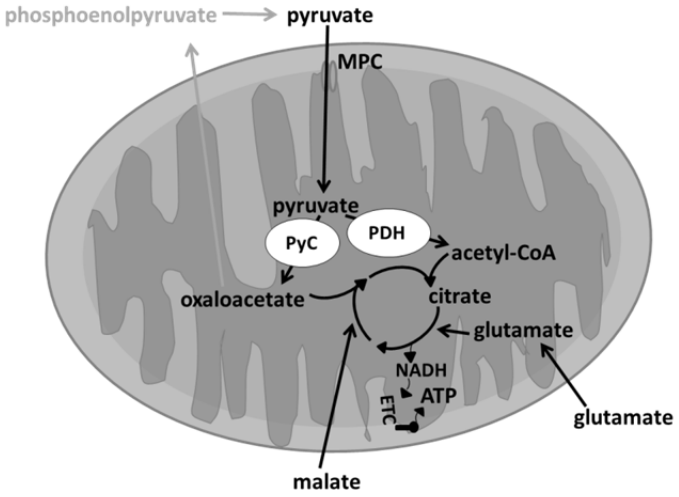

Figure 2: Complex 1 linked substrates for electron transport chain. After crossing outer mitochondrial membrane (OMM) via VDAC, pyruvate is transported into the matrix by mitochondrial pyruvate carrier (MPC). Pyruvate can either be oxidized to acetyl-CoA by pyruvate dehydrogenase complex (PDH) or carboxylated to oxaloacetate by pyruvate carboxylase (PyC) (only in gluconeogenic tissues). Glutamate is transported into mitochondria and oxidized by glutamate dehydrogenase to 2-oxoglutarate. ETC= electron transport chain.

2.3.2.2 Complex 2 associated substrate- Succinate

Succinate is transported into the matrix by the dicarboxylate carrier[186] and is the substrate for the succinate-dehydrogenase (C2) in the respiratory chain. Succinate is used together with rotenone (complex 1 inhibitor) to avoid accumulation of oxaloacetate, which is inhibiting succinate dehydrogenase, and a potential reverse flow of electrons through complex 1.[187,188]

2.3.2.3 Complex 1 and 2 associated substrates- Octanoyl-/Palmitoylcarnitine and Malate

The acyl-CoAs are imported into mitochondria via the carnitine-acylcarnitine translocase (CAT) (Figure 3). The acylchains are degraded by mitochondrial fatty acid β-oxidation (FAO) to acetyl-CoA, NADH and $FADH_2$.[189] Acetyl-CoA enters the TCA cycle, NADH is the substrate for complex 1, and $FADH_2$ simultaneously transfers electrons onto the electron-transferring flavoprotein complex (CETF), which supplies electrons to CoQ.[190]

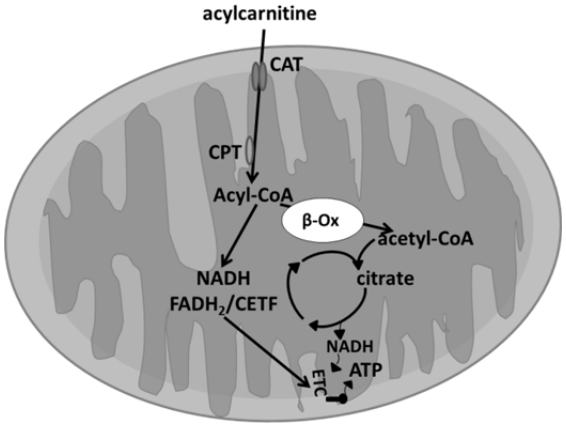

Figure 3: Complex 1 and 2 linked substrates for electron transport chain. Imported fatty acids are broken down via β-oxidation (β-Ox) to acetyl-CoA (further metabolised in the TCA cycle), NADH (electron transfer to complex 1) and FADH2 provide electrons via CETF to CoQ. TCA= tricarboxylic acid, ETC= electron transport chain, CPT= carnitine-palmitoyltransferase, CAT= carnitine-acylcarnitine-transporter, CoQ= coenzyme Q/ubiquinone, CETF= electron transfer flavoprotein complex.

2.3.3 Lipidome analyses of mitochondria

Lipidome analyses partly covering cardiolipins have previously been performed using liquid chromatography (LC)-mass spectrometry (MS)[166] and less often by shotgun analysis,[96] gas chromatography (GC)-MS,[164,191] Fourier transformation (FT)-MS[175] or matrix-assisted laser desorption/ionisation (MALDI)-TOF-MS techniques investigating mitochondria from various tissues,[162,165,171,174,192] macrophages[173] and yeast.[171,175] In addition to different analytical approaches, lipidomics data published so far originated from a variety of mitochondria isolation methods: either differential centrifugation (DC)[162-165] or ultracentrifugation (UC) on density gradients like iodixanol,[173] ficoll and sucrose,[96,174] or percoll.[163,165,172]

For mitochondrial lipid analyses, purified mitochondria are subjected to lipid extraction applying protocols such as the classic Folch method,[193] the modified Bligh/Dyer method[194] or the more recent and convenient methyl tert-butyl ether (MTBE)/MeOH/H_2O method,[195] which was also applied in the present work.

2.3.3.1 Reversed-phase (RP) chromatography

In this thesis, chromatographic separation of lipids is performed on RP high-performance liquid chromatography (HPLC) columns to determine fatty acyl chain length and composition based on their varying interaction with the non-polar stationary phase in a polar mobile phase. Lipid classes are eluted in a mixed pattern based on the length and unsaturation of fatty acyl chains. The stationary phase consists of hydrophobic long chain alkyl groups (e.g. C8, C18), that are chemically bonded to the silanol groups of silica particles. The mobile phase is typically a mixture of water and an organic solvent (e.g. acetonitrile, isopropyl alcohol or methanol). The choice and proportion of the “organic modifier” will affect the selectivity of the separation. In RP the lipophilic/hydrophobic interaction between the fatty acid molecules and the alkyl chains of the stationary phase determines the retention time. Re-

tention time decreases as the number of double bonds increases. Other HPLC-based methods used in lipidomics, but not applied in this thesis, are normal phase liquid chromatography (NPLC) and hydrophilic interaction liquid chromatography (HILIC). In both techniques, lipids are separated into classes based on their specific polar head groups. Compared to shotgun lipidomics, which relies on direct infusion of sample into a mass spectrometer without any chromatographic pre-separation of analytes, LC-MS based lipidomics approaches reduce ion suppression in analysing complex biological samples by adding the retention time as another factor to selectivity and allows the identification of isobaric compounds. Electrospray ionisation (ESI; see next chapter 2.3.3.2), which was applied in this work, enabled the coupling of LC with MS in a highly efficient manner described for the first time by Whitehouse et al. (1985)[196] The combination of LC and MS (LC-MS) has opened up new analytical perspectives.

2.3.3.2 Electrospray ionisation (ESI)

In the 1980s a soft ionisation procedure, electrospray ionisation (ESI), was introduced and first applied to molecules with low molecular weight.[196] The usage was then extended to large biomolecules.[197] Han et al. (1994)[198] were first to employ ESI for – analysing lipid molecules. ESI is an interface between LC and MS, which transforms biomolecules from liquid state to gas phase ions under atmospheric conditions in a non-destructive manner. Eluting from an LC column at µl or nl flowrate, the analyte solution passes through a narrow capillary (ESI emitter, ~10 µm inner diameter). Between the emitter and a counter electrode a potential difference of ±1.5 – 4.5 kV is applied. Due to the strong electric field, charges accumulate at the liquid surface at the tip of the emitter. Accumulated positive charges are attracted by the counter electrode (negative) by the repulsion of the emitter in positive ESI mode (same polarity) and accumulated negative charges are attracted by the counter electrode (positive) by the repulsion of the emitter in negative ESI mode. When the voltage reaches a threshold (Taylor voltage), the surface of liquid changes its shape to a “Taylor cone”, when ejected from the ESI emitter. The solvent evaporates from these charged droplets through use of a hot drying gas (e.g. N_2) and these droplets shrink until the surface tension can no longer uphold the charge repulsions (Rayleigh limit) leading to “Coulombic explosion” and small droplets are ejected. This desolvation process occurs repeatedly to form even smaller droplets until single ions are transferred to the gas phase, a process that is still not completely understood.[199] Other frequently used soft ionisation technologies in lipidomics are atmospheric pressure chemical ionisation (APCI)[200] and matrix-assisted laser desorption/ionisation (MALDI).[201] But also more recent technologies like desorption electrospray ionisation (DESI),[202] matrix-free laser desorption ionisation (LDI),[203] and laser ablation electrospray ionisation (LAESI)[204] are used.

2.3.3.3 Mass spectrometry (MS)

A mass spectrometer usually consists of an ion source (for example ESI), a mass analyser, a detector and data processing electronics. The mass analyser separates gas phase ions based on their mass-to-charge-ratio (m/z). Electric or electromagnetic fields are used for separating ions. Mass spectra are plots of ion intensity as a function of the m/z ratio. Three commonly used mass analysers for biomol-

ecule analysis are quadrupole, linear ion trap[205] and the Orbitrap.[206] Quadrupoles consist of four precisely parallel metal rods. Opposite electrodes are connected and one pair of rods gets a positive current and the other pair a negative current. A set oscillation (time dependent radiofrequency) of this electric field in the centre of the quadrupole allows only a narrow m/z ratio to pass the quadrupole on a stable trajectory. The quadrupole linear ion trap (LTQ) is similar to a quadrupole split into three sections. The middle section is the largest section and stores the ion, whereas the end sections are used for ion manipulation and application of trapping potential. The Orbitrap traps and analyses ions by electrostatic fields. It consists of one spindle and an outer barrel like electrode. Injected ions are electrostatically trapped while oscillating along the central electrode. This frequency is dependent on the m/z ratio. The oscillating ions induce an image current signal on the outer electrode, which are converted into frequencies by Fourier transformation. These characteristic frequencies are then converted into a mass spectrum. Other mass analysers used in lipidomics are time-of-flight (TOF), Fourier transform ion cyclotron resonance (FT-ICR).

2.3.3.4 Tandem mass spectrometry (MS/MS)

Hybrid MS systems were developed combining two or more mass analysers to allow specific fragmentation of chosen precursor ions to obtain in-depth information on the structure via MS/MS spectra or improved detection limits (triple quadrupole instrument). In tandem mass spectrometry (MS/MS),[207] ions are generated in the ion source (e.g. ESI) and separated by m/z ratio in the first stage of the mass spectrometer (MS1). A precursor ion of a particular m/z (precursor ions) is selected and fragment ions (product ions) are generated by collision-induced dissociation (CID) or other processes. In CID, the precursor ion is fragmented by collisions with inert gas atoms, which raises the energy in the molecule before bonds are broken.[208,209] The resulting product ions are then separated and detected in a second stage of the mass spectrometer (MS2).

Tandem mass spectrometric experiments can be performed by tandem-in-space and tandem-in-time instruments.[210] Separate mass analysers are utilised for each MS stage in tandem-in-space instruments (e.g. triple quadrupole mass spectrometer). In the approach of tandem-in-time instruments the various MS/MS stages are being performed in one mass analyser (e.g. linear ion trap) at different time points, principally allowing to conduct MS^n experiments.

2.3.3.5 “Top down” and “bottom up” lipidomics

Based on the strategies that are applied for lipid screening, the lipidomics approach is defined as “top-down” or “bottom-up”. The specificity of both, ”top-down” and “bottom-up” approaches, depend on the ability of a MS to distinguish between two neighbouring peaks of intact molecular ions or their fragments. This resolving power or resolution is usually the ratio of the ion peak mass to the peak width at 50% of its height to the mass of the peak (full width at half maximum [FWHM]).[211] The difference between the measured and the theoretical mass value is described in a relative manner (e.g. parts per million (ppm)) and is defined as the mass accuracy.

The “top-down” lipidomics approach, that was applied in this thesis, takes the unique elemental composition of lipid species of specific classes into account using high-resolution MS for exact mass measurement, for example the Orbitrap and FT-ICR.[212,213] Exemplarily, the applied LTQ-Orbitrap enables a high mass resolution exceeding 100 000, a mass error less than 2 ppm using internal standards and 5 ppm with external calibration.[206,214] Data are acquired at high resolution and accuracy with the Orbitrap, whereas MS/MS is recorded at high speed with low resolution in a linear ion trap mass analyser

An alternative, so called “bottom-up”, approach in tandem-MS utilizes the “building block” feature of lipids; precursor ions are identified and quantified due to their specific fragment ion. Differences in chemical properties of lipid classes such as charge state and polarity are taken into account. These can be used to determine individual molecular species of a class by scanning precursor ions or neutral losses that are indicative for head groups, fatty acyls or long-chain sphingoid bases, etc. (Table 1).[207]

Table 1: Examples of scanning modes and resulting mass-to-charge ratios (m/z) in lipidomics. PIS=precursor ion scanning, NLS=neutral loss scanning; PC= phosphatidylcholine, PE=phosphatidylethanolamine, PS=phosphatidylserine, PI=phosphatidylinositol, PG=phosphatidylglycerol, PA=phosphatidic acid, SM=sphingomyelin.

subclass	polarity	scan mode	m/z
PC	positive	PIS	184
	negative	PIS	168
PE	positive	NLS	141
	negative	PIS	195
PS	positive	NLS	185
	negative	NLS	87
PI	positive	NLS	277
	negative	PIS	241
PG	positive	NLS	189
PA	positive	NLS	115
Ceramide	positive	PIS	264
Hexosylceramide	positive	PIS	264
Lactosylceramide	positive	PIS	264
SM	positive	PIS	184
	negative	PIS	168
Cholesterol ester	positive	PIS	369
Cholesterol (as acetate)	positive	NLS	77

3 Material and Methods

3.1 Material

3.1.1 Chemicals

Relevant product codes and/or abbreviations in brackets

2-(*N*-morpholino)ethanesulfonic acid (MES)	Sigma-Aldrich, St. Louis, MO, USA
4-(2-Hydroxyethyl)piperazine-1- ethanesulfonic acid (HEPES)	Roth, Karlsruhe, Germany
5,5'-Dithiobis-2-nitrobenzoic acid (DTNB; 6334)	Roth, Karlsruhe, Germany
Acetonitrile (ACN)	Merck, Darmstadt, Germany
Acetyl-CoA (lithium salt, A2181)	Sigma-Aldrich, St. Louis, MO, USA
Acrylamide 30 (37.5:1)	Roth, Karlsruhe, Germany
Adenosine 5'-triphosphate disodium salt hydrate (Na_2ATPxH_2O)	Sigma-Aldrich, St. Louis, MO, USA
Adenosine diphosphate (ADP)	Calbiochem, Merck, Darmstadt, Germany
Agarose, peqgold Universal	Peqlab, Erlangen, Germany
Ammonium acetate	Sigma-Aldrich, St. Louis, MO, USA
Ammonium persulfate (APS)	Sigma-Aldrich, St. Louis, MO, USA
Antimycin A (A8674)	Sigma-Aldrich, St. Louis, MO, USA
Ascorbate (A4034)	Sigma-Aldrich, St. Louis, MO, USA
BigDye® Terminator sequencing buffer 5x	Applied Biosystems, Foster City, CA, USA
Bio-Rad protein assay	Biorad, München, Germany
Bovine serum albumin (BSA, A6003)	Sigma-Aldrich, St. Louis, MO, USA
Bromophenolblue	Sigma-Aldrich, St. Louis, MO, USA
Butylated hydroxytoluene (BHT)	Sigma-Aldrich, St. Louis, MO, USA
Calcium carbonate ($CaCO_3$)	Merck, Darmstadt, Germany
Calcium chloride ($CaCl_2$)	Sigma-Aldrich, St. Louis, MO, USA
Carbonyl cyanide-p-trifluoromethoxyphenylhydrazon (FCCP) (C2920)	Sigma-Aldrich, St. Louis, MO, USA
Catalase	Sigma-Aldrich, St. Louis, MO, USA
Citrate synthase (CS) from porcine heart (C2360)	Sigma-Aldrich, St. Louis, MO, USA
cOmplete protease inhibitor cocktail	Roche, Mannheim, Germany
Cytochrome c (C7752)	Sigma-Aldrich, St. Louis, MO, USA

Developer	Agfa Healthcare GmbH, Berlin, Germany
Dichloromethane (DCM)	Sigma-Aldrich, St. Louis, MO, USA
Digitonin (D141)	Sigma-Aldrich, St. Louis, MO, USA
Dimethyl sulfoxide (DMSO)	Roth, Karlsruhe, Germany
Dithiothreitol (DTT)	Sigma-Aldrich, St. Louis, MO, USA
Ethanol p.A.	Merck, Darmstadt, Germany
Ethylene glycol-bis(β-aminoethyl ether)-N,N,N',N'-tetraacetic acid (EGTA)	Roth, Karlsruhe, Germany
Ethylene diaminetetraacetic acid (EDTA)	Sigma-Aldrich, St. Louis, MO, USA
Gelatine	Merck, Darmstadt, Germany
Glucose aqueous solution for injection (20%)	B. Braun, Melsungen, Germany
Glutamate (G1251)	Sigma-Aldrich, St. Louis, MO, USA
Glycerol	Merck, Darmstadt, Germany
Glycine	Roth, Karlsruhe, Germany
H_2O, HPLC-grade	Merck, Darmstadt, Germany
Hydrochloric acid (HCl)	AppliChem, Darmstadt, Germany
Imidazole	Sigma-Aldrich, St. Louis, MO, USA
Insulin, human recombinant	Sigma-Aldrich, St. Louis, MO, USA
Isopropanol (IPA)	Merck (Darmstadt, Germany).
Ketamine- injectable aqueous solution	Ratiopharm GmbH, Ulm, Germany
K-lactobionate	Sigma-Aldrich, St. Louis, MO, USA
Luminol (3-Aminophthalhydrazide)	Sigma-Aldrich, St. Louis, MO, USA
Magnesium chloride ($MgCl_2$)	Sigma-Aldrich, St. Louis, MO, USA
Magnesium chloride hexahydrate ($MgCl_2(H_2O)_6$)	Serva Electrophoresis, Heidelberg, Germany
Malate (M9138)	Sigma-Aldrich, St. Louis, MO, USA
Methanol (MeOH)	Merck (Darmstadt, Germany).
Methanol Normapur	VWR, Darmstadt, Germany
Na-orthovanadate	Sigma-Aldrich, St. Louis, MO, USA
Na-pyrophosphate	Sigma-Aldrich, St. Louis, MO, USA
Octanoylcarnitine (0605)	Tocris Bioscience, Bristol, UK
Oxaloacetic acid (5000)	Calbiochem, Merck, Darmstadt, Germany
Palmitoyl-L-carnitine chloride (76178)	Sigma-Aldrich, St. Louis, MO, USA
Phosphocreatine	Sigma-Aldrich, St. Louis, MO, USA
Ponceau S-Solution	AppliChem, Darmstadt, Germany
Potassium chloride (KCl)	Sigma-Aldrich, St. Louis, MO, USA

Potassium dihydrogenphosphate (KH_2PO_4)	Merck, Darmstadt, Germany
Potassium hydroxid (KOH)	Sigma-Aldrich, St. Louis, MO, USA
Pyruvate (P2256)	Sigma-Aldrich, St. Louis, MO, USA
Ribonuclease A	Serva Electrophoresis, Heidelberg, Germany
Rotenone (R8875)	Sigma-Aldrich, St. Louis, MO, USA
Saponin from quillaja bark (S4521)	Sigma-Aldrich, St. Louis, MO, USA
Sepharose G-50 superfine	GE Healthcare, München, Germany
Sodium azide (S2002)	Sigma-Aldrich, St. Louis, MO, USA
Sodium chloride (NaCl)	Merck, Darmstadt, Germany
Sodium deoxycholate (NaDOC)	Sigma-Aldrich, St. Louis, MO, USA
Sodium dodecyl sulfate (SDS)	Biorad, München, Germany
Sodium fluoride (NaF)	Sigma-Aldrich, St. Louis, MO, USA
Sodium pyrophosphate ($Na_4P_2O_7$)	Sigma-Aldrich, St. Louis, MO, USA
Succinate (S3674)	Sigma-Aldrich, St. Louis, MO, USA
Sucrose	Roth, Karlsruhe, Germany
Taurine	Sigma-Aldrich, St. Louis, MO, USA
TE-buffer, sterile, pH 8.0	Sigma-Aldrich, St. Louis, MO, USA
TEMED (*N*,*N*,*N*',*N*'-tetramethylethylenediamine)	Roth, Karlsruhe, Germany
TMPD (*N,N,N',N'*-tetramethyl-*p*-phenylenediamine; T3134)	Sigma-Aldrich, St. Louis, MO, USA
Triethanolamine (90279)	Sigma-Aldrich, St. Louis, MO, USA
Tris(hydroxymethyl)aminomethane (TRIS)	Sigma-Aldrich, St. Louis, MO, USA
TRIS, ultra-pure (for ECL)	MP Biomedicals Inc., Solon, OH, USA
Triton-X-100	Sigma-Aldrich, St. Louis, MO, USA

Ultra-pure water was prepared by a Milli-Q system (Millipore, Billerica, MA, USA)

3.1.2 Buffers and solutions

All buffers and solutions were prepared with ultra-pure water.

3.1.2.1 General buffers

Lysis Buffer 1 (pH 7.5) (stored at 4 °C)	HEPES	50 mM
	NaCl	150 mM
	$MgCl_2$	1.5 mM
	EGTA	1 mM
	Glycerol	10%
	Triton-X-100	1%
	NaF	100 mM
	$Na_4P_2O_7$	10 mM

Lysis Buffer 1 was mixed with phosphatase inhibitors (see below) and cOmplete protease inhibitor shortly before use and was mainly used for cell lysis.

Lysis Buffer 2 (RIPA lysis buffer; pH 7.6) (stored at 4 °C)	TRIS pH 7.6	25 mM
	NaCl	150 mM
	SDS	0.1%
	NaDOC	0.5%
	Triton-X-100	1%

Lysis Buffer 2 was supplemented with phosphatase inhibitors (see below) and cOmplete protease inhibitor shortly before use and was mainly used for tissue lysis.

10 x Phosphatase inhibitors (stored at -20 °C)	NaF	10 mM
	Na-pyrophosphate	5 mM
	Na-orthovanadate	10 mM
	β-glycerophosphate	10 mM

Bradford working solution: Bio-Rad Protein Assay solution was diluted 1:5 with ultra-pure water and filtered through filter papers (MN 615 ¼, α-cellulose, Machery-Nagel GmbH Co KG Germany). Solutions were kept no longer than 4 weeks at 4 °C and protected from light.

5 x Laemmli sample buffer (pH 6.8) (stored at 4 °C)	TRIS/HCl	60 mM
	Glycerol	5.5%
	SDS	0.44%
	β-Mercaptoethanol	1.1%
	Bromophenolblue	0.21%
Stacking gel buffer (pH 6.8) (stored at RT)	TRIS	0.5 M
	SDS	2%
Separation gel buffer (pH 8.8) (stored at RT)	TRIS	1.5 M
	SDS	2%
10 x Electrophoresis buffer (stored at 4 °C)	TRIS	250 mM
	Glycine	2 M
	SDS	1%
10 x Blotting buffer (stored at RT)	TRIS	480 mM
	Glycine	390 mM
	SDS	0.4%
1 x Blotting buffer (stored at RT)	10 x Blotting buffer	10%
	Methanol	20%
	H_2O	70%
Stripping buffer (pH 6.8) (stored at RT)	TRIS	66 mM
	β-Mercaptoethanol	0.5%
	SDS	2%
10 x NET-G (stored at 4 °C)	Gelatine	2.5%
	NaCl	1.5 M
	EDTA	50 mM
	TRIS	500 mM
	Triton-X-100	0.5%

10 x NET-G was diluted 1:10 with ultra-pure water and the pH was adjusted to 7.4 using 37% HCl to obtain 1 x NET-G.

10 x TBS (TRIS-buffered saline) (stored at RT)	NaCl	1.5 M
	TRIS	250 mM

0.1% Tween20 was added to TBS for TBS-T buffer. 10 x TBS was diluted 1:10 with ultra-pure water and the pH was adjusted to 7.6 to obtain 1 x NET-G.

Solution A (pH 9.35)	TRIS, ultra-pure	0.1 M
	Luminol	4.4 mM (in DMSO)
	p-Iodophenol	4.4 mM (in DMSO)
Solution B (pH 9.35)	TRIS, ultra-pure	0.1 M
(both stored at 4 °C)	H_2O_2 (30%)	0.4%

Enhanced chemiluminescence (ECL) solution: Shortly before usage solutions A and B were mixed at a ratio of 1:1.

50 x TAE buffer (pH 8) (stored at RT)	TRIS	1.25 M
	Acetic acid	625 mM
	EDTA	50 mM

Cryopreservation medium for cells	Cell medium	80%
	FCS	20%
	DMSO	10%

3.1.2.2 Respiratory measurement buffers for high resolution respirometry (HRR) and Seahorse XF96 measurements

Mir05 (pH 7.1 at 30 °C with KOH) (stored at -20 °C)	EGTA	0.5 mM
	$MgCl_2(H_2O)_6$	3 mM
	K-lactobionate*	60 mM
	Taurin	20 mM
	KH_2PO_4	10 mM
	HEPES	20 mM
	Sucrose	110 mM
	BSA, fatty acid free	1 g/l

*Preparation of 0.5 M stock solution, pH 7.0 with KOH

2 x STE buffer (pH 7.4 with HCl) (stored at 4 °C)	Sucrose	500 mM
	TRIS (base)	10 mM
	EGTA	4 mM
	BSA fatty acid free	0.1%-0.5% (depending on the tissue/cells), freshly added on the day of the experiment

2 x STE buffer was diluted with ultra-pure water to achieve 1x STE.

MAS buffer (pH 7.2 at 37 °C) (stored at 4 °C)	Sucrose	70 mM
	Mannitol	220 mM
	KH_2PO_4	10 mM
	$MgCl_2$	5 mM
	HEPES	2 mM
	EGTA	1 mM
	BSA, fatty acid free	0.1%-0.5% depending on the tissue/cells, freshly added on the day of the experiment

Biopsy preservation solution (BIOPS) (pH 7.1 at 30 °C with KOH)	CaK_2EGTA*	2.77 mM
(stored at -20 °C)	K_2EGTA*	7.23 mM
	Na_2ATP	5.7 mM
	$MgCl_2(H_2O)_6$	6.56 mM
	Taurine	20 mM
	Na_2Phospho-creatine	15 mM
	Imidazole	20 mM
	Dithiothreitol	0.5 mM
	MES	50 mM
	*Preparation of 100 mM stock solutions K_2EGTA and CaK_2EGTA (see below)	

Stocks:

K_2EGTA: 100 mM EGTA and 200 mM KOH were mixed in H_2O, pH was adjusted to 7.0 with KOH.

CaK_2EGTA: 2.002 g $CaCO_3$ were dissolved in 100 mM hot (80 °C) aqueous solution of EGTA (7.608 g/ 200 ml). While stirring continuously, 2.3 g KOH were added, pH was adjusted to 7.0 with KOH.

Substrates, uncouplers and inhibitors for HRR of isolated mitochondria from tissue and permeablised muscle fibres	**Substrate**	**Stock conc. [mM]**	**Solvent**
	Malate	800-1000	H_2O
	Digitonin	8.1	H_2O
	Octanoylcarnitine	100	H_2O
	ADP	500	H_2O
	Pyruvate	1000	H_2O
	Succinate	500	H_2O
	Cytochrome c	4	H_2O
	FCCP	1-2.5	EtOH
	Rotenone	1-2.5	DMSO
	Antimycin A	2.5-5	DMSO
	Glutamate	500	H_2O
	Ascorbate	800	H_2O
	TMPD	200	EtOH
	Sodium Azide	4000	H_2O

Catalase stock solution (112 000 U/ml; stored -20 °C): catalase powder from bovine liver with 2800 U/mg was diluted in Mir05.

H_2O_2 stock solution (200 mM; freshly prepared every day):

190 µl of 30% H_2O_2 were filled up to 10 ml with H_2O.

Saponin stock solution (5 mg/ml; freshly prepared):

5 mg Saponin from quillaja bark were added into 1 ml BIOPS.

Substrates, uncouplers and inhibitors for Seahorse respiratory analyses	**Substrate**	**Stock conc [mM]**	**Solvent**
	Succinate	5	H_2O
	Rotenone	2	DMSO
	ADP	4.05	H_2O
	Oligomycin	2.5	DMSO
	FCCP	2.5	DMSO
	AA	2.5	DMSO
	Pyruvate	0.01	H_2O
	Malate	0.0005	H_2O
	Palmitoylcarnitine	0.00375	H_2O

3.1.2.3 Citrate synthase (CS) activity assay buffers

Acetyl-CoA solution (12.2 mM, stored at -20 °C) in H_2O, stored on ice during measurement.

Stable up to 4 weeks at 4 °C:

Tris-HCl buffer (1.0 M, pH 8.1 with 37% HCl) in H_2O.

Tris-HCl buffer (0.1 M, pH 7.0 with 37% HCl), prepared from Tris-HCl buffer (1.0 M) with H_2O.

Triethanolamine-HCl buffer (0.5 M, pH 8.0 with 37% HCl) + EDTA (5 mM) in H_2O.

Triton X-100 (10% solution), dissolved in H_2O by stirring.

Prepared freshly before experiment:

Triethanolamine-HCl-buffer (0.1 M, pH 8.0): prepared from 0.5 M triethanolamine HCl buffer

Oxaloacetate (10 mM, pH 8.0): oxaloacetate dissolved in 0.1 M triethanolamine-HCl-buffer of pH 8.0

DTNB (1.01 mM, pH 8.1): dissolved in 1M Tris-HCl-buffer of pH 8.1.

CS Standard (0.0172 $mg*cm^{-3}$): 2 µl citrate synthase + 998 µl of 0.1 M Tris-HCl-buffer of pH 7.0. The CS standard served as a control for chemicals and assay conditions.

3.1.3 Cells, animals and human biopsies

3.1.3.1 Cells

Human hepatocellular carcinoma cells (HEPG2)	DSMZ, Braunschweig, Germany
Murine myoblasts C2C12 (CRL-1772™)	ATCC, Manassas, Virginia, USA
Primary human skeletal muscle cells (hMT)	cultured from muscle biopsies (3.2.1.1)
Human embryonic kidney cells 293 (HEK)	ATCC, Wesel, Germany

3.1.3.2 Animals

Male C57/Bl6 mice, 10-weeks-old	Charles River Laboratories, Sulzfeld, Germany
129 S1/SvImJ mice, 3-months-old	Jax Mice, Maine, USA

3.1.3.2.1 Mouse diets

Product codes in brackets

diet	company	experiment
control diet (CON): 10 kJ% fat, 20 kJ% protein, 70 kJ% carbohydrates (D15072001) high-energy diet (HED): 40 kJ% fat, 40 kJ% protein, 20 kJ% carbohydrates (D15072002)	Research Diets, New Brunswick, NJ, USA	Establishing diet effectiveness (see 3.2.2.3.1)
control diet (CON): 10 kJ% fat, 20 kJ% protein, 70 kJ% carbohydrates (D12450J) high-energy diet (HED): 45 kJ% fat, 20 kJ% protein, 35 kJ% carbohydrates (D12451 (I) mod.)	Ssniff, Soest, Germany	Optimised diet and treadmill exercise experiment (see 3.2.2.3.2)

Fatty acid composition of control diet (CON) and high-energy diet (HED) derived from Ssniff

% FA diet	CON %	HED %
12:0	0.25%	0.23%
14:0	1.00%	1.33%
16:0	17.25%	24.42%
16:1	1.25%	2.84%
18:0	7.75%	10.49%
18:1	32.50%	43.15%
18:2	35.75%	15.85%
18:3	3.75%	1.69%
20:0	0.50%	

3.1.3.3 Human biopsies and tissues

Muscle biopsies were taken from the lateral portion of the vastus lateralis of the quadriceps femoris after local anesthesia under sterile conditions by Dr. Anja Böhm using a Bergstroem needle biopsy technique as described previously.[215] The Ethics Committee of the University of Tübingen approved the protocol according to the Helsinki Declaration (446/2016B02).

For the analysis of liver tissue samples, Caucasians undergoing liver surgery at the Department of General, Visceral and Transplant Surgery at the University Hospital of Tübingen, Germany, were included as described previously.[216] Subjects were tested negative for viral hepatitis and had no liver cirrhosis. Liver samples were taken from normal, non-diseased tissue during surgery and used freshly. Informed written consent was obtained from all participants and the Ethics Committee of the University of Tübingen approved the protocol according to the Helsinki Declaration (239/2013B01).

3.1.4 Gels

Most SDS gels were 1.5 mm thick and 20×10 cm in size. The total required gel volume was 25 ml (20 ml separation gel and 5 ml stacking gel).

Stacking gel (5 ml)	H_2O	2.85 mL
	TCE	25 µl
	Stacking gel buffer	1.25 ml
	Acrylamide 30 (37.5:1)	0.8 ml
	TEMED	8 µl
	APS (10%)	33 µl

Separation gel 12.5% (20 ml)	H_2O	6.4 ml
	TCE	100 µl
	Separation gel buffer	5 ml
	Acrylamide 30 (37.5:1)	8.33 ml
	TEMED	33 µl
	APS (10%)	133 µl

Separation gel as **gradient gel** (5 to 15% acrylamide):

The gradient gel (20x10 cm, 1.5 mm thick) was made using a gradient maker mixing the heavy (15%, 10 ml) and the light (5%, 10 ml) solution throughout pouring the gel. Stacking gels were prepared as described above.

Separation gel 15% (10 ml)	H_2O	1.37 ml
	TCE	50 µl
	Separation gel buffer	2.5 ml
	Glycerol	1 ml
	Acrylamide 30 (37.5:1)	5 ml
	TEMED	17 µl
	APS (10%)	67 µl

Separation gel 5% (10 ml)	H_2O	5.7 ml
	TCE	50 µl
	Separation gel buffer	2.5 ml
	Acrylamide 30 (37.5:1)	1.67 ml
	TEMED	17 µl
	APS (10%)	67 µl

Agarose gel (1%, 2%):

Agarose gels were prepared by dissolving agarose in 1 x TAE buffer to obtain 1% or 2% gels under heating.

3.1.5 Culture media and supplements

Amphotericin B	Sigma-Aldrich, St. Louis, MO, USA
Chicken extract	Seralab, West Sussex, UK
DMEM high glucose	Gibco, life technologies, Carlsbad, CA, USA
DMEM no glucose	Gibco, life technologies, Carlsbad, CA, USA
DPBS	Sigma-Aldrich, St. Louis, MO, USA
FCS superior	Biochrom GmbH, Berlin, Germany
Glucose solution 200 g/l	Gibco, life technologies, Carlsbad, CA, USA
Glutamine	Lonza Ltd, Basel, Switzerland
Ham's F-12	Lonza, Basel, Switzerland
Insulin human	Sigma-Aldrich, St. Louis, MO, USA
Oleate	Sigma-Aldrich, St. Louis, MO, USA
Palmitate	Sigma-Aldrich, St. Louis, MO, USA
Penicillin/ Streptomycin	Lonza Ltd, Basel, Switzerland
RPMI 1640	Gibco, life technologies, Carlsbad, CA, USA
Trypsin-EDTA (200 mg/l versene (EDTA), 170 000 U trypsin/ml)	Lonza Ltd, Basel, Switzerland
α-MEM	Lonza, Basel, Switzerland

Medium for HEPG2 cells:

Growth medium for HEPG2 was RPMI 1640 supplemented with 10% FCS, 1% penicillin (pen)/streptomycin (strep), 1% glutamine.

Medium for HEK cells:

Growth medium for HEPG2 was DMEM high glucose supplemented with 10% FCS, 1% pen/strep, 1% glutamine.

Media for C2C12:

Growth medium was DMEM high glucose supplemented with 10% FCS, 1% pen/strep, 1% glutamine. DMEM no glucose medium was supplemented with glucose solution to obtain either 25 mM (high) or 5.5 mM (low) glucose concentration in the fusion medium. Fusion medium for C2C12 myoblasts was

supplemented with 2% FCS, 1% pen/strep, 1% glutamine. Starving medium was solely supplemented with 1% pen/strep, 1% glutamine.

Media for primary skeletal muscle cells:

Growth medium was a 1:1 mixture of α-MEM and Ham's F-12 supplemented with 20% FCS, 1% chicken extract, 1% pen/strep, and 0.2% amphotericin. Fusion medium was α-MEM supplemented with 2% FCS, 1% glutamine, 1% pen/strep, and 0.2% amphotericin B. Starving medium was solely supplemented with 1% pen/strep, 1% glutamine.

3.1.6 Kits

Big Dye Terminator v1.1 cycle sequencing kit	Applied Biosystems, Foster City, CA, USA
CyQUANT cell proliferation assay kit	Molecular probes, Eugene, Oregon, USA
Immobilon western HRP substrate luminol reagent	Millipore, Billerica, MA, USA
MACS (human mitochondria isolation kit)	Miltenyi Biotec, Bergisch-Gladbach, Germany
MinElute PCR purification kit	Qiagen, Hilden, Germany
Pierce BCA protein assay kit	Thermo Fisher Scientific, Waltham, Massachusetts, USA
QIA quick PCR purification	Qiagen, Hilden, Germany
SOD activity assay	Sigma-Aldrich, St. Louis, MO, USA

3.1.7 Internal standards for lipidomics analysis

Synonyms and product codes in brackets

1,2-Dipentadecanoyl-*sn*-glycero-3-phosphoethanolamine (PE 15:0; 850704P)	Avanti Polar Lipids Inc., Alabaster, AL, USA
1,2-Dinonadecanoyl-*sn*-glycero-3-phosphocholine (PC 19:0; 850367P)	Otto Nordwald, Avanti Polar Lipids Inc., Alabaster, AL, USA
1-Nonadecanoyl-2-hydroxy-*sn*-glycero-3-phosphocholine (LPC 19:0; 855776P)	Otto Nordwald, Avanti Polar Lipids Inc., Alabaster, AL, USA
N-lauroyl-D-erythro-sphingosylphosphorylcholine (SM 12:0; d18:1/12:0; 860583P)	Otto Nordwald, Avanti Polar Lipids Inc., Alabaster, AL, USA
Tripentadecanoin (TG 45:0; T4257)	Sigma-Aldrich, St. Louis, MO, USA

N-heptadecanoyl-D-*erythro*-sphingosine (Cer 17:0; d18:1/17:0; 860517P)	Otto Nordwald, Avanti Polar Lipids Inc., Alabaster, AL, USA
Palmitic acid (7,7,8,8,-D4; DLM-2893-05)	Cambridge Isotope Laboratories Inc., Tewksbury, MA, USA
1,1,2,2 Tetramyristoyl cardiolipin (CL 14:0; 710332P)	Avanti Polar Lipids Inc., Alabaster, AL, USA
Cardiolipin Mix I (LM-6003):	Avanti Polar Lipids Inc., Alabaster, AL, USA
CL(1'-[14:1(9Z)/14:1(9Z)],3'[14:1(9Z)/15:1(10Z)])	
CL(1'-[15:0/15:0],3'-[15:0/16:1(9Z)])	
CL(1'[22:1(13Z)/22:1(13Z)],3'[22:1(13Z)/14:1(9Z)])	
CL(1'[24:1(15Z)/24:1(15Z)],3'[24:1(15Z)/14:1(9Z)])	
4β-Hydroxycholesterol-d7 (700042)	Otto Nordwald, Avanti Polar Lipids Inc., Alabaster, AL, USA
7α-Hydroxycholesterol- d7 (700043)	Otto Nordwald, Avanti Polar Lipids Inc., Alabaster, AL, USA
7-Oxocholesterol-d7 (700046)	Otto Nordwald, Avanti Polar Lipids Inc., Alabaster, AL, USA
25-Hydroxycholesterol-d6 (700053)	Otto Nordwald, Avanti Polar Lipids Inc., Alabaster, AL, USA
27-Hydroxycholesterol-d6 (700059)	Otto Nordwald, Avanti Polar Lipids Inc., Alabaster, AL, USA
Cholesterol-2,3,4-$^{13}C_3$ (749478)	Sigma-Aldrich, St. Louis, MO, USA

3.1.8 Enzymes and inhibitors

Product codes in brackets

Protease from *Bacillus licheniformis*, type VIII, 7-15 units/mg solid (P5380)	Sigma-Aldrich, St. Louis, MO, USA
Collagenase D (11088866001)	Roche, Mannheim, Germany
Dispase II (24693)	Sigma-Aldrich, St. Louis, MO, USA
Trypsin (T1426)	Sigma-Aldrich, St. Louis, MO, USA
Soy trypsin inhibitor (T9003)	Sigma-Aldrich, St. Louis, MO, USA

3.1.9 Molecular markers

Chameleon Duo pre-stained protein ladder (928-60000)	Licor, Lincoln, NE, U.S.A.
Precision Plus protein dual color standard	Bio-Rad, München, Germany
HiMark pre-stained	Novex, life technologies, Carlsbad, CA, USA
Quickload 1 kb DNA ladder	New England BioLabs, Beverly MA, USA

3.1.10 Consumables

96-well ELISA microplate, PS, flat bottom	Greiner Bio-One, Frickenhausen, Germany
96-well ELISA microplate, PS, flat bottom, black	Greiner Bio-One, Frickenhausen, Germany
Amersham hyperfilm ECL	GE Healthcare, München, Germany
Cell scraper	Corning B.V. Life Sciences, Amsterdam, The Netherlands
Centri-Sep spin columns	Thermo Fisher Scientific, Schwerte, Germany
Costar 150 mm TC-treated culture dish	Corning B.V. Life Sciences, Amsterdam, The Netherlands
Costar TC-treated 6-well plates	Corning B.V. Life Sciences, Amsterdam, The Netherlands
Cryocups	Greiner Bio-One, Frickenhausen, Germany
Filterpapers MN 615 ¼	Machery-Nagel, Düren, Germany
Gel blotting paper	VWR, Darmstadt, Germany
Immobilon-P membrane, PVDF, 0.45 µm, IPVH00010	Merck Millipore, Darmstadt, Deutschland
Nitrocellulose transfer membrane, BA 85, 0.45 µm	VWR, Darmstadt, Germany
Tissue culture dishes 87 mm and 137 mm	TPP, Trasadingen, Switzerland
Tissue culture test plates (6-well, 12-well)	TPP, Trasadingen, Switzerland

3.1.11 Laboratory equipment

8-channel electronic pipette Xplorer	Eppendorf, Hamburg, Germany
Agarose gel chamber midi	Harnischmacher Labortechnik, Kassel, Germany
Binocular microscope S4E	Leica, Wetzlar, Germany
BioCision™ CoolCell™ FTS30 cell freezing container	Thermo Fisher Scientific, Schwerte, Germany
Centrifuge Heraeus Pico 17	Thermo Fisher Scientific, Schwerte, Germany
Centrifuge Sorvall Super T21	Thermo Fisher Scientific, Schwerte, Germany
Centrifuges 5427 R, 5415 R, 5804 R, 5417 R	Eppendorf, Hamburg, Germany
ChemiDoc Touch imaging system	Bio-Rad, Hercules, CA, USA
Electrophoresis chamber for SDS-PAGE	Selfmade
ELISA reader model 680	Biorad, München, Germany
Freeze Dryer LDC1 alpha 2-4	Christ, Osterode am Harz, Germany
Gentle MACS	Miltenyi Biotec, Bergisch-Gladbach, Germany
Glass- glass douncer 2 ml	Sartorius, Goettingen, Germany
Glass- glass douncer 40 ml	Wheaton, Millville, NJ, USA
Gradient maker	Hoefer, Holliston, MA, USA
Heating block Thermostat Plus	Eppendorf, Hamburg, Germany
Hera Safe hood	Thermo Fisher Scientific, Schwerte, Germany
Incubator for cells BBD6220	Binder, Tuttlingen, Germany
Incubator for cells Cytoperm	Heraeus, Hanau, Germany
Incubator Function Line	Heraeus, Hanau, Germany
Laboratory balance ALJ160-4NM	Kern & Sohn, Balingen-Frommern, Germany
Laboratory balance BL1500	Sartorius, Göttingen, Germany
Lightcycler 480 system	Roche, Mannheim, Germany
Magnetic stirrer MH15	Roth, Karlsruhe, Germany
Microscope Axiovert 25	Zeiss, Oberkochen, Germany
Multivortexer DVX-2500	VWR, Darmstadt, Germany
Nanodrop 2000	Thermo Fisher Scientific, Schwerte, Germany
Neubauer chamber	Paul Marienfeld, Lauda-Königshofen, Germany

Odyssey infrared scanner	Licor, Lincoln, NE, USA
Optima Max-E ultracentrifuge	Beckman Coulter, Brea, CA, USA
Oxygraph-2k	Oroboros Instruments, Innsbruck, Austria
Parr nitrogen bomb	Parr Instrument Co., Moline, IL
PerfectBlue double-gelsystem twin ExW S	VWR Peqlab Biotechnologie GmbH, Erlangen, Germany
Power supply Consort E 802	Consort nv, Turnhout, Belgium
Precision scale ALJI60-4NM	Gottl. Kern & Sohn, Balingen, Germany
Rotational vacuum concentrator 2-33 IR	Christ, Osterode am Harz, Germany
Rotator RS-RD20	Phoenix Instruments GmbH, Garbsen, Germany
Scepter 2.0 handheld automated cell counter	Merck Millipore, Darmstadt, Deutschland
Seahorse XF96	Agilent, Santa Clara, CA ,USA
Semi dry blotting chamber	Hölzel, Wörth, Germany
Shaker incubator	Edmund Bühler, Hechingen, Germany
Sharp angular forceps 11252-20 Inox	Fine Science Tools, Heidelberg for Dumont Switzerland
Table shaker	Hecht Assistent, Sondheim, Germany;
Teflon- glass douncer 15 ml	Sartorius, Göttingen, Germany
Thermocycler Mastercycler 5330	Eppendorf, Hamburg, Germany
ThermoMixer C	Eppendorf, Hamburg, Germany
Thermoshaker Thermostat plus	Eppendorf, Hamburg, Germany
Tissue Lyser	Qiagen, Hilden, Germany
Vortex Genie 2	Scientific industries, USA
Water bath	Memmert, Schwabach, Germany

3.1.12 Software

DatLab 6	OROBOROS INSTRUMENTS, Innsbruck, Austria
Endnote X7	Clarivate Analytics, Philadelphia, PA, USA
GrapPad Prism 7	Graphpad Software, La Jolla, CA, USA
ImageLab 5.2.1	Bio-Rad, Hercules, CA, USA

Imagestudio Lite Ver5.2	Licor, Lincoln, NE, USA
JMP 11	SAS Institute, Cary, NC, USA
Lightcycler 480 software V1.5.0.39	Roche, Mannheim, Germany
MultiExperiment Viewer software	J. Craig Venter Institute, La Jolla, CA, Rockville, MD, USA
Seahorse Wave 2.3	Agilent, Santa Clara, CA , USA
Seahorse XF96	Agilent, Santa Clara, CA ,USA
SIMCA-P 11.5	Umetrics, Umeå, Sweden
Some pictures derived from	Servier Medical Art

3.1.13 Primers

3.1.13.1 Primers for real time PCR

Primer (product code)	Manufacturer
Crls1 (Cardiolipin Synthase 1; QT00171878)	Qiagen, Hilden, Germany
Lclat (Lysocardiolipin Acyltransferase; QT01064336)	Qiagen, Hilden, Germany
Tbp (Tata Box Binding Protein; QT00198443)	Qiagen, Hilden, Germany
SCD1 (Stearoyl-CoA desaturase; QT00291151)	Qiagen, Hilden, Germany
Taz (Tafazzin; FW: TTTTAGGATCCCCCAGAGATGA, Rev: TGCACAACAAGGAAGTGCTGTA)	designed by C. Hoffmann*

3.1.14 Antibodies

3.1.14.1 Primary antibodies

Antibody (product code)	Dilution	Manufacturer
Akt/PKB (610860)	1:1000	BD Transduction laboratories, Erembodegem, Belgium
phospho Akt/PKB T-308 (9275S)	1:1000	Cell Signaling Technology, Frankfurt, Germany
phospho Akt/PKB S-473 (9271L)	1:1000	Cell Signaling Technology, Frankfurt, Germany
β–actin (4970)	1:1000	Cell Signaling Technology, Frankfurt, Germany
ATP5A (ab110273)	1:1000	Abcam, Cambridge, UK
Calnexin (H-70) (sc11397)	1:1000	Santa Cruz Biotechnology, Santa Cruz, CA, USA

* A member of our group

Citrat Synthase (ab96600)	1:1000	Abcam, Cambridge, UK
COX 4 (4844S)	1:5000	Cell Signaling Technology, Frankfurt, Germany
GAPDH (8245)	1:20000	Abcam, Cambridge, UK
GFAT	1:3000	Selfmade (Nerlich et al. (1998)[217])
Giantin (ab24586)	1:5000	Abcam, Cambridge, UK
GRP78/BiP	1:5000	Santa Cruz Biotechnology, Santa Cruz, CA, USA
HADHA (ab54477)	1:500	Abcam, Cambridge, UK
Histone H3 (ab1220)	1:1000	Abcam, Cambridge, UK
Anti-4 Hydroxynonenal (ab46545)	1:1000	Abcam, Cambridge, UK
Lamin B (sc-6216)	1:1000	Santa Cruz Biotechnology, Santa Cruz, CA, USA
LAMP-1 (sc-17768)	1:1000	Santa Cruz Biotechnology, Santa Cruz, CA, USA
MCAD (E-5) (sc-365448)	1:400	Santa Cruz Biotechnology, Santa Cruz, CA, USA
Mitochondria Fraction Western Blot Cocktail (ab139416)	1:250	Abcam, Cambridge, UK
Monoclonal anti-Myosin, MHC-fast, Clone MY-32 (M4276)	1:1000	Sigma-Aldrich, St. Louis, MO, USA
Total OXPHOS Rodent WB Antibody Cocktail (ab110413)	1:1000	Abcam, Cambridge, UK
PDH phospho (pSer232, AP1063))	1:3000	Calbiochem, Merck, Darmstadt, Germany
PDH phospho (pSer293, ab92696)	1:400	Abcam, Cambridge, UK
PDH phospho (pSer300, AP1064)	1:1000	Merck, Darmstadt, Germany
PDH-E1α (sc377092)	1:250	Santa Cruz Biotechnology, Santa Cruz, CA, USA
PEX3.1	1:10000	Kind gift of Prof. Dodt
PLIN2/ADRP/Adipophilin/ADFP (GP40)	1:2000	Progen Biotechnik, Heidelberg, Germany
PLIN5/OXPAT/MLDP/PAT-1(GP31)	1:500	Progen Biotechnik, Heidelberg, Germany
Pyruvate carboxylase (SAB2500845)	1:2000	Sigma-Aldrich, St. Louis, MO, USA
SCD1 (E-15, sc-14720)	1:1000	Santa Cruz Biotechnology, Santa Cruz, CA, USA
SCD1 (S-15, sc-14719)	1:1000	Santa Cruz Biotechnology, Santa Cruz, CA, USA
VDAC (N-18, sc-8828)	1:1000	Santa Cruz Biotechnology, Santa Cruz, CA, USA

3.1.14.2 Secondary antibodies

Antibody (product code)	Dilution	Manufacturer
Goat anti mouse IgG-HRP	1:3000 to 1:10000	Santa Cruz Biotechnology, Santa Cruz, CA, USA
Goat anti rabbit IgG-HRP	1:3000 to 1:10000	Santa Cruz Biotechnology, Santa Cruz, CA, USA
Goat anti guinea-pig IgG-HRP	1:1000	Santa Cruz Biotechnology, Santa Cruz, CA,

		USA
IRDye Infrared Dye donkey anti-guinea pig 800CW (926-32411)	1:10000	Licor, Lincoln, NE, USA
IRDye Infrared Dye donkey anti-rabbit 680LT (926-68023)	1:10000	Licor, Lincoln, NE, USA
IRDye Infrared Dye donkey anti-goat 800CW (926-32214)	1:10000	Licor, Lincoln, NE, USA
IRDye Infrared Dye donkey anti-mouse 680LT (926-68022)	1:10000	Licor, Lincoln, NE, USA
IRDye Infrared Dye goat anti-mouse 680RD (68070)	1:10000	Licor, Lincoln, NE, USA
IRDye Infrared Dye goat anti-rabbit 800CW (32211)	1:10000	Licor, Lincoln, NE, USA
IRDye Infrared Dye donkey anti-mouse 800CW (926-32212)	1:10000	Licor, Lincoln, NE, USA
IRDye Infrared Dye donkey anti-rabbit 800LT (925-32213)	1:10000	Licor, Lincoln, NE, USA
IRDye Infrared Dye donkey anti-goat 680CW (925-68074)	1:10000	Licor, Lincoln, NE, USA

3.2 Methods

3.2.1 Cell culture

3.2.1.1 Cultivation, passaging and seeding for experiments

All cells were cultured at 37 °C at 95% humidity and 5% CO_2. Every work step was performed under sterile conditions using a bench.

For passaging C2C12, HEPG2, and HEK cells were trypsinated (trypsin described in 3.1.5) for 5 min for HEKs and for up to 15 min for C2C12 and HEPG2 cells. Trypsin action was stopped adding one volume of growth medium. The cell suspension was centrifuged to remove the supernatant and the pellet was resuspended in 10 ml growth medium. Cell number was counted using a Scepter™ 2.0. HEKs and C2C12 were split every 2 to 3 days at a ratio of 1:5 to 1:10. HEPG2 were split at a ratio of 1:4 every 3 to 4 days.

Primary skeletal muscle cells were cultured from satellite cells of biopsies from the vastus lateralis muscle. First two passages of sub-cultured cells were used. Cells were grown until 80% confluence and fused for at least 5 and up to 9 days.

3.2.1.1.1 HEPG2 hepatoma cells

HEPG2 cells were grown in RPMI 1640 medium with 10% FBS, 1% penicillin/streptomycin and 1% glutamine. Cells were seeded at 4 x 10^6 in 15 cm cell culture plates, cultured for 3 days and mitochondria were isolated as described 3.2.6.2.

3.2.1.1.2 C2C12 mouse skeletal muscle cells

C2C12 were grown in high glucose DMEM medium (with 10% FBS, 1% penicillin/streptomycin and 1% glutamine). Cells were seeded at 1.5 x 10^6 in 15 cm cell culture plates, 1 x 10^5 per well in 6 well plates or 2500 per well in a Seahorse XF96 cell microplate and cultured for 2 days (see Figure 4). Then, growth medium was replaced by high glucose fusion medium, DMEM with 2% FBS, 1% penicillin/streptomycin and 1% glutamine, to induce differentiation. After 3 days insulin resistance was induced by chronic hyperinsulinemia (1 µM) in the absence or presence of high glucose conditions (25 mM vs. control 5.5 mM) for 48 h. During the stimulation, cells were additionally provided with low concentrations of palmitate and oleate (50 µM each). 15 cm dishes were used for mitochondrial isolation as described in 3.2.6.3. 6 well plates were harvested as described in 3.2.1.2 for western blotting (3.2.4) or as described in 3.2.12 for qPCR. To investigate insulin signalling, cells from six well plates were first starved for 3 h, stimulated acutely with 100 nM insulin for 15 min, lysed (3.2.1.2) and analysed by western blotting (3.2.4).

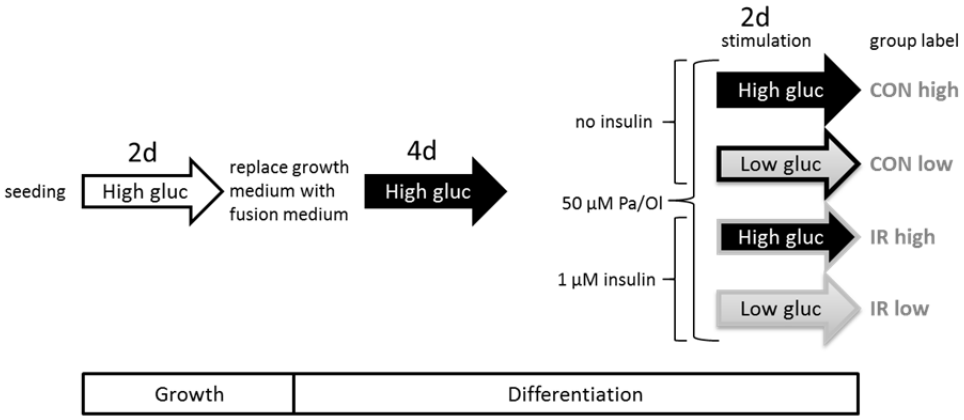

Figure 4: Treatment scheme of cultured C2C12 myotubes. Pa= palmitate, Ol= oleate, gluc= glucose, IR= insulin resistant, CON= control (no chronic insulin treatment), high= 25 mM glucose, low= 5.5 mM glucose, d= days

3.2.1.2 Cell lysis

For the preparation of cell lysates, plates were washed twice with PBS, lysed with 250 µl lysis Buffer 1/well of a 6 well plate or 750 µl per 15 cm plate and shaken on an orbital shaker for 30 min at 4 °C. The cells were scratched off and transferred into a reaction vessel. The lysate was centrifuged for 10 min at 13 000 g at 4 °C. Supernatant was transferred to a new cup and centrifugation was repeated. Supernatant was aliquoted and stored at -80 °C.

3.2.1.3 Cryopreservation of cell lines

Confluent cells from 15 cm dishes were trypsinated. After centrifuging the cell suspension the cell pellet was resuspended in 10 ml cryopreservation medium. Cell number was counted and the volume adjusted to a cell-line specific cell number per ml (e.g. 1x10^6 cells for C2C12). The suspension was immediately aliquoted into cryocups (1 ml aliquots) and frozen at -80 °C in a BioCision CoolCell FTS30

Cell Freezing Container to guarantee a controlled continuous decrease at a rate of -1 °C/min. After 24 h the cryocups were stored at -140 °C.

3.2.2 Animal studies

All animal experiments were conducted according to the National Institutes of Health Guide for the Care and Use of Laboratory Animals and the German law for the welfare of animals, and they were approved by local authorities (Regierungspraesidium Tuebingen, Baden-Wuerttemberg, Germany).

Unless not otherwise stated mice were C57/Bl6 mice.

3.2.2.1 Tissue lysis

Mouse liver and muscle were removed and directly placed in STE buffer (liver) or PBS (muscle) for mitochondrial experiments or directly in lysis Buffer 2 (RIPA). After weighing, tissue was homogenised in 1 ml lysis Buffer 2 (RIPA) using a TissueLyser (for 2 min at 20 Hz). For muscle tissue the homogenisation was repeated once. The lysate was centrifuged for 10 min at 13 000 g at 4 °C. Supernatant was transferred to a new cup and centrifugation was repeated. Supernatant was aliquoted and stored at -80 °C.

3.2.2.2 Liver tissue homogenisation for oxysterol extraction

Liver was removed and directly placed in either liquid nitrogen (“snap-frozen”) or in dichloromethane (DCM):methanol (MeOH) (1:1) ± BHT (5 µg/ml; stock solution 1 mg/ml in methanol) (“fresh”). DCM:MeOH (1:1) ± BHT (5 µg/ml) was also added to the frozen samples before extraction. After weighing, liver was homogenised using a TissueLyser (for 2 min at 20 Hz; Qiagen).

3.2.2.3 Mouse treadmill training and high-energy diet

3.2.2.3.1 Method establishment: diet and training effectiveness

The mouse handling was performed by Miriam Hoene[*]. Male C57/Bl6 mice, 10-weeks-old, randomly divided into four experimental groups based on bodyweight (see Table 2). Each group included four mice. Two groups were kept sedentary and two were trained on a treadmill five times a week for 30 min during 10 weeks. In the first week treadmill conditions were 9 m/min at 9° slope, which was increased in the second week to 12 m/min at 12° slope for nine more weeks. One of the two groups were either fed a control diet (D15072001) or a high-energy diet (D15072002), which were derived customised from Research Diets (New Brunswick, NJ, USA). Mice were weighed weekly. After 9 weeks mice were fasted overnight and metabolically characterised by an intraperitoneal glucose tolerance test. 2 g glucose solution (20%; B. Braun, Melsungen, Germany) per kilogram bodyweight was injected intraperitoneally. At baseline, blood glucose was measured after 15, 30, 60 and 120 min and a blood sample was drawn to measure insulin production. Last exercise training was performed at least 48 h

[*] a member of our group

before sacrificing the animals. After 10 weeks one mouse of every experimental group was processed per experimental day as described in the following: Mice were anaesthetised with ketamine-hydrochloride and xylazine, blood was taken by cardiac puncture and collected in EDTA tubes. Muscle subtypes (gastrocnemius, extensor digitorum longus (EDL), soleus, tibialis, plantaris) and pieces of liver were snap-frozen. Liver and pooled residual hind limb muscles were removed and mitochondria were purified by differential centrifugation following the protocol described in 3.2.6.4 for liver and 3.2.6.5 for muscle with a different enzymatic digestion. Skeletal muscle was digested using 7.2 U/g Collagenase D, 0.69 U/g Dispase II and 0.25 M $CaCO_2$ at 37 °C for 20 min with gentle shaking. DC mitochondria were used for respiratory analyses using a Seahorse XF96 (3.2.8.1.1) and were further purified as described in protocols 3.2.6.4/3.2.6.5 for lipidomics (3.2.10) and western blots (3.2.4).

Table 2: Experimental groups of the mouse experiment to investigate effects of high-energy diet and treadmill exercise

Experimental group	diet	exercise	abbreviation
1	Control diet	no	CON sed
2	Energy-rich diet	no	HED sed
3	Control diet	yes	CON run
4	Energy-rich diet	yes	HED run

3.2.2.3.2 Modified treadmill training and high-energy diet

The mouse handling was performed by Miriam Hoene as described in 3.2.2.3.1 with modifications. The experimental setup was repeated independently, leading to 8 mice per experimental group. The mice in the trained groups were trained for 6 weeks on a treadmill training three times a week for 1 h. The treadmill conditions were: in week 1 10 m/min at 12° slope, in week 2 11 m/min at 12° slope, in week 3 12 m/min at 12° slope, in week 4 12 m/min at 10° slope, in week 5 12 m/min at 9° slope and in the last week 12 m/min at 8° slope. The control diet (CON; 10 kJ% fat, 20 kJ% protein, 70 kJ% carbohydrates) and high-energy diet (HED; 45 kJ% fat, 20 kJ% protein, 35 kJ% carbohydrates) were derived from Ssniff (Soest, Germany). After 5 weeks mice were metabolically characterised as described in 3.2.2.3.1. Mice were killed on week 6. They were anaesthetised with ketamine-hydrochloride and xylazine and decapitated. Blood was collected in EDTA tubes. Muscle subtypes (gastrocnemius, extensor digitorum longus (EDL), soleus, tibialis, plantaris), pieces of liver, white adipose tissue (gonadal), heart and kidneys were snap-frozen. Liver and pooled residual hind limb muscles (pooled) were removed and mitochondria were purified by differential centrifugation (see protocols 3.2.6.4 and 3.2.6.5) for high-resolution respirometry (HRR, 3.2.8.2.2) and citrate synthase activity assay (3.2.7). DC mitochondria were further purified as described in protocol 3.2.6.4/3.2.6.5 for lipidomics (3.2.10), western blot (3.2.4) and SOD assays (3.2.11).

3.2.2.4 Oxidative stress induction in mice by doxorubicin treatment

Experiments were performed on 3-month-old wild-type 129 S1/SvImJ mice purchased from Jax Mice, USA. Mice were kept on a 12:12-h light-dark cycle and fed a standard diet (Ssniff, Soest, Germany) with tap water ad libitum. Oxidative stress was induced by a single intravenous injection of doxorubicin (14.5 µg/g body weight, Cell Pharm, Bad Vilbel, Germany) as described in Bohnert et al. (2015)[218] and Artunc et al. (2008)[219]. Control mice received NaCl 0.9% as vehicle. On day 8 after injection mice were euthanized by cervical dislocation under isoflurane anaesthesia. Mice handling was performed by Bernhard N Bohnert.[*] Liver was taken after median laparotomy.

3.2.3 Assays for determination of protein concentration

3.2.3.1 Bradford assay

For the determination of protein concentration, mitochondrial suspensions were diluted 1:10 to 1:200 in Bradford reagent. Absorbance was measured at 590 nm using a microplate reader and sample concentration was assessed using a BSA standard.

3.2.3.2 Bicinchoninic acid (BCA) assay

For the determination of protein concentration and further downstream analyses, sample pellets were resuspended in a small volume of PBS. Mitochondrial suspensions (prediluted 1:10 and 1:100 in PBS with 1% Triton-X-100) were diluted 1:200 in BCA protein assay reagent mix (Pierce™ BCA Protein Assay Kit, Rockford, USA). Absorbance was measured at 562 nm using a microplate reader and sample concentration was assessed using a BSA standard.

3.2.3.3 CyQUANT cell proliferation assay kit for in-plate protein determination

In-plate protein assay was used to determine protein concentration for C2C12 myotubes cultured and analysed on Seahorse XF96 cell microplates (96 well) as described in 3.2.8.1.2. CyQUANT is a fluorescent dye exhibiting enhanced fluorescence upon binding cellular nucleic acids. C2C12 myotubes were washed with PBS and frozen at -20 °C and further processed within 4 weeks. After thawing, 200 µl CyQUANT GR dye/cell-lysis buffer (CyQUANT GR 400 x diluted with 1 x cell lysis buffer) per well were added. A standard curve from bacteriophage-λ-DNA was used for quantification (0 to 1000 ng/ml final DNA concentrations). Fluorescence was measured with filters for excitation at 485 nm and emission at 535 nm.

3.2.4 SDS-PAGE

3.2.4.1 Western blotting

30 µg of protein from total lysate (3.2.1.2/3.2.2.1) or isolated mitochondrial fraction were separated by SDS-PAGE (12.5% or 5–12.5% gradient). The fixed volume of 8 µl mitochondrial suspension was

[*] Department of Internal Medicine 4, University Hospital Tuebingen, Tuebingen, Germany

used for blots performed in context with oxysterol analyses. 2,2,2-Trichloroethanol (TCE) was incorporated into the gels before polymerisation to visualise total protein amount via fluorescence on polyvinylidene difluoride (PVDF) membranes as described by Ladner et al. (2004)[220] for gels. Proteins were transferred to PVDF membranes (when secondary antibodies were fluorescent) or to nitrocellulose membrane (when secondary antibodies were conjugated to horseradish peroxidase (HRP)) by semi-dry electroblotting. PVDF membranes were then scanned for total protein quantification using a ChemiDoc Touch Imaging System (Bio-Rad, Hercules, CA, USA). Total protein was quantified densitometrically using the ImageLab Software (Bio-Rad, Hercules, CA, USA). Ponceau S solution was used to control protein transfer efficiency on nitrocellulose membranes. Membranes were blocked with NET-G buffer and incubated with the first antibody overnight at 4 °C or 2 h at room temperature. Membranes were washed with NET-G buffer.

3.2.4.2 Immunodetection

After incubation with the respective primary antibodies, bands were visualised with the appropriate secondary infrared antibodies (PVDF) and band intensity was measured using an Odyssey Infrared Imaging System (LI-COR, Lincoln, NE, USA). Nitrocellulose membranes were incubated with horseradish peroxidase-conjugated antibodies for 1 h at room temperature. Visualisation of immunocomplexes was performed by enhanced chemiluminescence as described previously[221] using a ChemiDoc Touch Imaging System (Bio-Rad, Hercules, CA, USA).

3.2.4.3 Stripping of membranes

Nitrocellulose membranes were incubated in stripping buffer at 56 °C (water bath) for 30 min and blocked afterwards with 1 x NET-G.

3.2.5 Oxidative stress assay by immunoblotting

Protein modification by 4-hydroxynonenal (4-HNE) was determined by immunoblotting as described in Section 3.2.4. Higher quantities of 4-HNE are attributed to endogenous lipid peroxidation caused by oxidative stress [222].

3.2.6 Mitochondrial isolation

3.2.6.1 Optimisation of mitochondrial isolation

Different steps throughout the mitochondrial isolation procedure were systematically optimised to increase purity and yield of mitochondria. Protein yield was investigated using BCA or Bradford assay (see 3.2.3). Enrichment of mitochondria or contaminations were evaluated using immunoblots (3.2.4) with respective antibodies. Tested parameters for differential centrifugation (DC) and ultracentrifugation (UC) from hMT, HEK, HEPG2 and C2C12 cells are listed in Supplementary Table 1. Cell homogenisation was optimised testing different dounce stroke numbers, cell numbers, dounce step repeats and buffer volumes in the douncer. In addition, an alternative homogenisation device, a Parr Nitrogen

bomb, was tested. Different pressures, buffer volumes and times under pressure were investigated in terms of cell disruption, mitochondrial integrity and feasibility for higher sample number throughput. Centrifugation conditions were varied for highest purity of mitochondria. For muscle cells, longer differentiation time effects on mitochondrial yield were tested additionally. Different muscle biopsy donors were compared as well. For further purification of the crude mitochondrial pellet after DC, mitochondria were layered on different density gradients using different conditions including a digestion with trypsin to remove contaminations. Tested parameters for magnetic bead-assisted isolation (MACS) from cells are listed in Supplementary Table 2. Homogenisation of different numbers of cells before magnetic bead-assisted isolation was optimised by testing different dounce strokes, using syringes with different gauge sizes and strokes and also testing a Parr nitrogen bomb for homogenisation. For further purification of MACS-isolated mitochondria the method was combined with different centrifugation conditions, a gradient and filter techniques. Tested parameters for mitochondrial isolation from liver, muscle and brown adipose tissue (BAT) are listed in Supplementary Table 3. Tissue homogenisation was optimised testing different amounts of tissue either disrupted using a douncer with different stroke numbers or a Gentle MACS following the manufacturer's instructions. For further purification of the mitochondria DC was combined with different gradients. For muscle tissue an enzymatic digestion step before homogenisation was established by testing different enzymes and different digestion conditions.

3.2.6.2 Mitochondria isolation procedures for HEPG2 cells

For DC and UC (see Figure 5) six 15 cm plates (approximately 90% confluent) were washed twice with ice-cold PBS, scraped and pooled into ice-cold STE buffer (250 mM sucrose, 5 mM Tris, 2 mM EGTA, pH 7.4 at 4 °C) containing 0.5% BSA. Small aliquots of this suspension were removed, stored at -80 °C for total cell lysates and the remainder was used for mitochondria isolation. From now on, all steps were performed at 4 °C or on ice. Cells were collected by centrifugation at 500 g for 5 min, resuspended in 20 ml ice-cold STE + BSA, homogenised using a loose fitted 40 ml glass-glass dounce homogeniser (Wheaton, Millville, NJ, USA) by applying 15 strokes, and centrifuged at 1 000 g for 10 min. The supernatant was transferred into a new centrifuge tube by filtering through 250 µM gauze. The pellet, which possibly contained unbroken cells, was resuspended in 15 ml fresh STE + BSA, homogenised again with 15 strokes and centrifuged at 1 000 g for 10 min. This supernatant was also transferred into a centrifuge tube by filtering through 250 µM gauze. The supernatants were combined and centrifuged at 10 400 g for 10 min to pellet the crude mitochondrial fraction. The pellet was resuspended in STE and centrifuged again at 10 400 g for 10 min. The crude mitochondrial pellet was carefully resuspended in 100 µl STE and transferred into a 2 ml reaction vessel. After centrifugation at 16 000 g for 2 min, the supernatant was removed and the DC pellets were frozen at -80 °C or subjected to UC. For UC, the pellets were resuspended in 200 µl STE, layered on 5 ml percoll gradient (25%) and centrifuged for 20 min at 80 000 g. The lower of the two layers appearing was collected with a glass Pasteur pipette and transferred into a new centrifuge tube, filled up with STE and centrifuged 10 min at 10 000 g. The pellet was resuspended in a small volume of STE buffer. After centrifugation at 16 000 g for 2 min the supernatant was removed and the UC mitochondrial pellet was frozen at -

80 °C. For MACS, the mitochondrial isolation was performed following the manufacturer´s instructions with some adaptions (see Figure 5). Cells were detached by scraping. $1x10^7$ cells (1.5 approximately 90% confluent plates, 15 cm) were counted and used for one mitochondrial isolation. Cell lysis was performed as recommended in the manual and by the company's technical support using a 27G 3/4 needle and syringe (15 strokes). Prior to the magnetic separation step, the sample was filtered through 70 µM gauze to avoid clogging of the column. After elution of the mitochondrial fraction and centrifugation at 16 000 g for 2 min, the pellet was resuspended in 100 µl of STE. After another centrifugation step, the supernatant was removed again and the pellet was frozen and stored at -80 °C.

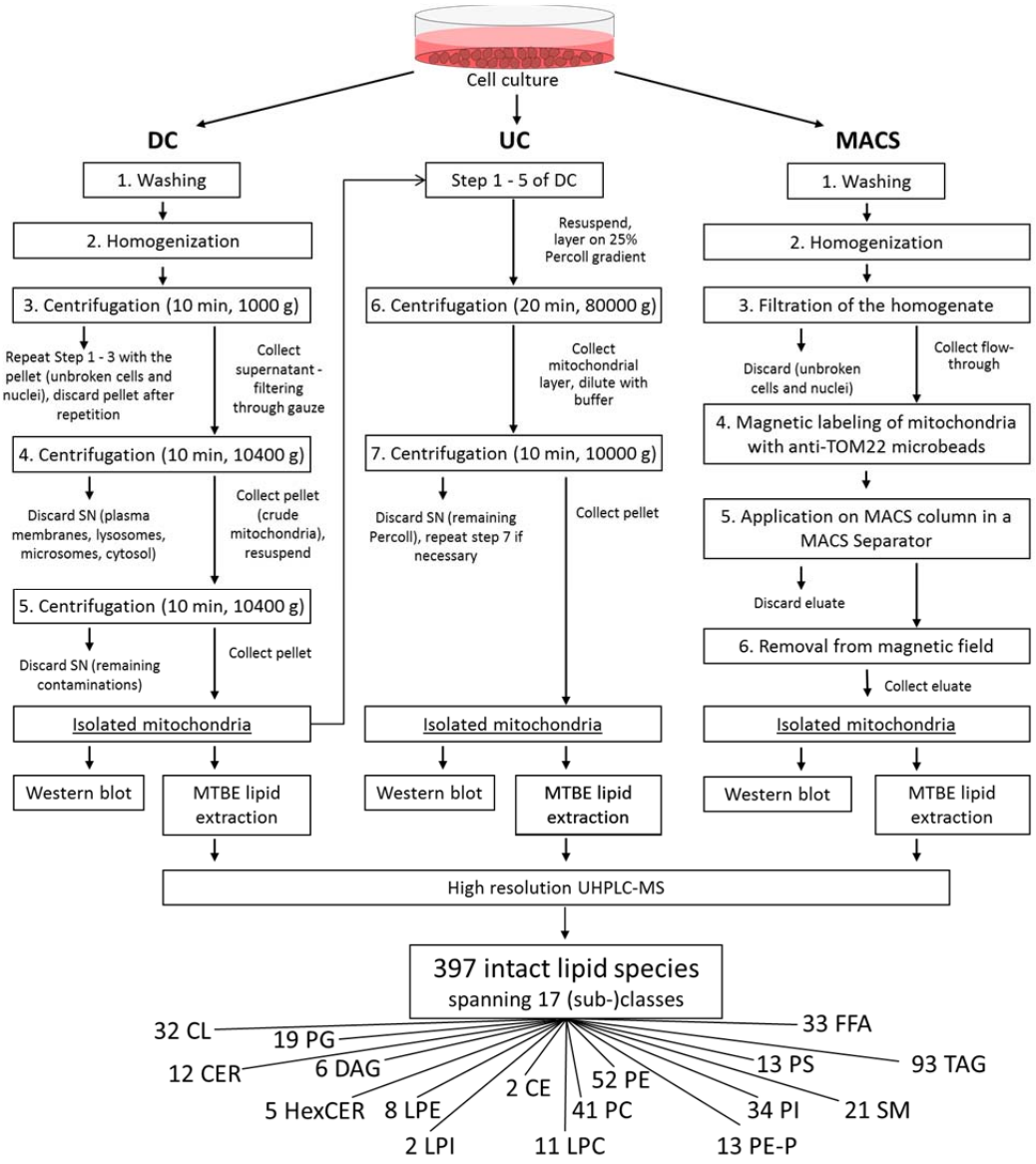

Figure 5: Experimental workflow from sample preparation to western blot and lipidomics analyses with subclasses of lipid species. Three mitochondria isolation methods, differential centrifugation (DC), ultracentrifugation (UC) and a magnetic bead-based method (MACS) were compared systematically; see Methods section for further details. SN, supernatant; MTBE= methyl tert-butyl ether; CE= cholesteryl ester; CER= ceramide; CL= cardiolipin; DAG= diacylglycerol; FFA= free fatty acids; HexCER= hexosyl-ceramide; LPC= lyso-phosphatidylcholine; LPE= lyso-phosphatidylethanolamine; LPI= lyso-phosphatidylinositol; PC= phosphatidylcholine; PE, phosphatidylethanolamine; PE-P, phosphatidylethanolamine plasmalogen; PG, phosphatidylglycerol; PI, phosphatidylinositol; PS= phosphatidylserine; SM= sphingomyelin; TAG= triacylglycerol.

3.2.6.3 Mitochondrial isolation protocol modified for C2C12 cells

Mitochondrial isolation of C2C12 cells was performed as described in 3.2.6.2 using UC with the following modifications: Cells were cultured and treated as described in Section 3.2.1.1. For UC five 15 cm plates (approximately 90% confluent) per group were washed once with ice-cold PBS, scraped and pooled into ice-cold STE buffer (250 mM sucrose, 5 mM Tris, 2 mM EGTA, pH 7.4 at 4 °C) containing only 0.1% BSA (Step 1, Figure 5). Cells were collected as described above, but were then homogenised using 20 strokes instead of 15 strokes (Step 2, Figure 5). The crude mitochondrial pellet was collected in 500 µl STE, layered on the percoll gradient and centrifuged for 30 min at 80 000 g (Step 6, Figure 5). After the collected layer was pelleted in STE, mitochondria were directly resuspended in PBS. If the pellet was still loose, caused by too high percoll remnants, the pellet was resuspended with PBS and centrifugation was repeated. The resuspended pellet was transferred to a 2 ml reaction vessel, centrifuged at 10 000 g for 10 min and resuspended again in a small volume of PBS (50 µl).

3.2.6.4 Mitochondrial isolation from mouse liver

Mitochondria isolation was performed as described (3.2.6.2) and previously published[130] with some modifications for liver tissue. 150 mg liver were directly placed into ice-cold STE buffer (250 mM sucrose, 5 mM Tris, 2 mM EGTA, 0.5% BSA, pH 7.4 at 4 °C). Throughout the whole protocol, all steps were performed at 4 °C or on ice. Tissue was cut into small pieces with a scissor, homogenised using a loosely fitted 2 ml glass-glass douncer (Sartorius, Goettingen, Germany) by applying 6 strokes, transferred to a 50 ml tube, filled up with STE + 0.5% BSA and centrifuged at 900 g for 10 min. The supernatant was transferred into a new centrifuge tube and centrifugation was repeated. The supernatant was then centrifuged at 9 000 g for 10 min to pellet the crude mitochondrial fraction. The pellet was resuspended in STE+ 0.1% BSA and centrifuged again at 9 000 g for 10 min. The crude mitochondrial pellet was carefully resuspended in 200 µl STE. An aliquot was used for respiration analyses (described 3.2.7) and protein determination by Bradford assay (3.2.3.1). The remaining sample was layered on 5 ml percoll gradient (25%) and centrifuged for 20 min at 80 000 g (accel/decel 5). The lower of the two appearing layers was collected with a Pasteur pipette and transferred to a new centrifuge tube, filled up with STE without BSA and centrifuged 10 min at 9 000 g. The pellet was resuspended in a small volume of STE buffer without BSA. After centrifugation at 16 000 g for 2 min the supernatant was removed, the pellet was resuspended in PBS and protein concentration was determined using BCA assay (described 3.2.3.2). Aliquots were frozen at -80 °C.

3.2.6.4.1 Liver mitochondria isolation for oxysterol analyses

Liver mitochondria isolation was performed as described in 3.2.6.4 with some additions. 150 mg liver were directly placed in ice-cold STE buffer either with or without BHT (5 µg/ml, stock solution 1 mg/ml in ethanol). This BHT concentration was used throughout the experiment. The crude mitochondrial pellet was resuspended in STE ± BHT and the percoll gradient was either with or without BHT. All buffers throughout the next steps were either with or without BHT. Aliquots with 50 µg mitochondria (by protein) were either used directly (“fresh”) for oxysterol extraction (3.2.10.4) or frozen at -80 °C (“frozen”) and extracted after thawing.

3.2.6.5 Mitochondria isolation from mouse skeletal muscle

Mitochondria isolation was performed as described for liver (3.2.6.4) with some modifications for skeletal muscle. 550 mg skeletal muscle tissue (pooled from remaining hind limb muscles after gastrocnemius, extensor digitorum longus (EDL), soleus, tibialis, plantaris were dissected and snap-frozen) were directly transferred into ice-cold PBS. Tissue was cut into small pieces with a scissor and further sheared using a razor blade (Herkenrath, Solingen, Germany). Cut muscle was transferred in a 50 ml tube and was digested for 3 min at 4 °C with a protease type 8. 1 ml enzyme solution (6 mg Protease (10 U/mg) per ml STE) was added to 100 mg tissue. After 3 min 10 ml STE + 0.1% BSA were added for dilution and the sample was centrifuged for 30 s at 900 g at 4 °C. Supernatant was removed, the tube filled up with STE + 0.1% BSA and centrifuged again. This washing step was repeated 3 times in total. Muscle suspension was homogenised using a 15 ml teflon-glass douncer (Sartorius, Goettingen, Germany) by applying six strokes. All following centrifugation steps and procedures were the same as already described for liver mitochondria after homogenisation (see 3.2.6.4).

3.2.6.6 Comparison of murine liver and muscle mitochondria

Using non-targeted UHPLC-MS lipidomics (see 3.2.10.3) and western blot analyses (3.2.4), we compared the lipid profiles of muscle and liver mitochondria from mice purified by ultracentrifugation (as described 3.2.6.4 and 3.2.6.5). Respiration of isolated mitochondria was measured after differential centrifugation in an Oxygraph-2k (3.2.8.2.2).

3.2.7 Citrate synthase activity assay

Citrate synthase (CS) activity was measured as quantitative marker for mitochondrial content in tissue and cells.[223] Citrate synthase is located in the mitochondrial matrix and therefore a common marker.[139,224] Briefly, the assay involves the following steps: CS irreversibly converts Elman's reagent (DTNB; 5,5'-dithiobis-(2-nitrobenzoic acid)) to 2-nitro-5-thiobenzoate (TNB), whose absorbance can be measured at 412 nm. Citrate synthase activity assay was established by Daniel Bleher in context of his bachelor´s thesis under supervision of Dr. Hoene and me. The citrate synthase activity assay was adjusted from Eigentler et al. (2015)[225] The assay was performed at room temperature in a 96 well plate in 200 µl total volume instead of a 1 ml cuvette. 15 µg protein lysate from tissue (3.2.2.1) or cells (3.2.1.2) were regarded ideal to achieve a linear calibration curve upon the reaction over the whole measurement duration. Protein concentration of the lysates (thawed and stored on ice) was determined using BCA (3.2.3.2), and adjusted to 1.5 mg/ml with ultra-pure water. A master mix was prepared consisting of Triton-X-100, Acetyl-CoA, DTNB and ultra-pure H_2O (Table 3). 15 µl oxaloacetate was added shortly before the measurement. A negative control (10 µl of H_2O_{dest}) and two positive controls (10 µl of 1:1 000 and 1:500 diluted citrate synthase) were performed in quadruplicates. Absorbance was measured in 10 s intervals for 3 min in a spectrophotometer (Microplate Reader from BIO-RAD, Model 680). Solutions in the plate were mixed for 4 s between measurements. Specific citrate synthase activity was calculated as described by Eigentler et al. (2015)[225]

Table 3 Components, added volumes per well and final concentration in the master mix for citrate synthase assay

Component	Vol. added [µl]	Final concentration
10% Triton-X-100	5	0.25%
Acetyl CoA	5	0.31 mM
1.01 mM DTNB	20	0.1 mM
Ultra-pure H2O	145 -Vsample	
Vsample	10 (1.5 mg/ml)	0.075 mg/ml
Oxaloacetate	15	0.5 mM

3.2.8 Respiration analyses

Mitochondrial respiration was analysed in isolated mitochondria, intact cells, digitonised cells, tissue homogenates or permeabilised muscle fibres.

Malate and octanoylcarnitine (Oxygraph 2k) or palmitoylcarnitine (Seahorse XF96) were injected to induce fatty acid oxidation (FAO). LEAK respiration is the oxygen consumption under non-phosphorylating conditions due to the proton leak. In Seahorse XF96 LEAK state is determined after ATP Synthase (C5/CV) inhibition using oligomycin, but since the Oxygraph-2k chambers showed carry-over effects of oligomycin between the measurements, LEAK was determined as state of no externally added ADP. ADP was added to induce oxidative phosphorylation ($_P$, OXPHOS). Pyruvate and glutamate were used as complex 1-associated substrates (C1/CI) and succinate as mainly complex 2-linked substrate (C2/CII). FCCP, a synthetic uncoupler, was titrated to uncouple the electron transport chain activity from ATP production and determine the maximal oxidative capacity of the electron transport chain ($_E$). Complex 1 was inhibited by rotenone to solely investigate complex 2-associated respiration. The non-mitochondrial background respiration or residual oxygen consumption (ROX) were determined by addition of antimycin A to inhibit the cytochrome c reductase (C3/CIII).

3.2.8.1 Seahorse XF96

The Seahorse XF96 Analyzer was used to analyse oxygen consumption of intact cells or isolated mitochondria in a 96-well plate format using probes with fluorescent sensors coupled to optical fibers.

3.2.8.1.1 Application to isolated mitochondria

Sensor cartridges were hydrated overnight in a Seahorse XF Calibrant solution 37 °C incubator (non-CO_2). Every subsequent step was performed on ice or at 4 °C. After protein determination by Bradford assay (3.2.3.1), isolated crude C2C12 mitochondria (protocol see 3.2.6.3), crude murine liver and muscle mitochondria (see protocols in Sections 3.2.6.4 and 3.2.6.5) suspensions were adjusted to the same protein concentration using STE buffer + BSA (2-5 mg/ml). This predilution was further adjusted to a final concentration of 3 µg/20 µl for liver and muscle mitochondria and to 5 µg/20 µl for C2C12 mitochondria using MAS buffer. 20 µl mitochondrial suspension were loaded per well (96 well Seahorse XF Cell Culture Microplate). Mitochondria were attached to the well bottom by centrifugation

at 2 000 g for 20 min at 4 °C. Compounds for ports (ADP, oligomycin, FCCP, antimycin A/rotenone) were prepared at a concentration 10 times higher than for the experiment and further diluted by serial automatic injection of the compounds into the wells. MAS buffer with either succinate and rotenone, pyruvate and malate or palmitoylcarnitine and malate as substrates was prepared (concentrations see 3.1.2.2). pH was checked for all buffers and compounds solutions. Since compound concentrations were kept constant, the loading volume per port of a hydrated sensor cartridge was adjusted. Compounds were loaded in following volumes**:** Port A 20 µl (ADP), Port B 22 µl (oligomycin), Port C 24 µl (FCCP), Port D 26 µl (antimycin A/rotenone). The sensor cartridge was first calibrated in the instrument. After the centrifugation, 160 µl MAS with substrates were added carefully to each well and the plate inserted into the Seahorse XF 96. First step was a 10 min waiting time to allow thermal equilibration of buffers and plates to 37 °C. Then, a programmed protocol was run by the system: injection Port A, mixing, measuring, injection Port B, mixing, measuring, injection Port C, mixing, measuring, injection Port D, mixing, measuring. Data were finally exported to an excel sheet.

Table 4: Substrates, inhibitors and uncouplers used in Seahorse XF96 analyses of isolated mitochondria; Ama= antimycin A, FCCP= carbonyl cyanide-p-trifluoromethoxyphenylhydrazone, ADP= adenosine diphosphate

Substrate	**Stock concentration [mM]**	**Final concentration [mM]**
Succinate	500	8
Rotenone	2	0.002
ADP	1000	6
Oligomycin	2.5	0.0025
FCCP	2.5	0.005
Ama	2.5	0.004
Pyruvate	1000	5
Malate	1000	5
Palmitoylcarnitine	50	0.04

3.2.8.1.2 Measurement of adherent cells (C2C12)

Ideal cell number was titrated aiming at 90% confluence. Assay medium was prepared by supplementing DMEM (Gibco, life technologies, Carlsbad, CA, USA) with glucose solution (Gibco, life technologies, Carlsbad, CA, USA) to a final concentration of 5.5 mM and 22 mM. Medium was warmed to 37 °C and pH adjusted with NaOH. Compounds were prepared as described above, but port loading varied: 20 µl Port A (oligomycin), 22 µl Port B (FCCP), 24 µl Port C (antimycin A/rotenone). Fusion medium was replaced by assay medium from cell plate in three steps using a multichannel pipette. Plate was incubated at 37 °C for one hour prior to measurements. For normalisation, the protein concentration per well was determined with the CyQUANT® Cell Proliferation Assay Kit (Molecular probes, Eugene, Oregon, USA) as described in 3.2.3.3.

3.2.8.2 O2k high-resolution respirometry (Oroboros)

An O2k-Oxygraph (Oroboros Instruments, Innsbruck, Austria) was used to analyse oxygen consumption in permeabilised muscle fibres, cells, tissue homogenates and isolated mitochondria. The instrument consists of two polarographic oxygen sensors (Clark type) in closed peltier-temperature controlled measuring chambers. Substrate-uncoupler-inhibitor titration (SUIT) protocols were performed to characterise mitochondrial pathways as shown in Table 5. After sample processing e.g. mitochondrial isolation cytochrome c was added during the SUIT protocol to determine intactness of the mitochondrial outer membrane and thereby ensure that no endogenous cytochrome c was released.

Table 5: Respiratory states induced in Oxygraph-2k analyses, Oct= octanoylcarnitine, M= malate, P= pyruvate, S= succinate, Rot= rotenone, Ama= antimycin A, CI= complex 1, CII= complex 2, FAO= fatty acid oxidation, OXPHOS= oxidative phosphorylation, ROX= residual oxygen consumption, subscript $_P$= phosphorylating condition after ADP addition, subscript $_E$= uncoupled condition after FCCP titration

injections	**states of respiration**	**state label**
OctM	LEAK	FAO
OctMP	OXPHOS	FAOP
PMOctP	OXPHOS	CI+FAOP
PMSOctP	OXPHOS	CI+CII+FAOP
PMSOctcP	OXPHOS	CI+CII+FAOC
PMSOctcE	Maximal electron transport chain capacity	CI+CII+FAOE
S(Rot)E	Maximal electron transport chain capacity	CIIE
AmaROX	Residual oxygen consumption	ROX

3.2.8.2.1 Respiratory measurements of permeabilised C2C12 cells

Cells were washed with PBS and then either trypsinated or scratched off, pelleted and resuspended in 10 ml fusion medium. 700 µl or approximately 400 000 cells were transferred to a 2 ml reaction vessel, pelleted by centrifugation (3 000 g, 4 min, RT). Afterwards, the supernatant was removed. Pellet was resuspended in 100 µl Mir05 by pipetting three times up and down. The suspension was injected into the Oxygraph-O2k. The applied SUIT protocol is shown in Table 6. Digitonin was titrated to permeabilise the cell membrane.

Table 6: Concentrations and injection sequence of the SUIT protocol (substrate, uncouplers, inhibitors) applied on C2C12 cells; Ama= antimycin A, FCCP= carbonyl cyanide-p-trifluoromethoxyphenylhydrazone, ADP= adenosine diphosphate, TMPD= N,N,N',N'-tetramethyl-p-phenylenediamine

Substrate	Stock conc. [mM]	Injected volume [µl]	Final concentration in Oxygraph-2k [mM]
Pyruvate	1 000	10	5
Malate	1 000	4	2
Digitonin	8.1	1	4.05
ADP	500	10	2.5
Glutamate	500	10	2.5
Succinate	500	10	2.5
Cytochrome c	4	5	0.01
FCCP	2.5	0.4	0.0005
Rotenone	2.5	1	0.00375
Ama	2.5	4	0.005
Ascorbate	800	5	2
TMPD	200	5	0.5
Sodium azide	4 000	100	200

3.2.8.2.2 Respiratory measurements of murine tissue homogenates and isolated mitochondria

Tissue was homogenated as described for mitochondrial isolation using DC (3.2.6). 10 µl of the homogenate were injected in the Oxygraph-2k. Protein concentrations of the homogenates were between 25 and 35 mg/ml. Therefore, protein concentrations of 125-175 µg/ml were analysed. Protein concentration was determined afterwards using a BCA assay (3.2.3.2). Respiration was normalised to protein amount. Mitochondria were isolated as described in 3.2.6. After DC mitochondrial protein concentration was determined using a Bradford assay (3.2.3.1). Protein concentration was adjusted to 2 mg/ml with STE+BSA, and 50 µl were injected in the Oxygraph-2k. The applied SUIT protocol is shown in Table 7.

Table 7: Concentrations and injection sequence of the SUIT protocol (substrate, uncouplers, inhibitors) applied on mouse tissue homogenates and isolated tissue mitochondria; Ama= antimycin A, FCCP= carbonyl cyanide-p-trifluoromethoxyphenylhydrazone, ADP= adenosine diphosphate

Substrate	**Stock conc. [mM]**	**Injected volume [µl]**	**Final concentration in Oxygraph-2k [mM]**
Malate	800	3,2	1.28
Octanoylcarnitine	100	10	0.5
ADP	500	10	2.5
Pyruvate	1 000	10	5
Succinate	1 000	10	5
Cytochrome c	4	5	0.01
FCCP	1	1 stepwise	0.0005 steps
Rotenone	2.5	1	0.00125
Ama	5	2	0.005

3.2.8.2.3 Respiratory measurements of murine skinned muscle fibre

The protocol was adapted from Pesta et al. (2012)[226] by Daniel Bleher during his bachelor thesis. Soleus muscle and gastrocnemius muscle from 129 S1/SvImJ mice were placed into 2 ml biopsy preservation solution (BIOPS) immediately after dissection. Fibre separation was performed under a binocular microscope in a glass petri-dish on ice. Two pairs of very sharp forceps (Inox) were used to remove connective tissue, hair, fat and separate the fibre bundles from each other. After separation, the fibres were transferred into one well of a 6 well plate with 2 ml BIOPS. 20 µl saponin stock solution (Sigma, S4521, 20-35% sapogenin, 5 mg/ml in BIOPS) were added to the well. The final saponin concentration was 50 µg/ml. The fibres were gently shaken at 4 °C for 30 min. 2 ml of MiR05 were added to another well in the 6-well plate and all fibres were transferred from the saponin solution into MiR05, followed by gentle shaking for 10 min in the cold room. To determine the weight, the fibres were placed on a dry filter paper for 3-5 s and placed in a Mir05 filled reaction vessel lid on the balance. The chambers of the Oxygraph-2k (set to 37 °C) were prefilled with Mir05 and 5 µl of catalase stock solution (112 000 U/ml), stirrers were turned off while 4-5 mg fibres were placed into the chambers. After closing the chambers, 5 µl of H_2O_2 stock solution (200 mM) were added. Oxygen concentration was kept between 270 µM and 450 µM O_2 during the complete SUIT protocol by adding H_2O_2 to avoid hypoxia in non-perfused fibre bundles as recommended by Pesta et al. (2012)[226]

3.2.8.2.4 Modification of the respiratory analyses for human skinned muscle fibre

The murine Oxygraph-2k protocol (3.2.8.2.3) had to be modified for human muscle fibres (3.1.3.3), since the skinned human muscle fibres showed too high cytochrome c responses. Muscle biopsies were directly placed into Mir05 buffer instead of BIOPS. After separation of the fibres, the fibres were not placed directly in a Mir05 filled well of a 6 well plate, but in a 70 µm cell strainer (BD Falcon,

Franklin Lakes, NJ, USA), which allowed an easier transfer of the fibres from well to well for washing reducing the losses. Saponin stock was prepared using a less concentrated saponin powder (Sigma, S7900, sapogenin >10%). Final saponin concentration was 50 µg/ml. After skinning, the fibres were washed three times instead of only once and the measurement in the Oxygraph-2k was performed under normal air oxygen-pressure without the usage of catalase and H_2O_2.

For the comparison of murine samples and human samples (reported in 4.2.2.1.1) some of the high-resolution respirometry analyses of human muscle fibres were performed by Christoph Hoffman, a member of our group.

3.2.8.2.5 Respiratory analyses for human liver tissue

For measurements of human liver samples (3.1.3.3), 2 mg tissue were cut in small pieces with a scissor and directly placed into pre-warmed Mir05 buffer in the Oxygraph-2k chamber. Digitonin was injected (12 mM) at the beginning to permeabilise intact cells. SUIT protocol as described in Table 7 was performed.

3.2.8.2.6 Analyses to investigate BHT and doxorubicin effect on respiration

Mitochondrial function was investigated by respiration measurements in an Oxygraph-2k. Mitochondria were isolated with or without BHT as described in 3.2.6.4.1. 100 µg mitochondria (Figure 27) or a constant volume of the mitochondrial suspension (Figure 29) were placed in Mir05 buffer in the Oxygraph-2k chambers. 1.28 mM malate, 0.5 mM octanoylcarnitine (fatty acid oxidation, FAO), 2.5 mM ADP (phosphorylating condition, $_P$), 5 mM pyruvate (complex I respiration), 2.5 mM succinate (complex II respiration), FCCP in 0.5 µM steps (uncoupled state, $_E$), 1.25 µM rotenone (complex I inhibitor) and 5 µM antimycin A (complex III inhibitor) were subsequently added to evaluate electron transport chain capacity. Data were corrected for non-mitochondrial background by subtraction of the values obtained for antimycin A.

3.2.9 Kinetics of sterols

To investigate stability and conversion products of cholesterol and selected oxysterols 0.3 µg 4β-hydroxycholesterol, 7-ketocholesterol, 27-hydroxycholesterol and cholesterol were incubated separately in PBS in open tubes at the following conditions: a) for 24 h at room temperature without BHT or at 4 °C with and without BHT; b) for 5 h at 4 °C with and without BHT (duration of mitochondria isolation procedure); c) oxysterols and cholesterol were directly processed after being dissolved in PBS by applying the oxysterol extraction procedure. Oxysterol extraction was performed as described in 3.2.10.4.

3.2.10 Lipidomics

3.2.10.1 Liquid–liquid MTBE extraction

Lipids were extracted with methyl tert-butyl ether (MTBE) as described previously[227] with slight modifications, which were based on a published MTBE extraction method described for lipidomics by Matyash et al. (2008)[195] Briefly, water was added to 100 µg (by protein) of mitochondrial or total cell lysate to reach a total volume of 100 µl. After this, 350 µl of ice-cold methanol (MeOH) including internal standards were added. Samples were briefly vortexed, 1 ml of MTBE was added, and the samples were shaken for 30 min at room temperature. After adding 250 µl of water and incubating the sample at room temperature for 10 min, samples were centrifuged for 20 min at 1 000 g and 4 °C to induce phase separation. With the relative amounts of MTBE:methanol:H_2O (20:6:7) a 2:1 ratio of upper (non-polar) to lower (polar) phase was yielded.

3.2.10.2 Lipidomics analyses and data processing of HEPG2 mitochondria

PhD Jia Li* performed lipidomics analysis of HEPG2 mitochondria. Lipidomics profiling was performed using Ultra Performance Liquid Chromatography (UPLC)-Linear Trap Quadrupole (LTQ)-Orbitrap-mass spectrometry (MS) as previously described[228]. A Waters ACQUITY UPLC system equipped with a C8 ACQUITY column (100 mm x 2.1 mm x 1.7 µm) (Milford, MA, USA) was applied for lipid separation. The elution solvents were A (acetonitrile (ACN):H_2O = 60:40) and B (isopropyl alcohol (IPA):ACN = 90:10), both containing 10 mM ammonium acetate. The following gradient was programmed: 32% B for the first 1.5 min, followed by linear increase to 85% B during the next 14 min. The solvent B was further increased to 97% during the next 0.1 min and maintained for 2.4 min, and then the column was equilibrated at 32% for 2 min prior to the next injection. The column temperature was set to 55 °C and the flow rate was 0.26 ml/min. Lipidomics data were acquired both in the positive and negative modes of electrospray ionisation (ESI) at a mass resolution of 30 000 with scan ranges of 400–2 000 and 90–2 000, respectively. The positive mode was operated at a source voltage of 4 kV, capillary temperature of 300 °C and sheath gas and auxiliary gas flows of 25 arb and 5 arb. The respective parameter settings in the negative mode were 5 kV, 325 °C, 45 arb and 8 arb. Lipid identities were assigned based on accurate mass measurement, MS/MS fragmentation and elution behaviour. All detected lipids were quantified by normalisation to the corresponding internal standard (described in Section 3.1.7: d4-palmitic acid, ceramide CER(d18:1/17:0), LPC(19:0), PC(19:0/19:0), PE(15:0/15:0), SM(d18:1/12:0), TAG(15:0/15:0/15:0), CL(14:0(4)), CL(24:1(3)-14:1), CL(14:1(3)15:1), CL(15:0(3)-16:1) and CL(22:1(3)-14:1)). The lipid nomenclature follows the LIPID MAPS classification and nomenclature system.[229]

* was formerly from Dalian Institute of Chemical Physics, Chinese Academy of Sciences, Dalian, China, now at Chinese academy of Agriculture Science

3.2.10.3 Lipidomics analyses and data processing of liver and muscle mitochondria

PhD Chunxiu Hu and Xiaoli Hou* performed lipidomics analysis of murine liver and muscle mitochondria. Lipidomics profiling was performed in a Waters UPLC system coupled with a Q Exactive HF mass spectrometer (Thermo Fisher Scientific, Rockford, IL, U.S.A.) Separation of lipid metabolites was achieved in a Waters UPLC C8 ACQUITY column (100 mm x 2.1 mm × 1.7 µm) (Milford, MA, USA). The elution solvents consisted of A (ACN:H_2O = 60:40, v/v) and B (IPA:ACN = 90:10, v/v), both containing 10 mM ammonium acetate. The elution gradient started at 32% B for the initial 1.5 min, followed by a linear increase to 85% B during the next 14 min. Within the subsequent 0.1 min, solvent B was rapidly increased to 97%, and then maintained for 2.4 min for column flush. Subsequently, the elution solvent was returned to 32% B within 0.1 min and kept for 2 min for column equilibration. The column temperature was set to 55 °C and the flow rate was 0.26 ml/min. Lipidomics data were acquired in both ESI positive and negative modes at scan ranges of 400 –1300 Da and 200 – 1 800 Da, respectively. The spray voltage was 3.5 kV for positive mode and -3.0 kV for negative mode. The capillary temperature was maintained at 300 °C. The auxiliary gas heater temperature was set to 350 °C. The flow rate of sheath gas and auxiliary gas was 45 arbitrary units (arb) and 10 arb, respectively. The S-lens RF level was 50. The AGC target was set to be 3×10^6 ion capacity and maximum IT was 200 ms. Mass resolution was 120 000 and 30 000 for full scan MS and data-dependent MS/MS. Lipid identities were assigned based on accurate mass measurement, MS/MS fragmentation and LC elution behaviour. All detected lipids were quantified by normalisation to the corresponding internal standard. The lipid nomenclature follows the LIPID MAPS classification and nomenclature system.

3.2.10.4 Oxysterol extraction

Oxysterols were extracted based on a method described in [230] with slight modifications. 10 µl of BHT (1 mg/ml in methanol), 10 µl deuterated oxysterol standard mix (0.25 - 0.5 µg/ml in methanol) and 1.4 ml of 1:1 dichloromethane (DCM):MeOH solution were added to 20 mg homogenised liver tissue or 50 µg mitochondria (by protein) in a 2.0 ml reaction tube (Eppendorf, Hamburg, Germany; Tube 1). Hydrolysis was performed by adding 100 µl of 1 M KOH, the tube was vigorously vortexed for 60 s and incubated at 37 °C in the Eppendorf ThermoMixer C (1 000 rpm) for 1.5 h. After hydrolysis, the tube was centrifuged at 1 180 g for 5 min at 25 °C, the supernatant was transferred into a 5.0 ml reaction tube (Tube 2) and 1.4 ml of Dulbecco's phosphate-buffered saline (DPBS) was added. Tube 2 was vortexed for 60 s and centrifuged at 4 500 g for 10 min at 25 °C, the organic (lower) layer was transferred into a new 2.0 ml reaction tube (Tube 3) and dried under vacuum. 1.4 ml DCM were added to the pelleted material in Tube 1, vortexed for 10 min and then centrifuged at 4 500 g for 10 min at 25 °C. The supernatant (in Tube 1) was transferred to Tube 2. Tube 2 was vortexed for 60 s and centrifuged at 4 500 g for 15 min at 25 °C, the organic (lower) layer was also transferred into Tube 3 and dried under vacuum. The dried samples were covered with N_2 to protect them from oxidation for short storage, reconstituted with 50 µl of 90% methanol followed by a centrifugation step at 9 660 g for 10 min at 25 °C, the supernatant was subjected to UPLC–MS analysis.

* Dalian Institute of Chemical Physics, Chinese Academy of Sciences, Dalian, China

3.2.10.5 UPLC–MS/MS-based oxysterol analyses and data processing

Oxysterol analyses were performed by Ping Luo and Qingqing Wang*. Targeted oxysterol profiling was performed using UPLC-MS as described previously.[230] An ACQUITY ultra performance liquid chromatography system equipped with a Q-Trap 5500 mass spectrometer (AB SCIEX, Framingham, MA, USA) was used for oxysterol separation. A XBridge™ C18 column (150 mm x 2.1 mm x 3.5 µm; Waters, Milford, MA, USA) was used for the chromatographic separation. The elution solvents were A (H_2O:ACN) = 3:7 (v/v)) and B (IPA:ACN= 1:1 (v/v)), both containing 5 mM ammonium acetate (NH_4OAc). The initial elution started with 0% B, was then linearly increased to 100% B during the next 7 min and held for 4 min. Another 4 min were used to equilibrate the system with 0% B prior to the next injection. The injection volume was 10 µl. The column temperature was set to 20 °C and the flow rate was 0.3 ml/min. For the mass spectrometer, curtain gas, gas1 and gas2 were at 0.241, 0.276 and 0.276 MPa, respectively. The electrospray ion source temperature was set to 50 °C. The spray voltage was set to 5.5 kV. Data were acquired in the positive electrospray ionisation (ESI+) mode. Peak alignment of the detected oxysterols was conducted by the instrument vendor software of Analyst (Version 1.6, AB SCIEX, Framingham, MA, USA). Oxysterol identification was based on accurate mass measurement, MS/MS fragmentation and retention time,[230] or confirmation with authentic standards. The lipid nomenclature follows the LIPID MAPS classification and nomenclature system.[229] The detected oxysterols were quantified by normalisation to a corresponding internal standard (deuterated standards of 4β-hydroxycholesterol-d7, 7-ketocholesterol-d7, 27-hydroxycholesterol-d6, 25-hydroxycholesterol-d6, 7α-hydroxycholesterol-d7).

3.2.11 SOD activity assay

Superoxide dismutase (SOD) activity assays were performed using the colorimetric SOD assay kit from Sigma-Aldrich, St. Louis, MO, USA following the manufacturer´s instructions.

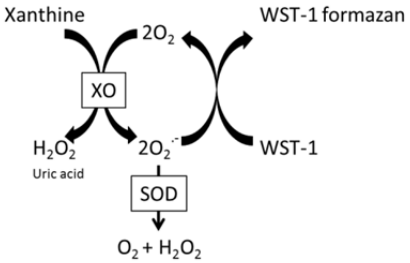

Figure 6: Principle of the SOD assay. WST-1= Dojindo´s tetrazolium salt, XO= xanthine oxidase, SOD= superoxide dismutase

Dojindo´s tetrazolium salt (WST-1; (2-(4-Iodophenyl)-3-(4-nitrophenyl)-5-(2,4-disulfophenyl)-2H-tetrazolium, monosodium salt) forms a formazan dye upon reduction with a superoxide anion. O_2 reduction rate is linearly dependent on the xanthine oxidase activity, which is inhibited by SOD. Since the detected absorbance is proportional to the $O_2^{\bullet-}$ amount, SOD activity is measured as the decrease

* Dalian Institute of Chemical Physics, Chinese Academy of Sciences, Dalian, China

in colour development (see Figure 6). Briefly, the protocol was: 20 µl (equivalent to 80 µg mitochondrial protein of C2C12, 40 µg for tissue mitochondria) sample SOD solution (standard dilution) or H_2O for Blanks 1 and 3 were added to a 96 well plate. 200 µl WST working solution were added. 20 µl of dilution buffer were added to Blanks 2 and 3. After quickly loading 20 µl enzyme solution to each sample and Blank 1, the plate was shaken and incubated at 37 °C for 20 min before detection at 450 nm in a microplate reader (BIO-RAD, Model 680, München, Germany).

3.2.12 Quantitative polymerase chain reaction (qPCR)

3.2.12.1 RNA extraction from cultured cells and liver tissue

RNA was extracted using the RNeasy Mini kit according to the manufacturer's instructions. Briefly, cells were lysed in 350 µl RLT- buffer plus 1% β-mercaptoethanol per well of a 6 well plate. Liver tissue was lysed in a TissueLyser (2 min, 20 Hz; Qiagen). After applying to QIAshredder spin columns samples were centrifuged for 2 min at 17 000 g at RT. The eluate was then mixed with 350 µl 70% ethanol and transferred to an RNeasy spin column placed in a 2 ml collection tube. Samples were centrifuged for 15 s at 17 000 g at RT. RNA was washed by adding 350 µl RW1 to the RNeasy column. After centrifugation at the previous conditions, samples were incubated 20 min with DNAse. RNA was washed again with RW1. Columns were washed twice with 500 µl RPE buffer. The last centrifugation step lastet 2 min at 17 000 g. RNA was eluted with RNAse-free water. RNA concentration was measured using a Nanodrop 2000 (Thermo Fisher Scientific, Schwerte, Germany).

3.2.12.2 Reverse transcriptase-reaction

RNA was reverse transcribed into cDNA using the Transcriptor First Strand cDNA Synthesis kit according to the manufacturer's instructions. Briefly, the concentration of RNA was adjusted to 1 µg/µl with water. 11 µl of RNA were transcribed. First, 2 µl of random hexamers (600 pmol/µl) were added and denaturation was performed at 65 °C for 10 min in the Mastercycler (Eppendorf, Germany). Then 4 µl 5x buffer, 2µl dNTPs, 0.5 µl RNAse inhibitor (40 U/µl) and 0.5 µl reverse transcriptase (20U/µl) were added as a master mix. Subsequently, the mix was heated to 25 °C for 10 min, 55 °C for 30 min and 85 °C for 5 min in a Mastercycler (Eppendorf). cDNA was aliquoted in 2 µl aliquots and stored at -20 °C.

3.2.12.3 Real time quantitative PCR in Lightcycler 480

Fluorescence of SYBR Green, a dye that emits a signal after binding to double stranded DNA, is measured after each cycle. Real time quantitative PCR was performed using reversed transcribed cDNA (3.2.12.2) following the manufacturer's instructions using the QuantiFast SYBR Green PCR kit from Qiagen. 2 µl cDNA were mixed with 18 µl master mix (10 µl 2x QuantiFast, 5.5 µl H_2O and 2 µl 10 µM primer solution in water) in a 96 well plate. Subsequently, the mix was heated to 95 °C for 5 min (de-

naturation step), 95 °C for 10 s and 60 °C for 30 s (40 x denaturation, annealing and elongation cycles), 95 °C for 10 s (denaturation), 62 °C for 5 s and continuously heated up to 98 °C (melting curve) and cooled down to 40 °C for 30 s (cooling) in a Lightcycler 480 (Roche, Mannheim, Germany). mRNA expression was quantified by running external standard curves for each gene. Standard PCR product was purified using the MinElute PCR purification kit from Qiagen according to the manufacturer's instructions. Standard range was from 5 pg/µl to 0.5 ag/µl. Concentration was measured using a Nanodrop 2000 (Thermo Fisher Scientific, Schwerte, Germany), adjusted to 5 ng/µl and aliquoted (5 µl) and stored at -20 °C. The mRNA expression was quantified with the Lightcycler 480 software by determining the crossing points (C_T) of standards and samples.

3.2.12.4 Selfmade primer quality control

The selfmade* primer for tafazzin was checked for specificity before usage. Size of the PCR products were controlled by separation on a 2% agarose gel after mixing with DNA loading buffer, containing GelRed (Biotium, Fremont, CA, USA) and H_2O). 1 kb DNA ladder (New England BioLabs, Beverly MA, USA) was used as marker. Gel was run for 30 min at 90 V, DNA was visualised using a Chemidoc Touch Imaging System (Bio-Rad). PCR product was purified using MinElute® PCR purification kit following the manufacturer's instructions. Concentration was determined using a Nanodrop 2000 and was adjusted to 5 ng/µl with ultra-pure H_2O and primer concentration to 1.6 µM. Sequencing was performed using the BigDye Terminator v1.1 Cycle Sequencing Kit (Thermo Fisher Scientific, Waltham, Massachusetts, USA). Ready reaction mix, primers, sequencing buffer and water were added and thermal cycles were performed as described in the manufacturer's protocol. Products were purified by via loading to sepharose beads and centrifugation at 1500 g for 3 min. The capillary electrophoresis, to determine the sequence, was performed by Roman Werner†.

3.2.13 Statistics applied in the different chapters of the results section

Data are presented as means ± standard deviation (SD). In the following, applied statistics are described for each chapter separately as entitled in the results section.

3.2.13.1 Data evaluation applied in 4.1.1.2 (Systematic comparison of optimised mitochondria isolation strategies in HEPG2 cells)

About 99% of all detected lipid peaks showed an RSD below 20% in four injections of the pooled sample during the 8-hour UPLC-MS run. Applying the 80% rule[231] and removing lipids with > 20% RSD, 397 lipids were quantified for further comparative analysis. Statistical significance was evaluated by one-way ANOVA and Tukey's post hoc test to account for multiple comparisons using GraphPad Prism (GraphPad Software, La Jolla, CA, USA). A p-value <0.05 was considered significant. Regression analysis was performed with the statistical software package JMP 11.0.0 (SAS Institute, Cary, NC, USA). Multivariate principal component analysis (PCA) was performed of the lipid concentrations (pmol/µg

* by Christoph Hoffmann, a member of our group

† a member of our group

mitochondrial protein) with SIMCA-P 11.5 (Umetrics AB, Umeå, Sweden). Values below the level of detection were set to 0. The open-source MultiExperiment Viewer software[232] was employed for heatmap generation using mean centred data pre-scaled to unit variance (uv).

3.2.13.2 Data evaluation applied in 4.1.2.2.1 (Respiratory measurements in permeabilised murine muscle fibres in Oxygraph-2k)

An unpaired t-test with Welch's correction was performed with GraphPad Prism (GraphPad Software, La Jolla, CA, USA). A value of $p < 0.05$ was considered significant.

3.2.13.3 Data evaluation applied in 4.1.3.1 (Establishment and optimisation of a valid mitochondrial oxysterol profiling strategy in liver tissue and hepatic mitochondria (fresh/frozen tissue, mitochondria isolation and oxysterol extraction fresh/frozen with or without butylated hydroxytoluene (BHT)))

Multifactorial ANOVA was performed with the statistical software package JMP 11.0.0 (SAS Institute, Cary, NC, USA). Benjamini-Hochberg-based false discovery rate (FDR) was used for statistical analysis, setting $p < 0.05$ and FDR <0.1 as the significance level. Student´s t-test was used to evaluate respiration measurements and immunoblots. Outliers were removed applying the ROUT method in GraphPad Prism (GraphPad Software, La Jolla, CA, USA), with Q set to 1% as recommended by the developers.[233]

3.2.13.4 Data evaluation applied in 4.2.1.1 (Skeletal muscle cell culture: Analysis of mitochondria from cultured skeletal muscle cells challenged with substrate overflow and insulin resistance: Insulin resistant murine C2C12 myotubes under low/high glucose conditions)

A paired Student´s t-test was performed for lipidomics and proteomics data. 2-way ANOVA was applied to western blot results, respiratory measurements and enzymatic assay results. 2way ANOVA (significances shown with "‾‾"), significances of multi comparison between groups indicated with the following mark "┌──┐".*= glucose had significant effects in ANOVA, #= insulin had significant effects in ANOVA.

3.2.13.5 Data evaluation applied in 4.2.2.1 (Tissue-specific comparison: liver and skeletal muscle mitochondria)

95% of all detected lipids showed a RSD below 20% throughout nine injections of a pooled sample during the whole UPLC-MS run. Statistical significance was evaluated by a Student´s t-test using GraphPad Prism (GraphPad Software, La Jolla, CA, USA). A p-value <0.05 was considered significant. Multivariate principal component analysis (PCA) was performed of the lipid concentrations per µg mitochondrial protein with SIMCA-P 11.5 (Umetrics, Umeå, Sweden). Values below the level of detection were set to 0. The open-source MultiExperiment Viewer software[232] was employed for heatmap

generation using mean centred data pre-scaled to unit variance (uv). Benjamini-Hochberg-based false discovery rate (FDR) was used for statistical analysis in

Figure 42 and Table 9, setting p <0.05 and FDR <0.05 as the significance level.

3.2.13.6 Data evaluation applied in 4.2.2.2 (Omics investigation of mitochondrial adaptions in liver and skeletal muscle to excess energy intake and physical exercise: Control diet versus energy-rich diet either with or without treadmill exercise)

2-way ANOVA was applied to western blot results, respiratory measurements and enzymatic assay results. 2way ANOVA (significances shown with "—"), significances of multi comparison between groups indicated with the following mark "┌──┐". *= diet had significant effects in ANOVA, #= training had significant effects in ANOVA using GraphPad Prism (GraphPad Software Inc., La Jolla, CA, USA). Multivariate principal component analysis (PCA) was performed of the lipid concentrations per µg mitochondrial protein with SIMCA-P 11.5 (Umetrics, Umeå, Sweden). Values below the level of detection were set to 0. The open-source MultiExperiment Viewer software (J. Craig Venter Institute, La Jolla, CA, USA)[232] was employed for heatmap generation using mean centred data pre-scaled to unit variance (uv). Data in Figure 52 were statistically evaluated by a Student´s t-test.

3.2.13.7 Levels of significance

p value	**level of significance**
≥ 0.05	no significance (ns)
< 0.05	*/#
< 0.01	**/##
< 0.001	***/###
< 0.0001	****/####

4 Results

4.1 Method establishment

4.1.1 Isolation of purified mitochondria

4.1.1.1 Mitochondria isolation from cell culture

Mitochondria isolation from primary human myotubes (hMT), human embryonic kidney 293 cells (HEK), murine myoblasts (C2C12) and human hepatocellular carcinoma cells (HEPG2) was optimised focussing on the purity of the mitochondrial fractions by depleting them from contaminations by other subcellular organelles. By employing western blot analysis, purity was investigated using organelle-specific markers for mitochondria as well as markers for endoplasmic reticulum (ER), nuclei, peroxisomes, lysosomes and cytosol as well as lipid droplets. Apart from the nuclear marker histone, all antibodies were directed against membrane proteins.

Experimental parameters considered for optimising mitochondria isolation were stroke numbers in different douncers, nitrogen bomb pressure, times and volumes, buffer composition, enzymatic digestions prior to homogenisation keeping mitochondrial integrity. Additionally, different approaches to perform mitochondrial isolation were tested namely the commonly used differential centrifugation (DC),[162-165] DC followed by ultracentrifugation (UC)[163,165,172] and a more recent magnetic bead assisted method (MACS, Miltenyi Biotec, Bergisch-Gladbach, Germany).[176,177] Briefly, for DC tissues or cells are minced and homogenised, commonly using a dounce homogeniser.[169-171] A slow centrifugation step is performed to sediment broken cells and cell debris, which is followed by a fast centrifugation step using the supernatant to pellet the mitochondria (Figure 5, left). DC-derived mitochondria were layered on different continuous and discontinuous gradients and centrifuged using an ultracentrifuge for further purification of mitochondrial fractions (Figure 5, middle). Lastly, the commercialised more rapid MACS approach to isolate mitochondria was investigated, which was first described by Hornig-Do et al. (2009)[176]. After sample homogenisation, mitochondria were coupled to anti-TOM22-antibodies conjugated to paramagnetic beads. Bead-coupled mitochondria were then be isolated in a magnetic field (Figure 5, right).

The pivotal steps and tested experimental parameters, which led to the optimised protocols finally applied in this thesis, are shown for DC, UC and MACS in the following. All tested conditions are summarised in Supplementary Table 1 and Supplementary Table 2. The optimised protocol for mitochondrial isolation from HEPG2 is described in 3.2.6.2 and from C2C12 in 3.2.6.3.

Cell homogenisation in nitrogen bomb: Different pressures for cell disruption in a N_2 bomb (Parr Instrument, Moline, IL, USA) were compared using C2C12 (Figure 7), HEKs, HEPG2 and hMTs cells (data not shown). Mitochondrial membrane ATP synthase 5 (ATP5) was used to confirm the presence of

mitochondria in total cell lysates and their enrichment in the isolated fractions (Figure 7). Dounced mitochondrial fractions and the harshest N_2 bomb conditions (condition 1, Figure 7) showed the strongest ATP5 signal, indicating the most pronounced enrichment in mitochondria. At the same time, the marker for nuclei (histone H3) was enriched in all samples disrupted in a N_2 bomb, indicating a concomitant disruption of the nuclei leading to contaminations not depletable by centrifugation. In addition, the marker for cytosol (GFAT) was present in all mitochondrial fractions, indicating an inevitable contamination of isolated mitochondria with cytosol. Based on these results, cells were disrupted using a douncer in further experiments.

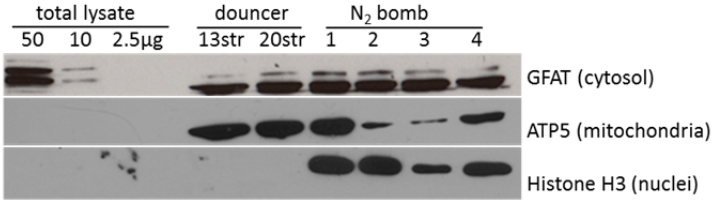

Figure 7: Analysis of organelle-specific proteins in total C2C12 cell lysates and in mitochondrial fractions obtained after homogenisation with a douncer or via cell disruption in a N_2 bomb. A representative western blot of C2C12 mitochondria isolations is shown. str= strokes; nitrogen bomb conditions: 1= 30 bar, 3 ml, 5 min; 2= 10 bar, 3 ml, 15 min; 3= 10 bar, 3 ml, 5 min; 4= 10 bar, 20 ml, 5 min. Mitochondrial membrane ATP synthase 5 (ATP5) was used as a marker for mitochondria. For the detection of potential contaminations, antibodies against histone H3 (nuclei marker) and GFAT (cytosol marker) were used. Further details are described in Section 3.2.6.

Cell homogenisation using a douncer: Next, the homogenisation using a douncer was further optimised. Dounce stroke repetitions and cell numbers keeping the total volume constant during homogenisation were varied. Solely results for C2C12 and HEPG2 are shown in Figure 8, since these cells were used in further experiments applied in this thesis. Three 15 cm plates of HEPG2 were not enough to yield a sufficient mitochondria enrichment showing no or only a weak ATP5 signal (Figure 8 left). Homogenisation of six 15 cm plates of HEPG2 dounced more than 10 times showed sufficient mitochondrial enrichment, but only in the homogenisation condition with 15 strokes nuclei contaminations indicated via the signal of histone H3 were depleted. Further mitochondrial isolations of HEPG2 cells were performed from six 15 cm plates applying 15 strokes. Both, homogenisation of three and six 15 cm plates C2C12, led to a distinct enrichment of the mitochondrial marker ATP5 (Figure 8 right). Douncing six plates, instead of only three, however, also enriched nuclei contamination, indicating a higher disruption of organelles when douncing higher cell numbers in the same volume. For further experiments three 15 cm plates of C2C12 were dounced 20 times for mitochondrial isolation by differential centrifugation as described in Section 3.2.6.

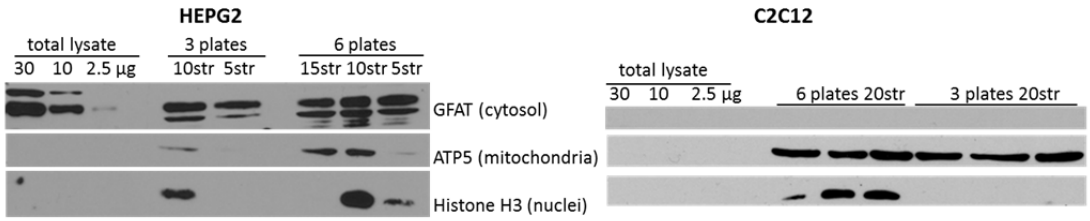

Figure 8: Analysis of organelle-specific proteins in HEPG2 (left) and C2C12 (right) cell lysates and in mitochondrial fractions obtained after homogenisation of cell suspensions from a different amount of cell plates with different stroke numbers. Mitochondrial membrane ATP synthase 5 (ATP5) was used as a marker for mitochondria. For the detection of potential contaminations, antibodies against histone H3 and GFAT were used. plate= 15 cm diameter cell plate of 90% confluence, str= strokes.

For a further purification of mitochondrial fractions, the ´crude` mitochondria (after differential centrifugation) were layered on density gradients and centrifuged at high speed.

Ultracentrifugation using a sucrose gradient: First, two different sucrose gradients were tested and the purity of the mitochondrial fractions were compared to both cell lysates and crude mitochondrial fractions. The first discontinuous sucrose gradient consisted of two layers (34 and 58% sucrose) and the second one of three layers (15, 22 and 50% sucrose) The results from Western Blot analysis are shown in Figure 9. Both gradients showed a stronger ATP5 signal in the mitochondria associated layer compared to crude mitochondrial fractions (Figure 9). Contamination with nuclei (histone H3 as a marker) was reduced after ultra-centrifugation, but all other contaminant proteins investigated like Calx and GRP78 (endoplasmic reticulum) and PEX3.1 (peroxisomes) showed stronger signals after ultracentrifugation. Other appearing layers contained minor protein amounts, contained also mitochondria and were enriched with ER contamination.

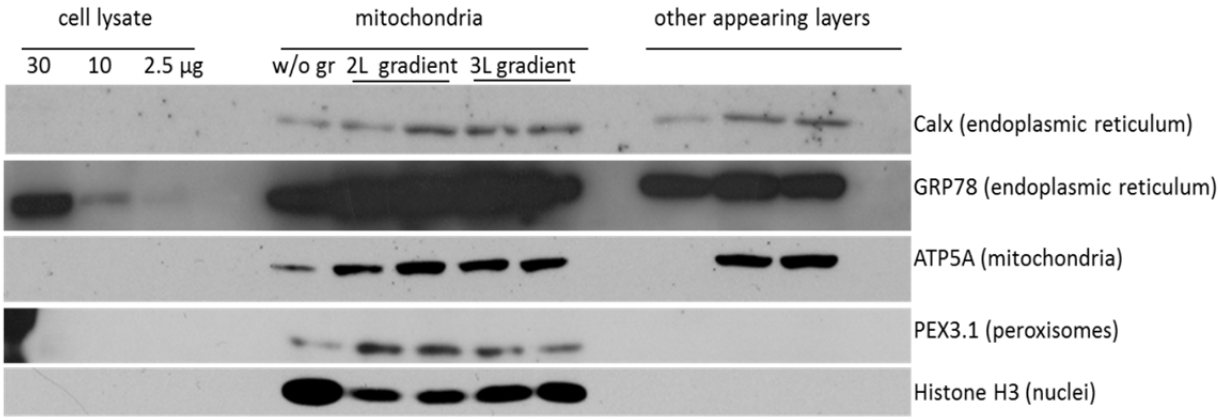

Figure 9: Analysis of organelle-specific proteins in C2C12 cell lysates and in mitochondrial fractions obtained after mitochondrial isolation using just differential centrifugation (w/o gr= without gradient, DC) or after further purification of these mitochondria using a sucrose gradient either with two layers (=2L; 34%, 58%) or three layers (=3L; 15%, 22%, 50%). Each gradient was performed in duplicates. Layers appearing after ultracentrifugation other than the mitochondrial enriched layer were also employed ("other appearing layers") to investigate their composition. Mitochondrial membrane ATP synthase 5 (ATP5) was used as a marker for mitochondria. For the detection of potential contaminations, antibodies against histone H3, calnexin, GRP78 and PEX3.1 were used.

Ultracentrifugation using a percoll gradient: Purification of crude mitochondrial fractions after DC was further modified by ultracentrifugation on a percoll gradient, in this case a continuous self-forming 25% gradient (Figure 10 A). Ultracentrifugation depleted the mitochondrial fraction appearing in the lower layer (see results in Figure 10 B; lane "w/o trypsin LL") from endoplasmic reticulum visualized via the marker calnexin (calx) while enriching mitochondria compared to crude mitochondria (Figure 10 B; lane "w/o gradient"). An additional trypsination of the crude mitochondrial pellet before layering on the gradient to dissociate mitochondria-associated organelles from mitochondria did not further improve the purification, but lead to a stronger signal of ATP5 in the upper layer (Figure 10 B; lane "Trypsin UL"), indicating a decreased amount of mitochondrial protein in the lower mitochondria-associated layer (Figure 10 B; "Trypsin LL").

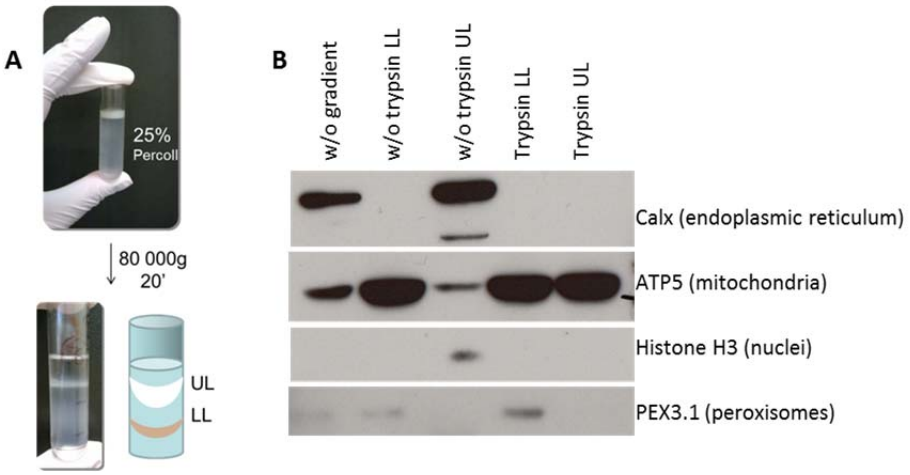

Figure 10: A: 25% Percoll gradient before and after ultracentrifugation forming two appearing layers. LL= lower layer after ultracentrifugation, UL= upper layer after ultracentrifugation. B: Analysis of organelle-specific proteins in mitochondrial fractions from HEPG2 obtained after mitochondrial isolation using just differential centrifugation (lane "w/o gradient") or after further purification of these mitochondria using a 25% continuous percoll gradient. Mitochondrial membrane ATP synthase 5 (ATP5) was used as a marker for mitochondria. For the detection of potential contaminations, antibodies against histone H3, calnexin and PEX3.1 were used. w/o trypsin= without trypsin digestion of the crude mitochondrial pellet, trypsin= crude mitochondrial pellet was trypsinated before layering on the percoll gradient to dissociate mitochondria-associated organelles from mitochondria.

MACS: As an alternative mitochondrial isolation approach, a more recent magnetic bead-assisted method (MACS) was investigated as described in 3.2.6.2. It is an anti-human antibody coupled magnetic bead assisted method. So, only human derived cell lines like HEPG2 and hMTs could be investigated, but not the murine cell line C2C12. Again, homogenisation was optimised testing different cell disruption methods: a douncer and a needle with different gauge sizes of the syringes and different stroke numbers (results are given in Figure 11). Compared to differentially centrifuged crude mitochondria (DC) MACS derived mitochondria showed stronger enrichment of and thus contamination with endoplasmic reticulum, indicated by the higher intensity of the calx protein. An increasing stroke number using a douncer led to a higher mitochondria (ATP5) enrichment, but ATP5 signal was strongest in needle and syringe homogenised samples. However, also the strongest signal of calx was detected in these samples, indicating the highest ER contamination. The evaluation was achieved from the results of densitometric quantification of the western blot signals of calx and ATP5. The ratio of

ATP5 to calx was highest in the needle and syringe homogenised samples, so this method was chosen for further MACS experiments (3.2.6.2). 27.75G gauge size of the syringe was preferred over the 30G gauge, because the 30G showed a PLIN2 signal, indicating a contamination with lipid droplets.

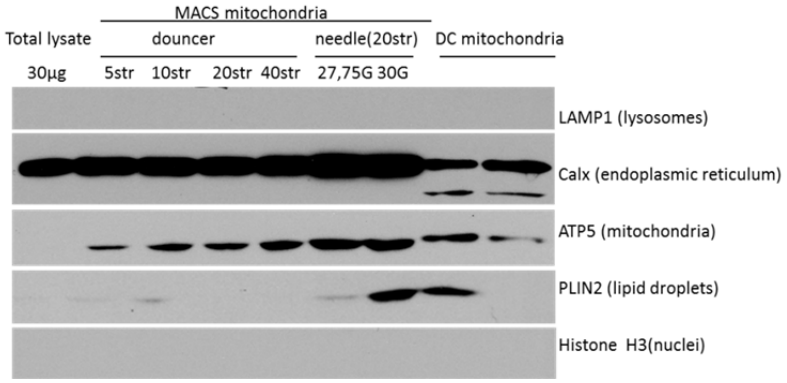

Figure 11: Analysis of organelle-specific proteins in mitochondrial fractions from HEPG2 obtained after mitochondrial isolation using MACS method (Miltenyi Biotec, Bergisch-Gladbach, Germany). Mitochondrial membrane ATP synthase 5 (ATP5) was used as a marker for mitochondria. For the detection of potential contaminations, antibodies against histone H3, calnexin (calx), PLIN2 and LAMP1 were used. str= strokes, G= gauge size of the needle, DC= differential centrifugation, MACS= magnetic bead assisted method. No signals were detected for histone H3 and LAMP1.

4.1.1.2 Systematic comparison of optimised mitochondria isolation strategies in HEPG2 cells

After optimisation of all three mitochondrial isolation methods DC, UC and MACS (reported in 4.1.1.1) focussing on purity and yield of the mitochondrial fraction on protein levels, we systematically compared the three isolation methods. For this isolated mitochondria from liver-derived HEPG2 cells were used to generate detailed lipid profiles using UPLC-MS to investigate whether lipidomics data alone can provide an estimate of the purity of mitochondrial samples. Each purification procedure was performed in at least five replicates and compared to the lipid profiles of total cell lysate.

4.1.1.2.1 Organelle-specific protein abundances in mitochondria extracts isolated by different purification methods

Mitochondrial enrichment and purity of the isolated fractions was first investigated by employing western blot analysis as previously described (4.1.1.1). Organelle-specific markers for mitochondria as well as markers for potential contaminations by endoplasmic reticulum (ER), nuclei and Golgi apparatus (Figure 12) as well as lipid droplets were investigated. With the exception of the nuclear marker histone, all antibodies were directed against membrane proteins. Equal protein amounts (30 µg, 3.2.4) of total cell lysates were assessed as controls to determine the organelle-specific protein levels before enrichment. Mitochondrial membrane ATP synthase 5 (ATP5) was analysed to confirm the presence of mitochondria in total cell lysates and their enrichment in the isolated fractions (Figure 12). UC samples showed the strongest ATP5 signal, indicating the most pronounced enrichment in mitochondria. At the same time, the markers for ER and nuclei were most efficiently depleted by UC. The lipid droplet marker PLIN2 was detectable in 90 µg of total HEPG2 lysate (Supplementary Figure 2), but not in 30 µg of total lysate and mitochondrial fractions, indicating no enrichment of lipid drop-

lets. In contrast, DC and in particular MACS samples contained prominent amounts of the markers for ER and nuclei (Figure 12). All mitochondria isolation procedures led to a decrease of giantin, the Golgi apparatus marker, compared to total cell lysates.

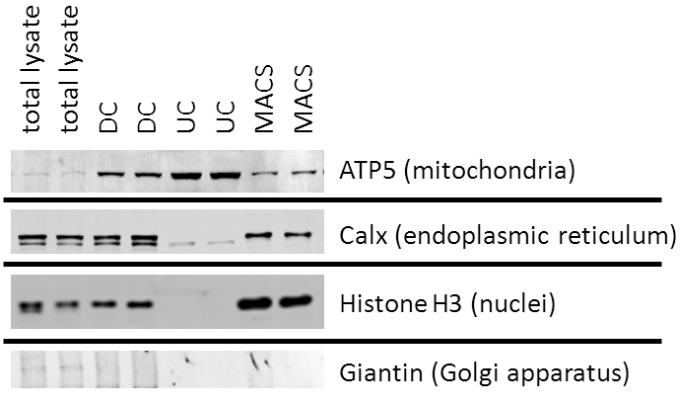

Figure 12: Analysis of organelle-specific proteins in total HEPG2 cell lysates and in mitochondrial fractions obtained by differential centrifugation (DC), ultracentrifugation (UC) and a magnetic bead-assisted method (MACS). A representative western blot of two mitochondria isolations per method is shown. Mitochondrial membrane ATP synthase 5 (ATP5) was used as a marker for mitochondria. For the detection of potential contaminations, antibodies against calnexin (calx), histone H3 and giantin were used. Details of the methods in Section 3.2.6.2.

4.1.1.2.2 Comparative lipid profiling of mitochondria isolated by different purification methods

The lipid species in the mitochondrial fractions were quantified using our UPLC-MS approach described in 3.2.10.2. In total, 397 lipids from 17 (sub-)classes, 12 ceramide (CER), 32 cardiolipin (CL), 2 cholesteryl ester (CE), 6 diacylglycerol (DAG), 5 hexosyl-ceramide (HexCER), 11 lyso-phosphatidylcholine (LPC), 8 lyso-phosphatidylethanolamine (LPE), 2 lyso-phosphatidylinositol (LPI), 41 phosphatidylcholine (PC), 52 phosphatidylethanolamine (PE), 13 phosphatidylethanolamine plasmalogen (PE-P), 19 phosphatidylglycerol (PG), 34 phosphatidylinositol (PI), 13 phosphatidylserine (PS), 21 sphingomyelin (SM), 93 triacylglycerol (TAG) and 33 free fatty acid (FFA) species could be quantified. We obtained a linear range over 2.0-3.2 orders of magnitude (r^2> 0.991) for the 5 CL standards (3.2.10.2) tested. About 80% quantitative data of all detected lipid species showed a relative standard deviation (RSD) below 30%, the RSD median value was 21.49% for the 6 different biological replicates obtained by UC purification. It is important to note that the precision is determined for the whole analytical workflow including biological replicates, mitochondrial isolation, lipid extraction and UPLC-MS analysis. Thus, overall a high precision and reliability of the whole (pre-)analytical procedure is demonstrated. The different isolation methods had no major effect on the total number of detected lipid species, but UC purification caused a depletion of 6 of the 93 TAG species to levels below the detection limit. The small sample amount employed, 100 µg (by protein) of purified mitochondria, did not cause a reduction in the number of detected lipid species compared to total cell lysate, but quantitative determination for 3 of the 32 cardiolipins was impossible due to not reaching the limit of detection in total cell lysates.

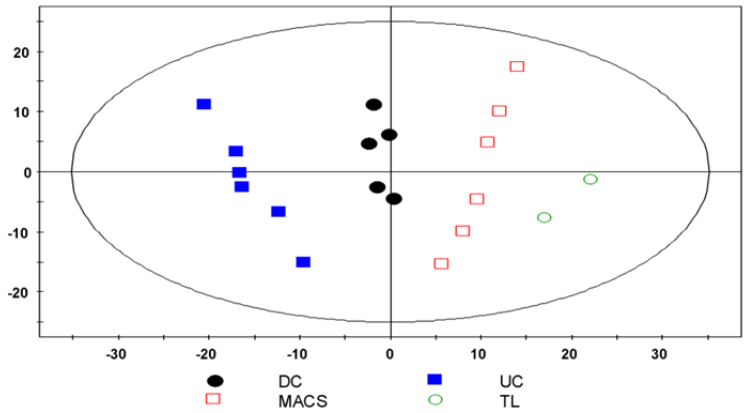

Figure 13: Principal Component Analysis (PCA) scores plot of the first two principal components (PC1= 0.41%, PC2= 0.21% of total variance) based on all detected lipids (relative standard deviation in the quality control samples< 20%; unit variance (uv) scaling (R2X= 0.865, Q2= 0.748)). Each spot represents one mitochondrial sample isolated from HEPG2 cells using three different methods: DC= differential centrifugation; UC= DC followed by ultracentrifugation; MACS= magnetic bead-assisted isolation; TL= total cell lysate.

To gain an initial overview of the effect of the isolation procedures on the lipid profiles, a multivariate principal component analysis (PCA, Figure 13) of the lipid compositions of the different mitochondrial samples and of total cell lysate was performed (3.2.13.1). In the direction of the first principal component a pronounced separation of the mitochondrial samples was detected, which clustered together dependent on the isolation methods. The difference from total cell lysate was smallest for MACS samples, followed by DC and UC. Thus, MACS isolation yielded mitochondrial samples whose lipid profile was closest to the profile of total cell lysate, whereas lipids from UC-isolated mitochondria were most distinct from total cell lysate.

4.1.1.2.3 Lipid profiles of mitochondrial samples isolated from HEPG2 cells by ultracentrifugation (UC) show the highest enrichment in mitochondria-specific cardiolipins

To assess how the isolation methods affected the lipid composition of the samples, a heatmap was generated using the summed amounts relative to mitochondrial protein amount of the individual lipid classes (Figure 14). Data were normalised by mean centring and scaled to unit variance. In accordance with the PCA analysis, the heatmap revealed that MACS samples were most similar to total cell lysate, both showing higher levels of FFA, CE, DAG and TAG and lower levels of the mitochondria-specific CL (2.2.2) and PG than the other isolation methods. While DC samples contained the highest amounts of PE-P, PS, HexCER and SM, UC samples showed the greatest enrichment of PE, PG and CL, indicating the highest mitochondrial enrichment. Lipids other than the mitochondrial signature lipid CL cannot be assigned to individual organelles, in previous observations in skeletal muscle tissue CL was suggested to be a superior marker of mitochondrial content.[223]

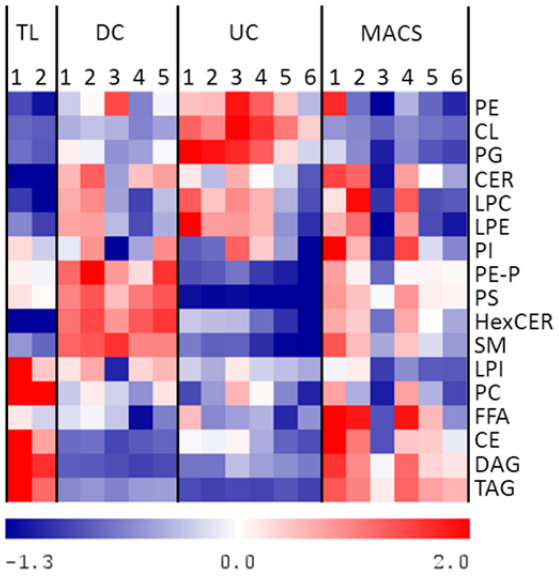

Figure 14: Heatmap visualisation of the different lipid (sub-)classes in total cell lysates (TL) and in mitochondrial samples isolated by three different methods: DC= Differential centrifugation, UC= ultracentrifugation, MACS= magnetic bead-assisted isolation. Each column represents an individual mitochondrial isolation labelled by a number. Values were centred to the mean of the respective lipid class and scaled to unit variance. White colour shows values close to the mean of the lipid class and red- and blue- coloured values are higher and lower, respectively, than the mean. CE= cholesteryl esters; CER= ceramides; CL= cardiolipins; DAG= diacylglycerols; FFA= free fatty acids; HexCER= hexosyl-ceramides; LPC= lyso-phosphatidylcholines; LPE= lyso-phosphatidylethanolamines; LPI= lyso-phosphatidylinositols; PC= phosphatidylcholines; PE= phosphatidylethanolamines; PE-P= phosphatidylethanolamine plasmalogens; PG= phosphatidylglycerols; PI= phosphatidyl-inositols; PS= phosphatidylserines; SM= sphingomyelins; TAG= triacylglycerols. The mitochondria-specific CLs were most enriched by UC.

While containing similar amounts of total lipids per µg of mitochondrial protein analysed, the different isolation methods yielded significantly different CL levels (Table 8). UC-purified mitochondria contained the highest relative CL amount (12.9 ± 1.7% of all phospholipids), DC was intermediate (3.6 ± 0.5% of all phospholipids) and MACS showed the lowest amount of CL (2.4 ± 0.3% of all phospholipids) ($p_{UC\text{-}DC} < 0.0001$, $p_{UC\text{-}MACS} < 0.0001$). A high PE/PC ratio is characteristic for mitochondria as a remnant of their possible bacterial background.[94] The lipids in the UC fraction exhibited the highest PE/PC ratio, 0.98 ± 0.08, followed by DC with 0.79 ± 0.19 and MACS with 0.66 ± 0.17.

Table 8: Summed content of lipid classes (pmol/µg protein) quantified by LC-MS lipid profiling of mitochondria purified using different isolation methods.

Lipid (sub-)	DC		UC		MACS		UC vs. DC	UC vs. MACS	DC vs. MACS
class	Mean	SD	Mean	SD	Mean	SD	*p*-value	*p*-value	*p*-value
CL	8.623	1.779	34.433	10.814	5.217	1.522	< 0.0001	< 0.0001	n.s.
CE	0.012	0.001	0.019	0.007	0.033	0.017	n.s.	n.s.	0.0135
CER	2.838	0.404	2.447	0.326	2.703	0.662	n.s.	n.s.	n.s.
DAG	0.092	0.007	0.129	0.018	0.283	0.077	n.s.	0.0002	< 0.0001
FFA	59.601	10.134	60.664	11.180	87.242	28.114	n.s.	n.s.	n.s.
HexCER	1.013	0.076	0.516	0.113	0.719	0.151	< 0.0001	0.0282	0.0033
LPC	1.625	0.459	1.834	0.476	1.709	0.727	n.s.	n.s.	n.s.
LPE	0.728	0.163	0.838	0.251	0.699	0.249	n.s.	n.s.	n.s.
LPI	0.081	0.032	0.064	0.010	0.052	0.021	n.s.	n.s.	n.s.
PC	91.406	5.802	86.358	11.261	89.657	14.345	n.s.	n.s.	n.s.
PE	72.193	17.171	85.393	16.767	60.249	24.064	n.s.	n.s.	n.s.
PE-P	1.313	0.243	0.526	0.136	0.916	0.166	< 0.0001	0.0064	0.0078
PG	6.198	1.495	12.973	4.579	3.582	1.639	0.0061	0.0003	n.s.
PI	41.717	7.223	39.157	8.012	44.678	9.599	n.s.	n.s.	n.s.
PS	11.296	1.444	1.200	0.335	8.494	1.630	< 0.0001	< 0.0001	0.0066
SM	8.185	0.619	3.090	0.662	5.834	1.642	< 0.0001	0.0020	0.0092
TAG	17.082	1.565	7.313	0.964	53.924	11.260	n.s.	< 0.0001	< 0.0001

DC= differential centrifugation; UC= ultracentrifugation; MACS= magnetic bead-assisted isolation; CE= cholesteryl esters; CER= ceramides; CL= cardiolipins; DAG= diacylglycerols; FFA= free fatty acids; HexCER= hexosyl-ceramides; LPC= lyso-phosphatidylcholines; LPE= lyso-phosphatidylethanolamines; LPI= lyso-phosphatidylinositols; PC= phosphatidylcholines; PE= phosphatidylethanolamines; PE-P= phosphatidylethanolamine plasmalogens; PG= phosphatidylglycerols; PI= phosphatidyl-inositols; PS= phosphatidylserines; SM= sphingomyelins; TAG= triacylglycerols. n.s.= not significant. Values are means of at least 5 purifications.

4.1.1.2.4 The lipid composition of mitochondrial samples isolated from HEPG2 cells by differential centrifugation (DC) and MACS underlines a relevant contamination with membranes from other organelles

Western blot analyses indicated that in addition to enriching the mitochondria-specific protein ATP5, DC and MACS also enriched markers of other contaminant organelles (Figure 12). UC-purified samples, in contrast, depleted histone H3 beyond detectability and only a very low signal was visible for the ER-marker calnexin (Figure 12). In a similar manner, DC and MACS also increased the relative amounts of other lipid classes that were not enriched by UC (Figure 15). Compared to UC, samples isolated by DC or MACS contained significantly higher amounts of PS, PE-P, SM, and HexCER (Table 8). Additionally, PE plasmalogens (PE-P) were significantly lower with UC than with the other isolation methods. A striking feature of the MACS and, to a lower degree, DC samples was their significantly

higher TAG content (Figure 14, Figure 15 and Table 8). Therefore, these findings indicate that UC, but not DC or MACS, yielded a pure mitochondrial fraction with little contamination by non-mitochondrial organelles employed by western blot analyses but also on lipid level.

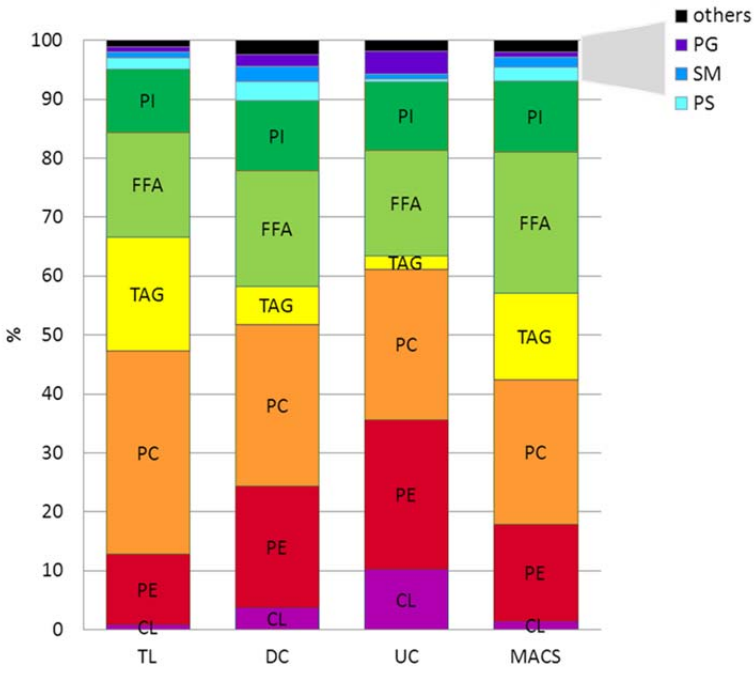

Figure 15: Contribution of the different lipid classes (amount in pmol/µg protein) to all lipids detected in mitochondria enriched by differential centrifugation (DC), ultracentrifugation (UC) or magnetic bead-assisted isolation (MACS) and in total cell lysates (TL). Values are means of at least 5 purifications or of 2 total cell lysates. Data in Table 8.

4.1.1.2.5 Lipid profiling as an estimate of purity of isolated mitochondria

To assess whether lipidomics data alone can provide an estimate of the purity of mitochondrial samples, we performed a direct comparison of lipidomics (Figure 16 A, C, E) and western blot data (Figure 16 B, D). Both CL, the signature lipid of mitochondria, and ATP5 were pronouncedly enriched in UC samples, resulting in a strong correlation between CL concentrations and ATP5 protein levels in the purified mitochondria (r^2= 0.79, p< 0.0001; Supplementary Figure 1; Figure 16 A, B).

On the other hand, two lipid classes, PS and SM, and the ER-specific protein calnexin were reduced in UC-purified samples in a similar fashion (Figure 16 C, D, E).

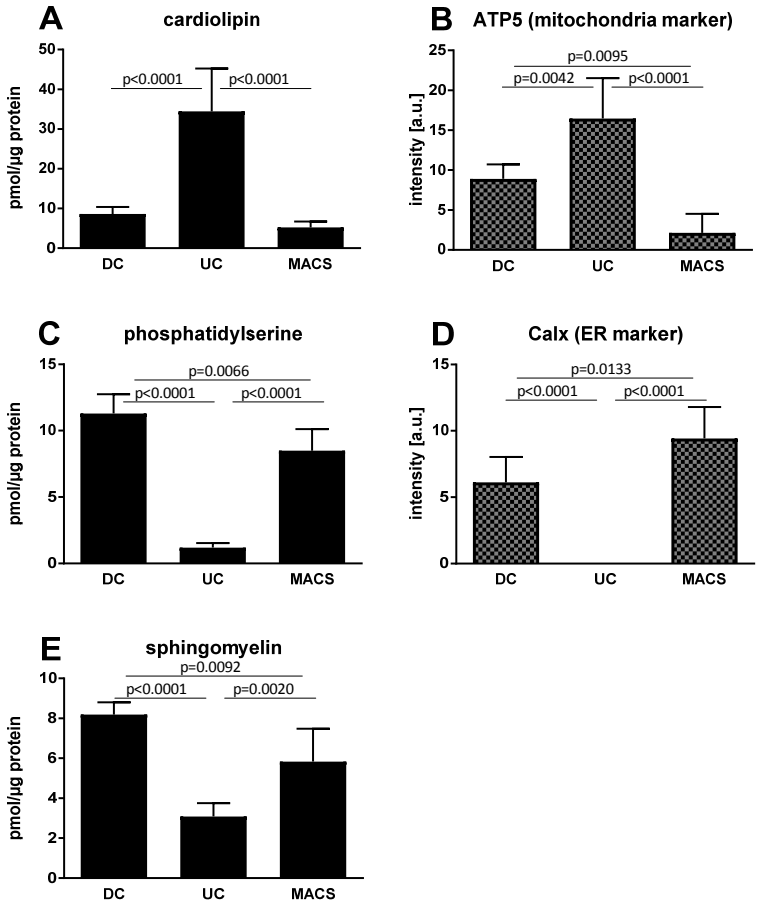

Figure 16: Comparison of distinct lipid (left) and protein contents (right) in mitochondrial samples isolated using three different procedures, differential centrifugation (DC), ultracentrifugation (UC), and magnetic bead-assisted isolation (MACS). Histograms show the sums of the lipid classes or the densitometric quantification of western blots normalised to total cell lysate. Values are means ± SD of at least 5 purifications.

4.1.1.3 Method establishment of mitochondria isolation from mouse liver and skeletal muscle tissue

In a first step, the homogenisation technique (douncer, Gentle MACS (Miltenyi Biotec, Bergisch-Gladbach, Germany), stroke number, tissue amount, tissue digestion procedures and gradient compositions were optimised (see tested conditions in Supplementary Table 3). Mitochondrial enrichment and contamination depletion was employed by western blot analyses. The optimised protocols are described in 3.2.6.4 for liver and 3.2.6.5 for skeletal muscle from mice.

First, the MACS method was applied to isolate mitochondria from tissue. Homogenisation of the tissue was performed testing two different devices: a tissue douncer and the gentle MACS provided by Miltenyi Biotec, which is in principle a semi-automated blender in volumes of a few millilitres. Western Blot analyses showed no difference in ATP signal intensity (Figure 17) and therefore mitochondrial enrichment, between the two homogenisation devices. MACS method did not deplete the muscle mitochondrial fraction from ER (calx band), observed with both gentle MACS and a tissue douncer

used for homogenisation. Based on these results purchasing the gentle MACS was avoided and a douncer was used instead for further tissue homogenisation.

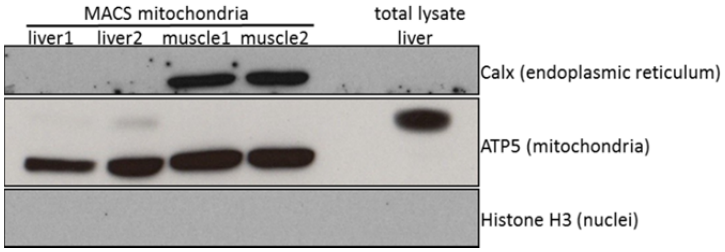

Figure 17: Analysis of organelle-specific proteins in total liver lysate and in mitochondrial fractions obtained by MACS purification or differential centrifugation (DC) from mouse liver and muscle. Homogenisation before MACS purification was performed either with Gentle MACS (=1; Miltenyi Biotec, Bergisch-Gladbach, Germany) following the manufacturer´s instructions or with a douncer (=2). Mitochondrial membrane ATP synthase 5 (ATP5) was used as a marker for mitochondria. For the detection of potential contaminations, antibodies against histone H3 and calx were used.

Next, MACS method was compared with two other commonly used mitochondria isolation methods: differential centrifugation (DC) and DC with subsequent ultracentrifugation (UC). Using liver tissue the MACS method led to the strongest ATP5 enrichment, while also showing a slight calx signal, indicating a higher contamination with endoplasmic reticulum (Figure 18).

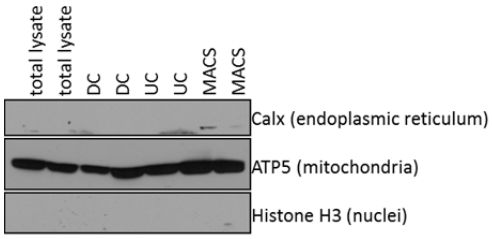

Figure 18: Analysis of organelle-specific proteins in liver lysates and in mitochondrial fractions obtained by differential centrifugation (DC), ultracentrifugation (UC) and a magnetic bead-assisted method (MACS). An exemplary western blot of 2 mitochondria isolations per method is shown. Mitochondrial membrane ATP synthase 5 (ATP5) was used as a marker for mitochondria. For the detection of potential contaminations, antibodies against calnexin (calx) and histone H3 were used.

Skeletal muscle was also isolated using the three different methods in comparison. Before DC and UC a tissue digestion was established. Without digestion, muscle tissue was not disrupted sufficiently in the douncer and mitochondrial yield was very low. Digestion time, enzyme concentration, digestion temperature and type of enzyme were optimised and controlled by employing western blot analyses and Oxygraph-2k analyses of the cytochrome c response. The latter analysis verifies the intactness of the mitochondrial outer membrane (data not shown). Comparison of DC, UC and MACS applied on skeletal muscle tissue showed strong ATP5 enrichment in all samples and slight ER contaminations (Figure 19 left). Different amounts of muscle were tested. Since 200 mg starting material did not yield enough mitochondrial protein to perform all experiments, 500 mg tissue was used for all following experiments. Different types of percoll gradients for ultracentrifugation were tested (3.2.6.4, 3.2.6.5). All showed strong ATP5 enrichment and slight ER contaminations (Figure 19 right). A continuous percoll gradient was chosen to further purify muscle mitochondria as established for liver mitochondrial isolation.

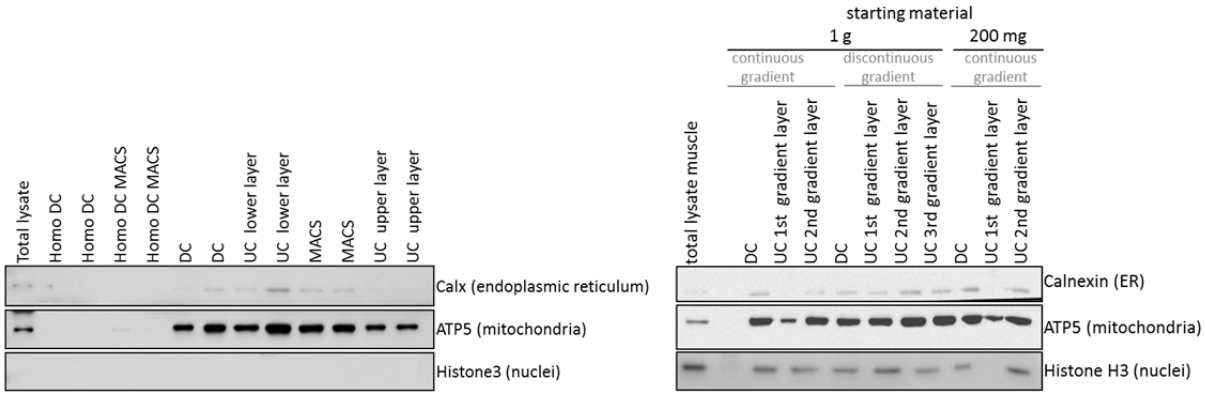

Figure 19: Analysis of organelle-specific proteins in skeletal muscle lysates and in mitochondrial fractions obtained by differential centrifugation (DC), ultracentrifugation (UC) and a magnetic bead-assisted method (MACS) (left). Homo= homogenate, DC= differential centrifugation, UC= DC plus subsequent ultracentrifugation, MACS= magnetic bead assisted mitochondria isolation, lower and upper layer= two appearing layers in the percoll gradient after ultracentrifugation. An exemplary western blot of 2 mitochondria isolations per method is shown. Mitochondrial membrane ATP synthase 5 (ATP5) was used as a marker for mitochondria. For the detection of potential contaminations, antibodies against calnexin (calx) and histone H3 were used.

We established and optimised a reliable and comprehensive method to obtain lipid and protein profiles from pure tissue-derived mitochondria isolated from liver and skeletal muscle. Briefly for liver (3.2.6.4), 150-200 mg of tissue were minced, homogenised applying 6 strokes in a douncer, followed by differential centrifugation (DC). The crude mitochondrial pellet was layered on a continuous 25% Percoll gradient (UC). Briefly for muscle tissue (3.2.6.5), around 500 mg were minced with a scissor and then a razor blade. Tissue was digested using a protease type 8 before homogenisation with 6 strokes in a douncer, followed by DC and UC. This tool was integrated in the following experiments.

4.1.2 Respiratory measurements

4.1.2.1 Respiratory analyses on a Seahorse XF96

Respiration analyses using a Seahorse XF96 were established and optimised for intact C2C12 myotubes and for isolated mitochondria from C2C12 cells and murine tissue.

Cell number per well was titrated for the adherent murine cell line C2C12. 2 500 cells per well of a Seahorse XF96 cell microplate were cultured for two days before adding fusion medium, to achieve 90% confluency of the cells. This was required to avoid multilayer growth of the cells and thereby a lagged substrate and inhibitor diffusion.

For isolated mitochondria from cells and tissue, the protein amount per well was also titrated. An ideal protein amount was determined by tracking O_2 concentration in each well over measurement time. A too high protein amount led to exhaustion of oxygen in the well during the measurement course and thereby a limitation of the oxygen consumption. This was due to an insufficient amount of time during mixing and waiting steps to allow the re-equilibration of the medium to ambient O_2 concentrations (Figure 20, red line). The ideal amount was chosen at equilibrium between oxygen con-

sumption and sufficient re-equilibration (Figure 20, blue line). Ideal concentrations were 3 µg/20 µl for liver and muscle mitochondria and 5 µg/20 µl for C2C12 as described in 3.2.8.1.

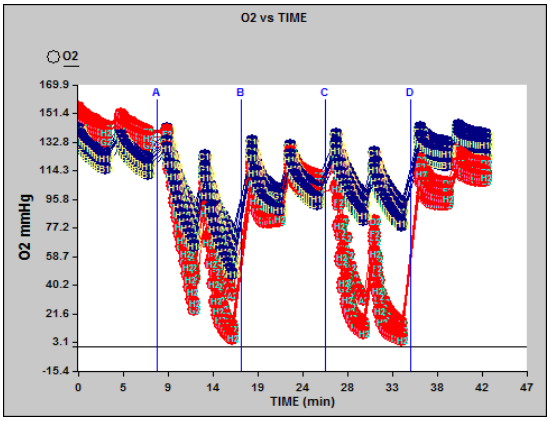

Figure 20: O_2 level data over the time course of a measurement. Too high number of cells or too high protein amount of isolated mitochondria leading to inadequate re-equilibration of the buffer to ambient O_2 concentration during mixing and waiting and consequently limiting respiration= red line. Ideal cell number or protein amount ensured adequate re-equilibration of the buffer= blue line. A= ADP injection, B= Oligomycin injection, C= FCCP injection, D= Antimycin A + Rotenone injection.

After protein amount and cell number were set, final concentrations of adenosine diphosphate (ADP) and carbonyl cyanide-p-trifluoromethoxyphenylhydrazone (FCCP) were titrated. Cell types and different tissues vary in the amount of ADP required for maximal oxidative phosphorylation induction and their response to the mitochondrial uncoupler FCCP. Substrates were added in excess and ADP and FCCP were injected in different concentrations to determine dose response data. ADP was injected after basal state to final concentrations of 0 to 16 mM (Figure 21 left graph) and FCCP was injected after ADP and oligomycin to final concentrations from 0 to 16 µM (Figure 21 right graph). The minimal ADP concentration necessary to maximally induce oxidative phosphorylation was 5 mM, therefore 6 mM were used in further assays (titration for isolated C2C12 mitochondria shown in Figure 21 left). An FCCP concentration of 5 µM was used ensuring a full uncoupling of respiration but avoiding a decrease in maximal respiration (shown for isolated C2C12 mitochondria, Figure 21 right).

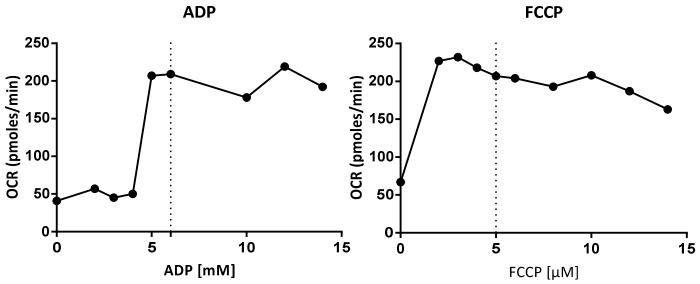

Figure 21: Seahorse XF96 - Titrations of ADP and FCCP to determine the final concentrations needed to induce maximal respiration. OCR= oxygen consumption rate. Dotted line shows chosen concentration in further experiments.

4.1.2.2 Respiratory analysis on an Oxygraph 2k

High-resolution respirometry (HRR) was established for permeabilised murine and human muscle fibers, isolated mitochondria, digitonised cells and tissue homogenates. Mild detergents, saponin for muscle fibres and digitonin for intact cells, were used to selectively perforate the cell membrane to facilitate substrate, uncoupler and inhibitor action on the electron transport chain. During mitochondrial isolation or tissue and sample preparation the outer mitochondrial membrane may become damaged leading to a release of cytochrome c, which then limits the respiration (Figure 22, upper graph). To check for the mitochondrial integrity cytochrome c was added exogenously in every measurement. Since cytochrome c cannot enter the outer mitochondrial membrane, no or only low increase of respiration after cytochrome c addition is an indicator for intact mitochondria and thus proofs a high quality of mitochondrial preparations (Figure 22, lower graph). Measurements with suspect cytochrome c responses were excluded and sample preparation was mildened as described in the methods section until cytochrome c response was acceptable.

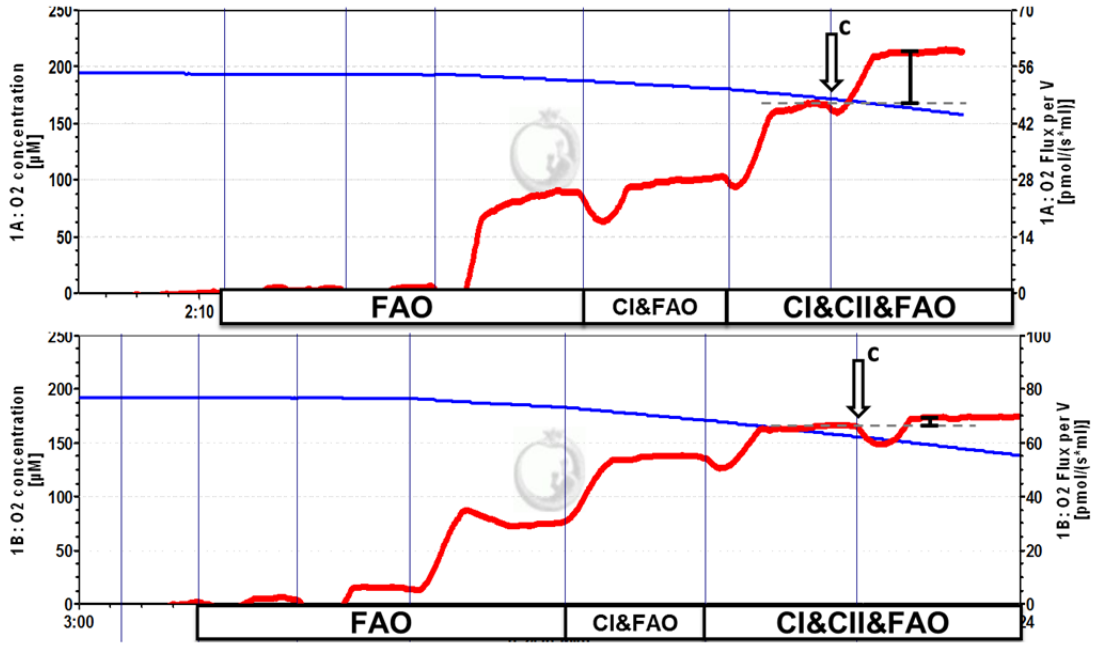

Figure 22: Testing the integrity of the outer mitochondrial membrane. Oxygen concentration (blue line) and respiration rate (red line) measured using a polarographic oxygen electrode. OXPHOS respiration is stimulated by the addition of the substrates octanoylcarnitine and malate for fatty acid oxidation (FAO) with ADP, pyruvate as complex 1 (CI) linked substrate and succinate as mainly complex 2 (CII) linked substrate. 10 µM cytochrome c (c) addition marked with black arrow) is added to assess outer membrane integrity. An increase in respiration with exogenously added cytochrome c is observed if the outer mitochondrial membrane is damaged (upper graph: 25.9% increase after cytochrome c addition). Lower graph shows a measurement of intact mitochondria (3.8%).

Final concentrations of substrates, uncoupler and digitonin (for intact cells) were titrated first for every tested sample material (Figure 23). The uncoupler FCCP was titrated individually in every analytical run. Substrates and digitonin were titrated once to investigate the final concentration necessary to

obtain the maximal possible induction of respiration. Final concentrations used for further experiments are tabulated in Section 3.2.8.2.

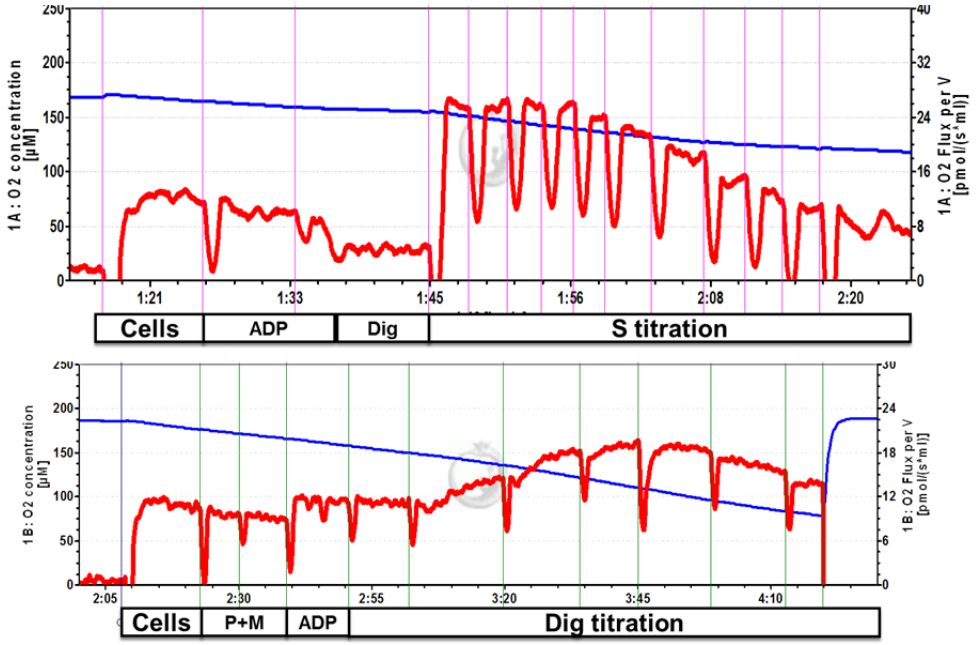

Figure 23: Titrating succinate (S; upper graph) and digitonin (Dig) to permeabilise cells (lower graph). Oxygen concentration (blue line) and respiration rate (red line) measured using a polarographic oxygen electrode. Optimal final succinate concentration was performed after cells were provided with rotenone, ADP and digitonised for permeabilisation (upper graph). Succinate concentration inducing the maximal respiration was used. Rotenone was added to avoid oxaloacetate accumulation and thereby a succinate dehydrogenase inhibition. Optimal digitonin concentration was investigated after addition of pyruvate (P), malate (M) and ADP to stimulate oxidative phosphorylation. Without permeabilisation by digitonin, substrates cannot enter the outer mitochondrial cell membrane. Accordingly, the addition of digitonin leads to an increase of respiration by enabling the substrates to enter the mitochondria. Titrations for other substrates are not shown.

4.1.2.2.1 Respiratory measurements in permeabilised murine muscle fibres in Oxygraph-2k

Respiratory measurements in permeabilised murine muscle fibres were optimised by testing different separation techniques by forceps, tissue handling, buffer compositions, saponine concentrations and incubation times. After modifying all steps permeabilised muscles from mouse soleus and gastrocnemius muscles were analysed following the protocol described in 3.2.8.2.3, leading to a cytochrome c injection response below 2%, indicating an intact outer mitochondrial membrane. The applied substrates and inhibitors were already described for isolated mitochondria (3.2.8.2.2). To test the reproducibility of the established sample preparation and the sensitivity of the Oxygraph-2k in general, two oxidatively distinct muscles were chosen as proof of principle application. Oxidative capacity was higher in soleus muscle throughout all respiratory states than in gastrocnemius muscle (Figure 24). The increase of oxygen flux in percent after ADP addition was significantly higher in soleus muscle (respiration on Oct and M) than in gastrocnemius muscle. After pyruvate addition, the percental increase of respiration was significantly higher in gastrocnemius muscle.

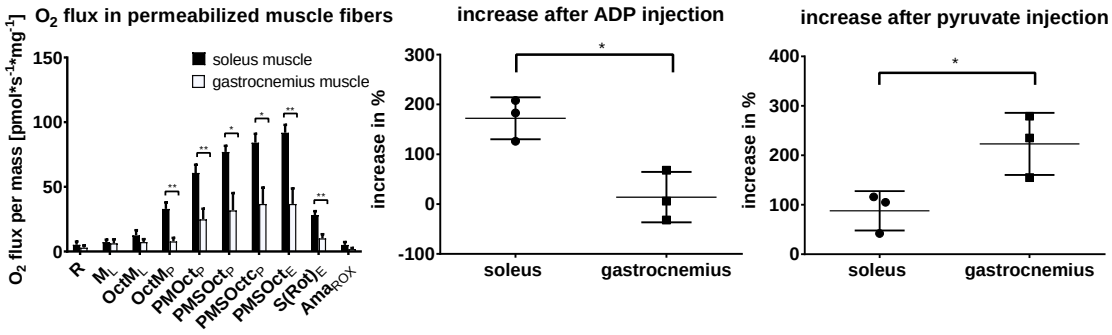

Figure 24: Oxygen fluxes per mass in soleus and gastrocnemius muscle (mean + SD; n= 3). Data were normalised for wet weight of the inserted sample. Malate and octanoylcarnitine (M, Oct) were injected to induce fatty acid oxidation. LEAK respiration (L) is the oxygen consumption under non-phosphorylating conditions due to the proton leak. ADP was added to induce oxidative phosphorylation (subscript $_P$, OXPHOS). Pyruvate (P) was used as complex 1-associated substrate and succinate (S) as mainly complex 2-linked substrate. FCCP, a synthetic uncoupler, was titrated to uncouple the electron transport chain activity from ATP production and determine the maximal oxidative capacity of the electron transport chain (subscript $_E$). Complex 1 was inhibited by rotenone (Rot) to investigate solely complex 2-associated respiration. The non- mitochondrial background respiration or residual oxygen consumption (ROX) were determined by addition of antimycin A (Ama) to inhibit the cytochrome c reductase. Students´s t-test was performed.

4.1.2.2.2 Respiratory measurements in permeabilised human muscle fibres on Oxygraph 2-k

The murine Oxygraph-2k protocol (3.2.8.2.3) had to be modified for human muscle fibres, because it led to an increase of respiration after cytochrome c injection over 2% in human muscle biopsies (data not shown). Fibre separation technique by forceps, tissue handling, buffer compositions, saponin purity, fibre handling and incubation times were optimised. Permeabilised muscles from biopsies from the vastus lateralis were analysed following the optimised protocol described in 3.2.8.2.4. The applied substrates and inhibitors were already described for isolated mitochondria (3.2.8.2.2). After modification of sample processing the cytochrome c response was below 2% (Figure 25), indicating an intact outer mitochondrial membrane.

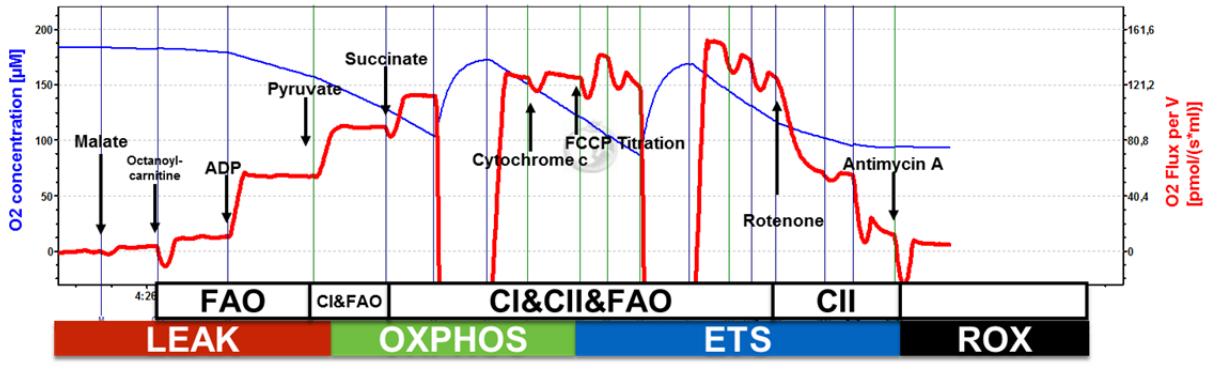

Figure 25: Exemplary run of an Oxygraph-2k measurement with permeabilised human muscle fibres. blue line: O_2 concentration [nmol/ml]; red line: O_2 flux [pmol/(s*ml)]. Malate and octanoylcarnitine (M, Oct) were injected to induce fatty acid oxidation (FAO). LEAK respiration is the oxygen consumption under non-phosphorylating conditions due to the proton leak. ADP was added to induce oxidative phosphorylation (OXPHOS). Pyruvate (P) was used as complex 1-associated substrate (CI) and succinate as mainly complex 2-linked substrate (CII). FCCP, a synthetic uncoupler, was titrated to uncouple the electron transport chain activity from ATP production and determine the maximal oxidative capacity of the electron transport chain (electron transfer system capacity= ETS). Complex 1 was inhibited by rotenone to investigate solely complex 2-associated respiration. The non-mitochondrial background respiration or residual oxygen consumption (ROX) were determined by addition of antimycin A to inhibit the cytochrome c reductase.

4.1.3 Animal experiments

4.1.3.1 Establishment and optimisation of a valid mitochondrial oxysterol profiling strategy in liver tissue and hepatic mitochondria (fresh/frozen tissue, mitochondria isolation and oxysterol extraction fresh/frozen with or without butylated hydroxytoluene (BHT))

Based on the pre-analytical inconsistency of the use[230,234,235] or non-use[113,129,236] of an antioxidant like butylated hydroxytoluene (BHT) in oxysterol analyses, the effect of BHT addition on oxysterol pattern was compared. The use of frozen instead of fresh samples, which simplifies the overall experimental processes, was also addressed. A robust and valid strategy for oxysterol analyses in liver tissue and liver mitochondria was defined, since so far to our knowledge a strategy for a quantitative oxysterol profile of mitochondria has not yet been defined in literature. The results were validated with functional and kinetic experiments and the strategy was applied on samples of an oxidative stress mouse model.

4.1.3.1.1 Liver tissue oxysterol profiling: Is the antioxidant BHT necessary and is it possible to use frozen instead of fresh tissue?

Two pivotal steps in liver tissue processing for oxysterol analyses were addressed. The effects on the oxysterol pattern of no antioxidant versus BHT addition were systematically investigated and the effects of using frozen instead of fresh tissue were examined. Therefore, all samples were extracted with or without BHT (5 µg/ml) and the oxysterol pattern in fresh and frozen liver tissue were compared (3.2.2.2). In total, 16 oxysterols were detected in 20 mg liver tissue irrespective of the presence of BHT or using fresh or frozen sample material. Unexpectedly, the absence of BHT did not significantly affect the yield of the 16 detected oxysterols in liver tissue (Figure 26 A). Furthermore, also frozen tissue can be used (Figure 26 B), no significant effect on the oxysterol yield and pattern was detected in comparison to fresh tissue.

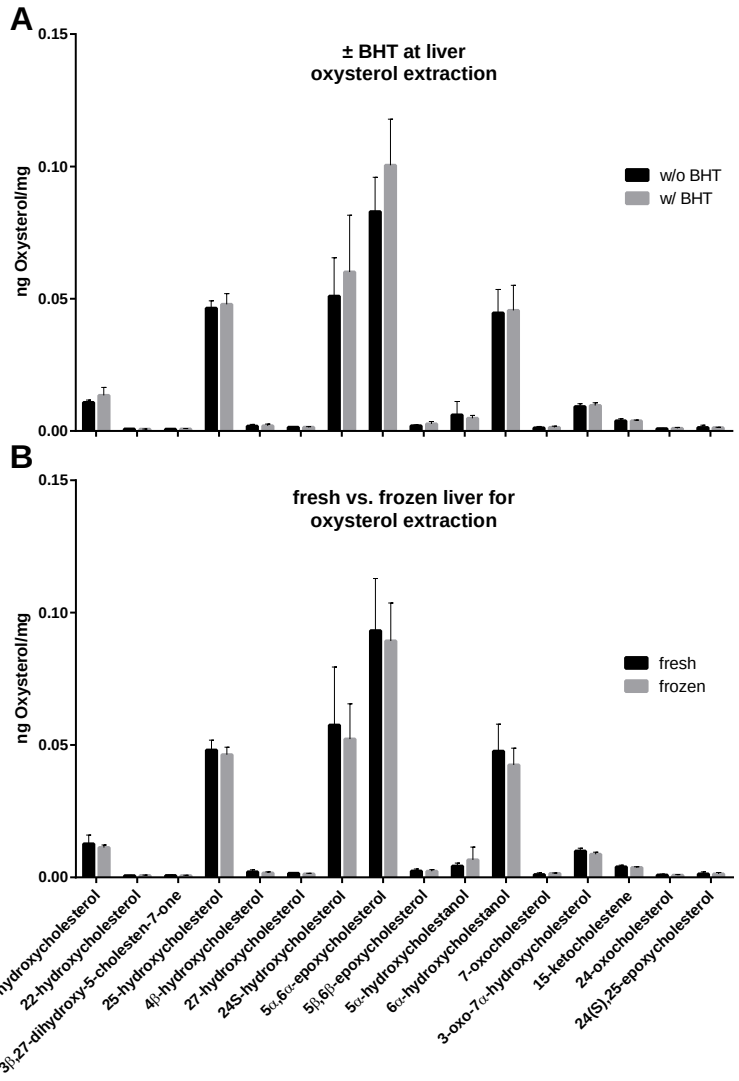

Figure 26: Oxysterols in liver tissue (n= 4-5 per group). A: Oxysterol extraction ± BHT; given are the means and the standard deviation of w/o and w/ BHT samples (fresh and frozen tissue taken together). B: Extraction from fresh vs. frozen liver. Given are the means and the standard deviation of fresh and frozen samples (samples w/o and w/ BHT taken together). BHT= butylated hydroxytoluene, fresh= tissue was extracted directly after harvesting, snap-frozen= extraction after one freeze-thaw-cycle.

4.1.3.1.2 Liver mitochondria oxysterol profiling: Is the antioxidant BHT necessary at every processing step and is it possible to use frozen instead of fresh mitochondria isolates?

To define a robust and valid method for oxysterol analyses in isolated mitochondria, different pivotal conditions throughout oxysterol analyses were systematically compared (Figure 27 A; 3.2.6.4.1): firstly, the presence or absence of BHT (5 µg/ml) during the mitochondrial isolation from fresh liver (ca. 150 mg), secondly, the usage of frozen vs. fresh mitochondria for oxysterol extraction (50 µg mitochondria by protein, 3.2.10.4) and thirdly, the presence or absence of BHT during oxysterol extraction from mitochondria. Finally, it was also tested if the presence of BHT during mitochondria isolation may alter mitochondrial function by analysing mitochondrial respiration (Oxygraph-2k, Oroboros; 3.2.8.2.6).

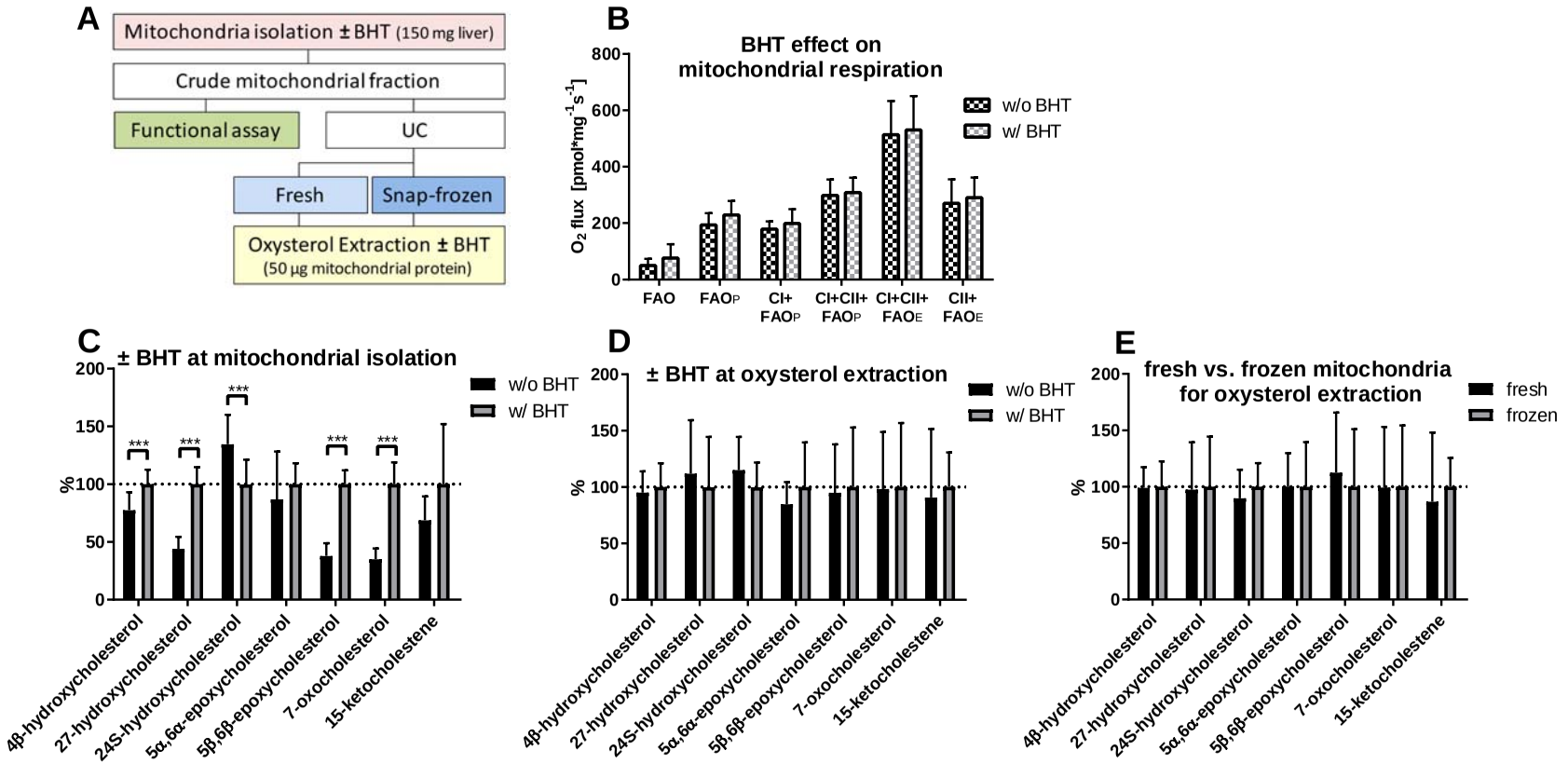

Figure 27: Oxysterols in liver mitochondria: A: experimental design, B: functional assay - investigation of BHT effect on mitochondrial respiration using an OROBOROS Oxygraph-2k; FAO= fatty acid oxidation (octanoylcarnitine + malate), p= phosphorylating (ADP), CI= complex I respiration (pyruvate), CII= complex II respiration (succinate), E= uncoupled maximal respiration (FCCP), C: Impact of BHT added during mitochondrial isolation on oxysterol yield - relative oxysterol levels of mitochondria isolated with and without BHT (relative data= w/ BHT set to 100%; fresh and frozen tissue and samples w/o and w/ BHT at oxysterol extraction taken together), D: Impact of BHT on oxysterol yield added during oxysterol extraction- relative oxysterol levels of mitochondria extracted with and without BHT (relative data, w/ BHT set to 100%; fresh and frozen tissue and samples w/o and w/ BHT during mitochondria isolation taken together), E: Impact of the usage of fresh or frozen mitochondria for oxysterol extraction- relative oxysterol levels of fresh vs. frozen mitochondria (relative data, frozen set to 100%; samples w/o and w/ BHT during oxysterol extraction and during mitochondria isolation taken together). Given are the means with standard deviation (n= 4/group in each experiment). B: student´s t-test, C, D, E: FDR; BHT= butylated hydroxytoluene, fresh= mitochondria were directly extracted after isolation, snap-frozen= extraction after one freeze-thaw-cycle. UC= ultracentrifugation.

BHT addition during mitochondrial isolation did not influence respiration of the isolated mitochondria (Figure 27 B). In contrast, the addition of BHT is highly relevant for the oxysterol pattern in isolated mitochondria. Of a total of 7 detected mitochondrial oxysterols, 5 were significantly influenced when BHT was absent during the isolation process (Figure 27 C). Without BHT, the yield of 4β-hydroxycholesterol, 27-hydroxycholesterol, 5β,6β-epoxycholesterol and 7-oxocholesterol was significantly lower and 24S-hydroxycholesterol was significantly higher (Figure 27 C). No changes were detected for 5α,6α-epoxycholesterol and 15-ketocholestene. The absence of BHT during the last step, the oxysterol extraction (3.2.10.4) from isolated mitochondria, did not influence the oxysterol level (Figure 27 D). Moreover, as for liver tissue, frozen mitochondria can also be used (Figure 27 E) given that BHT was present during the mitochondria isolation procedure. Notably, the usage of an antioxidant early in sample processing does not change mitochondrial function (Figure 27 B). Another finding was that frozen mitochondria can equally well be used.

4.1.3.1.3 Is autoxidation the culprit of the detected alterations in the mitochondrial oxysterol profiles?

Oxysterols can be autoxidised by air oxygen or oxidised by reaction with mitochondrial reactive oxygen species or enzymatically. To proof the relevance of autoxidation, the concentrations of pure oxysterol standards (4β-hydroxycholesterol, 27-hydroxycholesterol, 7-oxocholesterol) and cholesterol with and without BHT after 5 and 24 h incubations at 4 °C (Figure 28 A, 3.2.9) were determined. By this experimental setup not only oxysterol stability but also possible oxysterols autoxidised from cholesterol were investigated. The 5-h incubation at 4 °C in open tubes including shaking from time to time resembles the condition of mitochondrial isolation performed in this study, whereas the 24 h incubation at room temperature (RT) without BHT was performed to take possible extreme time delays and temperature variations into account.

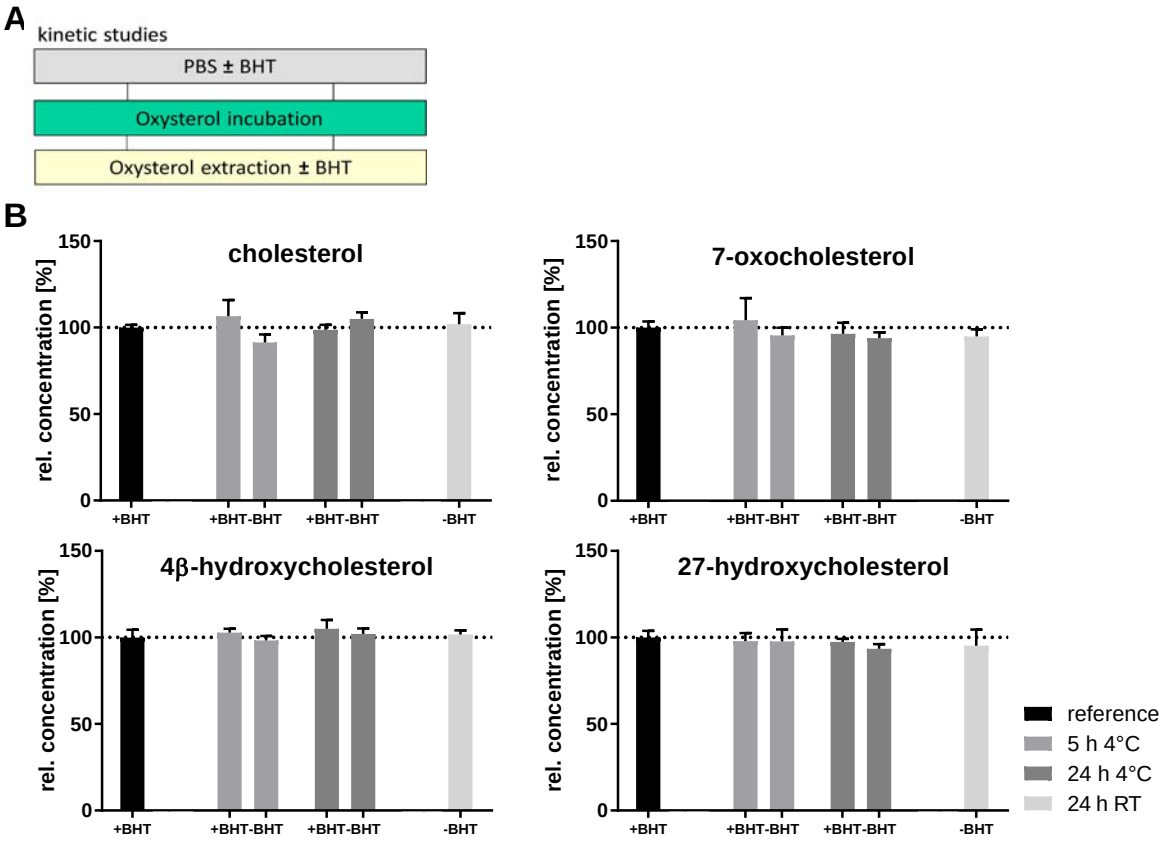

Figure 28: In vitro kinetics of oxysterol concentration incubated in PBS - investigation of stability and possible conversion products. A: experimental design, B: In vitro incubation of cholesterol, 7-oxocholesterol, 4β-hydroxycholesterol and 27-hydroxycholesterol in PBS either with or without BHT (+/- BHT), at different temperatures (4 °C and RT) and different durations (5 h and 24 h). Reference (set to 100%): cholesterol and the oxysterol standards were directly processed without any incubation delay. 5 h at 4 °C are mimicking the time and conditions during mitochondrial isolation. 24 h at RT without BHT were performed as an extreme condition for these oxidation-prone substances. RT= room temperature.

Neither the oxysterols 4β-hydroxycholesterol, 27-hydroxycholesterol and 7-oxocholesterol nor cholesterol showed significantly changed concentrations after up to 24 h even at RT (Figure 28 B). Autoxidation alone cannot explain the detected alterations in the mitochondrial oxysterol profiles (Figure 27).

4.1.3.1.4 Proof of principle experiment: Oxysterols in liver and liver mitochondria from mice after reactive oxygen stress induction

To validate the defined strategy, namely adding BHT from the beginning and using frozen tissue, tissue (3.2.2.2) and mitochondria samples (3.2.6.4.1) of an oxidative stress mouse model (Figure 29 A) were investigated. Oxidative stress was induced by a single dose of doxorubicin, a potent anti-cancer drug, already shown to induce oxidative stress by an increase of reactive oxygen species in liver.[237-239] In total, 13 oxysterols in 20 mg liver and 6 oxysterols in 50 µg mitochondria (by protein) were detected irrespective of doxorubicin treatment.

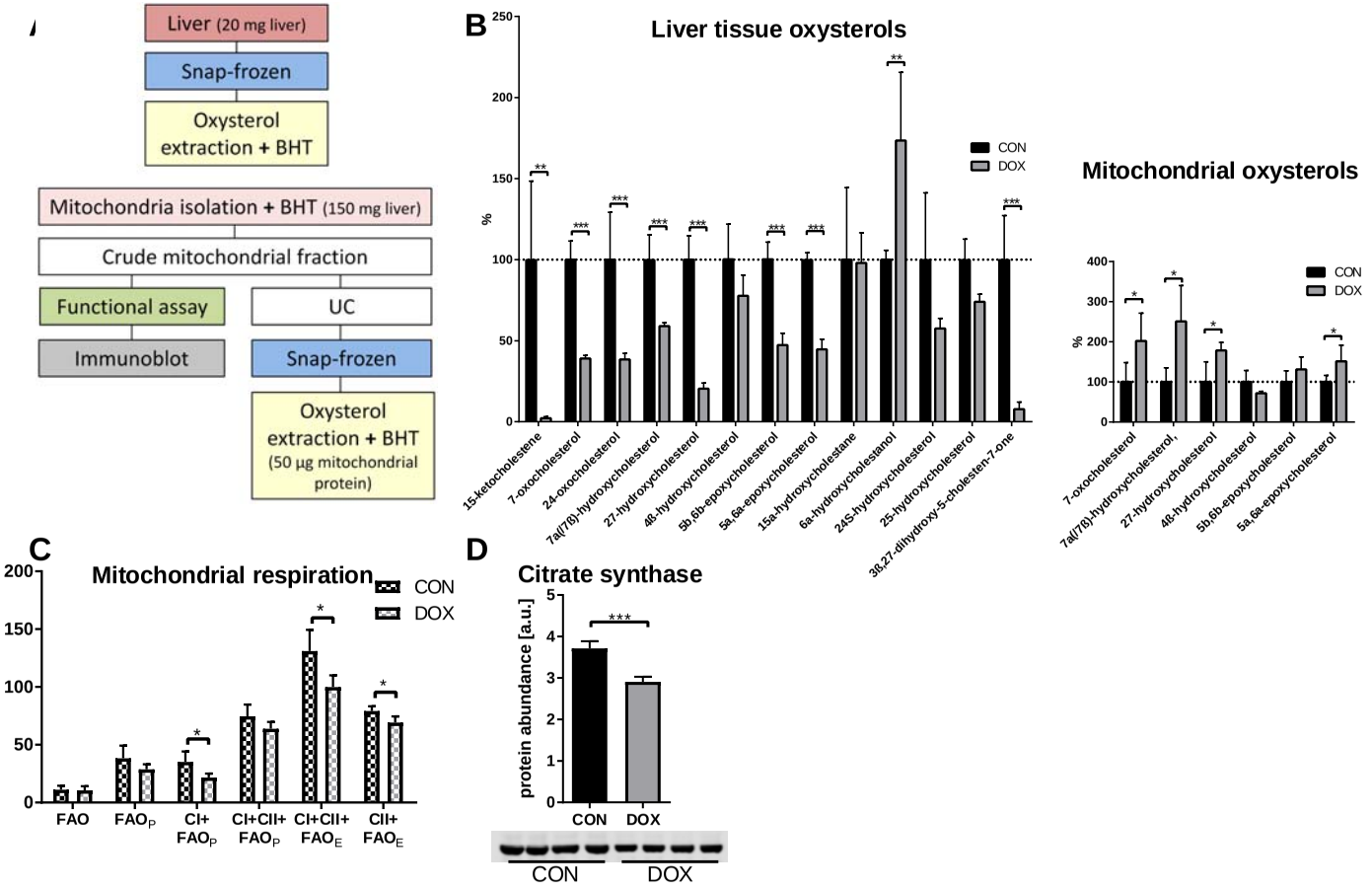

Figure 29: Doxorubicin (DOX) induced oxidative stress reduces mitochondrial oxidative capacity and increases the oxysterol amount in hepatic mitochondria, but not in liver (n= 4/group). A: experimental design, B: impact of DOX on oxysterol yield – relative oxysterol levels of mitochondria isolated from DOX-treated and control mice (CON set to 100%), C: functional analyses of mitochondria - effect of DOX treatment on mitochondrial respiration analysed in an Oxygraph-2k, OROBOROS, here: same volume of mitochondrial suspension was used, FAO= fatty acid oxidation (octanoylcarnitine + malate), p=phosphorylating (ADP), CI= complex I respiration (pyruvate), CII= complex II respiration (succinate), E= uncoupled maximal respiration (FCCP) D: Histogram of a western blot of citrate synthase as mitochondrial marker (same volume of mitochondrial suspension). Each band represents the citrate synthase protein abundance of one mouse sample. B: FDR was applied for testing significance. C, D: student´s t-test; CON= control, DOX= Doxorubicin, UC= ultracentrifugation, BHT= butylated hydroxytoluene, snap-frozen= extraction after one freeze-thaw-cycle.

Unexpectedly, the levels of the detected oxysterols in liver tissue of doxorubicin treated mice (DOX) were lower compared with control mice (Figure 29 B). In contrast, in liver mitochondria of DOX-treated mice an increased amount of the oxysterols was found. Solely 4β-hydroxycholesterol and 5β,6β-epoxycholesterol were not or only slightly changed (Figure 29 B).

The functional investigations given in Figure 29 C showed a reduced respiration in mitochondria isolated from the liver of doxorubicin treated mice (3.2.8.2.6). Also citrate synthase protein amount (Figure 29 D) was lower in doxorubicin treated mice.

4.2 Mitochondrial function and insulin resistance

4.2.1 Cell culture

4.2.1.1 Skeletal muscle cell culture: Analysis of mitochondria from cultured skeletal muscle cells challenged with substrate overflow and insulin resistance: Insulin resistant murine C2C12 myotubes under low/high glucose conditions

It is still unclear whether metabolic overflow leads to disturbances in substrate utilisation and, consequently, insulin resistance (IR) or if mitochondrial dysfunction is a consequence of impaired insulin signalling. Skeletal muscle IR is considered to be the initiating or primary defect that is evident decades before β-cell failure and hyperglycemia develops.[4] Effects of IR induced by chronic exposure to high concentrations of insulin in combination with substrate overflow through high glucose concentrations on skeletal muscle mitochondria were investigated. To this end, functional analyses, western blot analyses of isolated mitochondria from C2C12 myotubes and western blot analyses from total C2C12 cell lysates were performed.

4.2.1.1.1 Total cell lysates of C2C12 myotubes

As a first step, we investigated the efficiency of 48 h insulin treatment with 1 µM insulin (3.2.1.1.2) to induce insulin resistance in cell lysates from C2C12 cells treated either with high glucose concentrations and or chronic insulin on protein level. Each procedure was performed in three replicates. To investigate insulin signalling, cells were first starved for 3 h, stimulated acutely with 100 nM insulin for 15 min, lysed and analysed by western blotting (see 3.2.1.1.2). Phosphorylation of Akt at Ser473 and Thr308 was detected as marker for insulin signalling activation (see Figure 30).

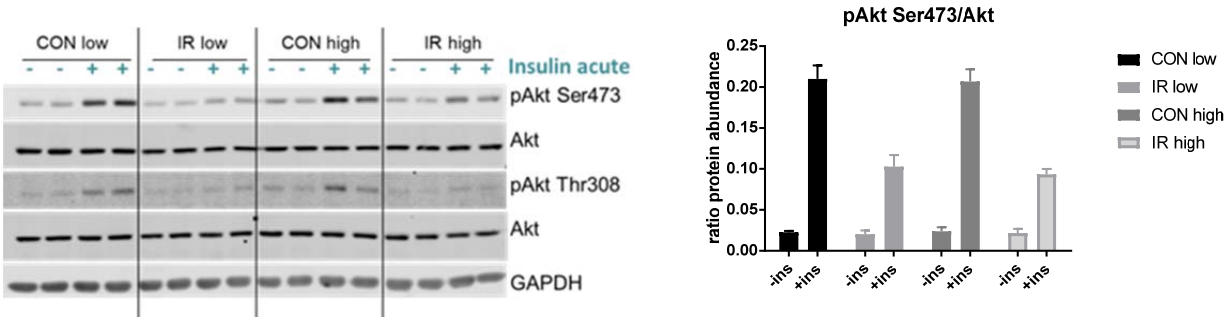

Figure 30: left: Representative western blot of C2C12 lysates using pAkt Ser473 and pAkt Thr308 antibodies to investigate insulin signalling. After starving the cells for 3 h from FCS, insulin signalling was activated by acute insulin stimulation with 100 nM insulin for 15 min (see 3.2.1.1.2). CON= control, IR= chronic insulin (1 µM), low= 5.5 mM glucose, high= 25 mM glucose; GAPDH was used as a housekeeper. Right: The histogram shows the sums of pAkt473/Akt ratio after densitometric quantification of western blots. Values are means ± SD of 3 sets.

C2C12 myotubes treated with chronic insulin showed lower signals of phosphorylated Akt after acute insulin stimulation than control groups, indicating an impaired insulin signalling as intended by this treatment. Further, western blot analyses of C2C12 lysates showed no difference in myosin heavy chain fast isoform (MYH fast) protein abundance (Figure 31) between the treatment groups, indicating no effect of the treatments on differentiation efficiency from myoblasts to myotubes. Thus, high glucose and chronic insulin led to insulin resistance without affecting fusion efficiency in skeletal muscle cells.

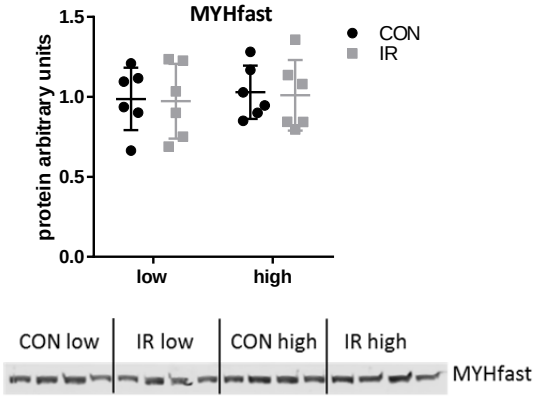

Figure 31: Representative western blot of four C2C12 lysates per group using an antibody against myosin heavy chain fast isoform (MYHfast) as differentiation control. CON= control, IR= chronic insulin (1 µM), low= 5.5 mM glucose, high= 25 mM glucose; histogram shows the sums of the densitometric quantifications of western blots. Values are means ± SD of 6 replicates.

4.2.1.1.2 Mitochondria from C2C12 myotubes

To investigate the effect of an oversupply with glucose and insulin on mitochondrial content in skeletal muscle cells, an activity assay of citrate synthase (Figure 32 A; 3.2.7), often used as a measure of mitochondrial amount,[223] was performed. Citrate synthase activity was not only significantly reduced by chronic insulin treatment but also under high glucose conditions, indicating a reduced mitochondrial content in states of insulin resistance and glucose oversupply. Citrate synthase protein amount

(CS) in total cell lysates (Figure 32 B) showed the same trends as observed in the citrate synthase activity assay.

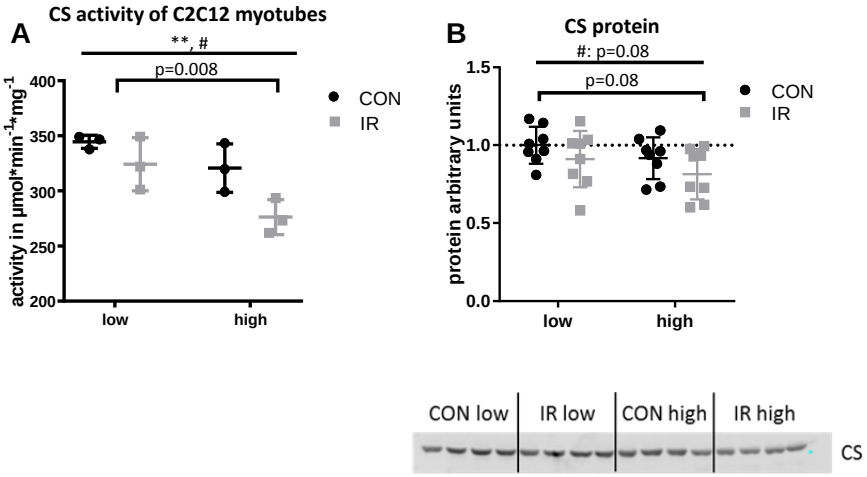

Figure 32: A: Citrate synthase activity in C2C12 lysates in µmol/min*mg[9], CON= control, IR= chronic insulin (1 µM), low= 5.5 mM glucose, high= 25 mM glucose; values are means ± SD of 3 replicates. B: histogram shows the sums of the densitometric quantifications of western blots. Values are means ± SD of at least 8 replicates. Representative western blot of four C2C12 lysates per group using an antibody against citrate synthase (CS) as mitochondrial content marker. 2way ANOVA (significances shown with "—"): *=significantly different for low to high glucose conditions, #=significantly different for CON to IR conditions. Multi comparison significances shown with "⌐¬".

To assess if the observed lower amount of mitochondria under insulin and high glucose treatment also affects the mitochondrial function, respiratory analyses were performed in permeabilised cells in an Oroboros Oxygraph-2k (Figure 33). Indeed, ADP-induced oxidative phosphorylation in the presence of the complex 1-associated substrate pyruvate with malate was significantly lower in mitochondria from cells under high glucose conditions. Insulin treatment, however, had no significant effect on mitochondrial respiration (Figure 33 B). The same trend was also seen for glutamate- and succinate-linked respiration and uncoupled respiration (Figure 33 A), indicating a decreased respiration due to a decreased mitochondrial content as observed in Figure 32 A. However, the contribution of complex 2-associated respiration towards maximal uncoupled respiration (C1 and C2) was higher under high glucose conditions than in low glucose conditions (Figure 33 C). These differences in oxidative phosphorylation and complex contributions to maximal respiration were further elucidated on protein level.

[9] Performed by bachelor student Daniel Bleher under supervision of Lisa Kappler and Miriam Hoene

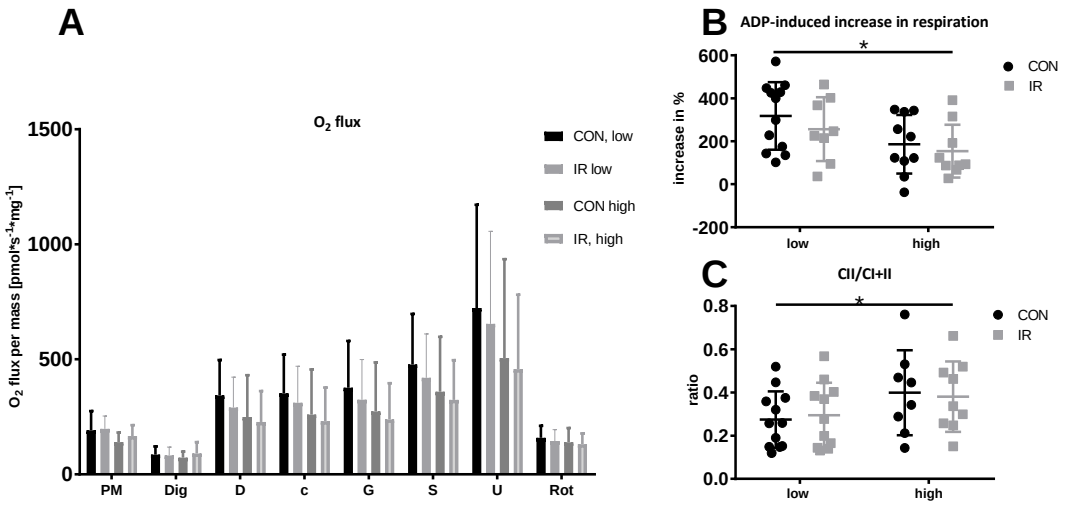

Figure 33: Mitochondrial respiration analyses in digitonised C2C12 myotubes using an Oxygraph-2k[10] CON= control, IR= chronic insulin (1 µM), low= 5.5 mM glucose, high= 25 mM glucose; A: O_2flux per mg cell lysate protein over the measurement course, PM= pyruvate and malate, Dig= digitonin, D= ADP, c= cytochrome c, G= glutamate, S= succinate, U= FCCP titration to uncouple respiration, Rot= rotenone, corrected for non-mitochondrial background. B: Percentaged increase of respiration after ADP addition with octanoylcarnitine and malate present as substrates. C: Contribution of C2-associated respiration towards maximal C1- and C2-associated maximal respiration. * significantly different between low glucose and high glucose condition, 2way-ANOVA (significances shown with "___").

[10] Performed by bachelor´s student Daniel Bleher under supervision of Lisa Kappler and Miriam Hoene

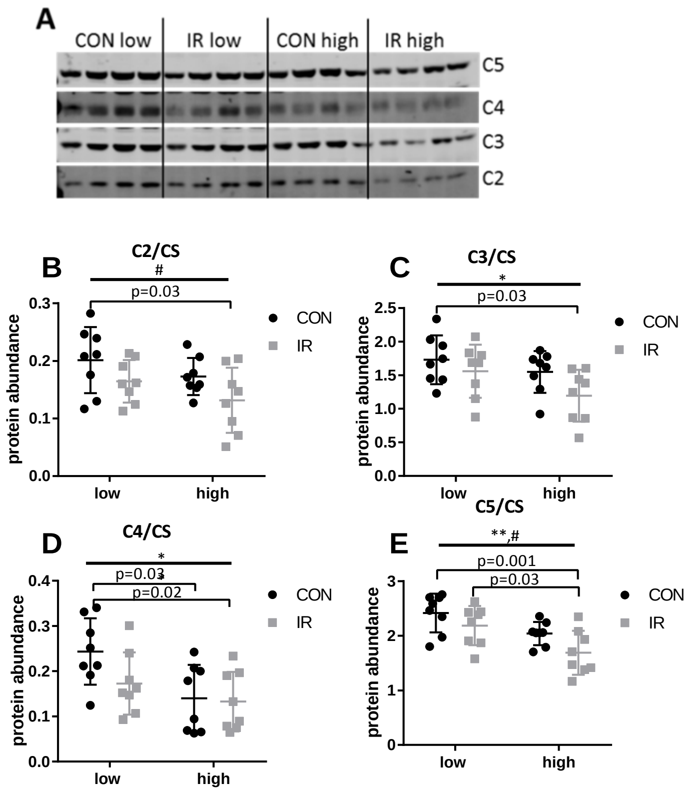

Figure 34: Representative western blot of four C2C12 lysates per group using antibodies against mitochondrial complexes (C2-C5, C1 was below detection limit). CON= control, IR= chronic insulin (1 µM), low= 5.5 mM glucose, high= 25 mM glucose; histograms show the sums of the densitometric quantifications of western blots. Values are means ± SD of 8 replicates. 2way ANOVA (significances shown with "▬"): *=significantly different for low to high glucose conditions, #=significantly different for CON to IR conditions. Multi comparison significances shown with "┌──┐".

Treatment group-specific abundances of proteins of the electron transport chain were quantified in cell lysates of C2C12 (Figure 34). Mitochondrial content was monitored using citrate synthase as a marker. Electron transport chain protein abundances of the complexes were normalised to mitochondrial content (CS protein abundance; Figure 32) to investigate their protein levels independently of a decreased mitochondrial content in states of glucose oversupply and insulin resistance. The abundance of complex 1 was below detection limit. complex 2 protein abundance was significantly lower in IR than in CON treated cells (Figure 34 B). Complex 3 and 4 protein abundances were significantly lower under high glucose conditions (Figure 34 C+D). Complex 5 was of significantly lower abundance following chronic insulin conditions (IR) and under high glucose conditions (Figure 34 E). Even after normalisation to mitochondrial content electron transport chain complexes are reduced after high glucose treatment or chronic insulin or even by both, indicating that the reduced mitochondrial amount is not the solely contributor to the altered mitochondrial function.

4.2.1.1.3 Decreased superoxide dismutase in mitochondria isolated from C2C12 myotubes

Increasing evidence suggests that oxidative stress plays a major role in the pathogenesis of type 2 diabetes mellitus.[85] Increased oxidative stress is associated with damage of cellular organelles and

enzymes, increased lipid peroxidation, and development of insulin resistance.[84] Mitochondria are major sources of reactive oxygen species in cells.[47] Approximately 0.01% to 5% of electrons passing down the electron transport chain leak to oxygen during oxidative respiration, which is converted to reactive oxygen species.[47,79] Hence, the detected changes in oxidative respiratory capacity due to high glucose treatment of C2C12 (Figure 33) might possibly also affect reactive oxygen production. Therefore, oxidative stress and related enzymes were investigated. Superoxide dismutase levels (SOD1 and 2) in whole cell lysates employed by western blot analyses were not changed by the high glucose and insulin treatment (Figure 35; treatment described in 3.2.1.1.2). High levels of 4-HNE are attributed to endogenous lipid peroxidation caused by oxidative stress,[222] but no concentration change was observed in our experiments. Investigating isolated mitochondria, however, lead to the indication of a treatment effect more prominent on mitochondrial level.

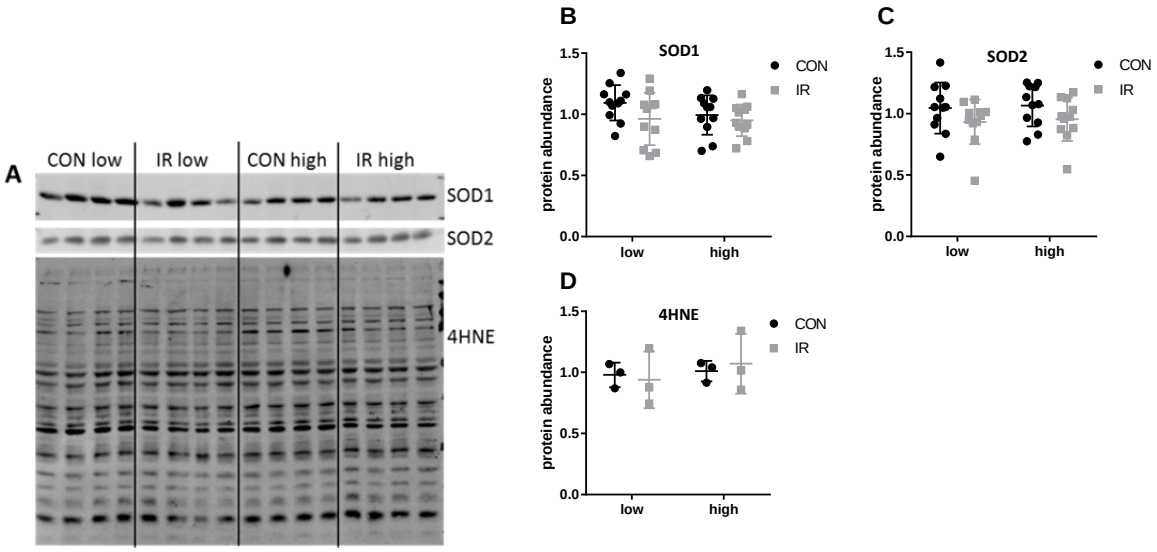

Figure 35: A: Representative western blot of four C2C12 lysates per group using antibodies against superoxide dismutases (SOD1, SOD2) and 4-hydroxynonenal (4HNE) as oxidative stress marker. CON= control, IR= chronic insulin (1 µM), low= 5.5 mM glucose, high= 25 mM glucose; B-D: histograms show the sums of the densitometric quantifications of western blots. Values are means ± SD of at least 3 replicates.

Both hyperinsulinemia and glucose oversupply caused a decreased SOD activity in isolated mitochondria (Figure 36 A). Western blot analyses of mitochondrial fractions showed also decreased SOD1 protein abundances under insulin treatment, not seen for SOD2 abundances (Figure 36 C+D). 4-Hydroxynonenal protein levels (3.2.5) in isolated mitochondria were not changed between the groups (data not shown).

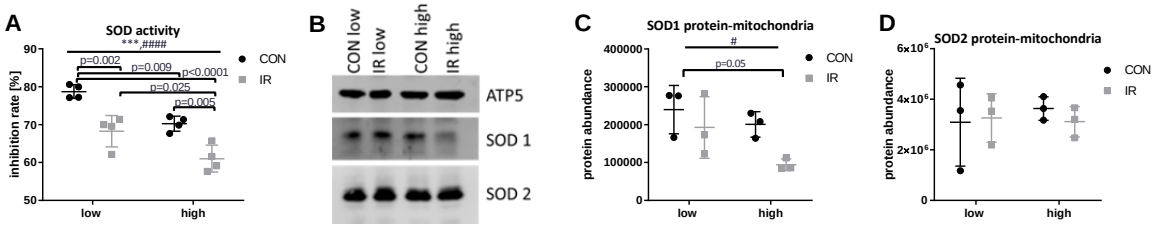

Figure 36: A: SOD activity in isolated mitochondria; B: Representative western blot of C2C12 mitochondrial fractions using antibodies against ATP-Synthase 5 (ATP5) as mitochondrial marker, superoxide dismutases (SOD1, SOD2). C+D: histograms show the sums of the densitometric quantifications of western blots. Values are means ± SD of 3 replicates. CON= control, IR= insulin (1 µM), low= 5.5 mM glucose, high= 25 mM glucose, SOD= superoxide dismutase. 2way ANOVA (significances shown with "⎯"): *=significantly different for low to high glucose conditions, #=significantly different for CON to IR conditions. Multi comparison significances shown with "⌐¬".

Effects of IR induced by chronic exposure to high concentrations of insulin in combination with substrate overflow through high glucose concentrations on skeletal muscle mitochondria were investigated. Chronic insulin treatment was shown to be an effective inducer of insulin resistance in C2C12 cells. While not affecting oxidative capacity of mitochondria, IR reduced mitochondrial content in the myotubes as well as SOD activity and SOD 1 protein abundance solely on mitochondrial levels. Independently of the decreased mitochondrial content insulin treated cells had lower abundances of complex 2 and complex 5 protein. Glucose oversupply reduced mitochondrial respiration probably due to a decreased mitochondrial amount. Oxidative defence was also reduced under high glucose conditions. Independently of the reduced mitochondrial amount, high glucose led to decreased complex protein abundances of C2, C4 and C5.

4.2.2 Mouse experiments

4.2.2.1 Tissue-specific comparison: liver and skeletal muscle mitochondria

4.2.2.1.1 Mitochondria show tissue-specific characteristics in respiratory functional analyses

High-resolution respirometry (HRR) of isolated mitochondria showed differing substrate preference between liver and muscle mitochondria (Figure 37, murine). With octanoylcarnitine and malate present, muscle mitochondria oxidised significantly larger amounts of the complex 1 substrate pyruvate (Figure 37 A), whereas liver mitochondria respired more after addition of the complex 2 associated substrate succinate (Figure 37 B). This finding was not only found in mice, but also detected when human liver samples and human muscle biopsies were compared (Figure 37 human; Supplementary Figure 3; protocol described in 3.2.8.2.4 and 3.2.8.2.5). Contribution of complex 2 associated substrate oxidation to maximal respiration on complex 1 and 2 substrates was higher in liver (Figure 37 C). Liver and muscle mitochondria also differed in their respiratory profiles: in muscle mitochondria ADP caused a higher increase of phosphorylating respiration compared to leak respiration in liver mitochondria (Figure 37 D). The P/E-ratio (phosphorylating respiration relative to the maximal uncou-

pled respiration) was not different between muscle and liver mitochondria (Figure 37 E). The P/E-ratio takes coupling and limitations of OXPHOS capacities into account.

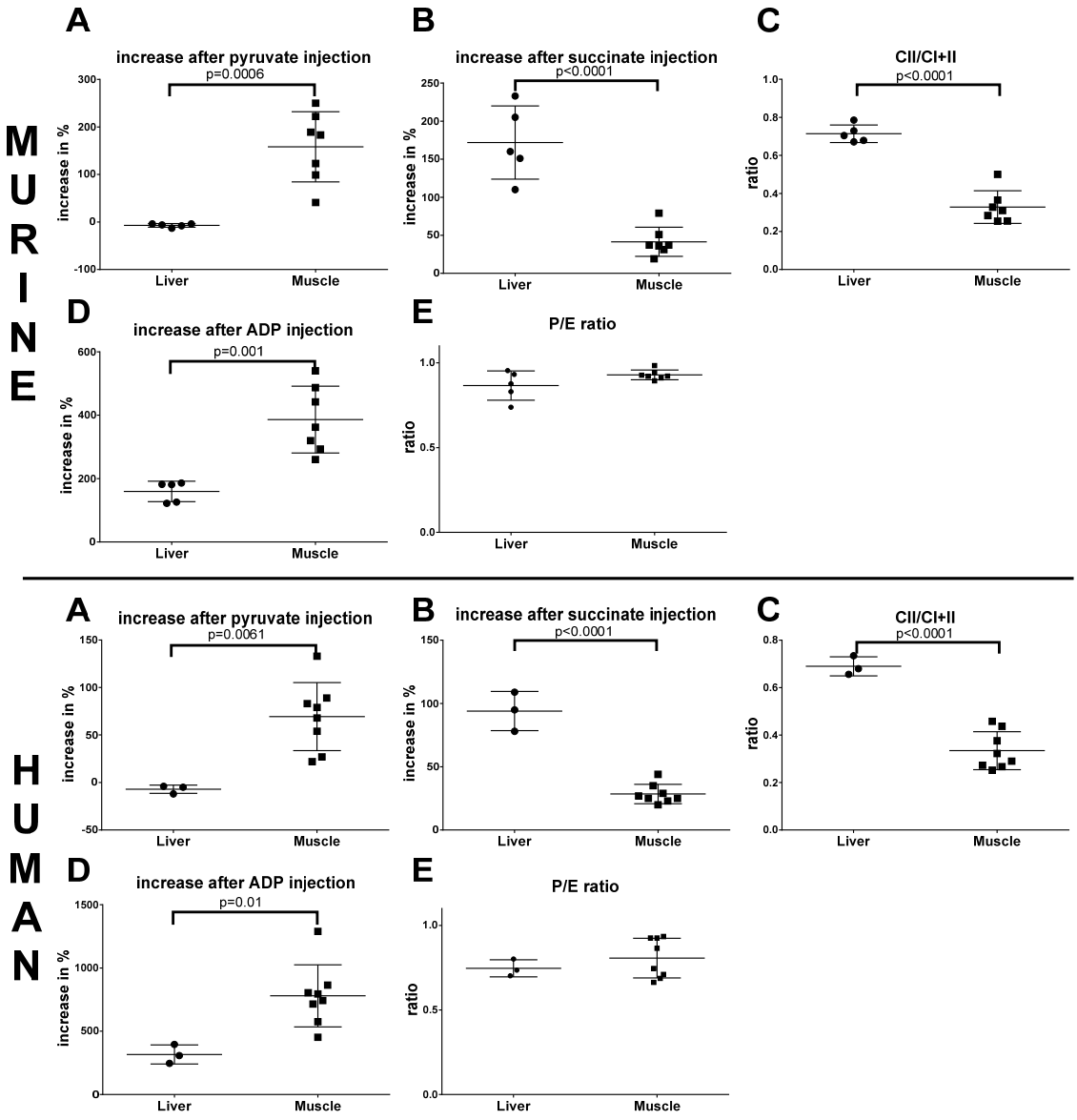

Figure 37: Respiratory analyses of murine liver and skeletal muscle mitochondria and human liver and skeletal muscle fibres on an Oxygraph-2k: A: increase of phosphorylating respiration after pyruvate (complex 1 substrate) injection; B: increase of phosphorylating respiration after succinate (complex 2 substrate) injection; C: Ratio of maximal uncoupled complex 2 respiration to total maximal uncoupled respiration with C1 and C2 substrates; D: Increase of respiration in % after ADP injection in the presence of octanoylcarnitine and malate; E: P/E ratio: phosphorylating respiration (after ADP injection) relative to uncoupled maximal respiration (titrated using the synthetic protonophore FCCP). High-resolution respirometry (HRR) of skeletal muscle mitochondria was performed for 7 mice (n= 7) and for liver mitochondria for 5 mice (n= 5). High-resolution respirometry (HRR) of human skeletal muscle fibres was performed in n= 8[11] and for human liver tissue in n= 3. Student´s t-test was performed.

Mitochondrial phospholipid content and composition have been shown to affect electron transport chain activity and respiratory function.[71,72,92] The relationship between mitochondrial function and

[11] High-resolution respirometry of human skeletal muscle fibers was partially performed by Christoph Hoffmann

mitochondrial lipid composition, particularly in tissue samples, still remains not completely understood.

4.2.2.1.2 Comparative lipid profiling of mitochondria isolated from mouse skeletal muscle and liver tissue

In total, 276 lipids from liver and 278 lipids from muscle from 16 (sub-)classes, 3 ceramide (CER), 24 cardiolipin (CL), 8 lyso-phosphatidylcholine (LPC), 8 lyso-phosphatidylethanolamine (LPE), 2 lyso-phosphatidylinositol (LPI), 51 phosphatidylcholine (PC), 4 phosphatidylcholine plasmalogen (PC-P), 55 for liver/57 for muscle phosphatidylethanolamine (PE), 16 for liver/17 for muscle phosphatidylethanolamine plasmalogen (PE-P), 19 for liver/17 for muscle phosphatidylglycerol (PG), 19 phosphatidylinositol (PI), 13 phosphatidylserine (PS), 5 for liver/6 for muscle phosphatidylserine plasmalogen (PS-P), 6 sphingomyelin (SM), 14 triacylglycerol (TAG) and 29 free fatty acid (FFA) species could be quantified (Figure 38).

The tissue had no major effect on the total number of detected lipid species in thereof isolated mitochondria. 2 PE, 1 PE-P, 1 PS-P species were solely detected in muscle mitochondria and 2 PG species were solely detected in liver mitochondria.

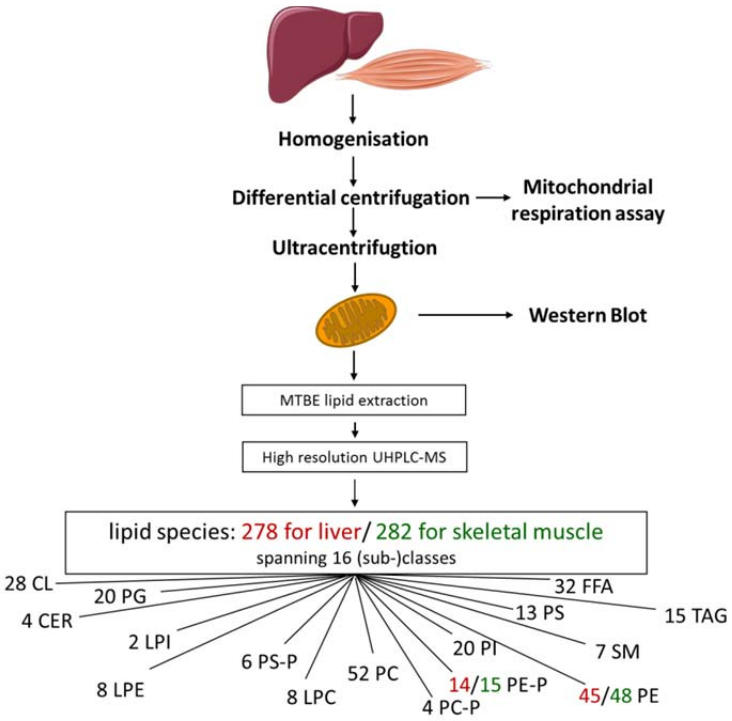

Figure 38: Experimental workflow from sample preparation to respiratory analyses, western blot and lipidomics analyses. See methods section for further details. CER= ceramide, CL= cardiolipin, LPC= lysophosphatidylcholine, LPE= lysophosphatidylethanolamine, PC= phosphatidylcholine, PC-P = phosphatidylcholine plasmalogen, PE= phosphatidylethanolamine, PE-P= phosphatidylethanolamine plasmalogen, PG= phosphatidylglycerol, LPI= lysophosphatidylinositol, PI= phosphatidylinositol, PS= phosphatidylserine, PS-P= phosphatidylserine plasmalogen, SM= sphingomyelin, TAG= triacylglycerol, FFA= free fatty acids, MTBE= methyl tert-butyl ether; liver and muscle picture: Servier Medical Art.

To gain an initial overview of the possible tissue differences in the lipid profiles, a multivariate principal component analysis (PCA, Figure 39; 3.2.13.5) was performed. In the direction of the first principal component a pronounced separation of the clustered hepatic and skeletal muscle-derived mitochondrial samples could be seen. One liver sample was excluded as an outlier as observed in the PCA (Liver 40-13 in Figure 39).

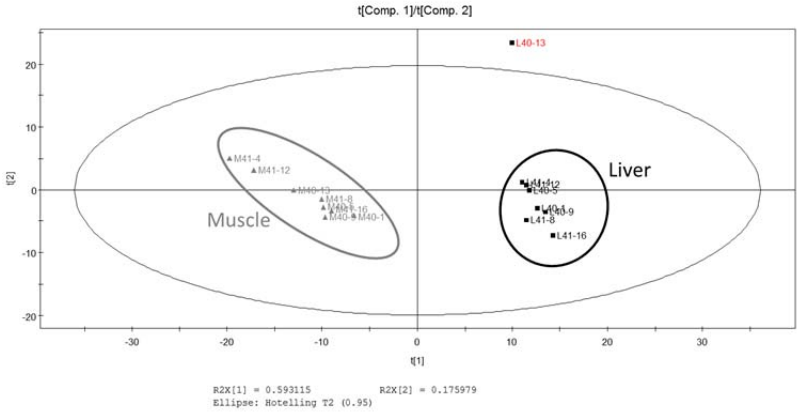

Figure 39: Principal Component Analysis (PCA) scores plot of the first two principal components based on all detected lipids (relative standard deviation in the quality control samples <20% and after par scaling). The first component explains 59.3% of the variation and the second one 17.6%. Each spot represents one mitochondrial sample isolated from mouse liver or skeletal muscle using ultracentrifugation. L= liver, M= skeletal muscle; L40-13 (marked in red) was excluded as outlier.

4.2.2.1.3 Mitochondrial samples isolated from murine skeletal muscle tissue show higher phospholipid levels than mitochondria from liver

To assess, how the lipid composition of the samples differed depending on their tissue origin, a heatmap was generated using the summed amounts of the individual lipid classes (Figure 40). Data were normalised by mean centring and scaled to unit variance. Heatmap analysis of the summed lipid classes indicated that muscle mitochondria had a higher total lipid amount than liver mitochondria (316±49 pmol/µg versus 221±39 pmol/µg total mitochondrial protein). In accordance with the PCA analysis, the heatmap revealed that muscle and liver mitochondria show distinctly different levels of lipids. Solely LPI and TG were lower in muscle-derived than in liver-derived mitochondria.

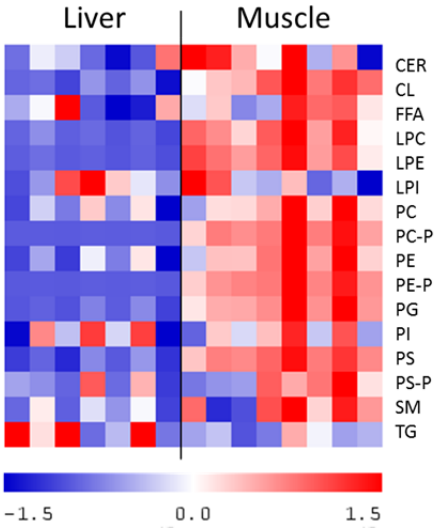

Figure 40: Heatmap visualisation of the sums of the different lipid (sub-)classes in mitochondrial samples from murine liver (n= 7) and muscle (n= 8). Each column represents an individual mitochondrial isolation. Values were centred to the mean of the respective lipid class and scaled to unit variance. White colour shows values close to the mean of the lipid class and red- and blue-coloured values are higher and lower, respectively, than the mean. CER= ceramides, CL= cardiolipins, LPC= lysophosphatidylcholines, LPE= lysophosphatidylethanolamines, PC= phosphatidylcholines, PC-P= phosphatidylcholine plasmalogens, PE= phosphatidylethanolamines, PE-P= phosphatidylethanolamine plasmalogens, PG= phosphatidylglycerols, LPI= lysophosphatidylinositols, PI= phosphatidylinositols, PS= phosphatidylserines, PS-P= phosphatidylserine plasmalogens, SM= sphingomyelins, TAG= triacylglycerols, FFA= free fatty acids.

To assess membrane composition of liver and muscle mitochondria, data were normalised to total phospholipid content due to the differences in total lipid amount. In skeletal muscle mitochondria the relative amounts of cardiolipin (CL) and of the CL precursor phosphatidylglycerol (PG) were significantly higher than in liver mitochondria after normalisation, also seen for phosphatidylethanolamines (PE) and phospatidylserines (PS), but to a less distinct extent (Figure 41; A,C,F,H). In liver mitochondria phosphatidylinositol (PI) and phosphatidylcholine (PC) were significantly higher than in muscle mitochondria. This was also significant for for ceramide (CER) and the sum of PC and PE (85.5±0.3% in liver, 76.5±0.3% in muscle, Figure 41; B,D,E,G), albeit with a lower p-value. PC and PE are the major phospholipids in mitochondrial membranes accounting for about 80% of all phospholipids throughout different tissues and cells.[23] The contribution of sphingomyelin to phospholipid content of mitochondria derived from liver or muscle was equal (Figure 41; I).

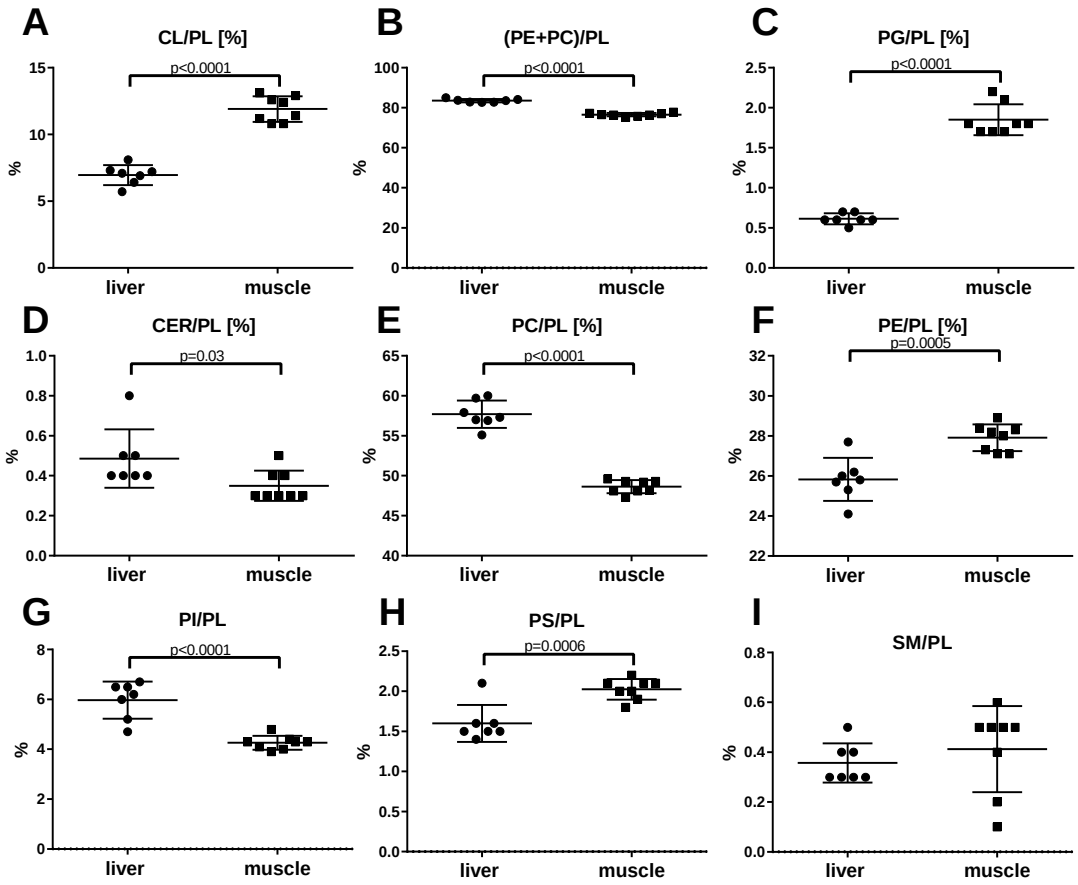

Figure 41: Cardiolipin (= CL), phosphatidylglycerol (= PG), phosphatidylcholine (= PC), phospatidylethanolamine (= PE), ceramide (= CER), phosphatidylinositol (= PI), phosphatidylserine (= PS), sphingomyelin (= SM) levels in isolated mitochondria from liver and muscle as percentage of the total phospholipid (= PL) amount. Student´s t-test was performed.

4.2.2.1.4 Mitochondrial samples isolated from murine skeletal muscle and liver tissue show different acyl chain compositions throughout several phospholipid classes including cardiolipins

Cardiolipin (CL) is the only signature lipid of mitochondria, it is a key player in the organisation of the general mitochondria membrane structure and in the organisation of the essential electron transport chain components into higher order assemblies being associated with higher oxidative phosphorylation in mitochondria.[92,97,99,101,102,240,241] Normalised to the sum of the lipid class, the relative amounts of specific lipid species were shown in percent for CL and its precursor phosphatidylglycerol (PG, Figure 42). Longer acyl chains with a higher degree of unsaturation, especially 22:6, were incorporated in muscle compared to liver mitochondria CLs. Interestingly, PGs containing 22:6 acyl chains were not detected in muscle but in liver, indicating a possible channelling of these acyl chains directly into CLs.

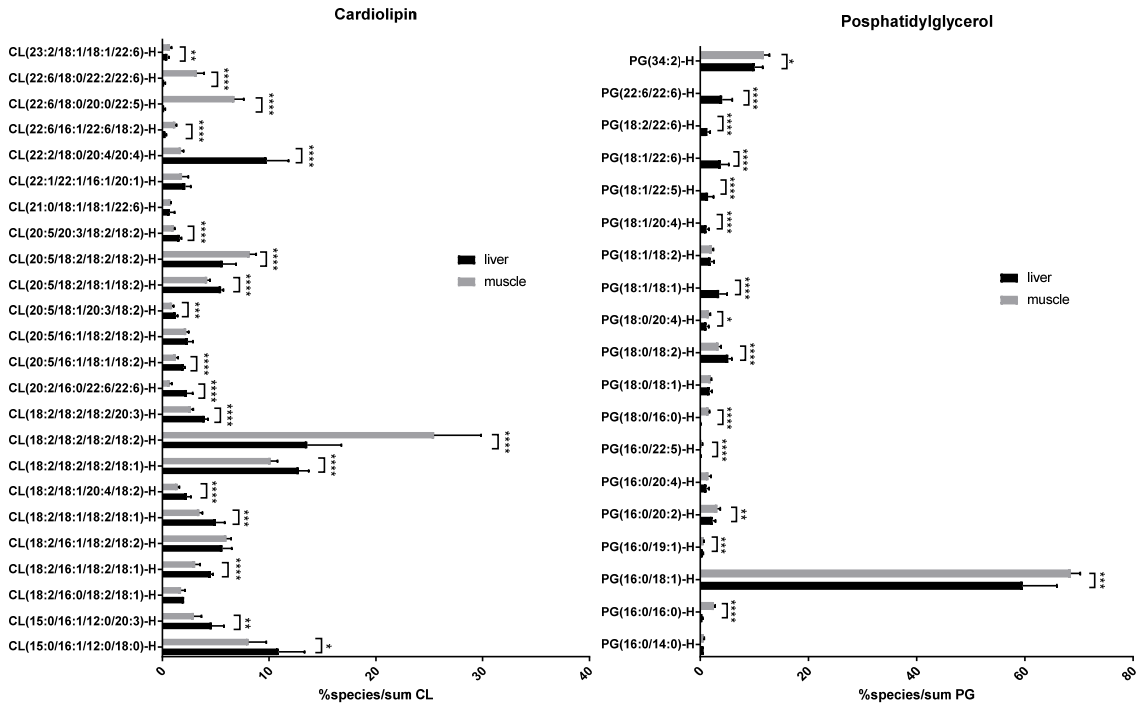

Figure 42: Cardiolipin (= CL) or phosphatidylglycerol (= PG) species as percentages of the total CL (left) or PG (right) amount. False discovery rate (FDR) was applied for testing significance.

The most abundant fatty acyl chain in mitochondrial cardiolipin of muscle and liver was 18:2 with 47.27% and 55.24% of all acyl chains (Table 9). Cardiolipin from mitochondria derived from liver showed higher amounts of mono-unsaturated fatty acids (MUFAs) whereas CL from muscle mitochondria contained more poly-unsaturated fatty acids (PUFAs). CL from liver mitochondria consisted more often of medium chain fatty acids (12C) than skeletal muscle mitochondria. Muscle mitochondria, however, contained predominantly long chain (15-21C) and very long chain fatty acids (>22C). The highest enrichment in liver compared to muscle, however, was found for 20:4 acyl chains (5.45% vs. 1.25%), whereas mitochondria derived from muscle showed higher abundances for 22:5 (1.69% vs. 0.04%), 22:6 (4.64% vs. 1.74%) and 20:0 (1.69% vs. 0.04%) (Table 9).

Table 9: Acyl chain composition in percent of cardiolipins from mitochondria derived from mouse liver and muscle, FA= fatty acid; FDR was applied for testing significance.

% FA	Liver	Muscle	adjusted p
20:4	5.45%	1.25%	0.003
20:2	0.57%	0.17%	0.003
22:2	2.48%	1.25%	0.003
16:0	1.09%	0.61%	0.003
20:3	2.87%	1.91%	0.003
12:0	3.88%	2.76%	0.011
15:0	3.88%	2.76%	0.011
18:1	10.73%	8.19%	0.003
16:1	8.15%	6.68%	0.010
18:2	47.27%	55.24%	0.011
23:2	0.12%	0.18%	0.015
22:6	1.74%	4.64%	0.003
20:0	0.04%	1.69%	0.003
22:5	0.04%	1.69%	0.003
20:5	4.62%	4.47%	0.209
20:1	0.54%	0.46%	0.227
22:1	1.09%	0.92%	0.227
21:0	0.18%	0.19%	0.515
18:0	5.24%	4.95%	0.643

The lipid species showing the largest differences in concentration between liver and muscle are phosphatidylethanolamines (PE). Their concentration was higher in muscle than in liver mitochondria. PE and CL are functionally converging in mitochondria stressing their individual, but also concerted importance for mitochondrial function,[242] especially with regard to their role in supporting oxidative phosphorylation.[71,72,92,97,99,101,102,240,241] Saturated fatty acids and MUFAs were significantly higher in PE in liver mitochondria than in muscle mitochondria, whereas PUFAs were significantly higher in PEs from muscle. Like similarly seen in CL, PEs from muscle contained prominently 22:6 acyl chains (30.4±1.1%) whereas liver mitochondria the acyl chains 20:4 (34.0±1.7%). Both were seen to have high abundances for 18:0 chains (27.6±0.6% for muscle and 24.3±1.5% for liver).

4.2.2.1.5 Protein abundances of mitochondria isolated from skeletal muscle and liver

As a next step, we systematically compared mitochondria isolated from mouse liver and muscle on protein level to investigate tissue-specific differences in protein abundances to gain deeper insights into the tissue-specific mitochondrial differences possibly associated with functional varieties. Each purification procedure was performed in eight replicates and compared to total cell lysate.

By employing western blot analysis, organelle-specific markers for mitochondria were investigated (Figure 43). In addition, also potential contaminations of the isolated mitochondria preparations by endoplasmic reticulum (ER) were controlled. Equal protein amounts (30 µg) of total cell lysates were assessed as controls to determine the organelle-specific protein levels before mitochondrial isolation. Signals were normalised to total protein abundance determined via stain-free TCE. Citrate synthase

(CS) was used to confirm the presence of mitochondria in total cell lysates and to quantify their enrichment in the isolated fractions (Figure 43 A). Citrate synthase protein abundance was significantly higher in muscle mitochondria compared to liver mitochondria. Mitochondria derived from muscle and liver did not show distinctly different abundances of Calnexin (calx), indicating no relevant difference in ER contamination (Figure 43 B). However, liver mitochondria had a much higher variability in ER protein abundance in the mitochondrial fractions, probably due to inter-experimental variances of the purification process. The densitometric data from the western blots of tissue lysates (Figure 43), western blot of tissue lysates, first two lanes) showed a clearly higher concentration of calx as a marker for ER in liver lysates compared to muscle samples. We ascribe this to a lower quantitative precision in mitochondrial purification. Complex 3 protein abundance was not significantly different between muscle and liver mitochondria (Figure 43 E). Muscle mitochondria showed significantly higher abundances of complex 1 and 2, Cox 4 and ATP Synthase (Figure 43 C, D, F, G).

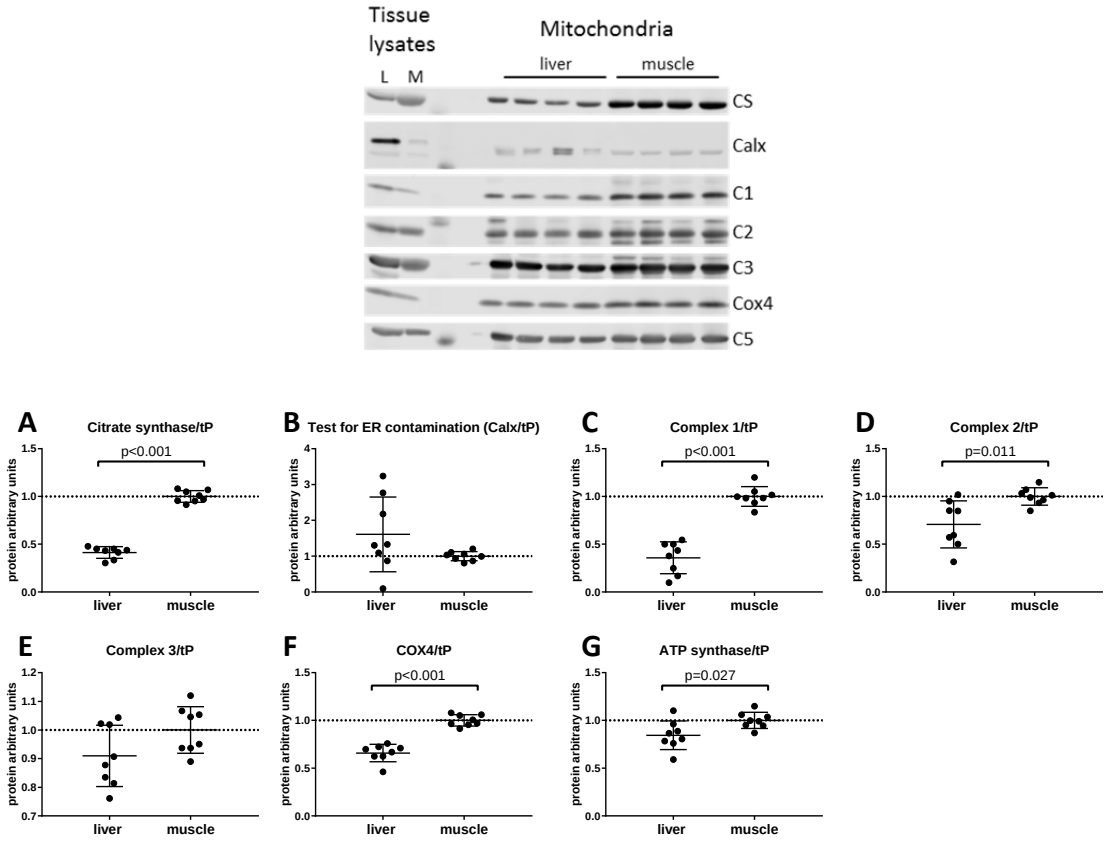

Figure 43: Analysis of specific proteins in mitochondrial fractions obtained by ultracentrifugation. A representative western blot of 4 mitochondria isolations per tissue is shown. Equal protein amounts (30 µg) of total cell lysates were assessed as controls on the mitochondrial blots to determine the protein levels before mitochondrial enrichment. A: Mitochondrial citrate synthase (CS) was used as a marker for mitochondrial content. B: Calnexin (calx) was investigated for potential contaminations by endoplasmic reticulum (ER). C-F: For the detection of the electron transport chain complexes with the exception of complex 4 (COX4; F), an antibody cocktail was used against complex 1 (C1), complex 2 (C2), complex 3 (C3), complex 5 (ATP synthase; C5). Histograms show the sums of the densitometric quantifications of western blots (Mean of "muscle" was set to 1, n= 8). Signals are normalised to total protein abundance. tP= total protein. Student´s t-test was performed.

4.2.2.1.6 Tissue-specific protein abundances in total lysates of skeletal muscle and liver

We further investigated (additionally to the tissue-specific mitochondrial protein equipment) the specific protein composition of tissue lysates from mouse liver and muscle determining the substrate supply for mitochondrial oxidation. In western blot analysis CS was used as a marker for mitochondrial matrix content (Figure 44 A). CS abundance was observed to be significantly higher in muscle tissue lysates compared to liver tissue lysates, indicating a higher mitochondrial content per unit protein. Protein abundances were normalised to total protein amount. Respiratory data (previously described in Section 4.2.2.1.1) showed that muscle mitochondria oxidised significantly more of the complex 1 substrate pyruvate in the presence of octanoylcarnitine/malate, whereas liver mitochondria respired more after addition of the complex 2 associated substrate succinate. In consistency with these results, western blot analyses of liver samples indicated higher abundance of mitochondria-specific proteins involved not only in gluconeogenesis but also in β-oxidation. Pyruvate carboxylase (PyC, Figure 44 B), medium-chain acyl-CoA dehydrogenase (MCAD, Figure 44 C) and hydroxyacyl-CoA dehydrogenase/3-ketoacyl-CoA thiolase/enoyl-CoA hydratase (trifunctional protein, HADHA, Figure 44 D) showed significantly stronger signals for liver compared to muscle tissue lysates. Hepatic pyruvate dehydrogenase (PDH, Figure 44 E) was significantly lower than in muscle tissue lysates.

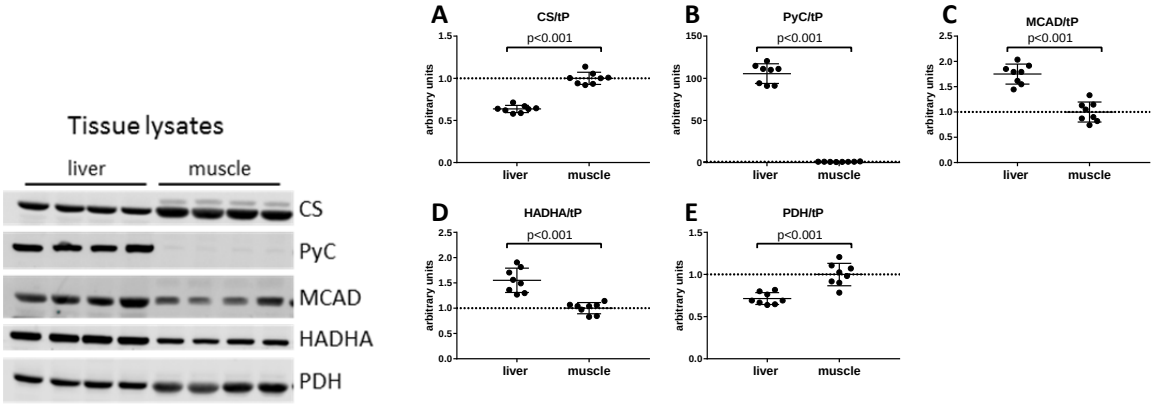

Figure 44: Analysis of specific proteins in tissue lysates of murine liver and skeletal muscle (left) and the densitometric quantification histograms (right). A representative western blot of four tissue lysates per tissue is shown. Mitochondrial citrate synthase (CS) was used as a marker for mitochondrial content. PyC= pyruvate carboxylase, MCAD= Medium-chain acyl-CoA dehydrogenase, HADHA=hydroxyacyl-CoA dehydrogenase/3-ketoacyl-CoA thiolase/enoyl-CoA hydratase (trifunctional protein), alpha subunit, PDH= pyruvate dehydrogenase. PyC and PDH were assessed to investigate pyruvate metabolism. MCAD and HADHA were used to assess β-oxidation. Histograms show the sums of the densitometric quantifications of western blots (Mean of "muscle" was set to 1, n=8). Signals are normalised to total protein abundance. tP= total protein. Student´s t-test was performed.

4.2.2.2 Omics investigation of mitochondrial adaptions in liver and skeletal muscle to excess energy intake and physical exercise: Control diet versus energy-rich diet either with or without treadmill exercise

The goal of the study was to investigate mitochondrial adaptions to states of excess energy intake complemented with training.

4.2.2.2.1 Method establishment: diet and training effectiveness in mice

Weight-matched mice were fed for 10 weeks with a high-energy diet (HED) or control diet (CON). Diets were derived from Research Diets (Diets, New Brunswick, NJ, USA) and were customised to match lipid composition (3.1.3.2.1). CON contained 10 kJ% fat, 20 kJ% protein and 70 kJ% carbohydrates, while HED was composed of 40 kJ% fat, 40 kJ% protein, 20 kJ% carbohydrates. Mice were kept either sedentary (sed) or trained (run) on a treadmill five times a week for 30 min for 10 weeks. 4 mice were in each of the four groups (CON sed, CON run, HED sed, HED run). In the first week treadmill conditions were 9 m/min at 9° slope, which was increased in the second week to 12 m/min at 12° slope for nine more weeks.

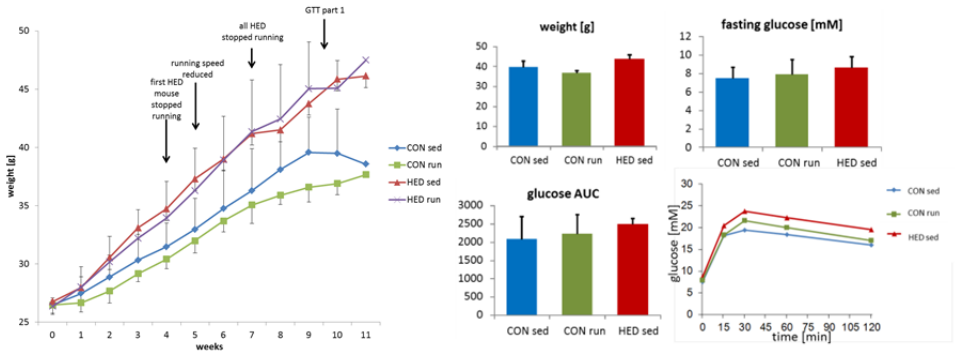

Figure 45: Body weight over time shown as mean ± SD, n= 4 for all time points (left). Final body weight in grams, fasting glucose, glucose area under the curve (AUC) after intraperitoneal glucose tolerance test, and blood glucose over 120 min after glucose bolus for glucose tolerance test (right). Intraperitoneal (i.p.) glucose tolerance tests (GTTs) were performed following overnight fast (~16 hours) through injection of glucose at 2 g/kg of body weight and measurement of plasma glucose concentration at the indicated time points (n= 4). HED run group was excluded, because mice stopped running on the treadmill before the intervention time was over. CON= control diet, HED= high-energy diet, sed= sedentary, run= treadmill trained.

After 4 weeks, one mouse of the HED fed group stopped running and was therefore excluded. In week five treadmill pace was decreased to keep the remaining HED mice running. After 7 weeks, all HED mice stopped running and this group was excluded from further experiments. Pace and slope were set back to previous conditions. After 10 weeks of diet and training neither body weights, fasting glucose levels, area under the curve (AUC) of blood glucose levels after an intraperitoneal glucose tolerance test nor the blood glucose response to the glucose bolus were significantly different between the three remaining groups (Figure 45). Respiratory analyses were performed with isolated mitochondria from liver using differential centrifugation as described in 3.2.2.1. No difference in oxidative

capacities between the three groups was detected using the mitochondrial substrates succinate and rotenone (Figure 46), pyruvate and palmitoylcarnitine plus malate (data not shown). Since training and diet did not result in phenotypical metabolic differences, these pretest treatments were optimised as described in 4.2.2.2.2. To ensure a consistent training and no drop-outs in all groups intervention time was reduced from 10 weeks to 6 weeks. Additionally, training frequency was reduced from 5 times a week to three times a week, but was performed 1 h instead of 30 min for compensation. Overall training intensity was kept comparable to the previous conditions, but pace was increased more slowly and slope was slightly reduced over experiment time to ensure HED mice running until the end of the intervention phase. The treadmill conditions were in week one 10 m/min at 12° slope, in week two 11 m/min at 12° slope, in week three 12 m/min at 12° slope, in week four 12 m/min at 10° slope, in week five 12 m/min at 9° slope and in the last week 12 m/min at 8° slope. The customised HED and CON leading to no difference in body weight after 10 weeks of feeding was replaced by a CON and HED combination with the CON composed of 10 kJ% fat, 20 kJ% protein and 70 kJ% carbohydrates and the HED of 45 kJ% fat, 20 kJ% protein and 35 kJ% carbohydrates. Both diets were already published as being effective for obesity and diet-induced insulin resistance.[243,244]

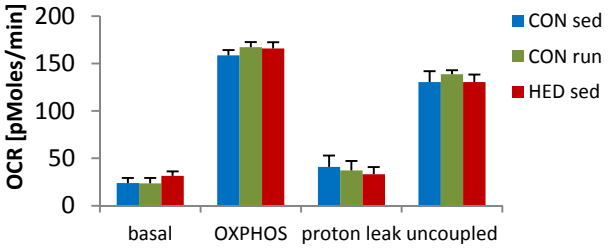

Figure 46: Respiratory measurement using a Seahorse XF96 performed with isolated liver mitochondria with palmitoylcarnitine and malate as substrates (=basal respiration), data not shown for other substrates, n= 4, CON= control diet, HED= high-energy diet, sed= sedentary, run= treadmill training, OCR= oxygen consumption rate. Oxidative phosphorylation (OXPHOS) was induced by ADP addition, proton leak was analysed after oligomycin and uncoupled respiration after FCCP addition.

4.2.2.2.2 High-energy diet leads to increased bodyweight, higher fasting insulin levels and an impaired glucose response, partially rescued by training

Weight-matched mice were fed for 6 weeks with a high energy diet (HED) or control diet (CON) and were either sedentary (sed) or trained (run) on a treadmill three times a week to investigate mitochondrial adaptions to states of excess energy intake and training (as described in 3.2.2.3.2). HED led to a significantly increased body weight in sedentary and trained mice. Weight gain by HED was significantly lower in trained mice compared to sedentary mice (Figure 47 A). An intraperitoneal glucose tolerance test was performed to metabolically characterise the mice after 5 weeks of diet and training. Fasting insulin levels were significantly higher in untrained high-energy diet fed mice than in control diet fed mice fed control diet (Figure 47 B). Training slightly rescued HED-fed mice from significantly increased fasting insulin levels. Same pattern was observed for the area under the curve (AUC) of the blood glucose levels during the intraperitoneal glucose tolerance test (Figure 47 C).

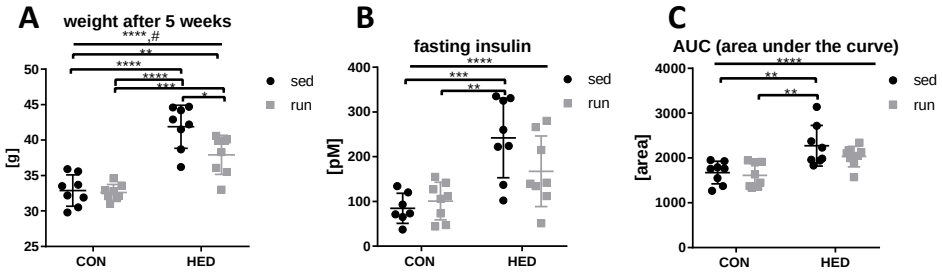

Figure 47: Mice body weights after 5 weeks of diet and training (A), fasting insulin levels (B) and blood glucose area under the curve (AUC) after an intraperitoneal glucose tolerance test (C); CON=control diet, HED= high-energy diet, sed= sedentary, run= treadmill training; 2way ANOVA (significances shown with "⎯⎯"): *=significantly different for CON to HED, #=significantly different for sed to run conditions. Multi comparison significances shown with "⌐¬".

4.2.2.2.3 Mitochondrial content is increased by high-energy diet in muscle but not in liver

Citrate synthase activity was measured to investigate mitochondrial content in tissue lysates from mouse skeletal muscle and liver. The tissue used for these lysates was from the same tissue pool used for mitochondrial isolation. Skeletal muscle tissue lysates derived from high-energy fed mice showed a slight but significant increase in citrate synthase activity compared to control-fed animals (Figure 48 A), indicating an increased mitochondrial amount after HED. No difference in citrate synthase activity was detected in liver tissue lysates (Figure 48 B).

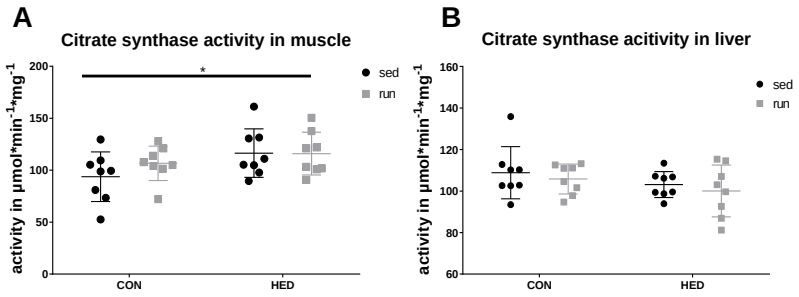

Figure 48: Citrate synthase activities of muscle (A) and liver lysates (B). Means + SD are given for n= 8. CON= control diet; HED= high-energy diet; sed= no training; run= training CS activity muscle. 2way ANOVA (significances shown with "⎯⎯"): *= significantly different for CON to HED.

As an additional measure to quantify mitochondrial content, the mitochondrial yield (by protein) after UC isolation was calculated per mg wet weight of the tissue amount used for analysis. As already observed in the citrate synthase activity assay, muscle mitochondrial yield was higher from tissues derived from high-energy fed animals than from control-fed mice (Figure 49 A). In addition, the yield from muscles of trained mice was higher than of sedentary mice. This was not seen for liver samples. Solely, a training effect was seen under HED. The analysis of samples labelled "HED run" showed a significantly higher mitochondrial yield per mg tissue compared to "HED sed" (Figure 49 B).

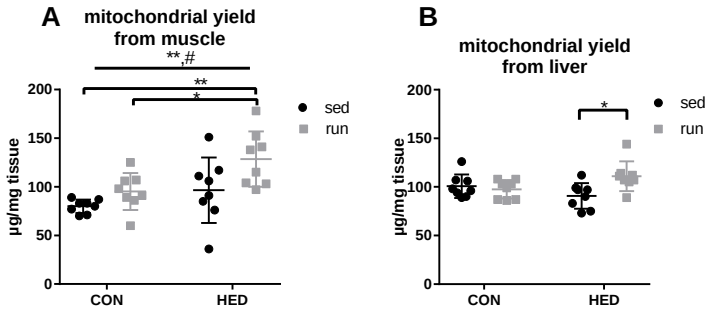

Figure 49: Yield of UC-isolated mitochondria (by protein) per mg wet weight of the tissue amount used. A: muscle mitochondrial yield after UC isolation B: liver mitochondrial yield after UC isolation. The mean + SD is given for n= 8, 2way ANOVA (significances shown with "⎯⎯"): *= significantly different for CON to HED, #= significantly different for sed vs. run conditions. Multi comparison significances shown with "⌐⎯⎯⌐".

4.2.2.2.4 Skeletal muscle mitochondrial respiration is affected by diet and training

Mitochondria from skeletal muscle were isolated by differential centrifugation as described in 3.2.6.5. High-resolution respirometry (HRR) of skeletal muscle mitochondria was performed for seven mice out of every group. Overview of the whole measurement course is shown in Supplementary Figure 4. When respiring on fatty acid oxidation substrates (octanoylcarnitine and malate) oxidative phosphorylation (after addition of ADP) was slightly higher in high-energy fed mice than in control fed mice ($p < 0.05$; Figure 50 A). Additional to the C8 acyl chain fatty acid octanoylcarnitine, the longer fatty acid chain palmitoylcarnitine (C16) was investigated as substrate for isolated mitochondria in a Seahorse XF96. Mitochondria derived from HED-fed mice showed a significantly higher phosphorylating respiration compared to mitochondria derived from CON-fed mice (Figure 50 G). The following pyruvate addition (complex 1 associated substrate), however, led to a significantly higher increase in muscle mitochondria from control diet-fed mice compared to high-energy diet-fed mice (Figure 50 B). In addition to the effect of high-energy diet on mitochondrial function in muscle, treadmill training led to a slight but significant increase in mitochondrial oxidative capacity on substrates for fatty acid oxidation (octanoylcarnitine and malate) and the complex 1 associated substrate pyruvate (Figure 50 C). This was persistent as a trend also after addition of succinate, a complex 2 associated substrates (Figure 50 D). After uncoupling the mitochondria with FCCP, muscle mitochondria derived from trained mice again showed a significantly higher oxidative capacity (Figure 50 E). The P/E-ratio (phosphorylating respiration relative to the maximal uncoupled respiration) was not changed in muscle mitochondria upon treatment (Figure 50 F). This ratio takes coupling and limitations of OXPHOS capacities into account.

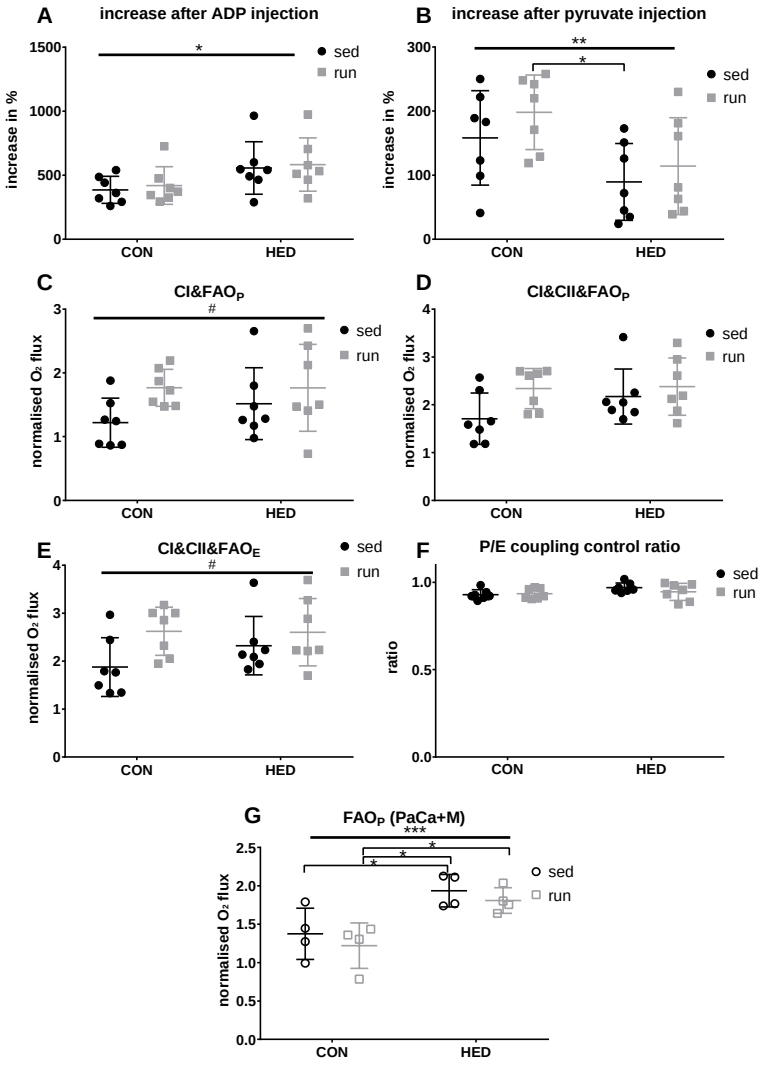

Figure 50: Normalised oxygen fluxes, flux increases in % and ratios of states in isolated muscle mitochondria (mean + SD, n= 7). Data were normalised for mitochondrial amount (by protein), dilution throughout the analysis and inter-day variances. CON= control diet; HED= high-energy diet; run= trained; sed= sedentary. 2way ANOVA (significances shown with "—"): * =significantly different for CON to HED, #= significantly different for sed to run conditions. Multi comparison significances shown with "⌐¬". A: Percentaged change of oxygen flux after ADP injection, malate and octanoylcarnitine present. B: Percentaged change of oxygen flux after pyruvate injection, ADP, malate and octanoylcarnitine present. C: Normalised oxidative phosphorylation (malate, octanoylcarnitine, ADP, pyruvate present). D: Normalised oxidative phosphorylation (malate, octanoylcarnitine, ADP, pyruvate, succinate present). E: Uncoupled maximal respiration. F: Ratio of maximal coupled respiration to uncoupled respiration. G: Normalised phosphorylating oxidative capacity using palmitoylcarnitine (PaCa) and malate (M) as substrates in isolated skeletal muscle mitochondria using a Seahorse XF96.

4.2.2.2.5 Liver mitochondrial respiration is solely affected by diet and not by training

HRR of liver mitochondria was performed for five mice from every group. The whole course of the measurement is shown in Supplementary Figure 5. Liver mitochondria derived from high-energy diet-fed mice showed significantly higher leak respiration with octanoylcarnitine and malate present than mitochondria derived from control-fed animals (Figure 51 A). The same pattern was observed under phosphorylating conditions and the additional complex 1 associated substrate pyruvate (Figure 51 B),

as well as the additional complex 2 associated substrate succinate (Figure 51 C). The higher oxidative capacity of mitochondria from high-energy-fed mice was also observed after uncoupling the electron transport chain from ATP production with FCCP (Figure 51 D). The P/E-ratio (phosphorylating respiration relative to the maximal uncoupled respiration) was not changed in liver mitochondria (Figure 51 E).

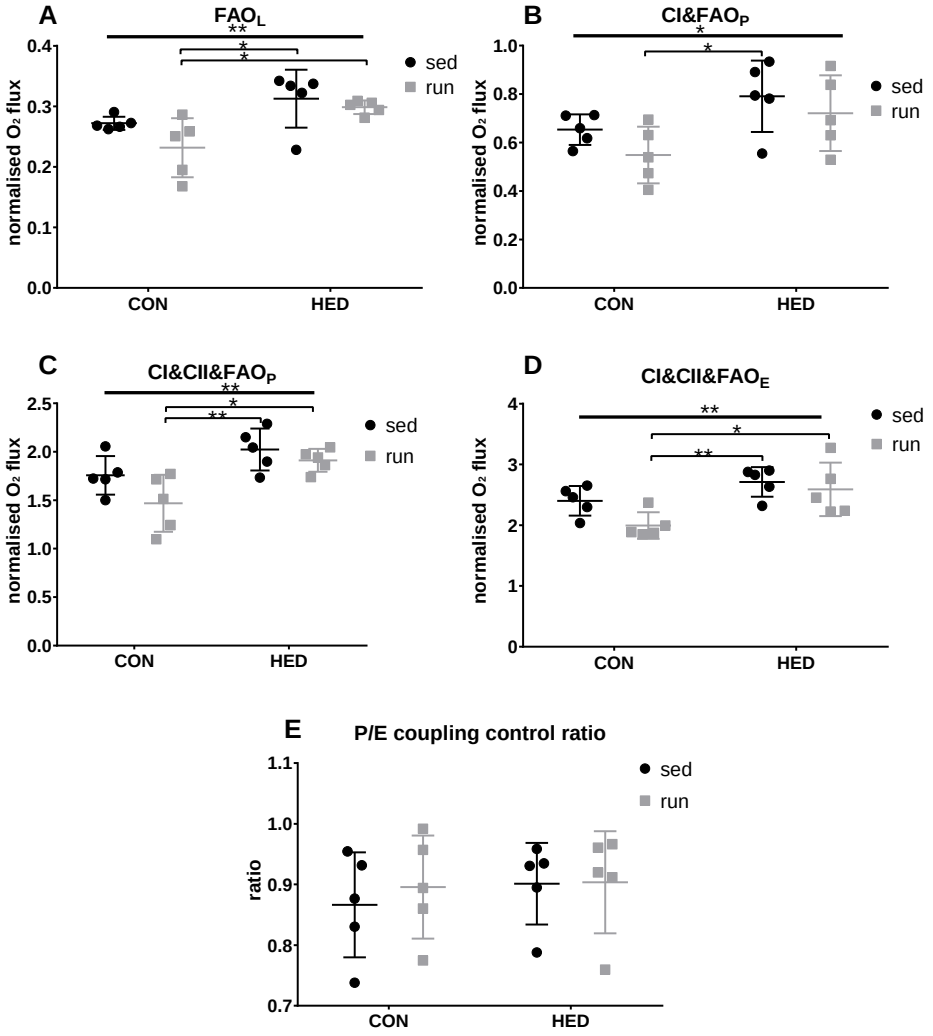

Figure 51: Normalised oxygen fluxes, flux increases in % and ratios of states in isolated liver mitochondria (mean + SD, n= 5). Data was normalised for mitochondrial amount (by protein), dilution throughout the analysis and inter-day variances. CON= control diet; HED= high-energy diet; run= trained; sed= sedentary. 2way ANOVA (significances shown with "___"): *= significantly different for CON to HED, #= significantly different for sed to run conditions. Multi comparison significances shown with "⌐¬". A: Leak respiration, malate and octanoylcarnitine present. B: Normalised oxidative phosphorylation (malate, octanoylcarnitine, ADP, pyruvate present). C: Normalised oxidative phosphorylation (malate, octanoylcarnitine, ADP, pyruvate, succinate present). D: Uncoupled maximal respiration. E: Ratio of maximal coupled respiration to uncoupled respiration.

To illustrate the effect of high-energy diet on mitochondrial respiration in liver, sedentary and trained samples were taken together and diet effects are shown in Figure 52. Throughout the SUIT (substrate-uncoupler-inhibitor-titration, 3.2.8.2) protocol HED mitochondria showed a significantly higher oxidative capacity. The non-mitochondrial background (Ama_{ROX}) was not different between the groups.

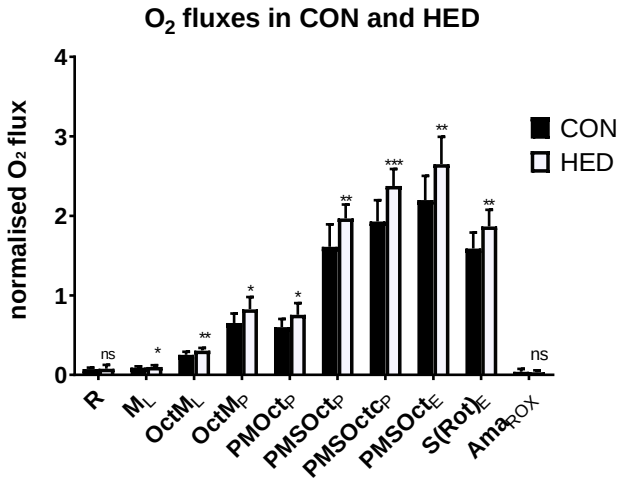

Figure 52: Liver mitochondria respiration (normalised oxygen flux, mean + SD, n = 10): Control diet vs. high-energy diet. Data were normalised for mitochondrial amount (by protein), dilution throughout the analysis and inter-day variances. CON= control diet; HED= high energy diet; trained and sedentary were summed. *= significantly different between CON and HED, Student´s t-test.

4.2.2.2.6 Diet associated effects dominate the mitochondrial lipid profile

To gain an initial overview of the possible intervention group differences in the lipid profiles, a multivariate principal component analysis (PCA, Figure 53, 3.2.13.6) was performed. In the direction of the first principal component, a pronounced separation of the clustered hepatic and skeletal muscle-derived mitochondrial samples could be seen as discussed in 4.2.2.1. However, in the direction of the third and fourth principal component a pronounced separation of the mitochondria could be seen due to the diet with no further separation of the training, indicating a much larger effect of diet on the mitochondrial lipid profiles than of the training intervention. Although the lipid composition was shown to be highly tissue-specific (Figure 39, first and second components of PCA explained 76.9% of the variation leading to tissue-dependant separation), the high-energy diet („HED“) had similar effects on the lipid composition in both tissues. The third and fourth component of the PCA explained additional 8.9% of the variation leading to the separation of the mitochondria by diet.

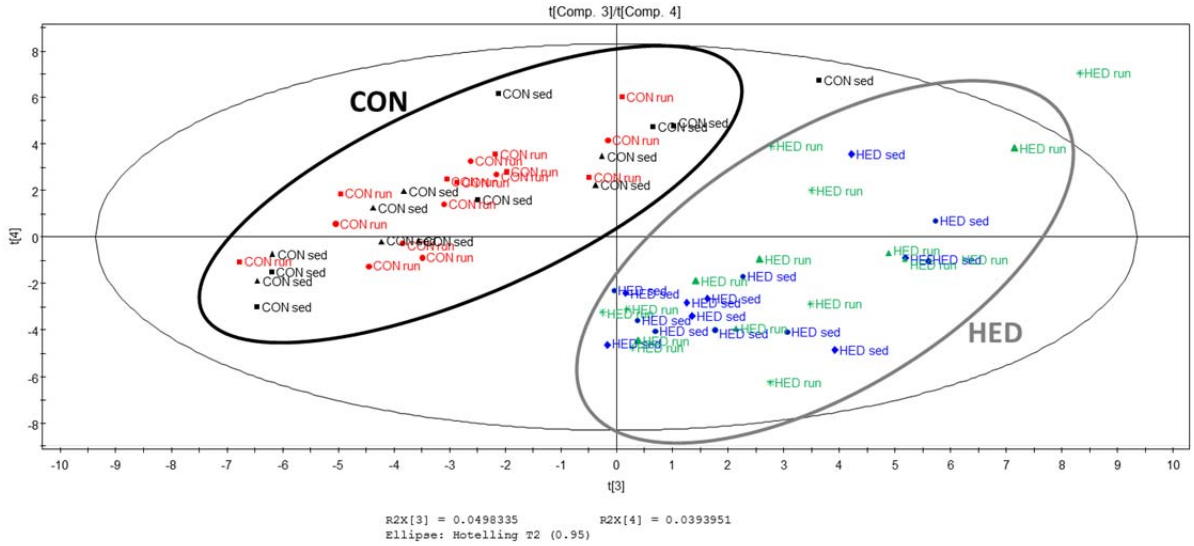

Figure 53: Principal Component Analysis (PCA) scores plot of the third and fourth principal components based on all ~300 detected lipids (relative standard deviation in the quality control samples < 20%, autotransformed). Each spot represents one mitochondrial sample isolated from mouse liver or skeletal muscle using ultracentrifugation. CON= control diet; HED= high-energy diet; run= trained; sed= sedentary. The third component explains 5.0% of the variation and the fourth component explains 3.9%.

CL content of mitochondria was not different between the groups (Figure 54 A, C), the most prominent cardiolipin, tetra-linoleoyl-CL (18:2/18:2/18:2/18:2), however, was higher abundant in liver mitochondria from HED-fed than in CON-fed mice (Figure 54 D), not seen in muscle (Figure 54 B).

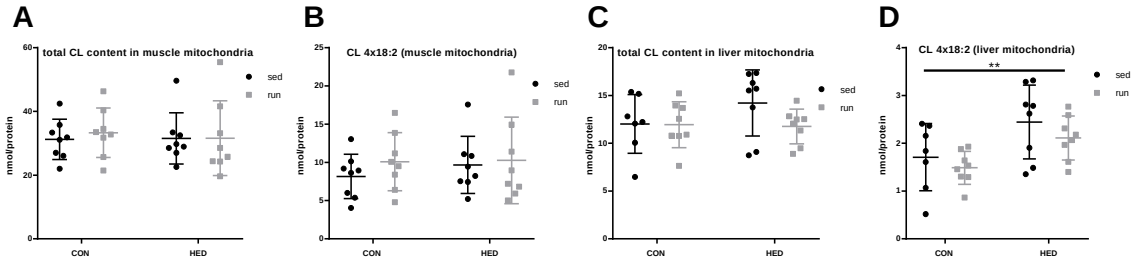

Figure 54: Summed cardiolipin content in muscle mitochondria (A) and liver mitochondria (B) and tetra-linoleoyl-CL (18:2/18:2/18:2/18:2) amount of muscle (B) and liver mitochondria (D). 2way ANOVA (significances shown with "▬"): *= significantly different for CON to HED.

4.2.2.2.7 Diet fatty acid composition does not reflect the fatty acid composition of mitochondrial lipids

From data provided by the manufacturer high-energy diet contained more 16:0, 16:1 and 18:1 fatty acids than CON diet (24.42% vs 17.25%, 2.84% vs 1.25%, 43.15% vs 32.5%). These fatty acids, however, were less abundant in the mitochondrial lipid profiles derived from HED-fed mice in cardiolipin (CL), phosphatidylcholine (PC), phosphatidylethanolamine (PE), the cardiolipin precursor phosphati-

dylglycerol (PG) and phosphatidylinositol (PI). In contrast, 18:0 fatty acid, which was higher in concentration in HED diet than in CON diet (10.49% vs 7.75%), was found to be also elevated in PC, PE, PG and PI in mitochondria derived from HED-fed mice. 18:2 and 18:3 fatty acids, however, were lower in the HED diet than in the CON diet (15.85% vs 35.75%, 1.68% vs 3.75%) and were also detected to be lower in the lipid classes PC, PE and PI in the mitochondria from HED-fed mice. 20:3 fatty acid was significantly increased in CL in mitochondria from HED-fed mice compared to CON-fed in either tissue. Higher energy diet led to a change in concentration of 56 lipid species in liver and 66 in muscle mitochondria, 32 of these were changed in both tissues. PS was not affected by HED.

4.2.2.2.8 The oxidative defence seems to be neither affected by high-energy diet nor treadmill training

Since mitochondria are major sources of reactive oxygen species (ROS) in cells primarily through respiratory complexes I, II and III, they are also a primarily affected target by ROS.[74-78] Additionally, mitochondrial ROS production has been discussed in the context of skeletal muscle insulin resistance.[245,246] But neither superoxide dismutase 1 (SOD1) nor SOD2 protein abundance was significantly affected by HED or training in mitochondria from muscle and liver (Figure 55; A-F).

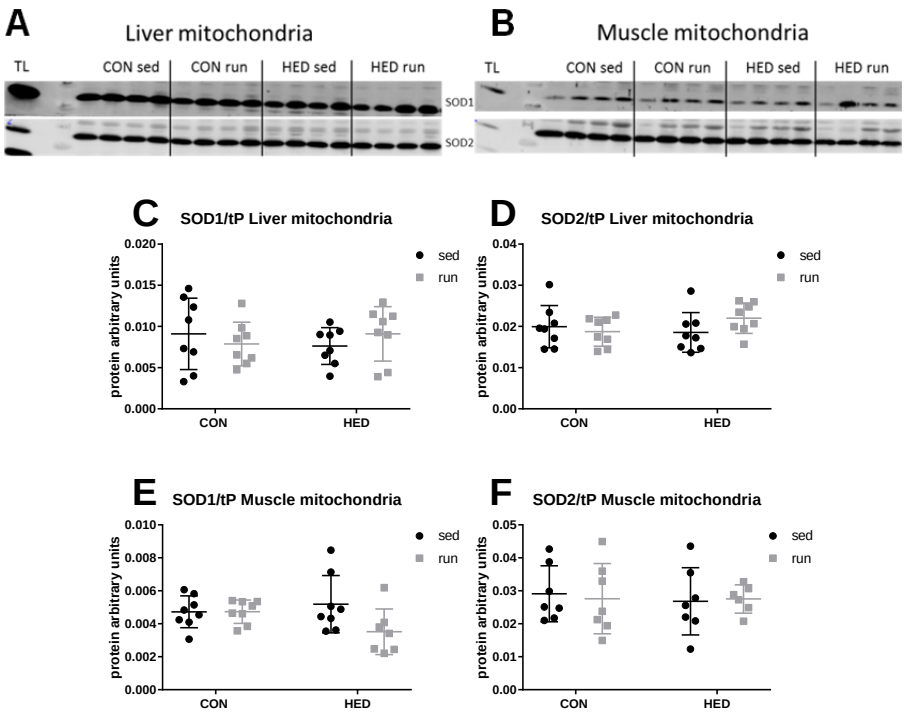

Figure 55: SOD protein levels in isolated mitochondria; representative western blots of liver (A) and muscle (B) mitochondrial fractions using antibodies against superoxide dismutases (SOD1, SOD2). Histograms (C to F) show the sums of the densitometric quantifications of western blots. Values are means ± SD (n= 8). CON= control, HED= high-energy diet fed, sed= sedentary, run= treadmill trained, SOD= superoxide dismutase. 2way ANOVA.

Since protein levels are not necessarily reflecting enzyme activities SOD activity was investigated in liver mitochondria and liver tissue lysates (Figure 56). These assays were not performed with muscle due to a more limited sample amount. SOD activity was not changed by HED or training neither in mitochondria nor in total liver lysates.

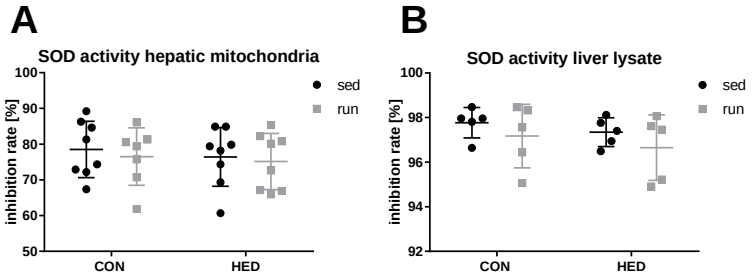

Figure 56: SOD activity in isolated hepatic mitochondria (A) and liver tissue lysates (B); Values are means ± SD (n= 5-8). CON= control, HED= high-energy diet fed, sed= sedentary, run= treadmill trained, SOD= superoxide dismutase. 2way ANOVA (significances shown with "—"): *=significantly different for CON to HED.

5 Discussion

5.1 Establishment of mitochondrial assays

5.1.1 Establishment and optimization of a reliable and precise mitochondria isolation strategy in HEPG2 cells is a prerequisite for lipidomics analyses

The yield of mitochondria is often the bottleneck when it comes to a limited sample amount available, e.g. small tissue samples like biopsies or samples with a low mitochondrial density. So far, published lipidomics analyses covering CLs required and used 250 µg[165] to 1.5 mg[162,192] (by protein) of mitochondria. Despite using as little as 100 µg, lipidomics analysis used in this thesis was sufficiently sensitive to detect 32 cardiolipin species, whereas previous publications reported a detection of 100 species,[96] 28 species[162] or less.[171,173,174,192] Compared to other lipid classes, the abundance of CL, a mitochondria-specific dimeric glycerophospholipid, is relatively low in whole cell lysates.[247] UC-purified mitochondria contained the highest relative amount, DC was intermediate and MACS showed the lowest amount of CL (4.1.1.2.3). In addition to CL, mitochondria also synthesise its precursor PG.[23] Thus, the elevated PG levels in UC samples further underpinned the higher mitochondria enrichment by UC compared to the other isolation methods. Compared to UC, samples isolated by DC or MACS contained significantly higher amounts of PS, PE-P, SM, and HexCER (4.1.1.2.3). Sphingolipids are characteristically high in ER, lysosomes, Golgi apparatus and plasma membranes.[23,248] As the mitochondrial sphingolipid content is normally very low, high levels of SM and HexCER in mitochondrial fractions can likely be attributed to contaminations by other organelles and membranes. Similarly, the PS content was reported to be higher in ER, Golgi, lysosomes and the plasma membrane than in mitochondria.[23] Contaminations could result from co-sedimentation (mainly during DC), from organelle-mitochondria interactions, or from non-specific interactions with the antibody or the solid phase during the MACS procedure. PE plasmalogens (PE-P) were significantly lower using UC than using the other isolation methods. Mitochondria from heart, brain, kidney, adrenal cortex and spleen are rich in PC and PE plasmalogens.[23,248] While the liver is the major site for plasmalogen synthesis,[249] PE-P are present only at low levels in liver mitochondria.[250-252] Since plasmalogens are also part of nuclear, ER and Golgi membranes,[250,251] the higher PE-P in the DC- and MACS-samples might indicate contaminations by these other organelles. MACS and, to a lower degree, DC samples had a significantly higher TAG content. While TAGs are mainly stored in lipid droplets, neutral lipid cores surrounded by a monolayer of phospholipids and associated proteins,[253] the ER is the major site of their production,[254] pointing towards a relevant contamination of the samples isolated by MACS and DC with ER membranes. Therefore, it was clearly shown that UC, but not DC or MACS, yielded a pure mitochondrial fraction with little contamination by non-mitochondrial organelles. Different from functional assays, which highly depend on mitochondrial integrity and viability, the validity of mitochondrial “omics” analyses is directly related to sample purity. Tests for contaminations or quality

controls of mitochondrial enrichment are rarely reported. However, lipidomics studies performed on DC- and MACS-isolated mitochondria may result in erroneous conclusions if the samples contain relevant contaminations by ER and other organelles, as indicated in this study. In addition, the application of different protocols with different degrees of contaminations might preclude comparison of results from different studies. For example, published CL contents range between 10 to 20%[23,255] of total phospholipids, which has been suggested to be caused not solely by different experimental conditions, but also by varying degrees of purity of the mitochondrial samples.[99] The strong correlation between ATP5 protein and cardiolipin concentration was in line with previous observations in skeletal muscle tissue that suggested CL to be a superior marker of mitochondrial content.[223] Since lipids other than CL cannot be assigned to individual organelles, protein analyses are better suited to classify residual ER or other contaminants in mitochondrial samples. A purity examination by western blot (Figure 12) or comparable assays in the early phase of an experiment to ensure the quality and reliability of subsequent publications reporting lipidomics analyses of mitochondrial samples is strongly recommended. Nevertheless, the higher sensitivity and the possibility to investigate contaminations in a quantitative fashion make lipidomics an appropriate tool to assess the purity of mitochondrial samples.

5.1.1.1 Conclusion

Mitochondria isolation by ultracentrifugation yielded the purest samples. Therefore, it is strongly recommended for lipidomics analyses of mitochondria obtained from cell culture models. The two other methods tested, DC and MACS, may result in misleading conclusions when isolating mitochondria for ”omics” analyses due contamination with other organelles. The lipidomics data obtained in this study confirmed CL to be a potent marker for mitochondrial content, comparable or even superior to purity controls by western blot analysis. In addition, it was demonstrated that elevated amounts of PS, HexCER, SM, and TAG may indicate contaminations by other organelles. Thus, a careful analysis of lipid profiles can be recommended as quality control of mitochondrial samples in analytical settings. Subcellular profiling is becoming increasingly relevant for basic and translational research. The implementation of valid, robust sample preparation strategies is one of the keys to success for these sophisticated studies. Although DC and MACS are much faster and easier to perform, it is highly recommended to use purification by UC to achieve reliable results when performing mitochondrial lipid profiling.

5.1.2 Establishment and optimisation of a valid mitochondrial oxysterol profiling strategy in liver tissue and hepatic mitochondria (fresh/frozen tissue, mitochondria isolation and oxysterol extraction fresh/frozen ±BHT)

Many reports about oxysterols in body fluids or tissues exist, but not in every analytical study, even in recent ones, the ease of cholesterol autoxidation was taken into account.[103] This is highly problematic, since some oxysterols formed enzymatically *in vivo* are identical to the products of autoxidation *ex vivo*[103] and furthermore oxysterols formed by *in vivo*-reaction with ROS, have the same structure as

those enzymatically produced *in vivo* or autoxidised *ex vivo.*[256,257] As a consequence, the presence[230,234,235] or absence[113,129,236] of an antioxidant like the synthetic commonly used butylated hydroxytoluene (BHT), protecting cholesterol from *ex vivo* oxidation during sample handling and storage, might lead to discrepant findings. Based on the pre-analytical inconsistency of the use[230,234,235] or non-use[113,129,236] of an antioxidant like BHT in oxysterol analyses, the effect of BHT on the oxysterol pattern was compared methodically. Additionally, the use of frozen samples instead of fresh samples was also addressed to simplify the overall experimental process. In liver, BHT addition did not change oxysterol levels (4.1.3.1.1). This might be due to the fact that liver tissue samples, in contrast to the isolation of mitochondria as discussed below, can be collected and processed very quickly (including harvesting within 15 min before oxysterol extraction). Furthermore, also frozen tissue can be used (4.1.3.1.1), since no significant effect on the oxysterol yield was detected in comparison to fresh tissue, which opens up additional perspectives for the analysis of liver tissue samples by simplifying the overall experimental procedure.

Quantitative data or protocols about mitochondrial oxysterols are pretty rare.[128,129] Studies so far mainly focused on enzymatic equipment and conversion products in mitochondrial incubations with oxysterols or cholesterol.[103,258] BHT addition during mitochondrial isolation changed oxysterol levels significantly (4.1.3.1.2), making the multi-step time-consuming mitochondria isolation procedure the most critical step. Summarised from these findings, the addition of BHT as early as possible at sample processing (here: addition to the tissue before mitochondrial isolation and all subsequent steps) is strongly recommended, since these data clearly showed that alterations in the oxysterol yield can be prevented and no side effects of BHT on mitochondrial function could be detected. In absence of BHT, the oxysterol yield could be falsely increased by further oxidation from cholesterol throughout sample processing or falsely decreased by further decomposing of the oxysterol. Structural differences between the oxysterols might be the reason for the oxysterols being differently prone to the protection by BHT in vital mitochondria. The primary hydroxyl group in 27-hydroxycholesterol for example can easily be oxidised, whereas the ketone group at C_{15} in 15-ketocholestene is more resistant to oxidation.

As investigated in a kinetic experiment (4.1.3.1.3), autoxidation by oxygen from air cannot explain the significantly changed mitochondrial oxysterol pattern when BHT was present during mitochondrial isolation. Thus, BHT might either prevent the generation of reactive oxygen species and their reaction with sterols or reduce the activity of sterol-oxidizing enzymes. BHT interferes with cytochrome P450 proteins (CYPs) as reported in microsomes.[259] In liver tissue many CYP species are involved in oxysterol formation such as CYP46A1, CYP7A1, CYP3A4 and CYP27, some of which are even localised in mitochondria.[119] Enzymes can still be active during the whole mitochondrial isolation from liver harvesting, homogenisation to purification and thereby probably change the oxysterol pattern due to the “stress” situation during the long isolation procedure.

These findings might not only be important for oxysterol analyses of mitochondria, but also for general lipid analyses of mitochondria. Analyses of oxidation-prone lipids like mitochondria-specific cardiolipins might also be affected during the quite long mitochondrial isolation process by presence or

absence of an antioxidant like BHT. So far to our knowledge in published protocols about lipid profiling of isolated mitochondria, BHT is, if at all[130,162,163], not added until the lipid extraction[260].

A mouse model for oxidative stress induced by injecting doxorubicin (4.1.3.1.4) was used as proof of principle experiment for the methods established in Sections 4.1.3.1.1 and 4.1.3.1.2. This oxidative stress model clearly illustrates that oxysterol profiles of tissue or cell lysate show distinct differences in comparison to the oxysterol profile on the subcellular level, hence implicating the relevance to go beyond the cellular level when profiling oxysterols. Especially the elevated mitochondrial levels of 7α/7β-hydroxycholesterol and 7-oxocholesterol might be a relevant finding for the pathogenesis of doxorubicin toxicity, since they are associated with oxysterol-induced apoptosis via the mitochondrial pathway.[118-120] The functional investigations given showed a reduced respiration in mitochondria isolated from the liver of doxorubicin-treated mice. This finding may possibly be due to an inhibitory effect of DOX on some of the respiratory chain complexes.[261] Moreover, it can be explained by the 42% lower yield of mitochondrial protein per mg liver tissue of the DOX-treated mice which is also evident by the lower citrate synthase protein amount. These data suggest a reduced amount of mitochondria in the livers of DOX-treated mice as already described by Dirks-Naylor et al. (2014)[262] This reduction might contribute to the observed decrease in certain oxysterols in total liver tissue. Several oxysterols showed a high abundance in mitochondria compared to total tissue (e.g. for 5β,6β-epoxycholesterol: 4.13-8.65 ng/mg mitochondria versus 0.1-0.27 ng/mg liver; including CON and DOX). Thus, a reduced mitochondrial content might result in reduced tissue level of these oxysterols.

5.1.2.1 Conclusion

Although BHT addition is recommended during oxysterol extraction from tissue or isolated mitochondria to achieve high quality quantitative oxysterol results, quick processing without the addition of BHT did not result in significant changes of the detected oxysterol profiles. Frozen liver tissue and mitochondria were also shown to be suitable for oxysterol analyses. More importantly, for the investigation of oxysterol profiles in mitochondria the addition of BHT is highly recommended as early as possible at long sample processing experiments (here: addition to the tissue before mitochondrial isolation and all subsequent steps), since the presence of an antioxidant early in sample processing does not influence mitochondrial function, but has significant impact on detected oxysterol levels. Lastly, using doxorubicin-treated mice as a model, it was shown that tissue levels of oxysterols may not reflect relevant changes in subcellular oxysterol pattern and important information about the contribution of oxysterols to pathomechanisms may be missed.

5.2 Skeletal muscle cell culture: Analysis of mitochondria from cultured skeletal muscle cells challenged with substrate overflow and insulin resistance: Insulin resistant murine C2C12 myotubes under low/high glucose conditions

The C2C12 cell line is a widely used *in vitro* model for skeletal muscle, especially due to its special feature of being capable to differentiate into muscle-like myotubes.[263-265] This cell differentiation process was controlled in this work not to be affected by treatment with chronically high insulin levels and high glucose concentrations using the marker myosin heavy chain (MYH, Figure 31), which is a typical marker for fully differentiated muscle cells.[266] The treatment effectively induces insulin resistance (Figure 30) as previously reported for L6 muscle cells[267] and C2C12.[268] Elevated glucose and insulin levels are two characteristic hallmarks of type 2 diabetes exacerbating insulin resistance and playing important roles in the pathogenesis of the disease.[269] Early in differentiation, murine myoblasts were reported to derive approximately 60% of their energy by lactate production from glucose despite oxidisable fuels present in the medium.[270] However, cells cultured in media with high glucose amounts tend to be highly glycolytic. This is called "Crabtree effect",[271] and should be kept in mind in metabolic investigations using such cell models. Mailloux et al. (2010)[272] confirmed the different phenotypes by showing higher amounts of lactic acid in the high glucose medium in C2C12 cells in a similar experimental setup as applied in this thesis. L6 myotubes treated with high glucose and insulin also showed a higher basal glucose uptake.[267] In this work both, citrate synthase activity and protein abundance were reduced by high glucose but also by chronic insulin treatment causing insulin resistance (Figure 32). A lower mitochondrial mass due to cultivation in high glucose conditions was reported for myotubes but not myoblasts.[273] This decrease in mitochondrial mass seen under high glucose conditions could be due to a more glycolytic phenotype of the cells not relying on oxidative phosphorylation (OXPHOS) for ATP production but on glycolysis. Insulin resistance had an additional decreasing effect on the mitochondrial mass, which was also observed in skeletal muscle of type 2 diabetics, insulin resistant patients and even the offspring of type 2 diabetics.[145] PGC-1α, a co-activator of nuclear receptors, plays an important role in controlling mitochondrial biogenesis.[274] A reduced expression of PGC1α and related genes was reported in microarray studies in skeletal muscle of type 2 diabetic patients,[275,276] possibly leading to a reduced mitochondrial mass. Contrarily, human myotubes derived from healthy participants showed an increase of mitochondrial mass due to cultivation in high glucose, whereas myotubes of patients with type 2 diabetes history lacked a response after 7 days in high glucose differentiation medium.[277,278]

A decreased mitochondrial content is discussed to play a role in the disruption of insulin signalling, leading to a decreased oxidative metabolism, especially reduced fatty acid oxidation, and accumulation of intracellular metabolites.[136,137,141,145] In this context, oxidative metabolism was investigated in permeabilised cells. Respiration on complex 1 linked substrates pyruvate with malate and glutamate and with added succinate tended to be higher throughout all respiratory states in cells cultivated in low glucose medium (Figure 33), probably due to a lower mitochondrial content in high glucose conditions. However, also different substrate preferences were detected in this work: high glucose signif-

icantly decreased the response of phosphorylating respiration on the complex 1 linked substrate pyruvate with malate compared to leak state, indicating that cells cultivated on low glucose levels have a higher complex 1 linked respiratory capacity. In concordance to the higher complex 1 linked respiration at low glucose concentrations, the contribution of complex 2 linked respiration to maximal respiration (complex 1 and 2) was significantly lower under these conditions. Similar studies published previously focused on other parameters such as different substrates for different phenotypes or slightly different experimental setups, which make a direct comparison rather difficult.[272,273,278] Consistent with our finding, but in intact cells, higher maximal O_2 consumption rates with glucose, l-glutamine, and pyruvate as substrates were observed in C2C12 cells differentiated in low glucose compared to high glucose medium.[272] This finding was explained by the more glycolytic phenotype of the cells cultivated under high glucose conditions. In a similar setup, maximal respiration and spare respiratory capacity were also decreased in C2C12 differentiated in high glucose medium.[273] Taken all results together a decreased oxidative capacity was observed in myotubes cultivated in high glucose conditions possibly due to the higher dependence on glycolysis for ATP generation. In addition, a lower mitochondrial mass was observed in these myotubes. High glucose conditions leading to less oxidation of substrates and a higher reliance on glycolysis for ATP production, were further investigated by characterising protein levels of electron transport chain complexes (Figure 34). Most of the complexes were less abundant due to high glucose conditions and insulin resistance, even after correction for mitochondrial mass (citrate synthase protein). Additionally, these cells seem to rely less on complex 1 (NADH) and more on complex 2 linked electron transport chain substrates (succinate), maybe also based on the higher glycolysis rate already providing the cell with NADH, produced during glycolysis. These specific substrate differences do not solely point towards a general decrease of respiration, due to the reasons mentioned above, but indicate a more specific alteration in mitochondria due to high glucose treatment.

Since mitochondria are major sources of reactive oxygen species (ROS) in cells primarily through respiratory complexes I, II and III, they are also a prime target of it.[74-78] Mitochondrial ROS production has been discussed in the context of skeletal muscle insulin resistance[245,246] and was propagated to induce mitochondrial dysfunction due to mitochondrial DNA mutations.[83] Oxidative stress quantified via 4-hydroxynonenal (4HNE) protein, produced by ROS–lipid interaction, did not differ between the groups (Figure 35). High glucose levels, however, were shown to increase ROS production in endothelial cells even without insulin stimulus.[279] This could be due to lipid peroxidation as measure for ROS production being a more long-term effect. SOD activity and SOD1 protein abundance in mitochondria (Figure 36), but not in whole tissue lysates (Figure 35), were decreased by high glucose conditions and by insulin resistance. The protein abundance was only decreased under high glucose conditions, indicating an effect solely on mitochondrial level and not on the whole cell. SOD is an antioxidant enzyme that catalyses the disproportionation of superoxide anion ($O_2^{\bullet -}$) into molecular oxygen (O_2) and hydrogen (H_2O_2).[280] The SOD activity assay does not distinguish between SOD1 or 2, but since the assay was performed in isolated mitochondria, it could be suggested that it is mainly the mitochondrial SOD2 activity that is decreased with high glucose and insulin resistance, although the protein abundance is not changed. SOD1, however, the cytosolic SOD, is also debated to eventually translocate to

mitochondria especially in context with amyotrophic lateral sclerosis.[281] In allonax-induced diabetes in rats, SOD activity was also reduced over disease time in muscle.[282] Similar results were reported in a high-fat diet rat model. The rats were preselected based on their low capacity to run.[283] In retina tissue of diabetic mice SOD activity was also reduced.[88] A reduced SOD activity would likely lead to a higher ROS exposure, which was linked to reduced insulin sensitivity,[246] but 4HNE levels remained unchanged in this experimental setup. Since SOD2 activity is putatively controlled by PGC-1α,[284] decreased PGC-1α in insulin resistance as described above could be an explanation for the decreased activity.

5.2.1 Conclusion

High glucose concentrations as also faced in hyperglycemia due to insulin resistance lead to a cell phenotype that seems to rely more on glycolysis for ATP generation than on oxidative phosphorylation. Mitochondrial content is thereby decreased as cause or consequence of the more glycolytic than OXPHOS oriented ATP generation under high glucose concentrations but also under chronic insulin treatment. Probably due to this lower mitochondrial mass the overall respiratory capacity is lower compared to the cells under normal glucose concentration. This is further underpinned by a lower relative protein abundance of the ETC complexes (even after normalisation for the mitochondrial marker protein citrate synthase). Lower respiration is usually associated with less ROS production. These proposedly lower ROS levels, however, might be balanced by the observed decrease in oxidative defense (SOD activity but also superoxide dismutase (SOD) 1 protein levels) in isolated mitochondria from high glucose treated, but also insulin treated cells. A lower complex 1, but higher complex 2 linked respiration, additionally points towards a substrate shift for oxidative phosphorylation, which relies less on NADH. Another possible aspect to be considered is the glycolytic phenotype. The fact that not only the function of mitochondria is altered after 48 h of treatment, but also protein levels, indicates a tight regulation and quick adjustment of mitochondria to external conditions. These data suggest, that metabolic overflow in these cells downregulates down-stream pathways from glycolysis. This might support the hypothesis of decreased mitochondrial oxidation leading to metabolite accumulation resulting in an impairment of insulin signalling.

5.3 Tissue-specific comparison: liver and skeletal muscle mitochondria

Mitochondria are the major sites of energy production through oxidative phosphorylation, but mitochondrial composition is tailored to the specific needs of different tissues. Transcriptional or post-translational events finely adjust the mitochondrial proteins leading to an adaption to the specific energy demand and environment of the tissue.[58,70,285] Comparing tissue lysates and isolated mitochondria from murine skeletal muscle and liver, tissue-specific differences were detected on protein and lipid level, but also on the function level.[152]

5.3.1 Muscle and liver mitochondria show distinct differences in substrate preference for mitochondrial respiration

In high-resolution respirometry (HRR) of isolated mitochondria a significantly different substrate preference for oxidative phosphorylation was detected for liver vs. muscle mitochondria (Figure 37). With octanoylcarnitine/malate present, muscle mitochondrial phosphorylating respiration increased significantly after the complex 1 linked substrate pyruvate was added while liver mitochondria did not respond to pyruvate addition (Figure 37 A). This corroborates published data reporting almost a doubled respiration on palmitoylcarnitine (PaCa) upon pyruvate addition compared to PaCa respiration without pyruvate in muscle. The respiration of liver mitochondria does not change by the addition of pyruvate to respiration on PaCa.[60] Pyruvate is transported into the mitochondria via mitochondrial pyruvate carrier (MCP1 and MCP2).[286] Protein levels employed by western blot showed higher levels of MPC protein in liver than in muscle,[287] therefore not providing a limitation of pyruvate import into liver compared to muscle explaining the non-response of liver mitochondria to pyruvate. However, pyruvate offered to mitochondria could have different metabolic fates: (1) it could be metabolised to acetyl-CoA by the pyruvate dehydrogenase complex (PDH), then be further metabolised in the TCA cycle feeding electrons into the respiratory chain and finally leading to an increase in respiration detectable in HRR. Indeed, PDH protein was found to be higher in tissue lysates from muscle compared to liver (Figure 44) indicating a more prominent channelling of pyruvate towards acetyl-CoA into oxidative phosphorylation. This potentially contributes to the higher muscular response to pyruvate. Additionally or alternatively, the regulation of PDH can be different as PDH is inhibited by pyruvate dehydrogenase kinase (PDK). Both muscle and liver express 3 isoforms of PDK (PDK1, 2 and 4), but all of them are more strongly expressed in muscle than in liver,[288] a finding which is inconsistent with the findings in HRR. (2) The second possible fate of pyruvate, at least in gluconeogenic liver tissue, is its metabolisation by pyruvate carboxylase (PyC) to oxaloacetate for gluconeogenesis. (3) A third option is a direct shuffling into other anabolic pathways (e.g. ketogenesis) in the form of acetyl-CoA. Liver is the main site for gluconeogenesis.[61] PyC expression in muscle is reported controversially with- if at all-relevance in muscle just to anaplerotically replenish the oxaloacetate in the TCA cycle.[289-291] Western blot analyses in this study revealed no detectable PyC protein in muscles samples, whereas it was prominently detected in liver (Figure 44), supporting the hypothesis that exogenously added pyruvate might be directly metabolised by PyC and channelled into oxaloacetate for gluconeogenesis in liver. Accordingly, no increase in respiration would be observed after pyruvate addition.

A closer look at the specific protein equipment of isolated mitochondria from muscle and liver by western blot analyses (Figure 43) revealed significantly lower levels of citrate synthase protein in liver mitochondria compared to muscle. Citrate synthase as the enzyme of the first step of the TCA cycle catalyses the condensation of acetyl-CoA with oxaloacetate to citrate. This finding together with the fact that protein levels of all electron transport chain (ETC) complexes except of complex 3 were significantly less abundant in liver mitochondria than in muscle, leads to the suggestion that muscle mitochondria preferably feed the TCA cycle and thereby oxidative phosphorylation to generate ATP. Liver mitochondria, however, provided with the glycolytic substrate pyruvate shuttle it into anabolic

pathways, leading to a lower need of ETC protein equipment than in muscle. Lower abundances of the ETC complex proteins of mitochondria in liver compared to muscle were reported previously.[55] Another factor possibly contributing to the liver-specific mitochondrial non-response to pyruvate might be the fact that the mitochondria are already respiring on a fatty acid as substrate before pyruvate is added. In addition, it is likely that the capacity for fatty acid vs. carbohydrate oxidation is elevated in liver compared to muscle This is corroborated by the fact that muscle is mainly using carbohydrates (glucose) in postprandial states for ATP production, which is responsible for most of the glucose disposal.[7,62] Thus, fatty acid oxidation might probably maximally feed the ETC via complex 1, with no further capacity or need for another complex 1 substrate. The significantly higher protein abundances of hydroxylacyl-CoA dehydrogenase (HADHA) and medium-chain acyl-CoA dehydrogenase (MCAD) detected in western blot analyses of whole tissue lysates underpin this higher capacity to oxidise fatty acids in liver than in muscle (Figure 44).

With the onset of phosphorylating respiration with ADP, the absolute change from leak respiration on octanoylcarnitine and malate (OctM; Figure 37 D) was significantly higher in mitochondria in muscle than in liver. On the one hand this possibly indicates a higher capacity of muscle for oxidative phosphorylation to generate ATP generally needed due to the great energy demands during exercise,[62,63,292] but it could also reflect the possible tendency of liver mitochondria to not fully oxidise the fuels, but instead transferring them continuously into anabolic processes as discussed above. Additionally, citrate synthase protein, a mitochondrial mass marker, was significantly higher in abundance in muscle lysates compared to liver lysates (Figure 44), indicating a higher mitochondrial content in muscle than in liver. This may also contribute to a much higher respiratory capacity due to high ATP demands during training. Accordingly, Benard et al. (2006)[55] reported higher citrate synthase activity in muscle than in liver. Additionally, the muscle is metabolically more flexible than the liver and able to switch between carbon sources for ATP production.[63] This is another explanation for the higher response of skeletal muscle mitochondria to the addition of another glycolytic substrate, while already respiring on fatty acids.

Mitochondrial phosphorylating respiration of liver, however, showed a significantly higher increase compared to muscle mitochondria when providing the complex 2-associated substrate succinate in addition to the substrates OctM and pyruvate (Figure 37 B, see the SUIT protocol in Table 5). These data likely indicate either a saturated ETC in the muscle mitochondria already achieved providing OctM and pyruvate as substrates or a saturated complex 2 pathway by OctM oxidation, possibly explaining why the addition of a further complex 2 substrate did not further increase respiration.

In liver mitochondria, oxidative phosphorylation can still be increased after OctM and pyruvate via feeding complex 2 with succinate (Figure 37 B), indicating no saturation of that pathway with fatty acids. This higher capacity of complex 2 observed in liver mitochondria is also supported by the finding of a significantly higher contribution of complex 2 respiration towards maximal respiration (uncoupled) on complex 1 and 2 in liver mitochondria than in muscle (Figure 37 C). The observation of complex 2 carrying out most of the maximal electron transport chain capacity in liver was also reported by Holmstrom et al. (2012)[152] Jorgensen et al. (2012)[60] reported that liver displays a much smaller

succinate effect than muscle when respiring already on PaCa, but this finding was entitled as ´unexpected´.

Thus, taking all the results together, complex 2 activity was observed to be indicatively higher in liver mitochondria than in muscle mitochondria. This could not be explained by higher complex 2 protein abundance in liver, since all complexes except of complex 3 were higher abundant in muscle mitochondria as verified by western blot analysis. Accordingly, a saturation of the ETC as discussed above is more likely.

5.3.2 Tissue-specific lipid composition of mitochondria

Mitochondrial phospholipid content and composition have been shown to also affect electron transport chain activity and respiratory function.[71,72,92,97,99,101,102,240,241] As lipidomics data revealed, cardiolipin (CL) levels, as well as their precursor phosphatidylglycerol (PG), were significantly higher in skeletal muscle than in liver mitochondria (Figure 41). This might be due to a higher density of cristae, since cardiolipins are mainly located in the inner membrane of mitochondria.[23] Consistent with this explanation is, that CL may predominantly facilitate tight membrane folding.[293,294] Cardiolipin synthase expression was observed to be higher in skeletal muscle than in liver[295] according to the higher CL levels detected. Cardiolipin, the signature lipid of mitochondria, has been shown to be a key player in the organisation of the general mitochondria membrane structure and of the essential electron transport chain components into higher order assemblies. High cardiolipin concentrations are associated with higher oxidative phosphorylation in mitochondria.[92,97,99,101,102,240,241] In contrast, reduced CL levels due to mutated tafazzin in Barth syndrome are associated with deficits in mitochondrial function in oxidative phosphorylation (OXPHOS).[296] The lipidomics data determined in this thesis are in line with the hypothesis that the significantly higher CL levels in skeletal muscle mitochondria (Figure 41) rely more on OXPHOS (as discussed above). A theory by Cheng et al. (2008)[297], who investigated brain mitochondrial lipidomes, described the cardiolipin composition to be tailored to the metabolic needs of the surrounding tissue. Accordingly, tissues with high mitochondrial activity like muscle and liver are equipped with CL that are especially suited for supporting mitochondrial function, whereas other tissues where mitochondrial function is of lower relevance, e.g. in brain, mostly rely on glucose. These tissues have no need for specifically adapted tetra-linoleoyl-CL (18:2/18:2/18:2/18:2) and lipid profiles can be expected to be much more diverse. To this extent, acyl chain composition of lipids, especially of CL, were investigated (Figure 42). However, cardiolipin synthase is not specific for acyl chains.[298,299] Instead, the specificity for acyl chains stems from remodelling the cardiolipin. Tafazzin as example, a phospholipid-lysophospholipid transacylase is one of the most important enzymes involved in cardiolipin remodelling.[300] The mutated tafazzin in Barth syndrome patients mostly affects heart and skeletal muscle leading to the assumption of a higher expression in these tissues. However, expression levels of tafazzin were comparable between all tested tissues including heart, muscle but also liver.[301] Additionally, higher enrichment of heart, skeletal muscle and liver CL with linoleic acid was observed not to be due to increased tafazzin mRNA expression,[301] indicating that tafazzin expression does not reflect mature CL levels. Acyl-CoA:lysocardiolipin acyltransferase-1 (LCLAT1) catalyses

another important step in CL remodelling, that is the acylation of lysocardiolipin (or in general polyglycerophospholipids) with acyl groups from linoleoyl-CoA or oleoyl-CoA back to cardiolipin, and converts saturated CL into more unsaturated CL. ALCAT1 expression is increased in response to oxidative stress. This would support the finding of more unsaturated fatty acids in muscle mitochondria,[302] the organ confronted with peaks of oxidative stress by physical activity.[303-305] However, LCLAT1 is more highly expressed in liver than in muscle.[306,307] Since expression levels not always reflect protein levels or activity, the tissue-specific fatty acid specificity remains unclear.

The dominance of tetra-linoleoyl-CLs in the muscle and liver mitochondria is an example for the extraordinary selectivity of the cardiolipin remodelling process. It is the most abundant PUFA-CL species in liver and in muscle mitochondria as already published previously,[308,309] but the relative amount is higher in muscle (25.5% ± 4.3%) than in liver mitochondria (13.6% ± 3.2%), see Figure 42. Previously published percentages of tetra-linoleoyl-CL in rat liver mitochondria were higher with 56.5% ± 4.7%, but concentrations in heart muscle mitochondria (probably comparable to skeletal muscle) were in the same range as observed in this work (21.4% ± 1.8%).[310] 18:2-CL is speculated to play an important role in the response to high energy demands in tissue as described for the contractile function in heart.[311,312] This could be an explanation of higher levels in muscle mitochondria than in liver. In skeletal muscle, the second most abundant PUFA was 22:6 in CL but also PE (4.2.2.1.4), which was even published to be the most abundant PUFA in summed phospholipids in muscle of mice.[313] In mouse heart, over 50% of all CL species contained 22:6 acyl chains.[310] In liver mitochondria 20:4 acyl chains was the second most abundant PUFA (4.2.2.1.4), again being published to be the most abundant PUFA in summed PLs of mouse liver.[313] Cortie et al. (2015)[313] however, failed to detect CLs, instead, the acyl chain percentages were summed from PC, PE, PS, PG, PA. PEs were shown to consist of more PUFA in muscle than liver (4.2.2.1.4). PE and CL make up for 32% of all phospholipids in liver mitochondria and for almost 40% in muscle, dominating overall phospholipid profiles. PE and CL are functionally converging in mitochondria stressing their individual, but also combined importance for mitochondrial function.[242] Mutant prokaryotic cells lacking the ability to synthesise phosphatidylserine, the precursor of PE, and therefore devoid of PE, showed compensatory increased CL, PG and to a lesser extent PA levels.[314] This correlative relationship was also observed in yeast when PE or CL were depleted.[315]

A higher degree of unsaturation is associated with an increased susceptibility of membrane lipids to peroxidise depending on the number of bisallylic methylene groups present in PUFA.[316,317] CL containing 20:4 and 22:6 acyl chains are subject to passive CL oxidation (a non-selective process). CL is peroxidised, leading to decreased activity of respiratory chain complexes (I, III, and IV) as well as decreased supercomplex assemblage.[318-320] The oxidation to highly diverse unsaturated CLs is discussed as a source for lipid mediators.[321] Selective CL oxidation is required for induction of apoptosis;[322] but also enzymatically regulated oxidation of phospholipids might play a role in signaling.[323] The degree of polyunsaturation of the mitochondrial membrane was previously published to be positively correlated with mitochondrial proton leak.[324-326] Therefore, the higher amount of PUFA in PE and CL of muscle mitochondria than in liver mitochondria (4.2.2.1.4) are in concordance with the muscle mitochondrial

proton leak being assumed to account for 17-21% of standard metabolic rate whereas liver mitochondrial proton leak accounts for only 3-5%.[327] Leak respiration (OctM without exogenous ADP) in this thesis cannot be directly compared due to normalisation of the data.

Longer and more unsaturated acyl chains, especially 22:6, in cardiolipin seem to be directly channelled from phosphatidylglycerol (PG), the precursor of CL, to CL in skeletal muscle mitochondria (Figure 42). This might lead to a depletion of 22:6 acyl chains in muscle mitochondrial PG, whereas PGs consisting of the same acyl chains are still abundant in liver. Thus, we raise the hypothesis that these 22:6 acyl chain-enriched cardiolipins might be essential to provide the higher oxidative phosphorylation flexibility in muscle to cover higher ATP demands during exercise. This is supported by an observed increase of these 22:6 acyl chains in phospholipids in the glycolytic EDL muscle of mice after exercise.[328] Also in endurance trained men phospholipid 22:6 level were positively correlated with type 1 oxidative fibres.[329] The upregulation of selective incorporation of 22:6 acyl chains in PC and PE upon exercise was recently investigated by Valentine et al. (2017)[330] suggesting lysophosphatidic acid acyltransferase 3 as being responsible. A twelve week fish oil supplementation in men led to incorporation of 22:6 acyl chains in PC and PE in mitochondrial membranes, led to no change in respiration, but increased mitochondrial ADP sensitivity and maximal mitochondrial ROS emission.[191] However, an increased remodelling of CL towards 22:6 acyl chains was also observed in diabetic mouse heart.[331]

Among others, another possible explanation for the tissue-specific fatty acid profiles is the responsiveness of tissue to certain fatty acids. Significantly higher proportion of radiolabelled LDL (^{3}H-cholesteryl oleate tracer) enriched in DHA was found in heart, brown adipose and brain tissues relative to liver LDL.[332] This higher accumulation of DHA in tissues, skeletal muscle, due to their myogenic precursor,[333,334] could be indicative for a more efficient uptake of these fatty acids, probably providing more 22:6 acyl chains for remodeling and synthesis of CL and PE. Isolated heart mitochondria of rats contained higher amounts of tetra-linoleoyl-CLs and CLs containing 22:6 acyl chains after supplementation with docosahexaenoic and eicosapentaenoic acid,[335] indicating an impact of dietary long-chain PUFAs on mitochondrial phospholipid composition.[336] Supplementation with 22:6 acyl chains was reported to increase both 22:6 and 20:5 acyl chains and decrease 20:4 acyl chains in cardiac mitochondrial phospholipids. This is discussed as a cardioprotective effect of these fatty acids.[337] Since 22:6 acyl chain levels of the standard mouse diet were not provided, also precursor fatty acids may preferably be taken up and synthesised to acyl chains 22:6. Another possible explanation is related to liver being the major site of *de novo* lipogenesis.[64]

Of all detected lipid classes, the most distinctly different lipid species were within the lipid class of phosphatidylethanolamine (PE) showing higher levels in muscle mitochondria compared to liver (Figure 41). Previously published data showed that depletion of mitochondrial PE in cells led to defective ETC complexes and a decreased respiratory capacity.[72] This is in conformity with a higher electron transport chain activity and respiration of PE N-methyltransferase (PEMT) lacking cells accumulating PE. Mice lacking PEMT accumulating PE in hepatic mitochondria shifted pyruvate metabolisation towards decarboxylation and energy production instead of carboxylation and glucose production.[71] This shift in pyruvate metabolisation by higher amounts of PE might also be relevant in the muscle and

liver-specific mitochondrial response to pyruvate as discussed above. A higher increase of respiration after pyruvate addition of muscle mitochondria and significantly higher levels of PE were detected in muscle than in liver mitochondria.

Several pathways for PE synthesis exist. The CDP-ethanolamine pathway in the ER is the preferred pathway in rat liver[338] and hamster heart.[339] This pathway was shown to result in PE species enriched in mono- or di-unsaturated fatty acids in the sn-2 position, while the phosphatidylserine decarboxylation (Psd) pathway, residing in mitochondria, generates PE species with polyunsaturated fatty acids.[340] CDP-ethanolamine pathway published to be dominant in rat liver could be a possible explanation for the lower PUFA fatty acid composition in liver PE compared to muscle PE.

These tissue-specific differences in mitochondrial equipment and function could play a major role in disease pathologies and form a basis for drug targeting. In skeletal muscle evidence points to either a decreased mitochondrial function in diabetes at least in humans,[137-139,141-143,275,276] or unchanged function.[341-345] This is in contrast to an increased mitochondrial function in liver of insulin resistant, diabetic or non-alcoholic fatty liver disease (NAFLD) patients.[154,346-350] Much less data reporting a decreased mitochondrial function in liver in diabetes exist,[159] being more strongly associated with a progression towards nonalcoholic steatohepatitis (NASH).[154,351] Thus, the results of this thesis are part of a more comprehensive understanding of the molecular and functional differences of mitochondria between tissues and provide new insights into tissue-specific mitochondrial contribution to disease developments and states, which might play an important aspect in targeting these organelles by drugs affecting their function.

5.3.3 Conclusion

We established and optimised a reliable and comprehensive method to obtain tissue-specific lipid profiles from pure muscle and liver mitochondria. We integrated this tool into a systems biological analysis of isolated mitochondria covering not only lipidomics but also functional and mitochondrial protein analyses.

The lack of response of liver but not muscle mitochondria to pyruvate addition detected in respirometric analyses supports the hypothesis of mitochondria being tailored to specific tissue demands. Thus, liver might shuttle added pyruvate directly into anabolic processes such as gluconeogenesis instead of using it for ATP production via oxidative phosphorylation when fatty acids are also present. Not only abundances of proteins involved in gluconeogenesis but also in β-oxidation were higher in liver than in muscle lysates as employed by western blot, supporting a higher shuttling of added substrates into anabolic processes. Muscle mitochondria seem to more strongly rely on oxidative phosphorylation. This finding is supported by a higher protein abundance of electron transport chain complexes, a generally higher mitochondrial mass as well as higher amounts of lipids like cardiolipins and phosphatidylethanolamines, which are associated with a higher electron transport chain activity, respiration and supercomplex assembly. Fatty acid composition was distinctly different between liver and muscle mitochondria highlighting specific fatty acids. E.g. 20:6 acyl chains in CLs seem especially important in supporting the tissue-specific function of muscle mitochondria, which seem to more

strongly rely on OXPHOS. In contrast to that, 22:6 acyl chains were only detectable in liver in the CL precursor PG, but not in CL itself.

These results may build the base for further investigations on mitochondrial specificities of liver and skeletal muscle as two insulin target organs, responsible for endogenous glucose production and disposal. They also help elucidating organ cross-talks in health (e.g. exercise) and disease. They might lead to more target-specific treatments of mitochondrial dysfunctions associated with, for example, insulin resistance and type 2 diabetes.

5.4 Omics investigation of mitochondrial adaptions in liver and skeletal muscle to excess energy intake and physical exercise: Control diet versus energy-rich diet either with or without treadmill training

Training of the mice led to a significantly reduced weight gain induced by high-energy diet (Figure 47 A). This result is concomitant with slightly lower fasting insulin levels and a slightly lower area under the curve (AUC) of the blood glucose levels during the intraperitoneal glucose tolerance test (Figure 47 B+C), indicating training-associated rescue effects of the insulin sensitivity in trained compared to sedentary mice. In Goto-Kakizaki rats, which spontaneously develop T2Dm with age, the progression of the disease was shown to differently affect muscle and liver mitochondria. Particularly, a reduced complex 2 flux was only observed in liver (not in muscle), raising the hypothesis of a tissue-specific involvement and role of mitochondria in T2Dm pathology.[60] In high resolution respirometric (HRR) and Seahorse XF96 measurements performed in this thesis the oxidative phosphorylation of fatty acid oxidation substrates (octanoylcarnitine and malate, OctM and palmitoylcarnitine and malate, PaCaM) was significantly higher in muscle mitochondria of high-energy fed mice than in control fed mice independent of training (Figure 50 A+G). Additionally to this higher fatty acid oxidation capacity, a higher citrate synthase activity in muscle lysates of HED fed mice was observed (Figure 48), a marker for mitochondrial mass.[352] The higher mitochondrial amount is supported by a higher mitochondrial yield of mitochondria being isolated from HED muscle than from CON muscle (Figure 49). This is in concordance with animal studies investigating insulin resistance and mitochondrial function, hereby reporting increased fatty acid oxidation capacity, increased mitochondrial content and increased oxidative protein activities.[25,148-152] This effect is discussed as compensatory effect to overcome excess substrate flows at early stages of disease development.[25,148-152] Both rats with high capacity to run and low capacity to run were reported also to increase fatty acid oxidation after high fat feeding.[283] However, high fat feeding of mice led to an increase of citrate synthase, HADHA and MCAD activity in muscle, that was not observed in liver.[151]

Contrarily, in human studies, the relationship between insulin resistance, obesity and mitochondrial function is discussed more controversially, suggesting that this compensatory effect could be specific to the animal model chosen. Mice experiments in inbred strains however allow in a very controlled

way to induce insulin resistance and to investigate underlying molecular mechanisms, whereas humans are much more heterogeneous.

Some research groups did not observe mitochondrial alterations like reduced oxidative capacity,[27,139] or the reduced mitochondrial content[27,140] in obesity or insulin resistance in humans. In addition, contrary findings to our animal studies were reported, for example a lowered oxidative capacity in muscle biopsy material from T2Dm patients or obese compared to healthy subjects.[136-140] This effect even remained after the commonly applied normalisation to mitochondrial content (mtDNA, CS activity) except for one study,[139] and was also confirmed in isolated mitochondria.[141]

Since the animal study reported in this thesis is in accordance with previously published animal studies, but only with some of the studies in humans, it can be speculated that this observed discrepancy is species-dependent. The differences observed in respiration between mitochondria derived from CON-fed and HED-fed mice are not explicable by differences in mitochondrial mass, since mass was even increased in HED. Additionally an apparent substrate switch of respiration was observed in this thesis. Pyruvate addition (complex 1-associated substrate) to mitochondria respiring on OctM led to a significantly higher increase in muscle mitochondria from control diet-fed mice compared to high-energy diet fed mice (Figure 50 B). A saturation of the electron transport chain (ETC) being fed with electrons into complex 1 and 2 from fatty acid oxidation, can be reasoned as this would not cause a further increase in respiration by an additional complex 1 substrate. Another explanation could be upregulated pyruvate dehydrogenase kinase (PDK) isoforms in skeletal muscle as reported due to high-fat feeding in rats.[353] PDK upregulation could lower pyruvate dehydrogenase activity and thus metabolisation of the added pyruvate. In addition to the effect of high-energy diet on mitochondrial function in muscle, treadmill training led to a significantly increased mitochondrial oxidative capacity on substrates for fatty acid oxidation (OctM) combined with the complex 1-associated substrate pyruvate (Figure 50 C). This trend was persistent after addition of succinate, a complex 2-associated substrate, causing the electron transport chain to be fully activated under phosphorylating (ATP generating) conditions (Figure 50 D). Similarly, after 6 weeks of training ATP production in humans was observed to be enhanced by 92% in skeletal muscle.[354] After uncoupling the electron transport chain from ATP production in mitochondria using the protonophore FCCP, muscle mitochondria derived from trained mice showed the significantly higher maximal oxidative capacity again (Figure 50 E). The activity of cytochrome oxidase (COX) proposed to be rate-limiting in ETC[355,356] was shown to be increased in rat muscle after 12 weeks of running.[357] Likewise, ten weeks of aerobic training of healthy and diabetic men increased mitochondrial respiration.[358] This higher oxidative capacity could be due to a compensatory increase to cover a lower mitochondrial mass. In contrast, citrate synthase activity in muscle of these individuals was not changed by training in this study. Citrate synthase was discussed to be regulated acutely rather than by chronic exercise in humans questioning its role as a marker in exercise studies.[359,360] This leads to the assumption that citrate synthase protein might be a better measure. However, a training effect was not observed on citrate synthase protein level (data not shown). However, it was even possible to obtain a higher amount of mitochondria from trained mouse muscle than from untrained muscle, indicating a higher mitochondrial mass although not be-

ing reflected on citrate synthase level (Figure 49 A). Training did not show an effect on mitochondrial function of liver mitochondria, proposing a distinct tissue-specific difference between the training responses of mitochondria. High-energy diet, however, affected liver mitochondrial respiration. Given the different responses to the same stimulus in muscle and liver mitochondria, mitochondria seem to be tailored to the specific energy demands of the specific tissue as discussed in 5.3. Liver mitochondria from HED-fed mice showed a higher oxidative capacity than CON-fed mice (Figure 52). This pattern was observed under phosphorylating conditions respiring on fatty acids, but also with the additional complex 1-associated substrate pyruvate and with the additional complex 2-associated substrate succinate (Figure 51, Figure 52). The higher oxidative capacity of mitochondria from HED fed mice was also observed after uncoupling the electron transport chain from ATP production with FCCP (Figure 51, Figure 52). This corroborates previously published observations of higher oxidative capacity in isolated liver mitochondria in an obese mouse model compared with its obese-resistant congenic strain.[361] Accordingly, liver biopsies of obese insulin resistant humans with and without non-alcoholic fatty liver (NAFL) but not steatohepatitis (NASH) were observed to have higher oxidative capacity in whole liver tissue, as well as in isolated mitochondria.[154] This finding was independent of an increased mitochondrial mass, which is in conformity with results in this thesis showing no differences in citrate synthase activity in liver, the mitochondrial mass marker, between the interventions (Figure 48 B). The higher oxidative capacity was also seen in indirect methods to assess hepatic mitochondria.[155,156] A previous study revealed higher fatty acid oxidation of obese (ob/ob) mice compared to lean, but also reported higher citrate synthase levels.[362] Contrarily, in humans there is also evidence of a normal oxidative phosphorylation in T2Dm compared to lean and obese patients assessed by HRR.[157] Even an impaired hepatic mitochondrial function in T2Dm in humans was described,[158,159] also seen in diabetic rats after high-caloric feeding.[160] Liver mitochondria derived from mice fed with high-energy diet showed significantly higher leak respiration with octanoylcarnitine and malate present than mitochondria derived from control-fed animals (Figure 51 A). This could be due to a stronger uncoupling by protein 2 activity (UCP2), which uncouples respiration from oxidative phosphorylation. UCP2 mRNA and protein was shown to be induced in obese (ob/ob) mice.[363,364] This decrease of efficiency in ATP production is currently discussed as a mechanism to cope with excess substrate supply and thereby to avoid too much reactive oxygen species (ROS) production by an overload of the ETC.

To investigate the oxidative defence and ROS load, SOD activity and protein content in isolated mitochondria and tissue lysates were investigated (4.2.2.2.8). The activity of mitochondrial superoxide dismutase is putatively controlled by PGC-1α,[284] a co-activator of nuclear receptors, which plays an important role in controlling mitochondrial biogenesis.[274] Although oxidative capacity (ETC complexes are the major source for ROS[74-78]) and mitochondrial mass was increased at least in muscle due to diet and training, the oxidative defence by superoxide dismutase (SOD) was unchanged both on activity and on protein level for muscle and liver. A reduced SOD activity would likely lead to a higher ROS exposure. Exercise was previously published to promote generation of ROS,[303-305] which is associated with insulin sensitising. The latter may stem from the upregulation of ROS-sensitive transcriptional regulators of insulin sensitivity and increased antioxidative defence e.g. by SOD.[305,365] Due to this link

of ROS to positive effects of exercise,[305,365] but evidently also to reduced insulin sensitivity,[246] the role of ROS still remains paradoxical.

Availability of certain fatty acids was speculated to form the limiting factor determining mitochondrial lipid composition, since investigated cardiolipins were built from acyl groups dominant in the respective tissue.[24] This is supported by higher amounts of tetra-linoleoyl-CLs and CLs containing 22:6 acyl chains in isolated heart mitochondria of rats after supplementation with docosahexaenoic and eicosapentaenoic acid.[335] This indicates dietary long-chain PUFAs to have an effect on mitochondrial phospholipid composition.[336] This hypothesis can also be supported by the results for high-energy diet where similar changes in liver and muscle mitochondrial lipid composition were induced, although their lipid composition was highly tissue-specific (Figure 53). Mitochondrial membranes are discussed to adapt to the lipid composition provided by the diet.[21] Fatty acid composition of the mitochondrial lipids, however, did not completely reflect the fatty acid composition provided by the high-energy diet, indicating regulating or limiting factors beyond the availability of certain fatty acids (4.2.2.2.7).

Higher amounts of cardiolipin (CL) the signature lipid of mitochondria, which has been shown to be a key player in the organisation of the general mitochondria membrane structure and in the organisation of the essential electron transport chain components into higher order assemblies were associated with higher oxidative phosphorylation in mitochondria.[92,97,99,101,102,240,241] Defective CL remodelling was discussed in both type 1 and 2 diabetes.[366-368] It was shown that at a very early stage of pathological development in a diabetic mouse, CL in heart is abnormally remodelled. CL content is decreased and the usual prime tetra-linoleoyl-CL is depleted and replaced by longer and more unsaturated fatty acids.[331] A decreased level of unsaturation of human skeletal muscle phospholipids was directly related to impaired insulin action.[369] Absolute CL content of mitochondria was not observed to be different between CON-fed mice and HED-fed mice in this work, and tetra-linoleoyl-CL was significantly increased solely in liver, but not in muscle, due to HED (Figure 54), which led to reduced insulin sensitivity (Figure 47). Absence of CL was shown to be partially compensated in respiratory chain activity by its precursor PG in mitochondria.[370] Furthermore, absolute PG levels remained the same in the groups in this work, indicating no elevation of PG to compensate the lower tetra-linoleoyl-CL levels in liver mitochondria of CON-fed mice.

Stearoyl-CoA desaturase-1 (SCD1) is located in the ER and catalyses the formation of MUFAs from saturated fatty acids, especially the major components of membrane phospholipids oleate and palmitoleate from stearoyl-CoA and palmitoyl-CoA.[371] Insulin-resistant muscle of ZDF mice showed increased SCD1 levels,[372] indicating a possible role of SCD1 in insulin resistance development. Reversely, pure deficiency of insulin action present in muscle-specific insulin receptor knockout (MIRKO) mice results in downregulation of SCD1.[373] The possible role of SCD1 and its contribution to insulin resistance makes it an interesting feature in follow-up experiments.

Eight weeks of regular treadmill training were previously reported to significantly increase the peroxidative stress (measured as hydroperoxide amount) in liver mitochondrial membranes of rats fed a diet enriched in olive or sunflower oil. The same was observed in muscle mitochondria upon olive oil diet.[41] Treadmill training was hypothesised to increase peroxidative stress by increased PUFA

amounts in liver mitochondria seen under sunflower oil diet and for muscle mitochondria under olive oil enriched diet.[41] Due to the almost 6 fold lower amounts of hydroperoxide levels reported in muscle compared to liver, Mataix et al. (1998)[41] speculated muscle to be more resistant to oxidative stress induced by a high degree of unsaturated fatty acids in the diet. This was based on the increase of mitochondrial oxidative defence (measured via SOD activity) with training.[374] The same working group published higher amounts of saturated fatty acids, lower amounts of MUFA and higher amounts of PUFA levels in liver mitochondria due to exercise in rats and lower PUFAs in muscle mitochondria.[21] The lower amount of MUFAs solely seen in liver, was discussed to be due to the higher metabolic rate of this tissue.[21] Another study from this working group revealed, that rats fed with a diet enriched in sun flower oil showed increased SFA, MUFA and PUFA (n-6) percentages in liver but not in muscle mitochondrial lipids after 8 weeks of submaximal training.[42]

Summarizing, the positive health effect of exercise might be rather subtle at least on lipid levels, since only little data, and partly inconclusive ones, are available on the effect of exercise on mitochondrial lipid composition in liver or muscle.[21,41,42] This hypothesis is supported by the observed effects of exercise on the mitochondrial lipid profile which were much lower than the impact of the high-energy diet in this work, as also described for skeletal muscle phospholipids.[375]

5.4.1 Conclusion

A higher mitochondrial mass in high-energy fed mice in muscle but not in liver does not only support the hypothesis of a tissue-specific involvement in disease pathology, but also the hypothesis of a compensatorily increased mitochondrial function in insulin resistance to overcome excess substrate supply. This was often observed in animal models in muscle. Muscle oxidative capacity was affected by both diet and training, while liver was solely and greatly affected by diet, leading to the assumption that the training effects might only influence mitochondrial respiratory function of the trained muscle, but not liver. Since muscle insulin resistance plays a role in the early development of T2Dm, the positive impact of training on muscle mitochondrial function might cause the slightly improved insulin sensitivity in trained HED-fed mice. Although function of muscle and liver mitochondria was affected differently by training and high-energy diet feeding, diet had a much greater impact on lipid composition of the mitochondria than training. Interestingly, although having highly tissue-specific lipid compositions muscle and liver mitochondria were affected similarly facing the high-energy diet. However, the fact that the dietary fatty acid composition did not always reflect the mitochondrial fatty acid composition of the detected lipids, raises the hypothesis of mitochondrial lipid composition not necessarily being randomly determined just by the provided lipid pool, pointing towards a selective process for lipids being incorporated into mitochondria.

6 Summary

Dysfunctional mitochondria are widely discussed to be involved in the pathophysiology of human diseases such as cancer or diabetes. However, it is still unclear whether metabolic overflow leads to disturbances in mitochondrial substrate utilisation and, consequently, to insulin resistance or if mitochondrial dysfunction is a consequence of impaired insulin signalling. This work aimed at elucidating this controversially discussed role of mitochondrial dysfunction in the etiology of insulin resistance and diabetes. In this context, mitochondrial adaptions to excess energy intake, insulin resistance and exercise were addressed on multiple levels using systems biological analyses of isolated mitochondria from cell culture and tissues from mouse models and humans. The applied techniques covered sample preparation, lipidomics approaches and also protein and functional analyses including enzymatic assays and high-resolution respirometry.

Changes in lipid homeostasis are very likely to affect mitochondrial membrane composition which, in turn, regulates mitochondrial structure and function. Since most lipids are not specific for individual organelles and therefore challenging to quantify in cell or tissue lysates in a mitochondria-specific fashion, an accurate, comprehensive lipid profiling strategy which first enriches mitochondria and minimises contaminations by membranes from other organelles was established and published in the context of this thesis as a prerequisite to investigate the contribution of individual lipids to mitochondrial (dys-)function (Kappler et al. (2016)[130]). Mitochondria isolation by ultracentrifugation yielded the purest samples and was used for further lipidomics analyses of mitochondria obtained from cell culture models and mouse tissues in this thesis. The two other methods tested in this work, differential centrifugation and an antibody coupled-magnetic bead assisted method, revealed more contaminations from other organelles. Therefore, they may result in misleading conclusions when isolating only impure mitochondria for ”omics” analyses. The established lipidomics approach was further modified by adding the antioxidant butylated hydroxytoluene for analyses of a special class of oxidised lipids, the oxysterols.

To study the hypothesis that skeletal muscle insulin resistance is the primary defect that is evident decades before β-cell failure and hyperglycemia develops, isolated mitochondria of a murine skeletal muscle cell line were investigated after induction of insulin resistance by chronic hyperinsulinemia and in the absence or presence of high glucose conditions. In this thesis it is shown, that chronic high glucose and insulin stimulation led to a decrease of mitochondrial mass in the C2C12 myotubes. This could be caused by the lower reliance on oxidative phosphorylation for ATP generation supported by the observed lower oxidative respiratory capacity. This hypothesis is further underlined by a concomitant switch in electron transport chain substrate preference. Hence, the cell culture findings of this thesis support the hypothesis that insulin resistance can be the cause of decreased or incomplete mitochondrial oxidation leading to metabolite accumulation, further impairing insulin signalling. Additionally, this thesis reveals that both hyperinsulinemia and glucose oversupply caused decreased superoxide dismutase (SOD) activity and SOD 1 protein abundance on a mitochondria-specific level,

since it was observed solely in isolated mitochondria, but not whole cell lysates. Mitochondria are the major sites for reactive oxygen species (ROS) production and increasing evidence suggests that oxidative stress plays a major role in the pathogenesis of type 2 diabetes mellitus. The observed change in antioxidative defence and its impact on ROS levels are an interesting finding worthwhile to be further investigated.

To gain further comprehensive understanding of the molecular changes underlying the alterations in mitochondrial function and metabolic control induced by an energy-rich western diet and additionally to unravel the mechanisms by which exercise compensates overnutrition and prevents mitochondrial dysfunction, a high energy diet feeding mouse experiment including regular treadmill exercise training with subsequent lipidomics and functional investigations was employed. Whereas the higher fatty acid oxidation capacity observed under high-energy feeding was concomitant with an increased mitochondrial mass in skeletal muscle, this was not observed in liver. A higher mitochondrial oxidative capacity in high-energy-fed mice could be due to a compensatory increased mitochondrial function in insulin resistance to overcome excess substrate supply. The fact that this is mainly observed in skeletal muscles of animal models, makes it a probable rodent-specific phenomenon and therefore relevance for humans remains inconclusive. Muscle oxidative capacity was affected by both diet and training, while liver was solely and greatly affected by diet. Although function of muscle and liver mitochondria was affected differently by training and high-energy diet feeding, diet had a much greater impact on the lipid composition of the mitochondria in both tissues than training. The highly tissue-specific lipid compositions of muscle and liver mitochondria, as shown in this thesis, were affected similarly facing the high-energy diet. Training adaptions on lipid level seem to be rather subtle. Quantitative proteomics analyses, that are currently performed might further elucidate tissue-specific mitochondrial adaptations and a tissue-specific contribution to disease pathologies. Notably, mitochondrial fatty acid composition of the detected lipid classes did not always reflect the dietary fatty acid composition. This points to a selective process for lipid incorporation into mitochondria.

Besides differences in the adaptation to diet and exercise, the comparison of liver and muscle mitochondria revealed clear differences in lipid composition, enzyme abundance and respiration. Contrary to muscle, isolated hepatic mitochondria did not show an increase in respiration after adding pyruvate as an additional substrate to fatty acids. This detected “non-response” to pyruvate in respiration of isolated liver, but not muscle mitochondria supports the hypothesis of mitochondria being tailored to specific tissue demands. When fatty acids are already present, the findings of this thesis suggest that externally provided pyruvate is directly shuttled into anabolic processes such as gluconeogenesis or ketogenesis. Pyruvate is thus not used for ATP production via oxidative phosphorylation. In contrast, in muscle mitochondria, pyruvate can be used for oxidative phosphorylation even in the presence of fatty acids to react to the great changes in energy demand in this tissue for example during exercise. This was not only supported by a higher protein abundance of electron transport chain complexes and in general a higher mitochondrial mass, but also by a higher amount of lipids like cardiolipins and phosphatidylethanolamines, all associated with a higher electron transport chain activity, respiration and supercomplex assembly. Investigations on mitochondrial specificities of liver and

skeletal muscle as two insulin target organs, responsible for endogenous glucose production and disposal, could help to elucidate the tissue-specific role in health (e.g. exercise) and disease and might lead to more target-specific treatments of mitochondrial dysfunctions associated with for example insulin resistance and type 2 diabetes.

A further broadening of the knowledge about the mitochondrial role in development and prevention of type 2 diabetes is needed. A special focus should be on ruling out the controversy of published data, probably also caused by many different functional approaches applied in the studies all referring to the broad and general term “mitochondrial function”. This may be achieved by highly comparable and standardised experiments (e.g. suitable surrogate markers for mitochondrial mass) taking into account species and tissue specific mitochondrial differences. The methodology developed in this thesis can form a basis for future standardisation.

7 Zusammenfassung

Mitochondriale Dysfunktion wird wegen ihrer zentralen Rolle im Stoffwechsel oft in Zusammenhang mit der Pathophysiologie von humanen Krankheiten wie zum Beispiel Diabetes und Krebs gebracht. Es ist jedoch noch ungeklärt, ob eine erhöhte Energieaufnahme und damit Angebot an Metaboliten zu einer gestörten mitochondrialen Substratoxidation mit resultierender Insulinresistenz führt, oder ob eine mitochondriale Dysfunktion Folge einer gestörten Insulinsignalkaskade ist. Das Ziel dieser Arbeit war die kontroverse Rolle der mitochondrialen Dysfunktion in der Ätiologie von Insulinresistenz und Diabetes zu untersuchen. Zu diesem Zweck wurden mitochondriale Veränderungen infolge von überschüssiger Energieaufnahme, Insulinresistenz und Sport mittels systembiologischer Analysen in isolierten Mitochondrien aus Zellkultur, murinen und humanen Geweben untersucht. Die angewendeten Techniken umfassten die Probenvorbereitung, Lipidomics-Analysen, aber auch Protein- und Funktionsanalysen sowie enzymatische Tests und hochauflösende Atmungsmessungen.

Veränderungen in der Lipidhomeostase beeinflussen sehr wahrscheinlich die Zusammensetzung der mitochondrialen Membranen mit Folgen für die Mitochondrienstruktur und -funktion. Da die meisten Lipide nicht spezifisch für einzelne Zellorganellen sind, ist es eine Herausforderung, Mitochondrien-spezifische Lipide in Zell- oder Gewebelysaten zu quantifizieren. Um den Beitrag einzelner Lipide zur mitochondrialen Funktion/Dysfunktion untersuchen zu können wurde eine präzise und umfassende Methode zur Analyse von Mitochondrien-spezifischen Lipiden als Teil dieser Doktorarbeit etabliert und bereits publiziert (Kappler et al. (2016)[130]).Die Isolierung von Mitochondrien mittels Ultrazentrifugation führte zur besten Aufreinigung und wurde daher für die Lipidanalysen von Mitochondrien aus Zellkultur und Gewebe in dieser Doktorarbeit verwendet. Zur Mitochondrienisolation wurden auch die differentielle Zentrifugation und ein Ansatz basierend auf Beads mit gekoppeltem Antikörper in dieser Doktorarbeit getestet. Beide Methoden führten zu mehr Verunreinigungen mit anderen Organellen und die Aufreinigung von unreinen Mitochondrien könnte daher möglicherweise eine Missinterpretation von Ergebnissen in OMICS-Analysen nach sich ziehen. Die etablierte Methode zur Lipidanalyse wurde durch die Zugabe von dem antioxidativen butyliertem Hydroxytoluen modifiziert, um oxidierte Lipide, die sogenannten Oxysterole analysieren zu können.

Basierend auf der Hypothese, dass sich die Insulinresistenz im Skelettmuskel schon Jahrzehnte vor dem β-Zellversagen und der Hyperglykämie manifestiert, wurden Mitochondrien einer murinen Skelettmuskelzelllinie nach Induktion von Insulinresistenz mit chronischer Hyperinsulinämie in der An- oder Abwesenheit von Hyperglykämie isoliert und untersucht. In dieser Doktorarbeit konnte gezeigt werden, dass chronisch hohe Glukose- und Insulinkonzentrationen zu einer erniedrigten Mitochondrienmasse in C2C12 Myotuben führten. Dies könnte durch eine geringere Abhängigkeit der Zellen von der oxidativen Phosphorylierung zur ATP Produktion bedingt sein. Dafür spricht auch die ebenfalls beobachtete verringerte oxidative Kapazität und eine geänderte Substratpräferenz der Elektronentranportkette. Somit unterstützen die Ergebnisse dieser Doktorarbeit die Hypothese, dass Insulinresistenz zu einer verminderten oder inkompletten mitochondriale Oxidation führen könnte, wodurch

Metabolite akkumulieren, die die Insulinsignalkaskade weiter beeinträchtigen. Zusätzlich konnte in dieser Doktorarbeit gezeigt werden, dass sowohl Hyperinsulinämie als auch ein Überangebot an Glukose eine reduzierte Superoxid Dismutase (SOD) Enzymaktivität und SOD1 Proteinabundanz ausschließlich in Mitochondrien hervorrufen, da diese Veränderungen nur in isolierten Mitochondrien nicht jedoch im Gesamtzelllysat beobachtet wurden. Mitochondrien sind die Hauptquelle für die Bildung von Sauerstoffradikalen (ROS) und es gibt zunehmend Hinweise, dass oxidativer Stress eine wichtige Rolle in der Pathogenese des Typ 2 Diabetes spielt. Die beobachteten Veränderungen in der antioxidativen Abwehr und deren Auswirkungen auf die ROS Level sind ein interessanter Befund und werden weiter untersucht.

Um ein umfassenderes Verständnis für die molekularen Veränderungen der Mitochondrien durch funktionelle und metabolische Adaptionen an eine Hoch-Energie-Diät und Ausdauertraining zu erlangen wurde ein Mausexperiment durchgeführt. Zusätzlich wurden Lipidomics und funktionelle Analysen durchgeführt, um die Mechanismen von Ausdauertraining aufzuklären, welche die Folgen von Überernährung kompensieren und eine mitochondriale Dysfunktion verhindern. Hoch-Energie-Diät erhöhte nicht nur die Fettsäureoxidation im Muskel, sondern auch die Mitochondrienmenge. Dies wurde in der Leber nicht beobachtet. Die erhöhte oxidative Kapazität unter Hoch-Energie-Diät könnte einen Kompensationsmechanismus der Mitochondrien darstellen, um dem Überangebot an Substraten in der Insulinresistenz entgegenzuwirken. Die Tatsache, dass dies hauptsächlich im Skelettmuskel von Tiermodellen beobachtet wurde legt die Vermutung nahe, dass es sich hierbei um ein spezifisches Phänomen im Nager handeln könnte und die Relevanz für den Menschen daher fraglich ist. Die oxidative Kapazität im Muskel wurde durch Diät und Training beeinflusst, wohingegen in Leber nur ein Einfluss der Diät zu beobachten war. Obwohl die Funktion von Mitochondrien aus Muskel und Lebergewebe durch Training und Hoch-Energie-Diät unterschiedlich beeinflusst wurde, hatte die Diät einen bedeutend größeren Einfluss auf die Lipidkomposition der Mitochondrien in beiden Geweben. In dieser Doktorarbeit konnte gezeigt werden, dass die Lipidzusammensetzung von Mitochondrien in Muskel und Leber äußerst Gewebe-spezifisch ist, aber in ähnlicher Weise durch die Hoch-Energie-Diät beeinflusst wurde. Die Effekte von Ausdauertraining auf Lipide der Mitochondrien scheinen eher gering zu sein. Quantitative Proteomanalysen, die momentan durchgeführt werden, könnten helfen die gewebespezifischen mitochondriellen Adaptionen und ihren Beitrag zur Krankheitsentwicklung aufzuklären. Bemerkenswerterweise spiegelte die mitochondriale Fettsäurezusammensetzung in den detektieren Lipidklassen nicht immer die Fettsäurezusammensetzung der Diäten wieder. Dies deutet darauf hin, dass die Lipidaufnahme in Mitochondrien ein selektiver Prozess ist.

Abgesehen von einer unterschiedlichen Adaption an Diät und Training, zeigte der Vergleich von Leber- und Muskelmitochondrien auch klare Unterschiede in der Lipidzusammensetzung, Enzymabundanz und mitochondrialer Respiration. Im Gegensatz zu isolierten Mitochondrien aus Muskel, zeigten Mitochondrien aus Leber keinen Anstieg in der Respiration nach Zugabe von Pyruvat als zusätzliches Atmungskettensubstrat neben Fettsäuren. Dieses Nichtansprechen von isolierten Lebermitochondrien, aber nicht von Muskelmitochondrien, auf Pyruvat in Atmungsmessungen, unterstützt die Hypothese, dass Mitochondrien auf die Ansprüche des jeweiligen Gewebes zugeschnitten und

angepasst sind. Die Ergebnisse dieser Doktorarbeit deuten darauf hin, dass wenn Fettsäuren bereits anwesend sind, extern zugeführtes Pyruvat in Lebermitochondrien direkt in anabole Prozesse wie Gluconeogenese oder Ketogenese überführt wird und daher nicht zur ATP Produktion über die oxidative Phosphorylierung verwendet wird. In Muskelmitochondrien hingegen, wird Pyruvat selbst in der Anwesenheit von Fettsäuren der oxidativen Phosphorylierung zugeführt, um die großen Schwankungen im Energiebedarf des Muskels zum Beispiel bei Sport erfüllen zu können. Die Hypothese wird weiter unterstützt durch eine höhere Abundanz der Elektronentransportkettenproteine, einer generell höheren Menge an Mitochondrien und auch durch eine höhere Menge an Lipiden wie Cardiolipin und Phosphatidylenthanolamin, die mit einer höheren Elektronentransportkettenaktivität, Atmung und Superkomplexbildung assoziiert werden.

Untersuchungen bezüglich der Spezifitäten von Mitochondrien aus insulinempfindlichen Organen wie Skelettmuskel und Lebe, welche für die endogene Glukoseproduktion und –abbau verantwortlich sind, könnten dabei helfen eine gewebespezifische Rolle der Mitochondrien bei zum Beispiel Sport und Krankheiten zu ermitteln. Dies könnte zu einer mehr zielgerichteten Behandlung von mitochondrialer Dysfunktion führen, welche im Zusammenhang mit Insulinresistenz und Diabetes diskutiert wird.

Die Beteiligung von Mitochondrien an der Entwicklung und Prävention von Typ 2 Diabetes muss noch weiter untersucht werden. Hierbei sollte ein besonderer Fokus darauf liegen, die kontroverse Datenlage bereits publizierter Studien zu klären. Diese beruht wahrscheinlich teilweise darauf, dass unter dem sehr breiten und allgemeinen Begriff der „Mitochondrienfunktion“ diverse verschiedene experimentelle Ansätze angewendet und publiziert werden. Eine Standardisierung der Experimente unter Einbeziehung von Speziesunterschieden und Gewebeunterschieden wie auch die Einführung von vereinheitlichten Parametern wie zum Beispiel zur Quantifizierung von Mitochondrien könnten helfen. Die Methodik welche in dieser Doktorarbeit entwickelt wurde kann zur weiteren Standardisierung beitragen.

8 References

(1) World Health Organization: Geneva, 2014.

(2) Schwitzgebel, V. M. "Many faces of monogenic diabetes"; *Journal of diabetes investigation* **2014**, *5*, 121-133.

(3) Billings, L. K.; Florez, J. C. "The genetics of type 2 diabetes: what have we learned from GWAS?"; *Annals of the New York Academy of Sciences* **2010**, *1212*, 59-77.

(4) Warram, J. H.; Martin, B. C.; Krolewski, A. S.; Soeldner, J. S.; Kahn, C. R. "Slow glucose removal rate and hyperinsulinemia precede the development of type II diabetes in the offspring of diabetic parents"; *Annals of internal medicine* **1990**, *113*, 909-915.

(5) Lillioja, S.; Mott, D. M.; Spraul, M.; Ferraro, R.; Foley, J. E.; Ravussin, E.; Knowler, W. C.; Bennett, P. H.; Bogardus, C. "Insulin resistance and insulin secretory dysfunction as precursors of non-insulin-dependent diabetes mellitus. Prospective studies of Pima Indians"; *The New England journal of medicine* **1993**, *329*, 1988-1992.

(6) Kitabchi, A. E.; Temprosa, M.; Knowler, W. C.; Kahn, S. E.; Fowler, S. E.; Haffner, S. M.; Andres, R.; Saudek, C.; Edelstein, S. L.; Arakaki, R.; Murphy, M. B.; Shamoon, H. "Role of insulin secretion and sensitivity in the evolution of type 2 diabetes in the diabetes prevention program: effects of lifestyle intervention and metformin"; *Diabetes* **2005**, *54*, 2404-2414.

(7) DeFronzo, R. A.; Jacot, E.; Jequier, E.; Maeder, E.; Wahren, J.; Felber, J. P. "The effect of insulin on the disposal of intravenous glucose. Results from indirect calorimetry and hepatic and femoral venous catheterization"; *Diabetes* **1981**, *30*, 1000-1007.

(8) DeFronzo, R. A.; Alvestrand, A.; Smith, D.; Hendler, R.; Hendler, E.; Wahren, J. "Insulin resistance in uremia"; *Journal of Clinical Investigation* **1981**, *67*, 563.

(9) Chan, D. C.; Gan, S. K.; Wong, A. T.; Barrett, P. H.; Watts, G. F. "Association between skeletal muscle fat content and very-low-density lipoprotein-apolipoprotein B-100 transport in obesity: effect of weight loss"; *Diabetes, Obesity and Metabolism* **2014**, *16*, 994-1000.

(10) Machann, J.; Häring, H.; Schick, F.; Stumvoll, M. "Intramyocellular lipids and insulin resistance"; *Diabetes, Obesity and Metabolism* **2004**, *6*, 239-248.

(11) Pan, D. A.; Lillioja, S.; Kriketos, A. D.; Milner, M. R.; Baur, L. A.; Bogardus, C.; Jenkins, A. B.; Storlien, L. H. "Skeletal Muscle Triglyceride Levels Are Inversely Related to Insulin Action"; *Diabetes* **1997**, *46*, 983-988.

(12) Goodpaster, B. H.; He, J.; Watkins, S.; Kelley, D. E. "Skeletal muscle lipid content and insulin resistance: evidence for a paradox in endurance-trained athletes"; *The Journal of Clinical Endocrinology & Metabolism* **2001**, *86*, 5755-5761.

(13) Russell, A. P.; Gastaldi, G.; Bobbioni-Harsch, E.; Arboit, P.; Gobelet, C.; Dériaz, O.; Golay, A.; Witztum, J. L.; Giacobino, J.-P. "Lipid peroxidation in skeletal muscle of obese as compared to endurance-trained humans: a case of good vs. bad lipids?"; *FEBS Letters* **2003**, *551*, 104-106.

(14) Hegarty, B. D.; Furler, S. M.; Ye, J.; Cooney, G. J.; Kraegen, E. W. "The role of intramuscular lipid in insulin resistance"; *Acta physiologica Scandinavica* **2003**, *178*, 373-383.

(15) Yu, C.; Chen, Y.; Cline, G. W.; Zhang, D.; Zong, H.; Wang, Y.; Bergeron, R.; Kim, J. K.; Cushman, S. W.; Cooney, G. J.; Atcheson, B.; White, M. F.; Kraegen, E. W.; Shulman, G. I. "Mechanism by which

fatty acids inhibit insulin activation of insulin receptor substrate-1 (IRS-1)-associated phosphatidylinositol 3-kinase activity in muscle"; *Journal of Biological Chemistry* **2002**, *277*, 50230-50236.

(16) Griffin, M. E.; Marcucci, M. J.; Cline, G. W.; Bell, K.; Barucci, N.; Lee, D.; Goodyear, L. J.; Kraegen, E. W.; White, M. F.; Shulman, G. I. "Free fatty acid-induced insulin resistance is associated with activation of protein kinase C theta and alterations in the insulin signaling cascade"; *Diabetes* **1999**, *48*, 1270-1274.

(17) Lazar, M. A. "How obesity causes diabetes: not a tall tale"; *Science* **2005**, *307*, 373-375.

(18) Wallace, D. C.; Fan, W. "Energetics, epigenetics, mitochondrial genetics"; *Mitochondrion* **2010**, *10*, 12-31.

(19) Ott, M.; Gogvadze, V.; Orrenius, S.; Zhivotovsky, B. "Mitochondria, oxidative stress and cell death"; *Apoptosis* **2007**, *12*, 913-922.

(20) Adam-Vizi, V.; Chinopoulos, C. "Bioenergetics and the formation of mitochondrial reactive oxygen species"; *Trends in Pharmacological Sciences* **2006**, *27*, 639-645.

(21) Quiles, J. L.; Huertas, J. R.; Manas, M.; Battino, M.; Mataix, J. "Physical exercise affects the lipid profile of mitochondrial membranes in rats fed with virgin olive oil or sunflower oil"; *British Journal of Nutrition* **1999**, *81*, 21-24.

(22) Paradies, G.; Paradies, V.; De Benedictis, V.; Ruggiero, F. M.; Petrosillo, G. "Functional role of cardiolipin in mitochondrial bioenergetics"; *Biochimica et Biophysica Acta (BBA) - Bioenergetics* **2014**, *1837*, 408-417.

(23) Horvath, S. E.; Daum, G. "Lipids of mitochondria"; *Progress in Lipid Research* **2013**, *52*, 590-614.

(24) Schlame, M.; Ren, M.; Xu, Y.; Greenberg, M. L.; Haller, I. "Molecular symmetry in mitochondrial cardiolipins"; *Chemistry and Physics of Lipids* **2005**, *138*, 38-49.

(25) Hancock, C. R.; Han, D.-H.; Chen, M.; Terada, S.; Yasuda, T.; Wright, D. C.; Holloszy, J. O. "High-fat diets cause insulin resistance despite an increase in muscle mitochondria"; *Proceedings of the National Academy of Sciences of the United States of America* **2008**, *105*, 7815-7820.

(26) Turner, N.; Bruce, C. R.; Beale, S. M.; Hoehn, K. L.; So, T.; Rolph, M. S.; Cooney, G. J. "Excess lipid availability increases mitochondrial fatty acid oxidative capacity in muscle"; *Diabetes* **2007**, *56*, 2085-2092.

(27) Toledo, F. G. S.; Johannsen, D. L.; Covington, J. D.; Bajpeyi, S.; Goodpaster, B.; Conley, K. E.; Ravussin, E. "Impact of prolonged overfeeding on skeletal muscle mitochondria in healthy individuals"; *Diabetologia* **2017**, 1-10.

(28) Toledo, F. G.; Goodpaster, B. H. "The role of weight loss and exercise in correcting skeletal muscle mitochondrial abnormalities in obesity, diabetes and aging"; *Molecular and Cellular Endocrinology* **2013**, *379*, 30-34.

(29) Russell, A. P.; Foletta, V. C.; Snow, R. J.; Wadley, G. D. "Skeletal muscle mitochondria: a major player in exercise, health and disease"; *Biochimica et Biophysica Acta (BBA)-General Subjects* **2014**, *1840*, 1276-1284.

(30) Toledo, F. G. S.; Menshikova, E. V.; Ritov, V. B.; Azuma, K.; Radikova, Z.; DeLany, J.; Kelley, D. E. "Effects of Physical Activity and Weight Loss on Skeletal Muscle Mitochondria and Relationship With Glucose Control in Type 2 Diabetes"; *Diabetes* **2007**, *56*, 2142-2147.

(31) Jacobs, R. A.; Fluck, D.; Bonne, T. C.; Burgi, S.; Christensen, P. M.; Toigo, M.; Lundby, C. "Improvements in exercise performance with high-intensity interval training coincide with an increase in skeletal muscle mitochondrial content and function"; *Journal of Applied Physiology* **2013**, *115*, 785-793.

(32) Hoene, M.; Lehmann, R.; Hennige, A. M.; Pohl, A. K.; Häring, H. U.; Schleicher, E. D.; Weigert, C. "Acute regulation of metabolic genes and insulin receptor substrates in the liver of mice by one single bout of treadmill exercise"; *The Journal of Physiology* **2009**, *587*, 241-252.

(33) Hoene, M.; Franken, H.; Fritsche, L.; Lehmann, R.; Pohl, A.; Häring, H.; Zell, A.; Schleicher, E.; Weigert, C. "Activation of the mitogen-activated protein kinase (MAPK) signalling pathway in the liver of mice is related to plasma glucose levels after acute exercise"; *Diabetologia* **2010**, *53*, 1131–1141.

(34) Hu, C.; Hoene, M.; Zhao, X.; Haring, H. U.; Schleicher, E.; Lehmann, R.; Han, X.; Xu, G.; Weigert, C. "Lipidomics analysis reveals efficient storage of hepatic triacylglycerides enriched in unsaturated fatty acids after one bout of exercise in mice"; *PLoS One* **2010**, *5*, e13318.

(35) Petridou, A.; Nikolaidis, M. G.; Matsakas, A.; Schulz, T.; Michna, H.; Mougios, V. "Effect of exercise training on the fatty acid composition of lipid classes in rat liver, skeletal muscle, and adipose tissue"; *European Journal of Applied Physiology* **2005**, *94*, 84-92.

(36) Mitchell, T. W.; Turner, N.; Hulbert, A.; Else, P. L.; Hawley, J. A.; Lee, J. S.; Bruce, C. R.; Blanksby, S. J. "Exercise alters the profile of phospholipid molecular species in rat skeletal muscle"; *Journal of Applied Physiology* **2004**, *97*, 1823-1829.

(37) Petriz, B. A.; Gomes, C. P.; Almeida, J. A.; de Oliveira, G. P.; Ribeiro, F. M.; Pereira, R. W.; Franco, O. L. "The effects of acute and chronic exercise on skeletal muscle proteome"; *Journal of Cellular Physiology* **2017**, *232*, 257-269.

(38) Fiebig, R.; Griffiths, M. A.; Gore, M. T.; Baker, D. H.; Oscai, L.; Ney, D. M.; Ji, L. L. "Exercise training down-regulates hepatic lipogenic enzymes in meal-fed rats: fructose versus complex-carbohydrate diets"; *The Journal of nutrition* **1998**, *128*, 810-817.

(39) Wirth, A.; Heuck, C. C.; Holm, G.; Björntorp, P. "Changes in the composition of fatty acids of total lipids in various tissues and serum due to physical training and food restriction in the rat"; *Scandinavian Journal of Clinical and Laboratory Investigation* **1980**, *40*, 55-62.

(40) Szabo, A.; Romvari, R.; Febel, H.; Bogner, P.; Szendro, Z. "Training-induced alterations of the fatty acid profile of rabbit muscles"; *Acta veterinaria Hungarica* **2002**, *50*, 357-364.

(41) Mataix, J.; Quiles, J. L.; Huertas, J. R.; Battino, M.; Manas, M. "Tissue specific interactions of exercise, dietary fatty acids, and vitamin E in lipid peroxidation"; *Free Radical Biology and Medicine* **1998**, *24*, 511-521.

(42) Quiles, J. L.; Huertas, J. R.; Manas, M.; Ochoa, J. J.; Battino, M.; Mataix, J. "Dietary fat type and regular exercise affect mitochondrial composition and function depending on specific tissue in the rat"; *Journal of Bioenergetics and Biomembranes* **2001**, *33*, 127-134.

(43) Miller, W. L. "Steroid hormone synthesis in mitochondria"; *Molecular and Cellular Endocrinology* **2013**, *379*, 62-73.

(44) Laffel, L. "Ketone bodies: a review of physiology, pathophysiology and application of monitoring to diabetes"; *Diabetes/metabolism research and reviews* **1999**, *15*, 412-426.

(45) McGarry, J. D.; Foster, D. W. "Regulation of hepatic fatty acid oxidation and ketone body production"; *Annual review of biochemistry* **1980**, *49*, 395-420.

(46) Atamna, H. "Heme, iron, and the mitochondrial decay of ageing"; *Ageing research reviews* **2004**, *3*, 303-318.

(47) Boveris, A.; Chance, B. "The mitochondrial generation of hydrogen peroxide. General properties and effect of hyperbaric oxygen"; *Biochemical Journal* **1973**, *134*, 707-716.

(48) Weisiger, R. A.; Fridovich, I. "Mitochondrial superoxide simutase. Site of synthesis and intramitochondrial localization"; *Journal of Biological Chemistry* **1973**, *248*, 4793-4796.

(49) Kaczanowski, S. "Apoptosis: its origin, history, maintenance and the medical implications for cancer and aging"; *Phys Biol* **2016**, *13*, 031001.

(50) Contreras, L.; Drago, I.; Zampese, E.; Pozzan, T. "Mitochondria: The calcium connection"; *Biochimica et Biophysica Acta (BBA) - Bioenergetics* **2010**, *1797*, 607-618.

(51) Rizzuto, R.; De Stefani, D.; Raffaello, A.; Mammucari, C. "Mitochondria as sensors and regulators of calcium signalling"; *Nature Reviews Molecular Cell Biology* **2012**, *13*, 566-578.

(52) Wallace, D. C. "Mitochondrial diseases in man and mouse"; *Science* **1999**, *283*, 1482-1488.

(53) Finsterer, J. "Inherited mitochondrial neuropathies"; *Journal of the neurological sciences* **2011**, *304*, 9-16.

(54) D'Aquila, P.; Bellizzi, D.; Passarino, G. "Mitochondria in health, aging and diseases: the epigenetic perspective"; *Biogerontology* **2015**, 1-17.

(55) Benard, G.; Faustin, B.; Passerieux, E.; Galinier, A.; Rocher, C.; Bellance, N.; Delage, J.-P.; Casteilla, L.; Letellier, T.; Rossignol, R. "Physiological diversity of mitochondrial oxidative phosphorylation"; *American Journal of Physiology - Cell Physiology* **2006**, *291*, C1172-C1182.

(56) Kunz, W. S. "Different Metabolic Properties of Mitochondrial Oxidative Phosphorylation in Different Cell Types - Important Implications for Mitochondrial Cytopathies"; *Experimental physiology* **2003**, *88*, 149-154.

(57) Johnson, D. T.; Harris, R. A.; Blair, P. V.; Balaban, R. S. "Functional consequences of mitochondrial proteome heterogeneity"; *Am J Physiol Cell Physiol* **2007**, *292*, C698-707.

(58) Johnson, D. T.; Harris, R. A.; French, S.; Blair, P. V.; You, J.; Bemis, K. G.; Wang, M.; Balaban, R. S. "Tissue heterogeneity of the mammalian mitochondrial proteome"; *American Journal of Physiology - Cell Physiology* **2007**, *292*, C689-697.

(59) Mootha, V. K.; Bunkenborg, J.; Olsen, J. V.; Hjerrild, M.; Wisniewski, J. R.; Stahl, E.; Bolouri, M. S.; Ray, H. N.; Sihag, S.; Kamal, M.; Patterson, N.; Lander, E. S.; Mann, M. "Integrated Analysis of Protein Composition, Tissue Diversity, and Gene Regulation in Mouse Mitochondria"; *Cell* **2003**, *115*, 629-640.

(60) Jorgensen, W.; Jelnes, P.; Rud, K. A.; Hansen, L. L.; Grunnet, N.; Quistorff, B. "Progression of type 2 diabetes in GK rats affects muscle and liver mitochondria differently: pronounced reduction of complex II flux is observed in liver only"; *American Journal of Physiology - Endocrinology And Metabolism* **2012**, *303*, E515-523.

(61) Rothman, D. L.; Magnusson, I.; Katz, L. D.; Shulman, R. G.; Shulman, G. I. "Quantitation of hepatic glycogenolysis and gluconeogenesis in fasting humans with 13C NMR"; *Science* **1991**, *254*, 573-576.

(62) Glaister, M. "Multiple Sprint Work- Physiological Responses, Mechanisms of Fatigue and the Influence of Aerobic Fitness"; *Sports medicine (Auckland, N.Z.)* **2005**, *35*, 757-777.

(63) Corpeleijn, E.; Saris, W. H.; Blaak, E. E. "Metabolic flexibility in the development of insulin resistance and type 2 diabetes: effects of lifestyle"; *Obesity Reviews* **2009**, *10*, 178-193.

(64) Patel, M. S.; Owen, O. E.; Goldman, L. I.; Hanson, R. W. "Fatty acid synthesis by human adipose tissue"; *Metabolism: clinical and experimental* **1975**, *24*, 161-173.

(65) Pullen, D. L.; Liesman, J. S.; Emery, R. S. "A species comparison of liver slice synthesis and secretion of triacylglycerol from nonesterified fatty acids in media"; *J Anim Sci* **1990**, *68*, 1395-1399.

(66) Postic, C.; Dentin, R.; Girard, J. "Role of the liver in the control of carbohydrate and lipid homeostasis"; *Diabetes & Metabolism* **2004**, *30*, 398-408.

(67) Furler, S. M.; Cooney, G. J.; Hegarty, B. D.; Lim-Fraser, M. Y.; Kraegen, E. W.; Oakes, N. D. "Local factors modulate tissue-specific NEFA utilization: assessment in rats using 3H-(R)-2-bromopalmitate"; *Diabetes* **2000**, *49*, 1427-1433.

(68) Skeie, B.; Kvetan, V.; Gil, K. M.; Rothkopf, M. M.; Newsholme, E. A.; Askanazi, J. "Branch-chain amino acids: their metabolism and clinical utility"; *Critical care medicine* **1990**, *18*, 549-571.

(69) Monirujjaman, M.; Ferdouse, A. "Metabolic and Physiological Roles of Branched-Chain Amino Acids"; *Advances in Molecular Biology* **2014**, *2014*, 6.

(70) Forner, F.; Foster, L. J.; Campanaro, S.; Valle, G.; Mann, M. "Quantitative proteomic comparison of rat mitochondria from muscle, heart, and liver"; *Molecular and Cellular Proteomics* **2006**, *5*, 608-619.

(71) van der Veen, J. N.; Lingrell, S.; da Silva, R. P.; Jacobs, R. L.; Vance, D. E. "The Concentration of Phosphatidylethanolamine in Mitochondria Can Modulate ATP Production and Glucose Metabolism in Mice"; *Diabetes* **2014**, *63*, 2620-2630.

(72) Tasseva, G.; Bai, H. D.; Davidescu, M.; Haromy, A.; Michelakis, E.; Vance, J. E. "Phosphatidylethanolamine Deficiency in Mammalian Mitochondria Impairs Oxidative Phosphorylation and Alters Mitochondrial Morphology"; *Journal of Biological Chemistry* **2013**, *288*, 4158-4173.

(73) Mårtensson, C. U.; Doan, K. N.; Becker, T. "Effects of lipids on mitochondrial functions"; *Biochimica et Biophysica Acta (BBA) - Molecular and Cell Biology of Lipids* **2017**, *1862*, 102-113.

(74) Barja, G. "Mitochondrial oxygen radical generation and leak: sites of production in states 4 and 3, organ specificity, and relation to aging and longevity"; *Journal of Bioenergetics and Biomembranes* **1999**, *31*, 347-366.

(75) Turrens, J. F.; Alexandre, A.; Lehninger, A. L. "Ubisemiquinone is the electron donor for superoxide formation by complex III of heart mitochondria"; *Archives Biochemistry Biophysics* **1985**, *237*, 408-414.

(76) Turrens, J. F.; Boveris, A. "Generation of superoxide anion by the NADH dehydrogenase of bovine heart mitochondria"; *Biochemical Journal* **1980**, *191*, 421-427.

(77) Betarbet, R.; Sherer, T. B.; Greenamyre, J. T. "Animal models of Parkinson's disease"; *BioEssays : news and reviews in molecular, cellular and developmental biology* **2002**, *24*, 308-318.

(78) Trojanowski, J. Q. "Rotenone neurotoxicity: a new window on environmental causes of Parkinson's disease and related brain amyloidoses"; *Experimental neurology* **2003**, *179*, 6-8.

(79) Brand, M. D. "Mitochondrial generation of superoxide and hydrogen peroxide as the source of mitochondrial redox signaling"; *Free Radical Biology and Medicine* **2016**, *100*, 14-31.

(80) McCord, J. M.; Fridovich, I. "Superoxide dismutase. An enzymic function for erythrocuprein (hemocuprein)"; *Journal of Biological Chemistry* **1969**, *244*, 6049-6055.

(81) Reczek, C. R.; Chandel, N. S. "ROS-dependent signal transduction"; *Current Opinion in Cell Biology* **2015**, *33*, 8-13.

(82) Sies, H. "Role of Metabolic H2O2 Generation: Redox Signaling and Oxidative Stress"; *Journal of Biological Chemistry* **2014**, *289*, 8735-8741.

(83) Hiona, A.; Leeuwenburgh, C. "The role of mitochondrial DNA mutations in aging and sarcopenia: implications for the mitochondrial vicious cycle theory of aging"; *Experimental gerontology* **2008**, *43*, 24-33.

(84) Maritim, A.; Sanders, a.; Watkins, r. J. "Diabetes, oxidative stress, and antioxidants: a review"; *Journal of Biochemical and Molecular Toxicology* **2003**, *17*, 24-38.

(85) Wanagat, J.; Hevener, A. L. "Mitochondrial quality control in insulin resistance and diabetes"; *Current Opinion in Genetics & Development* **2016**, *38*, 118-126.

(86) Lowell, B. B.; Shulman, G. I. "Mitochondrial dysfunction and type 2 diabetes"; *Science* **2005**, *307*, 384-387.

(87) Brownlee, M. "The Pathobiology of Diabetic Complications- A Unifying Mechanism"; *Diabetes* **2005**, *54*, 1615-1625.

(88) Kowluru, R. A.; Kowluru, V.; Xiong, Y.; Ho, Y.-S. "Overexpression of mitochondrial superoxide dismutase in mice protects the retina from diabetes-induced oxidative stress"; *Free Radical Biology and Medicine* **2006**, *41*, 1191-1196.

(89) Nishikawa, T.; Brownlee, M.; Araki, E. "Mitochondrial reactive oxygen species in the pathogenesis of early diabetic nephropathy"; *Journal of diabetes investigation* **2015**, *6*, 137-139.

(90) Al-Lahham, R.; Deford, J. H.; Papaconstantinou, J. "Mitochondrial-generated ROS down regulates insulin signaling via activation of the p38MAPK stress response pathway"; *Molecular and Cellular Endocrinology* **2016**, *419*, 1-11.

(91) Kunau, W.-H.; Dommes, V.; Schulz, H. "β-Oxidation of fatty acids in mitochondria, peroxisomes, and bacteria: A century of continued progress"; *Progress in Lipid Research* **1995**, *34*, 267-342.

(92) Lu, Y.-W.; Claypool, S. M. "Disorders of phospholipid metabolism: an emerging class of mitochondrial disease due to defects in nuclear genes"; *Frontiers in Genetics* **2015**, *6*, 1-27.

(93) Tamura, Y.; Sesaki, H.; Endo, T. "Phospholipid Transport via Mitochondria"; *Traffic* **2014**, *15*, 933-945.

(94) van Meer, G.; Voelker, D. R.; Feigenson, G. W. "Membrane lipids: where they are and how they behave"; *Nature Reviwes Molecular Cell Biology* **2008**, *9*, 112-124.

(95) Daum, G.; Vance, J. E. "Import of lipids into mitochondria"; *Progress in Lipid Research* **1997**, *36*, 103-130.

(96) Kiebish, M. A.; Han, X.; Cheng, H.; Lunceford, A.; Clarke, C. F.; Moon, H.; Chuang, J. H.; Seyfried, T. N. "Lipidomic analysis and electron transport chain activities in C57BL/6J mouse brain mitochondria"; *Journal of Neurochemistry* **2008**, *106*, 299-312.

(97) Claypool, S. M. "Cardiolipin, a critical determinant of mitochondrial carrier protein assembly and function"; *Biochimica et Biophysica Acta* **2009**, *1788*, 2059-2068.

(98) Claypool, S. M.; Koehler, C. M. "The complexity of cardiolipin in health and disease"; *Trends in Biochemical Sciences* **2012**, *37*, 32-41.

(99) Osman, C.; Voelker, D. R.; Langer, T. "Making heads or tails of phospholipids in mitochondria"; *The Journal of Cell Biology* **2011**, *192*, 7-16.

(100) Frohman, M. "Role of mitochondrial lipids in guiding fission and fusion"; *Journal of Molecular Medicine* **2015**, *93*, 263-269.

(101) Schlame, M.; Ren, M. "The role of cardiolipin in the structural organization of mitochondrial membranes"; *Biochimica et Biophysica Acta (BBA) - Biomembranes* **2009**, *1788*, 2080-2083.

(102) Unsay, J. D.; Cosentino, K.; Subburaj, Y.; García-Sáez, A. J. "Cardiolipin Effects on Membrane Structure and Dynamics"; *Langmuir* **2013**, *29*, 15878-15887.

(103) Schroepfer, G. J., Jr. "Oxysterols: modulators of cholesterol metabolism and other processes"; *Physiological reviews* **2000**, *80*, 361-554.

(104) Javitt, N. B. "Oxysterols: novel biologic roles for the 21st century"; *Steroids* **2008**, *73*, 149-157.

(105) Russell, D. W. "The enzymes, regulation, and genetics of bile acid synthesis"; *Annual review of biochemistry* **2003**, *72*, 137-174.

(106) Björkhem, I.; Diczfalusy, U. "Oxysterols Friends, Foes, or Just Fellow Passengers?"; *Arteriosclerosis, thrombosis, and vascular biology* **2002**, *22*, 734-742.

(107) Pikuleva, I. A. "Cholesterol-metabolizing cytochromes P450"; *Drug Metabolism and Disposition* **2006**, *34*, 513-520.

(108) Smith, L. L. In *Autoxidation in Food and Biological Systems*, Simic, M. G.; Karel, M., Eds.; Springer US: Boston, MA, 1980, pp 119-132.

(109) Murphy, R. C.; Johnson, K. M. "Cholesterol, reactive oxygen species, and the formation of biologically active mediators"; *Journal of Biological Chemistry* **2008**, *283*, 15521-15525.

(110) Leonarduzzi, G.; Gargiulo, S.; Gamba, P.; Testa, G.; Sottero, B.; Rossin, D.; Staurenghi, E.; Poli, G. "Modulation of cell signaling pathways by oxysterols in age-related human diseases"; *Free Radical Biology and Medicine* **2014**, *75 Suppl 1*, S5.

(111) Lange, Y.; Ye, J.; Strebel, F. "Movement of 25-hydroxycholesterol from the plasma membrane to the rough endoplasmic reticulum in cultured hepatoma cells"; *The Journal of Lipid Research* **1995**, *36*, 1092-1097.

(112) Smith, L. L.; Johnson, B. H. "Biological activities of oxysterols"; *Free Radical Biology and Medicine* **1989**, *7*, 285-332.

(113) Ahonen, L.; Maire, F. B.; Savolainen, M.; Kopra, J.; Vreeken, R. J.; Hankemeier, T.; Myohanen, T.; Kylli, P.; Kostiainen, R. "Analysis of oxysterols and vitamin D metabolites in mouse brain and cell line samples by ultra-high-performance liquid chromatography-atmospheric pressure photoionization-mass spectrometry"; *Journal of Chromatography A* **2014**, *1364*, 214-222.

(114) Stewart, C. R.; Wilson, L. M.; Zhang, Q.; Pham, C. L.; Waddington, L. J.; Staples, M. K.; Stapleton, D.; Kelly, J. W.; Howlett, G. J. "Oxidized cholesterol metabolites found in human atherosclerotic lesions promote apolipoprotein C-II amyloid fibril formation"; *Biochemistry* **2007**, *46*, 5552-5561.

(115) Nieva, J.; Song, B.-D.; Rogel, Joseph K.; Kujawara, D.; Altobel Iii, L.; Izharrudin, A.; Boldt, Grant E.; Grover, Rajesh K.; Wentworth, Anita D.; Wentworth Jr, P. "Cholesterol Secosterol Aldehydes Induce Amyloidogenesis and Dysfunction of Wild-Type Tumor Protein p53"; *Chemistry & Biology* **2011**, *18*, 920-927.

(116) Cygan, N. K.; Scheinost, J. C.; Butters, T. D.; Wentworth, P., Jr. "Adduction of cholesterol 5,6-secosterol aldehyde to membrane-bound myelin basic protein exposes an immunodominant epitope"; *Biochemistry* **2011**, *50*, 2092-2100.

(117) Poli, G.; Biasi, F.; Leonarduzzi, G. "Oxysterols in the pathogenesis of major chronic diseases"; *Redox Biology* **2013**, *1*, 125-130.

(118) Ryan, L.; O'Callaghan, Y. C.; O'Brien, N. M. "The role of the mitochondria in apoptosis induced by 7β-hydroxycholesterol and cholesterol-5β,6β-epoxide"; *British Journal of Nutrition* **2007**, *94*, 519-525.

(119) Vejux, A.; Malvitte, L.; Lizard, G. "Side effects of oxysterols: cytotoxicity, oxidation, inflammation, and phospholipidosis"; *Brazilian Journal of Medical and Biological Research* **2008**, *41*, 545-556.

(120) Panini, S. R.; Sinensky, M. S. "Mechanisms of oxysterol-induced apoptosis"; *Current Opinion in Lipidology* **2001**, *12*, 529-533.

(121) Liu, H.; Wang, T.; Huang, K. "Cholestane-3β,5α,6β-triol-induced reactive oxygen species production promotes mitochondrial dysfunction in isolated mice liver mitochondria"; *Chemico-biological interactions* **2009**, *179*, 81-87.

(122) Liu, H.; Wang, T.; Huang, K. "Cholestane-3beta,5alpha,6beta-triol-induced reactive oxygen species production promotes mitochondrial dysfunction in isolated mice liver mitochondria"; *Chemico-biological interactions* **2009**, *179*, 81-87.

(123) Omura, T. "Mitochondrial P450s"; *Chemico-biological interactions* **2006**, *163*, 86-93.

(124) Nelson, E. R.; Wardell, S. E.; Jasper, J. S.; Park, S.; Suchindran, S.; Howe, M. K.; Carver, N. J.; Pillai, R. V.; Sullivan, P. M.; Sondhi, V.; Umetani, M.; Geradts, J.; McDonnell, D. P. "27-Hydroxycholesterol Links Hypercholesterolemia and Breast Cancer Pathophysiology"; *Science* **2013**, *342*, 1094-1098.

(125) Björkhem, I.; Andersson, O.; Diczfalusy, U.; Sevastik, B.; Xiu, R. J.; Duan, C.; Lund, E. "Atherosclerosis and sterol 27-hydroxylase: evidence for a role of this enzyme in elimination of cholesterol from human macrophages"; *Proceedings of the National Academy of Sciences of the United States of America* **1994**, *91*, 8592-8596.

(126) Kölsch, H.; Heun, R.; Kerksiek, A.; Bergmann, K. v.; Maier, W.; Lütjohann, D. "Altered levels of plasma 24S- and 27-hydroxycholesterol in demented patients"; *Neuroscience Letters* **2004**, *368*, 303-308.

(127) Wu, Q.; Ishikawa, T.; Sirianni, R.; Tang, H.; McDonald, Jeffrey G.; Yuhanna, Ivan S.; Thompson, B.; Girard, L.; Mineo, C.; Brekken, Rolf A.; Umetani, M.; Euhus, David M.; Xie, Y.; Shaul, Philip W. "27-Hydroxycholesterol Promotes Cell-Autonomous, ER-Positive Breast Cancer Growth"; *Cell Reports* **2013**, *5*, 637-645.

(128) Musman, J.; Pons, S.; Barau, C.; Caccia, C.; Leoni, V.; Berdeaux, A.; Ghaleh, B.; Morin, D. "Regular treadmill exercise inhibits mitochondrial accumulation of cholesterol and oxysterols during myocardial ischemia-reperfusion in wild-type and ob/ob mice"; *Free Radical Biology and Medicine* **2016**, *101*, 317-324.

(129) Ren, S.; Hylemon, P.; Zhang, Z. P.; Rodriguez-Agudo, D.; Marques, D.; Li, X.; Zhou, H.; Gil, G.; Pandak, W. M. "Identification of a novel sulfonated oxysterol, 5-cholesten-3beta,25-diol 3-sulfonate, in hepatocyte nuclei and mitochondria"; *The Journal of Lipid Research* **2006**, *47*, 1081-1090.

(130) Kappler, L.; Li, J.; Häring, H.-U.; Weigert, C.; Lehmann, R.; Xu, G.; Hoene, M. "Purity matters: A workflow for the valid high-resolution lipid profiling of mitochondria from cell culture samples"; *Scientific Reports* **2016**, *6*, 21107.

(131) Yamada, T.; Ida, T.; Yamaoka, Y.; Ozawa, K.; Takasan, H.; Honjo, I. "Two distinct patterns of glucose intolerance in icteric rats and rabbits. Relationship to impaired liver mitochondria function"; *Journal of Laboratory and Clinical Medicine* **1975**, *86*, 38-45.

(132) Ruderman, N. B.; Saha, A. K.; Vavvas, D.; Witters, L. A. "Malonyl-CoA, fuel sensing, and insulin resistance"; *American Journal of Physiology* **1999**, *276*, E1-e18.

(133) Morino, K.; Petersen, K. F.; Shulman, G. I. "Molecular mechanisms of insulin resistance in humans and their potential links with mitochondrial dysfunction"; *Diabetes* **2006**, *55*.

(134) Koves, T. R.; Ussher, J. R.; Noland, R. C.; Slentz, D.; Mosedale, M.; Ilkayeva, O.; Bain, J.; Stevens, R.; Dyck, J. R.; Newgard, C. B.; Lopaschuk, G. D.; Muoio, D. M. "Mitochondrial overload and incomplete fatty acid oxidation contribute to skeletal muscle insulin resistance"; *Cell metabolism* **2008**, *7*, 45-56.

(135) Kelley, D. E.; Goodpaster, B.; Wing, R. R.; Simoneau, J. A. "Skeletal muscle fatty acid metabolism in association with insulin resistance, obesity, and weight loss"; *American Journal of Physiology* **1999**, *277*, E1130-1141.

(136) Kim, J. Y.; Hickner, R. C.; Cortright, R. L.; Dohm, G. L.; Houmard, J. A. "Lipid oxidation is reduced in obese human skeletal muscle"; *American Journal of Physiology - Endocrinology And Metabolism* **2000**, *279*, E1039-1044.

(137) Kelley, D. E.; He, J.; Menshikova, E. V.; Ritov, V. B. "Dysfunction of Mitochondria in Human Skeletal Muscle in Type 2 Diabetes"; *Diabetes* **2002**, *51*, 2944-2950.

(138) Phielix, E.; Schrauwen-Hinderling, V. B.; Mensink, M.; Lenaers, E.; Meex, R.; Hoeks, J.; Kooi, M. E.; Moonen-Kornips, E.; Sels, J.-P.; Hesselink, M. K. C.; Schrauwen, P. "Lower Intrinsic ADP-Stimulated Mitochondrial Respiration Underlies In Vivo Mitochondrial Dysfunction in Muscle of Male Type 2 Diabetic Patients"; *Diabetes* **2008**, *57*, 2943-2949.

(139) Boushel, R.; Gnaiger, E.; Schjerling, P.; Skovbro, M.; Kraunsøe, R.; Dela, F. "Patients with type 2 diabetes have normal mitochondrial function in skeletal muscle"; *Diabetologia* **2007**, *50*, 790-796.

(140) Ritov, V. B.; Menshikova, E. V.; Azuma, K.; Wood, R.; Toledo, F. G. S.; Goodpaster, B. H.; Ruderman, N. B.; Kelley, D. E. "Deficiency of electron transport chain in human skeletal muscle mitochondria in type 2 diabetes mellitus and obesity"; *American Journal of Physiology - Endocrinology and Metabolism* **2010**, *298*, E49-E58.

(141) Mogensen, M.; Sahlin, K.; Fernstrom, M.; Glintborg, D.; Vind, B. F.; Beck-Nielsen, H.; Hojlund, K. "Mitochondrial respiration is decreased in skeletal muscle of patients with type 2 diabetes"; *Diabetes* **2007**, *56*, 1592-1599.

(142) Chomentowski, P.; Coen, P. M.; Radikova, Z.; Goodpaster, B. H.; Toledo, F. G. "Skeletal muscle mitochondria in insulin resistance: differences in intermyofibrillar versus subsarcolemmal subpopulations and relationship to metabolic flexibility"; *The Journal of Clinical Endocrinology & Metabolism* **2011**, *96*, 494-503.

(143) Ritov, V. B.; Menshikova, E. V.; He, J.; Ferrell, R. E.; Goodpaster, B. H.; Kelley, D. E. "Deficiency of subsarcolemmal mitochondria in obesity and type 2 diabetes"; *Diabetes* **2005**, *54*, 8-14.

(144) Heilbronn, L. K.; Gan, S. K.; Turner, N.; Campbell, L. V.; Chisholm, D. J. "Markers of Mitochondrial Biogenesis and Metabolism Are Lower in Overweight and Obese Insulin-Resistant Subjects"; *The Journal of Clinical Endocrinology & Metabolism* **2007**, *92*, 1467-1473.

(145) Patti, M. E.; Butte, A. J.; Crunkhorn, S.; Cusi, K.; Berria, R.; Kashyap, S.; Miyazaki, Y.; Kohane, I.; Costello, M.; Saccone, R. "Coordinated reduction of genes of oxidative metabolism in humans with insulin resistance and diabetes: Potential role of PGC1 and NRF1"; *Proceedings of the National Academy of Sciences of the United States of America* **2003**, *100*, 8466-8471.

(146) Petersen, K. F.; Dufour, S.; Befroy, D.; Garcia, R.; Shulman, G. I. "Impaired mitochondrial activity in the insulin-resistant offspring of patients with type 2 diabetes"; *The New England journal of medicine* **2004**, *350*, 664-671.

(147) Holloway, G. P.; Thrush, A. B.; Heigenhauser, G. J.; Tandon, N. N.; Dyck, D. J.; Bonen, A.; Spriet, L. L. "Skeletal muscle mitochondrial FAT/CD36 content and palmitate oxidation are not decreased in obese women"; *American Journal of Physiology - Endocrinology And Metabolism* **2007**, *292*, E1782-1789.

(148) Turner, N.; Bruce, C. R.; Beale, S. M.; Hoehn, K. L.; So, T.; Rolph, M. S.; Cooney, G. J. "Excess lipid availability increases mitochondrial fatty acid oxidative capacity in muscle: evidence against a role for reduced fatty acid oxidation in lipid-induced insulin resistance in rodents"; *Diabetes* **2007**, *56*, 2085-2092.

(149) de Wilde, J.; Mohren, R.; van den Berg, S.; Boekschoten, M.; Dijk, K. W.-V.; de Groot, P.; Müller, M.; Mariman, E.; Smit, E. "Short-term high fat-feeding results in morphological and metabolic adaptations in the skeletal muscle of C57BL/6J mice"; *Physiological Genomics* **2008**, *32*, 360-369.

(150) Garcia-Roves, P.; Huss, J. M.; Han, D. H.; Hancock, C. R.; Iglesias-Gutierrez, E.; Chen, M.; Holloszy, J. O. "Raising plasma fatty acid concentration induces increased biogenesis of mitochondria in skeletal muscle"; *Proceedings of the National Academy of Sciences of the United States of America* **2007**, *104*, 10709-10713.

(151) Turner, N.; Hariharan, K.; TidAng, J.; Frangioudakis, G.; Beale, S. M.; Wright, L. E.; Zeng, X. Y.; Leslie, S. J.; Li, J.-Y.; Kraegen, E. W.; Cooney, G. J.; Ye, J.-M. "Enhancement of Muscle Mitochondrial

Oxidative Capacity and Alterations in Insulin Action Are Lipid Species Dependent- Potent Tissue-Specific Effects of Medium-Chain Fatty Acids"; *Diabetes* **2009**, *58*, 2547-2554.

(152) Holmstrom, M. H.; Iglesias-Gutierrez, E.; Zierath, J. R.; Garcia-Roves, P. M. "Tissue-specific control of mitochondrial respiration in obesity-related insulin resistance and diabetes"; *American Journal of Physiology - Endocrinology And Metabolism* **2012**, *302*, E731-739.

(153) Han, D.-H.; Hancock, C. R.; Jung, S. R.; Higashida, K.; Kim, S. H.; Holloszy, J. O. "Deficiency of the Mitochondrial Electron Transport Chain in Muscle Does Not Cause Insulin Resistance"; *PLoS One* **2011**, *6*, e19739.

(154) Koliaki, C.; Szendroedi, J.; Kaul, K.; Jelenik, T.; Nowotny, P.; Jankowiak, F.; Herder, C.; Carstensen, M.; Krausch, M.; Knoefel, W. T.; Schlensak, M.; Roden, M. "Adaptation of hepatic mitochondrial function in humans with non-alcoholic Fatty liver is lost in steatohepatitis"; *Cell metabolism* **2015**, *21*, 739-746.

(155) Koliaki, C.; Roden, M. "Hepatic energy metabolism in human diabetes mellitus, obesity and non-alcoholic fatty liver disease"; *Molecular and Cellular Endocrinology* **2013**, *379*, 35-42.

(156) Sunny, N. E.; Parks, E. J.; Browning, J. D.; Burgess, S. C. "Excessive hepatic mitochondrial TCA cycle and gluconeogenesis in humans with nonalcoholic fatty liver disease"; *Cell metabolism* **2011**, *14*, 804-810.

(157) Lund, M. T.; Kristensen, M.; Hansen, M.; Tveskov, L.; Floyd, A. K.; Støckel, M.; Vainer, B.; Poulsen, S. S.; Helge, J. W.; Prats, C.; Dela, F. "Hepatic mitochondrial oxidative phosphorylation is normal in obese patients with and without type 2 diabetes"; *The Journal of Physiology* **2016**, *594*, 4351-4358.

(158) Schmid, A. I.; Szendroedi, J.; Chmelik, M.; Krssak, M.; Moser, E.; Roden, M. "Liver ATP synthesis is lower and relates to insulin sensitivity in patients with type 2 diabetes"; *Diabetes care* **2011**, *34*, 448-453.

(159) Szendroedi, J.; Chmelik, M.; Schmid, A. I.; Nowotny, P.; Brehm, A.; Krssak, M.; Moser, E.; Roden, M. "Abnormal hepatic energy homeostasis in type 2 diabetes"; *Hepatology (Baltimore, Md.)* **2009**, *50*, 1079-1086.

(160) Bouderba, S.; Sanz, M. N.; Sánchez-Martín, C.; El-Mir, M. Y.; Villanueva, G. R.; Detaille, D.; Koceïr, E. A. "Hepatic Mitochondrial Alterations and Increased Oxidative Stress in Nutritional Diabetes-Prone Psammomys obesus Model"; *Experimental Diabetes Research* **2012**, *2012*.

(161) Gross, V. S.; Greenberg, H. K.; Baranov, S. V.; Carlson, G. M.; Stavrovskaya, I. G.; Lazarev, A. V.; Kristal, B. S. "Isolation of functional mitochondria from rat kidney and skeletal muscle without manual homogenization"; *Analytical Biochemistry* **2011**, *418*, 213-223.

(162) Bird, S. S.; Marur, V. R.; Sniatynski, M. J.; Greenberg, H. K.; Kristal, B. S. "Lipidomics profiling by high-resolution LC-MS and high-energy collisional dissociation fragmentation: focus on characterization of mitochondrial cardiolipins and monolysocardiolipins"; *Analytical Chemistry* **2011**, *83*, 940-949.

(163) Minkler, P. E.; Hoppel, C. L. "Separation and characterization of cardiolipin molecular species by reverse-phase ion pair high-performance liquid chromatography-mass spectrometry"; *Journal of lipid research* **2010**, *51*, 856-865.

(164) Barzanti, V.; Battino, M.; Baracca, A.; Cavazzoni, M.; Cocchi, M.; Noble, R.; Maranesi, M.; Turchetto, E.; Lenaz, G. "The effect of dietary lipid changes on the fatty acid composition and function of liver, heart and brain mitochondria in the rat at different ages"; *British Journal of Nutrition* **1994**, *71*, 193-202.

(165) Timmons, M. D.; Bradley, M.; Lovell, M. A.; Lynn, B. C. "Comparison of Sprague Dawley rat mitochondrial fatty acid profiles isolated from various tissues"; *Neurobiology of Lipids* **2012**, *11*.

(166) Pollard, A. K.; Ortori, C. A.; Stoger, R.; Barrett, D. A.; Chakrabarti, L. "Mouse mitochondrial lipid composition is defined by age in brain and muscle"; *Aging* **2017**, *9*, 986-998.

(167) Schöttl, T.; Kappler, L.; Braun, K.; Fromme, T.; Klingenspor, M. "Limited mitochondrial capacity of visceral versus subcutaneous white adipocytes in male C57BL/6N mice"; *Endocrinology* **2014**, *156*, 923-933.

(168) Frezza, C.; Cipolat, S.; Scorrano, L. "Organelle isolation: functional mitochondria from mouse liver, muscle and cultured filroblasts"; *Nature Protocols* **2007**, *2*, 287-295.

(169) Bird, S. S.; Stavrovskaya, I. G.; Gathungu, R. M.; Tousi, F.; Kristal, B. S. In *Methods in Molecular Biology*, 2015, pp 441-452.

(170) Daum, G.; Böhni, P.; Schatz, G. "Import of proteins into mitochondria. Cytochrome b2 and cytochrome c peroxidase are located in the intermembrane space of yeast mitochondria"; *Journal of Biological Chemistry* **1982**, *257*, 13028-13033.

(171) Angelini, R.; Vitale, R.; Patil, V. A.; Cocco, T.; Ludwig, B.; Greenberg, M. L.; Corcelli, A. "Lipidomics of intact mitochondria by MALDI-TOF/MS"; *The Journal of Lipid Research* **2012**, *53*, 1417-1425.

(172) Timmons, M. D.; Bradley, M. A.; Lovell, M. A.; Lynn, B. C. "Procedure for the isolation of mitochondria, cytosolic and nuclear material from a single piece of neurological tissue for high-throughput mass spectral analysis"; *Journal of Neuroscience Methods* **2011**, *197*, 279-282.

(173) Andreyev, A. Y.; Fahy, E.; Guan, Z.; Kelly, S.; Li, X.; McDonald, J. G.; Milne, S.; Myers, D.; Park, H.; Ryan, A.; Thompson, B. M.; Wang, E.; Zhao, Y.; Brown, H. A.; Merrill, A. H.; Raetz, C. R. H.; Russell, D. W.; Subramaniam, S.; Dennis, E. A. "Subcellular organelle lipidomics in TLR-4-activated macrophages"; *The Journal of Lipid Research* **2010**, *51*, 2785-2797.

(174) Kiebish, M. A.; Han, X.; Seyfried, T. N. "Examination of the brain mitochondrial lipidome using shotgun lipidomics"; *Methods in Molecular Biology* **2009**, *579*, 3-18.

(175) Leonov, A.; Arlia-Ciommo, A.; Bourque, S. D.; Koupaki, O.; Kyryakov, P.; Dakik, P.; McAuley, M.; Medkour, Y.; Mohammad, K.; Di Maulo, T.; Titorenko, V. I. "Specific changes in mitochondrial lipidome alter mitochondrial proteome and increase the geroprotective efficiency of lithocholic acid in chronologically aging yeast"; *Oncotarget* **2017**, *8*, 30672-30691.

(176) Hornig-Do, H. T.; Gunther, G.; Bust, M.; Lehnartz, P.; Bosio, A.; Wiesner, R. J. "Isolation of functional pure mitochondria by superparamagnetic microbeads"; *Analytical Biochemistry* **2009**, *389*, 1-5.

(177) Franko, A.; Baris, O. R.; Bergschneider, E.; von Toerne, C.; Hauck, S. M.; Aichler, M.; Walch, A. K.; Wurst, W.; Wiesner, R. J.; Johnston, I. C.; de Angelis, M. H. "Efficient isolation of pure and functional mitochondria from mouse tissues using automated tissue disruption and enrichment with anti-TOM22 magnetic beads"; *PLoS One* **2013**, *8*, e82392.

(178) Reed, L. J. "A trail of research from lipoic acid to alpha-keto acid dehydrogenase complexes"; *Journal of Biological Chemistry* **2001**, *276*, 38329-38336.

(179) Perham, R. N. "Domains, motifs, and linkers in 2-oxo acid dehydrogenase multienzyme complexes: a paradigm in the design of a multifunctional protein"; *Biochemistry* **1991**, *30*, 8501-8512.

(180) Patel, M. S.; Roche, T. E. "Molecular biology and biochemistry of pyruvate dehydrogenase complexes"; *The FASEB Journal* **1990**, *4*, 3224-3233.

(181) McCommis, K. S.; Finck, B. N. "Mitochondrial pyruvate transport: a historical perspective and future research directions"; *Biochemical journal* **2015**, *466*, 443-454.

(182) Meyer, J.; Vignais, P. M. "Kinetic study of glutamate transport in rat liver mitochondria"; *Biochimica et Biophysica Acta (BBA) - Bioenergetics* **1973**, *325*, 375-384.

(183) Azzi, A.; Chappell, J. B.; Robinson, B. H. "Penetration of the mitochondrial membrane by glutamate and aspartate"; *Biochemical and Biophysical Research Communications* **1967**, *29*, 148-152.

(184) Owen, O. E.; Kalhan, S. C.; Hanson, R. W. "The Key Role of Anaplerosis and Cataplerosis for Citric Acid Cycle Function"; *Journal of Biological Chemistry* **2002**, *277*, 30409-30412.

(185) Dolce, V.; Cappello, A. R.; Capobianco, L. "Mitochondrial tricarboxylate and dicarboxylate–Tricarboxylate carriers: from animals to plants"; *IUBMB Life* **2014**, *66*, 462-471.

(186) Palmieri, F.; Quagliariello, E.; Klingenberg, M. "Kinetics and Specificity of the Oxoglutarate Carrier in Rat-Liver Mitochondria"; *European Journal of Biochemistry* **1972**, *29*, 408-416.

(187) Lambert, A. J.; Brand, M. D. "Inhibitors of the Quinone-binding Site Allow Rapid Superoxide Production from Mitochondrial NADH:Ubiquinone Oxidoreductase (Complex I)"; *Journal of Biological Chemistry* **2004**, *279*, 39414-39420.

(188) Loschen, G.; Flohé, L. "Respiratory chain linked H2O2 production in pigeon heart mitochondria"; *FEBS Letters* **1971**, *18*, 261-264.

(189) Houten, S. M.; Wanders, R. J. A. "A general introduction to the biochemistry of mitochondrial fatty acid β-oxidation"; *Journal of Inherited Metabolic Disease* **2010**, *33*, 469-477.

(190) Ruzicka, F. J.; Beinert, H. "A new iron-sulfur flavoprotein of the respiratory chain"; *Journal of Biological Chemistry* **1977**, *252*, 8440-8445.

(191) Herbst, E. A.; Paglialunga, S.; Gerling, C.; Whitfield, J.; Mukai, K.; Chabowski, A.; Heigenhauser, G. J.; Spriet, L. L.; Holloway, G. P. "Omega-3 supplementation alters mitochondrial membrane composition and respiration kinetics in human skeletal muscle"; *The Journal of Physiology* **2014**, *592*, 1341-1352.

(192) Minkler, P. E.; Hoppel, C. L. "Separation and characterization of cardiolipin molecular species by reverse-phase ion pair high-performance liquid chromatography-mass spectrometry"; *Journal of lipid research* **2010**, *51*, 856-865.

(193) Folch, J.; Lees, M.; Sloane Stanley, G. H. "A simple method for the isolation and purification of total lipides from animal tissues"; *Journal of Biological Chemistry* **1957**, *226*, 497-509.

(194) Bligh, E. G.; Dyer, W. J. "A rapid method of total lipid extraction and purification"; *Canadian Journal of Biochemistry and Physiology* **1959**, *37*, 911-917.

(195) Matyash, V.; Liebisch, G.; Kurzchalia, T. V.; Shevchenko, A.; Schwudke, D. "Lipid extraction by methyl-tert-butyl ether for high-throughput lipidomics"; *The Journal of Lipid Research* **2008**, *49*, 1137-1146.

(196) Whitehouse, C. M.; Dreyer, R. N.; Yamashita, M.; Fenn, J. B. "Electrospray interface for liquid chromatographs and mass spectrometers"; *Analytical Chemistry* **1985**, *57*, 675-679.

(197) Fenn, J. B.; Mann, M.; Meng, C. K.; Wong, S. F.; Whitehouse, C. M. "Electrospray ionization for mass spectrometry of large biomolecules"; *Science* **1989**, *246*, 64-71.

(198) Han, X.; Gross, R. W. "Electrospray ionization mass spectroscopic analysis of human erythrocyte plasma membrane phospholipids"; *Proceedings of the National Academy of Sciences of the United States of America* **1994**, *91*, 10635-10639.

(199) Wilm, M. S.; Mann, M. "Electrospray and Taylor-Cone theory, Dole's beam of macromolecules at last?"; *International Journal of Mass Spectrometry and Ion Processes* **1994**, *136*, 167-180.

(200) Lee, S. H.; Williams, M. V.; DuBois, R. N.; Blair, I. A. "Targeted lipidomics using electron capture atmospheric pressure chemical ionization mass spectrometry"; *Rapid Communications in Mass Spectrometry* **2003**, *17*, 2168-2176.

(201) Fuchs, B.; Suss, R.; Schiller, J. "An update of MALDI-TOF mass spectrometry in lipid research"; *Progress in Lipid Research* **2010**, *49*, 450-475.

(202) Wiseman, J. M.; Puolitaival, S. M.; Takáts, Z.; Cooks, R. G.; Caprioli, R. M. "Mass Spectrometric Profiling of Intact Biological Tissue by Using Desorption Electrospray Ionization"; *Angewandte Chemie International Edition* **2005**, *44*, 7094-7097.

(203) Son, J.; Lee, G.; Cha, S. "Direct Analysis of Triacylglycerols from Crude Lipid Mixtures by Gold Nanoparticle-Assisted Laser Desorption/Ionization Mass Spectrometry"; *Journal of the American Society for Mass Spectrometry* **2014**, *25*, 891-894.

(204) Nemes, P.; Woods, A. S.; Vertes, A. "Simultaneous Imaging of Small Metabolites and Lipids in Rat Brain Tissues at Atmospheric Pressure by Laser Ablation Electrospray Ionization Mass Spectrometry"; *Analytical Chemistry* **2010**, *82*, 982-988.

(205) Schwartz, J. C.; Senko, M. W.; Syka, J. E. P. "A two-dimensional quadrupole ion trap mass spectrometer"; *Journal of the American Society for Mass Spectrometry* **2002**, *13*, 659-669.

(206) Makarov, A.; Denisov, E.; Kholomeev, A.; Balschun, W.; Lange, O.; Strupat, K.; Horning, S. "Performance evaluation of a hybrid linear ion trap/orbitrap mass spectrometer"; *Analytical Chemistry* **2006**, *78*, 2113-2120.

(207) Brügger, B.; Erben, G.; Sandhoff, R.; Wieland, F. T.; Lehmann, W. D. "Quantitative analysis of biological membrane lipids at the low picomole level by nano-electrospray ionization tandem mass spectrometry"; *Proceedings of the National Academy of Sciences of the United States of America* **1997**, *94*, 2339-2344.

(208) Hayes, R. N.; Gross, M. L. "Collision-induced dissociation"; *Methods in enzymology* **1990**, *193*, 237-263.

(209) McLuckey, S. A. "Principles of collisional activation in analytical mass spectrometry"; *Journal of the American Society for Mass Spectrometry* **1992**, *3*, 599-614.

(210) Johnson, J. V.; Yost, R. A.; Kelley, P. E.; Bradford, D. C. "Tandem-in-space and tandem-in-time mass spectrometry: triple quadrupoles and quadrupole ion traps"; *Analytical Chemistry* **1990**, *62*, 2162-2172.

(211) Gross, J. H. *Mass spectrometry: a textbook*; Springer Science & Business Media, 2006.

(212) Murphy, R. C.; Axelsen, P. H. "Mass spectrometric analysis of long-chain lipids"; *Mass spectrometry reviews* **2011**, *30*, 579-599.

(213) Brügger, B. "Lipidomics: Analysis of the Lipid Composition of Cells and Subcellular Organelles by Electrospray Ionization Mass Spectrometry"; *Annual review of biochemistry* **2014**, *83*, 79-98.

(214) Schwudke, D.; Hannich, J. T.; Surendranath, V.; Grimard, V.; Moehring, T.; Burton, L.; Kurzchalia, T.; Shevchenko, A. "Top-Down Lipidomic Screens by Multivariate Analysis of High-Resolution Survey Mass Spectra"; *Analytical Chemistry* **2007**, *79*, 4083-4093.

(215) Boehm, A.; Hoffmann, C.; Irmler, M.; Schneeweiss, P.; Schnauder, G.; Sailer, C.; Schmid, V.; Hudemann, J.; Machann, J.; Schick, F.; Beckers, J.; Hrabe de Angelis, M.; Staiger, H.; Fritsche, A.; Stefan, N.; Niess, A. M.; Haring, H. U.; Weigert, C. "TGF-beta Contributes to Impaired Exercise Response by Suppression of Mitochondrial Key Regulators in Skeletal Muscle"; *Diabetes* **2016**, *65*, 2849-2861.

(216) Peter, A.; Kovarova, M.; Staiger, H.; Machann, J.; Schick, F.; Konigsrainer, A.; Koenigsrainer, I.; Schleicher, E. D.; Fritsche, A.; Haring, H. U.; Stefan, N. "The Hepatokines Fetuin-A and Fetuin-B are up-regulated in the State of Hepatic Steatosis and may differently impact on Glucose Homeostasis in Humans"; *American Journal of Physiology - Endocrinology And Metabolism* **2017**, ajpendo.00262.02017.

(217) Nerlich, A. G.; Sauer, U.; Kolm-Litty, V.; Wagner, E.; Koch, M.; Schleicher, E. D. "Expression of glutamine:fructose-6-phosphate amidotransferase in human tissues: evidence for high variability and distinct regulation in diabetes"; *Diabetes* **1998**, *47*, 170-178.

(218) Bohnert, B. N.; Daniel, C.; Amann, K.; Voelkl, J.; Alesutan, I.; Lang, F.; Heyne, N.; Häring, H. U.; Artunc, F. "Impact of Phosphorus Restriction and Vitamin D-Substitution on Secondary Hyperparathyroidism in a Proteinuric Mouse Model"; *Kidney and Blood Pressure Research* **2015**, *40*, 153-165.

(219) Artunc, F.; Nasir, O.; Amann, K.; Boini, K. M.; Haring, H. U.; Risler, T.; Lang, F. "Serum- and glucocorticoid-inducible kinase 1 in doxorubicin-induced nephrotic syndrome"; *American journal of physiology. Renal physiology* **2008**, *295*, F1624-1634.

(220) Ladner, C. L.; Yang, J.; Turner, R. J.; Edwards, R. A. "Visible fluorescent detection of proteins in polyacrylamide gels without staining"; *Analytical Biochemistry* **2004**, *326*, 13-20.

(221) Bouaboula, M.; Legoux, P.; Pességué, B.; Delpech, B.; Dumont, X.; Piechaczyk, M.; Casellas, P.; Shire, D. "Standardization of mRNA titration using a polymerase chain reaction method involving co-amplification with a multispecific internal control"; *Journal of Biological Chemistry* **1992**, *267*, 21830-21838.

(222) Benedetti, A.; Comporti, M.; Esterbauer, H. "Identification of 4-hydroxynonenal as a cytotoxic product originating from the peroxidation of liver microsomal lipids"; *Biochimica et Biophysica Acta (BBA) - Lipids and Lipid Metabolism* **1980**, *620*, 281-296.

(223) Larsen, S.; Nielsen, J.; Hansen, C. N.; Nielsen, L. B.; Wibrand, F.; Stride, N.; Schroder, H. D.; Boushel, R.; Helge, J. W.; Dela, F.; Hey-Mogensen, M. "Biomarkers of mitochondrial content in skeletal muscle of healthy young human subjects"; *The Journal of Physiology* **2012**, *590*, 3349-3360.

(224) Fernstrom, M.; Bakkman, L.; Tonkonogi, M.; Shabalina, I. G.; Rozhdestvenskaya, Z.; Mattsson, C. M.; Enqvist, J. K.; Ekblom, B.; Sahlin, K. "Reduced efficiency, but increased fat oxidation, in mitochondria from human skeletal muscle after 24-h ultraendurance exercise"; *Journal of Applied Physiology* **2007**, *102*, 1844-1849.

(225) Eigentler, A.; Draxl, A.; Wiethüchter, A.; Kuznetsov, A.; Lassing, B.; Gnaiger, E. In *Protocols Enzymes*, Network, M. P., Ed., 2015.

(226) Pesta, D.; Gnaiger, E. "High-resolution respirometry: OXPHOS protocols for human cells and permeabilized fibers from small biopsies of human muscle"; *Methods in Molecular Biology* **2012**, *810*, 25-58.

(227) Chen, S.; Hoene, M.; Li, J.; Li, Y.; Zhao, X.; Häring, H.-U.; Schleicher, E. D.; Weigert, C.; Xu, G.; Lehmann, R. "Simultaneous extraction of metabolome and lipidome with methyl tert-butyl ether from a single small tissue sample for ultra-high performance liquid chromatography/mass spectrometry"; *Journal of Chromatography A* **2013**, *1298*, 9-16.

(228) Li, J.; Hoene, M.; Zhao, X.; Chen, S.; Wei, H.; Haring, H. U.; Lin, X.; Zeng, Z.; Weigert, C.; Lehmann, R.; Xu, G. "Stable isotope-assisted lipidomics combined with nontargeted isotopomer filtering, a tool to unravel the complex dynamics of lipid metabolism"; *Analytical Chemistry* **2013**, *85*, 4651-4657.

(229) Fahy, E.; Subramaniam, S.; Murphy, R. C.; Nishijima, M.; Raetz, C. R. H.; Shimizu, T.; Spener, F.; van Meer, G.; Wakelam, M. J. O.; Dennis, E. A. "Update of the LIPID MAPS comprehensive classification system for lipids"; *The Journal of Lipid Research* **2009**, *50*, S9-S14.

(230) McDonald, J. G.; Smith, D. D.; Stiles, A. R.; Russell, D. W. "A comprehensive method for extraction and quantitative analysis of sterols and secosteroids from human plasma"; *The Journal of Lipid Research* **2012**, *53*, 1399-1409.

(231) Bijlsma, S.; Bobeldijk, I.; Verheij, E. R.; Ramaker, R.; Kochhar, S.; Macdonald, I. A.; van Ommen, B.; Smilde, A. K. "Large-scale human metabolomics studies: a strategy for data (pre-) processing and validation"; *Analytical Chemistry* **2006**, *78*, 567-574.

(232) Saeed, A. I.; Sharov, V.; White, J.; Li, J.; Liang, W.; Bhagabati, N.; Braisted, J.; Klapa, M.; Currier, T.; Thiagarajan, M.; Sturn, A.; Snuffin, M.; Rezantsev, A.; Popov, D.; Ryltsov, A.; Kostukovich, E.; Borisovsky, I.; Liu, Z.; Vinsavich, A.; Trush, V.; Quackenbush, J. "TM4: A free, open-source system for microarray data management and analysis"; *BioTechniques* **2003**, *34*, 374-378.

(233) Motulsky, H. J.; Brown, R. E. "Detecting outliers when fitting data with nonlinear regression – a new method based on robust nonlinear regression and the false discovery rate"; *BMC Bioinformatics* **2006**, *7*, 123.

(234) Honda, A.; Yamashita, K.; Hara, T.; Ikegami, T.; Miyazaki, T.; Shirai, M.; Xu, G.; Numazawa, M.; Matsuzaki, Y. "Highly sensitive quantification of key regulatory oxysterols in biological samples by LC-ESI-MS/MS"; *The Journal of Lipid Research* **2009**, *50*, 350-357.

(235) Yoshioka, N.; Adachi, J.; Ueno, Y.; Yoshida, K.-I. "Oxysterols increase in diabetic rats"; *Free Radical Research* **2005**, *39*, 299-304.

(236) Griffiths, W. J.; Hornshaw, M.; Woffendin, G.; Baker, S. F.; Lockhart, A.; Heidelberger, S.; Gustafsson, M.; Sjövall, J.; Wang, Y. "Discovering Oxysterols in Plasma: A Window on the Metabolome"; *Journal of Proteome Research* **2008**, *7*, 3602-3612.

(237) Mostafa, M. G.; Mima, T.; Ohnishi, S. T.; Mori, K. "S-allylcysteine ameliorates doxorubicin toxicity in the heart and liver in mice"; *Planta medica* **2000**, *66*, 148-151.

(238) Tacar, O.; Sriamornsak, P.; Dass, C. R. "Doxorubicin: an update on anticancer molecular action, toxicity and novel drug delivery systems"; *Journal of Pharmacy and Pharmacology* **2013**, *65*, 157-170.

(239) Patel, N.; Joseph, C.; Corcoran, G. B.; Ray, S. D. "Silymarin modulates doxorubicin-induced oxidative stress, Bcl-xL and p53 expression while preventing apoptotic and necrotic cell death in the liver"; *Toxicology and Applied Pharmacology* **2010**, *245*, 143-152.

(240) Zhang, M.; Mileykovskaya, E.; Dowhan, W. "Gluing the respiratory chain together. Cardiolipin is required for supercomplex formation in the inner mitochondrial membrane"; *Journal of Biological Chemistry* **2002**, *277*, 43553-43556.

(241) Pfeiffer, K.; Gohil, V.; Stuart, R. A.; Hunte, C.; Brandt, U.; Greenberg, M. L.; Schagger, H. "Cardiolipin stabilizes respiratory chain supercomplexes"; *Journal of Biological Chemistry* **2003**, *278*, 52873-52880.

(242) Gohil, V. M.; Thompson, M. N.; Greenberg, M. L. "Synthetic lethal interaction of the mitochondrial phosphatidylethanolamine and cardiolipin biosynthetic pathways in Saccharomyces cerevisiae"; *Journal of Biological Chemistry* **2005**, *280*, 35410-35416.

(243) Haluzik, M.; Gavrilova, O.; LeRoith, D. "Peroxisome Proliferator-Activated Receptor-α Deficiency Does Not Alter Insulin Sensitivity in Mice Maintained on Regular or High-Fat Diet: Hyperinsulinemic-Euglycemic Clamp Studies"; *Endocrinology* **2004**, *145*, 1662-1667.

(244) Van Heek, M.; Compton, D. S.; France, C. F.; Tedesco, R. P.; Fawzi, A. B.; Graziano, M. P.; Sybertz, E. J.; Strader, C. D.; Davis, H. R. "Diet-induced obese mice develop peripheral, but not central, resistance to leptin"; *Journal of Clinical Investigation* **1997**, *99*, 385-390.

(245) Abdul-Ghani, M. A.; Jani, R.; Chavez, A.; Molina-Carrion, M.; Tripathy, D.; Defronzo, R. A. "Mitochondrial reactive oxygen species generation in obese non-diabetic and type 2 diabetic participants"; *Diabetologia* **2009**, *52*, 574-582.

(246) Anderson, E. J.; Lustig, M. E.; Boyle, K. E.; Woodlief, T. L.; Kane, D. A.; Lin, C. T.; Price, J. W., 3rd; Kang, L.; Rabinovitch, P. S.; Szeto, H. H.; Houmard, J. A.; Cortright, R. N.; Wasserman, D. H.; Neufer, P.

D. "Mitochondrial H2O2 emission and cellular redox state link excess fat intake to insulin resistance in both rodents and humans"; *Journal of Clinical Investigation* **2009**, *119*, 573-581.

(247) Han, X.; Yang, J.; Cheng, H.; Ye, H.; Gross, R. W. "Toward fingerprinting cellular lipidomes directly from biological samples by two-dimensional electrospray ionization mass spectrometry"; *Analytical Biochemistry* **2004**, *330*, 317-331.

(248) Zambrano, F.; Fleischer, S.; Fleischer, B. "Lipid composition of the Golgi apparatus of rat kidney and liver in comparison with other subcellular organelles"; *Biochimica et Biophysica Acta* **1975**, *380*, 357-369.

(249) Vance, J. E. "Lipoproteins secreted by cultured rat hepatocytes contain the antioxidant 1-alk-1-enyl-2-acylglycerophosphoethanolamine"; *Biochimica et Biophysica Acta* **1990**, *1045*, 128-134.

(250) Braverman, N. E.; Moser, A. B. "Functions of plasmalogen lipids in health and disease"; *Biochimica et Biophysica Acta (BBA) - Molecular Basis of Disease* **2012**, *1822*, 1442-1452.

(251) Honsho, M.; Yagita, Y.; Kinoshita, N.; Fujiki, Y. "Isolation and characterization of mutant animal cell line defective in alkyl-dihydroxyacetonephosphate synthase: Localization and transport of plasmalogens to post-Golgi compartments"; *Biochimica et Biophysica Acta (BBA) - Molecular Cell Research* **2008**, *1783*, 1857-1865.

(252) Brites, P.; Waterham, H. R.; Wanders, R. J. "Functions and biosynthesis of plasmalogens in health and disease"; *Biochimica et Biophysica Acta* **2004**, *1636*, 219-231.

(253) Martin, S.; Parton, R. G. "Lipid droplets: a unified view of a dynamic organelle"; *Nature Reviews Molecular Cell Biology* **2006**, *7*, 373-378.

(254) Walther, T. C.; Farese, R. V., Jr. "The life of lipid droplets"; *Biochimica et Biophysica Acta* **2009**, *1791*, 459-466.

(255) Colbeau, A.; Nachbaur, J.; Vignais, P. M. "Enzymac characterization and lipid composition of rat liver subcellular membranes"; *Biochimica et Biophysica Acta (BBA) - Biomembranes* **1971**, *249*, 462-492.

(256) Shinkyo, R.; Xu, L.; Tallman, K. A.; Cheng, Q.; Porter, N. A.; Guengerich, F. P. "Conversion of 7-dehydrocholesterol to 7-ketocholesterol is catalyzed by human cytochrome P450 7A1 and occurs by direct oxidation without an epoxide intermediate"; *Journal of Biological Chemistry* **2011**, *286*, 33021-33028.

(257) Larsson, H.; Bottiger, Y.; Iuliano, L.; Diczfalusy, U. "In vivo interconversion of 7beta-hydroxycholesterol and 7-ketocholesterol, potential surrogate markers for oxidative stress"; *Free Radical Biology and Medicine* **2007**, *43*, 695-701.

(258) Aringer, L.; Eneroth, P.; Nordström, L. "Side chain hydroxylation of cholesterol, campesterol and beta-sitosterol in rat liver mitochondria"; *The Journal of Lipid Research* **1976**, *17*, 263-272.

(259) Guarisco, J. A.; Hall, J. O.; Coulombe Jr, R. A. "Mechanisms of butylated hydroxytoluene chemoprevention of aflatoxicosis—inhibition of aflatoxin B1 metabolism"; *Toxicology and Applied Pharmacology* **2008**, *227*, 339-346.

(260) Zhong, H.; Lu, J.; Xia, L.; Zhu, M.; Yin, H. "Formation of electrophilic oxidation products from mitochondrial cardiolipin in vitro and in vivo in the context of apoptosis and atherosclerosis"; *Redox Biology* **2014**, *2*, 878-883.

(261) Nicolay, K.; de Kruijff, B. "Effects of adriamycin on respiratory chain activities in mitochondria from rat liver, rat heart and bovine heart. Evidence for a preferential inhibition of complex III and IV"; *Biochimica et Biophysica Acta (BBA) - Bioenergetics* **1987**, *892*, 320-330.

(262) Dirks-Naylor, A. J.; Kouzi, S. A.; Bero, J. D.; Phan, D. T.; Taylor, H. N.; Whitt, S. D.; Mabolo, R. "Doxorubicin alters the mitochondrial dynamics machinery and mitophagy in the liver of treated animals"; *Fundamental & Clinical Pharmacology* **2014**, *28*, 633-642.

(263) Blau, H. M.; Chiu, C. P.; Webster, C. "Cytoplasmic activation of human nuclear genes in stable heterocaryons"; *Cell* **1983**, *32*, 1171-1180.

(264) Yaffe, D.; Saxel, O. R. A. "Serial passaging and differentiation of myogenic cells isolated from dystrophic mouse muscle"; *Nature* **1977**, *270*, 725-727.

(265) Burattini, S.; Ferri, P.; Battistelli, M.; Curci, R.; Luchetti, F.; Falcieri, E. "C2C12 murine myoblasts as a model of skeletal muscle development: morpho-functional characterization"; *European Journal of Histochemistry* **2004**, *48*, 223-233.

(266) Brown, D. M.; Parr, T.; Brameld, J. M. "Myosin heavy chain mRNA isoforms are expressed in two distinct cohorts during C2C12 myogenesis"; *Journal of muscle research and cell motility* **2012**, *32*, 383-390.

(267) Huang, C.; Somwar, R.; Patel, N.; Niu, W.; Torok, D.; Klip, A. "Sustained exposure of L6 myotubes to high glucose and insulin decreases insulin-stimulated GLUT4 translocation but upregulates GLUT4 activity"; *Diabetes* **2002**, *51*, 2090-2098.

(268) Kumar, N.; Dey, C. S. "Development of insulin resistance and reversal by thiazolidinediones in C2C12 skeletal muscle cells"; *Biochemical pharmacology* **2003**, *65*, 249-257.

(269) Zierath, J. R.; Krook, A.; Wallberg-Henriksson, H. "Insulin action and insulin resistance in human skeletal muscle"; *Diabetologia* **2000**, *43*, 821-835.

(270) Leary, S. C.; Battersby, B. J.; Hansford, R. G.; Moyes, C. D. "Interactions between bioenergetics and mitochondrial biogenesis"; *Biochimica et Biophysica Acta (BBA)-Bioenergetics* **1998**, *1365*, 522-530.

(271) Ibsen, K. H. "The Crabtree effect: a review"; *Cancer Research* **1961**, *21*, 829-841.

(272) Mailloux, R. J.; Harper, M. E. "Glucose regulates enzymatic sources of mitochondrial NADPH in skeletal muscle cells; a novel role for glucose-6-phosphate dehydrogenase"; *The FASEB Journal* **2010**, *24*, 2495-2506.

(273) Elkalaf, M.; Anděl, M.; Trnka, J. "Low Glucose but Not Galactose Enhances Oxidative Mitochondrial Metabolism in C2C12 Myoblasts and Myotubes"; *PLoS One* **2013**, *8*, e70772.

(274) Lin, J.; Handschin, C.; Spiegelman, B. M. "Metabolic control through the PGC-1 family of transcription coactivators"; *Cell metabolism* **2005**, *1*, 361-370.

(275) Mootha, V. K.; Lindgren, C. M.; Eriksson, K. F.; Subramanian, A.; Sihag, S.; Lehar, J.; Puigserver, P.; Carlsson, E.; Ridderstrale, M.; Laurila, E.; Houstis, N.; Daly, M. J.; Patterson, N.; Mesirov, J. P.; Golub, T. R.; Tamayo, P.; Spiegelman, B.; Lander, E. S.; Hirschhorn, J. N.; Altshuler, D.; Groop, L. C. "PGC-1alpha-responsive genes involved in oxidative phosphorylation are coordinately downregulated in human diabetes"; *Nature genetics* **2003**, *34*, 267-273.

(276) Patti, M. E.; Butte, A. J.; Crunkhorn, S.; Cusi, K.; Berria, R.; Kashyap, S.; Miyazaki, Y.; Kohane, I.; Costello, M.; Saccone, R.; Landaker, E. J.; Goldfine, A. B.; Mun, E.; DeFronzo, R.; Finlayson, J.; Kahn, C. R.; Mandarino, L. J. "Coordinated reduction of genes of oxidative metabolism in humans with insulin resistance and diabetes: Potential role of PGC1 and NRF1"; *Proceedings of the National Academy of Sciences of the United States of America* **2003**, *100*, 8466-8471.

(277) Costford, S. R.; Crawford, S. A.; Dent, R.; McPherson, R.; Harper, M. E. "Increased susceptibility to oxidative damage in post-diabetic human myotubes"; *Diabetologia* **2009**, *52*, 2405-2415.

(278) Aguer, C.; Gambarotta, D.; Mailloux, R. J.; Moffat, C.; Dent, R.; McPherson, R.; Harper, M.-E. "Galactose Enhances Oxidative Metabolism and Reveals Mitochondrial Dysfunction in Human Primary Muscle Cells"; *PLoS One* **2011**, *6*, e28536.

(279) Nishikawa, T.; Edelstein, D.; Du, X. L.; Yamagishi, S.-i. "Normalizing mitochondrial superoxide production blocks three pathways of hyperglycaemic damage"; *Nature* **2000**, *404*, 787.

(280) Fridovich, I. "Superoxide dismutases. An adaptation to a paramagnetic gas"; *Journal of Biological Chemistry* **1989**, *264*, 7761-7764.

(281) Tafuri, F.; Ronchi, D.; Magri, F.; Comi, G. P.; Corti, S. "SOD1 misplacing and mitochondrial dysfunction in amyotrophic lateral sclerosis pathogenesis"; *Frontiers in Cellular Neuroscience* **2015**, *9*, 336.

(282) Gumieniczek, A.; Hopkala, H.; Wojtowicz, Z.; Nieradko, M. "Differences in antioxidant status in skeletal muscle tissue in experimental diabetes"; *Clinica Chimica Acta* **2001**, *314*, 39-45.

(283) Naples, S. P.; Borengasser, S. J.; Rector, R. S.; Uptergrove, G. M.; Morris, E. M.; Mikus, C. R.; Koch, L. G.; Britton, S. L.; Ibdah, J. A.; Thyfault, J. P. "Skeletal Muscle Mitochondrial and Metabolic Responses to a High Fat Diet in Female Rats Bred for High and Low Aerobic Capacity"; *Applied physiology, nutrition, and metabolism* **2010**, *35*, 151-162.

(284) St-Pierre, J.; Lin, J.; Krauss, S.; Tarr, P. T.; Yang, R.; Newgard, C. B.; Spiegelman, B. M. "Bioenergetic Analysis of Peroxisome Proliferator-activated Receptor γ Coactivators 1α and 1β (PGC-1α and PGC-1β) in Muscle Cells"; *Journal of Biological Chemistry* **2003**, *278*, 26597-26603.

(285) Mootha, V. K.; Bunkenborg, J.; Olsen, J. V.; Hjerrild, M.; Wisniewski, J. R.; Stahl, E.; Bolouri, M. S.; Ray, H. N.; Sihag, S.; Kamal, M.; Patterson, N.; Lander, E. S.; Mann, M. "Integrated Analysis of Protein Composition,Tissue Diversity, and Gene Regulation in Mouse Mitochondria"; *Cell* **2003**.

(286) Herzig, S.; Raemy, E.; Montessuit, S.; Veuthey, J. L.; Zamboni, N.; Westermann, B.; Kunji, E. R.; Martinou, J. C. "Identification and functional expression of the mitochondrial pyruvate carrier"; *Science* **2012**, *337*, 93-96.

(287) Vigueira, Patrick A.; McCommis, Kyle S.; Schweitzer, George G.; Remedi, Maria S.; Chambers, Kari T.; Fu, X.; McDonald, William G.; Cole, Serena L.; Colca, Jerry R.; Kletzien, Rolf F.; Burgess, Shawn C.; Finck, Brian N. "Mitochondrial Pyruvate Carrier 2 Hypomorphism in Mice Leads to Defects in Glucose-Stimulated Insulin Secretion"; *Cell Reports* **2014**, *7*, 2042-2053.

(288) Patel, M. S.; Korotchkina, L. G. "Regulation of the pyruvate dehydrogenase complex"; *Biochemical Society transactions* **2006**, *34*, 217-222.

(289) Ariane D. Minet, M. G. "Pyruvate carboxylase is expressed in human skeletal muscle"; *Biochemical and Biophysical Research Communications* **2010**, *402*, 196–197.

(290) Crabtree, B.; Higgins, S. J.; Newsholme, E. A. "The activities of pyruvate carboxylase, phosphoenolpyruvate carboxylase and fructose diphosphatase in muscles from vertebrates and invertebrates"; *Biochemical Journal* **1972**, *130*, 391-396.

(291) Utter, M. F.; Keech, D. B. "Pyruvate Carboxylase: I. Nature of the reaction"; *Journal of Biological Chemistry* **1963**, *238*, 2603-2608.

(292) Bangsbo, J. "Muscle oxygen uptake in humans at onset of and during intense exercise"; *Acta physiologica Scandinavica* **2000**, *168*, 457-464.

(293) Phan, M. D.; Shin, K. "Effects of cardiolipin on membrane morphology: a Langmuir monolayer study"; *Biophysical journal* **2015**, *108*, 1977-1986.

(294) Laganowsky, A.; Reading, E.; Allison, T. M.; Ulmschneider, M. B.; Degiacomi, M. T.; Baldwin, A. J.; Robinson, C. V. "Membrane proteins bind lipids selectively to modulate their structure and function"; *Nature* **2014**, *510*, 172-175.

(295) Chen, D.; Zhang, X.-Y.; Shi, Y. "Identification and functional characterization of hCLS1, a human cardiolipin synthase localized in mitochondria"; *Biochemical Journal* **2006**, *398*, 169-176.

(296) McKenzie, M.; Lazarou, M.; Thorburn, D. R.; Ryan, M. T. "Mitochondrial respiratory chain supercomplexes are destabilized in Barth Syndrome patients"; *Journal of molecular biology* **2006**, *361*, 462-469.

(297) Cheng, H.; Mancuso, D. J.; Jiang, X.; Guan, S.; Yang, J.; Yang, K.; Sun, G.; Gross, R. W.; Han, X. "Shotgun lipidomics reveals the temporally dependent, highly diversified cardiolipin profile in the mammalian brain: temporally coordinated postnatal diversification of cardiolipin molecular species with neuronal remodeling"; *Biochemistry* **2008**, *47*, 5869-5880.

(298) Nowicki, M.; Muller, F.; Frentzen, M. "Cardiolipin synthase of Arabidopsis thaliana"; *FEBS Letters* **2005**, *579*, 2161-2165.

(299) Hostetler, K. Y.; Galesloot, J. M.; Boer, P.; Van Den Bosch, H. "Further studies on the formation of cardiolipin and phosphatidylglycerol in rat liver mitochondria. Effect of divalent cations and the fatty acid composition of CDP-diglyceride"; *Biochimica et Biophysica Acta* **1975**, *380*, 382-389.

(300) Maguire, J. J.; Tyurina, Y. Y.; Mohammadyani, D.; Kapralov, A. A.; Anthonymuthu, T. S.; Qu, F.; Amoscato, A. A.; Sparvero, L. J.; Tyurin, V. A.; Planas-Iglesias, J.; He, R.-R.; Klein-Seetharaman, J.; Bayır, H.; Kagan, V. E. "Known unknowns of cardiolipin signaling: The best is yet to come"; *Biochimica et Biophysica Acta (BBA) - Molecular and Cell Biology of Lipids* **2017**, *1862*, 8-24.

(301) Houtkooper, R. H.; Turkenburg, M.; Poll-The, B. T.; Karall, D.; Pérez-Cerdá, C.; Morrone, A.; Malvagia, S.; Wanders, R. J.; Kulik, W.; Vaz, F. M. "The enigmatic role of tafazzin in cardiolipin metabolism"; *Biochimica et Biophysica Acta (BBA) - Biomembranes* **2009**, *1788*, 2003-2014.

(302) Li, J.; Romestaing, C.; Han, X.; Li, Y.; Hao, X.; Wu, Y.; Sun, C.; Liu, X.; Jefferson, L. S.; Xiong, J.; LaNoue, K. F.; Chang, Z.; Lynch, C. J.; Wang, H.; Shi, Y. "Cardiolipin Remodeling by ALCAT1 Links Oxidative Stress and Mitochondrial Dysfunction to Obesity"; *Cell metabolism* **2010**, *12*, 154-165.

(303) Sahlin, K.; Shabalina, I. G.; Mattsson, C. M.; Bakkman, L.; Fernstrom, M.; Rozhdestvenskaya, Z.; Enqvist, J. K.; Nedergaard, J.; Ekblom, B.; Tonkonogi, M. "Ultraendurance exercise increases the production of reactive oxygen species in isolated mitochondria from human skeletal muscle"; *Journal of Applied Physiology* **2010**, *108*, 780-787.

(304) Ghosh, S.; Lertwattanarak, R.; Lefort, N.; Molina-Carrion, M.; Joya-Galeana, J.; Bowen, B. P.; Garduno-Garcia Jde, J.; Abdul-Ghani, M.; Richardson, A.; DeFronzo, R. A.; Mandarino, L.; Van Remmen, H.; Musi, N. "Reduction in reactive oxygen species production by mitochondria from elderly subjects with normal and impaired glucose tolerance"; *Diabetes* **2011**, *60*, 2051-2060.

(305) Ristow, M.; Zarse, K.; Oberbach, A.; Kloting, N.; Birringer, M.; Kiehntopf, M.; Stumvoll, M.; Kahn, C. R.; Bluher, M. "Antioxidants prevent health-promoting effects of physical exercise in humans"; *Proceedings of the National Academy of Sciences of the United States of America* **2009**, *106*, 8665-8670.

(306) Cao, J.; Liu, Y.; Lockwood, J.; Burn, P.; Shi, Y. "A novel cardiolipin-remodeling pathway revealed by a gene encoding an endoplasmic reticulum-associated acyl-CoA:lysocardiolipin acyltransferase (ALCAT1) in mouse"; *Journal of Biological Chemistry* **2004**, *279*, 31727-31734.

(307) Cao, J.; Shen, W.; Chang, Z.; Shi, Y. "ALCAT1 is a polyglycerophospholipid acyltransferase potently regulated by adenine nucleotide and thyroid status"; *American Journal of Physiology - Endocrinology And Metabolism* **2009**, *296*, E647-E653.

(308) Schlame, M.; Brody, S.; Hostetler, K. Y. "Mitochondrial cardiolipin in diverse eukaryotes"; *European Journal of Biochemistry* **1993**, *212*, 727-733.

(309) Fajardo, V. A.; McMeekin, L.; Saint, C.; LeBlanc, P. J. "Cardiolipin linoleic acid content and mitochondrial cytochrome c oxidase activity are associated in rat skeletal muscle"; *Chemistry and Physics of Lipids* **2015**, *187*, 50-55.

(310) Minkler, P. E.; Hoppel, C. L. "Separation and characterization of cardiolipin molecular species by reverse-phase ion pair high-performance liquid chromatography-mass spectrometry"; *The Journal of Lipid Research* **2010**, *51*, 856-865.

(311) Hatch, G. M. "Cardiolipin biosynthesis in the isolated heart"; *Biochemical Journal* **1994**, *297*, 201-208.

(312) Sparagna, G. C.; Lesnefsky, E. J. "Cardiolipin remodeling in the heart"; *Journal of cardiovascular pharmacology* **2009**, *53*, 290-301.

(313) Cortie, C.; Hulbert, A.; Hancock, S.; Mitchell, T.; McAndrew, D.; Else, P. "Of mice, pigs and humans: An analysis of mitochondrial phospholipids from mammals with very different maximal lifespans"; *Experimental gerontology* **2015**, *70*, 135–143.

(314) Rietveld, A. G.; Killian, J. A.; Dowhan, W.; de Kruijff, B. "Polymorphic regulation of membrane phospholipid composition in Escherichia coli"; *Journal of Biological Chemistry* **1993**, *268*, 12427-12433.

(315) Osman, C.; Haag, M.; Potting, C.; Rodenfels, J.; Dip, P. V.; Wieland, F. T.; Brugger, B.; Westermann, B.; Langer, T. "The genetic interactome of prohibitins: coordinated control of cardiolipin and phosphatidylethanolamine by conserved regulators in mitochondria"; *The Journal of Cell Biology* **2009**, *184*, 583-596.

(316) Holman, R. T. "Autoxidation of fats and related substances"; *Progress in the chemistry of fats and other lipids* **1954**, *2*, 51-98.

(317) Cosgrove, J. P.; Church, D. F.; Pryor, W. A. "The kinetics of the autoxidation of polyunsaturated fatty acids"; *Lipids* **1987**, *22*, 299-304.

(318) Paradies, G.; Petrosillo, G.; Pistolese, M.; Ruggiero, F. M. "The effect of reactive oxygen species generated from the mitochondrial electron transport chain on the cytochrome c oxidase activity and on the cardiolipin content in bovine heart submitochondrial particles"; *FEBS Letters* **2000**, *466*, 323-326.

(319) Paradies, G.; Petrosillo, G.; Pistolese, M.; Ruggiero, F. M. "Reactive oxygen species generated by the mitochondrial respiratory chain affect the complex III activity via cardiolipin peroxidation in beef-heart submitochondrial particles"; *Mitochondrion* **2001**, *1*, 151-159.

(320) Paradies, G.; Petrosillo, G.; Pistolese, M.; Ruggiero, F. M. "Reactive oxygen species affect mitochondrial electron transport complex I activity through oxidative cardiolipin damage"; *Gene* **2002**, *286*, 135-141.

(321) Tyurina, Y. Y.; Poloyac, S. M.; Tyurin, V. A.; Kapralov, A. A.; Jiang, J.; Anthonymuthu, T. S.; Kapralova, V. I.; Vikulina, A. S.; Jung, M. Y.; Epperly, M. W.; Mohammadyani, D.; Klein-Seetharaman, J.; Jackson, T. C.; Kochanek, P. M.; Pitt, B. R.; Greenberger, J. S.; Vladimirov, Y. A.; Bayir, H.; Kagan, V. E. "A mitochondrial pathway for biosynthesis of lipid mediators"; *Nature chemistry* **2014**, *6*, 542-552.

(322) Kagan, V. E.; Tyurin, V. A.; Jiang, J.; Tyurina, Y. Y.; Ritov, V. B.; Amoscato, A. A.; Osipov, A. N.; Belikova, N. A.; Kapralov, A. A.; Kini, V.; Vlasova, I. I.; Zhao, Q.; Zou, M.; Di, P.; Svistunenko, D. A.; Kurnikov, I. V.; Borisenko, G. G. "Cytochrome c acts as a cardiolipin oxygenase required for release of proapoptotic factors"; *Nature Chemical Biology* **2005**, *1*, 223-232.

(323) Niki, E.; Yoshida, Y.; Saito, Y.; Noguchi, N. "Lipid peroxidation: Mechanisms, inhibition, and biological effects"; *Biochemical and Biophysical Research Communications* **2005**, *338*, 668-676.

(324) Porter, R. K.; Hulbert, A. J.; Brand, M. D. "Allometry of mitochondrial proton leak: influence of membrane surface area and fatty acid composition"; *American Journal of Physiology* **1996**, *271*, R1550-1560.

(325) Brookes, P.; A Buckingham, J.; Tenreiro, A.; Hulbert, A.; Brand, M. "The Proton Permeability of the Inner Membrane of Liver Mitochondria from Ectothermic and Endothermic Vertebrates and from Obese Rats: Correlations with Standard Metabolic Rate and Phospholipid Fatty Acid Composition"; *Comparative Biochemistry and Physiology - Part B: Biochemistry & Molecular Biology* **1998**, *119*, 325-334.

(326) Brand, M. D.; Turner, N.; Ocloo, A.; Else, P. L.; Hulbert, A. J. "Proton conductance and fatty acyl composition of liver mitochondria correlates with body mass in birds"; *Biochemical Journal* **2003**, *376*, 741-748.

(327) Rolfe, D. F.; Brand, M. D. "Contribution of mitochondrial proton leak to skeletal muscle respiration and to standard metabolic rate"; *American Journal of Physiology* **1996**, *271*, C1380-1389.

(328) Senoo, N.; Miyoshi, N.; Goto-Inoue, N.; Minami, K.; Yoshimura, R.; Morita, A.; Sawada, N.; Matsuda, J.; Ogawa, Y.; Setou, M.; Kamei, Y.; Miura, S. "PGC-1alpha-mediated changes in phospholipid profiles of exercise-trained skeletal muscle"; *Journal of lipid research* **2015**, *56*, 2286-2296.

(329) Andersson, A.; Sjodin, A.; Hedman, A.; Olsson, R.; Vessby, B. "Fatty acid profile of skeletal muscle phospholipids in trained and untrained young men"; *Am J Physiol Endocrinol Metab* **2000**, *279*, E744-751.

(330) Valentine, W. J.; Tokuoka, S. M.; Hishikawa, D.; Kita, Y.; Shindou, H.; Shimizu, T. "Lysophosphatidic Acid Acyltransferase 3 Incorporates Docosahexaeneoic Acid into Skeletal Muscle Cell Membranes and Is Upregulated by PPARdelta Activation"; *Journal of lipid research* **2017**.

(331) Han, X.; Yang, J.; Yang, K.; Zhao, Z.; Abendschein, D. R.; Gross, R. W. "Alterations in myocardial cardiolipin content and composition occur at the very earliest stages of diabetes: a shotgun lipidomics study"; *Biochemistry* **2007**, *46*, 6417-6428.

(332) Polozova, A.; Gionfriddo, E.; Salem Jr, N. "Effect of docosahexaenoic acid on tissue targeting and metabolism of plasma lipoproteins"; *Prostaglandins, Leukotrienes and Essential Fatty Acids* **2006**, *75*, 183-190.

(333) Timmons, J. A.; Wennmalm, K.; Larsson, O.; Walden, T. B.; Lassmann, T.; Petrovic, N.; Hamilton, D. L.; Gimeno, R. E.; Wahlestedt, C.; Baar, K. "Myogenic gene expression signature establishes that brown and white adipocytes originate from distinct cell lineages"; *Proceedings of the National Academy of Sciences of the United States of America* **2007**, *104*, 4401-4406.

(334) Seale, P.; Bjork, B.; Yang, W.; Kajimura, S.; Chin, S.; Kuang, S.; Scime, A.; Devarakonda, S.; Conroe, H. M.; Erdjument-Bromage, H.; Tempst, P.; Rudnicki, M. A.; Beier, D. R.; Spiegelman, B. M. "PRDM16 controls a brown fat/skeletal muscle switch"; *Nature* **2008**, *454*, 961-967.

(335) O'Shea, K. M.; Khairallah, R. J.; Sparagna, G. C.; Xu, W.; Hecker, P. A.; Robillard-Frayne, I.; Des Rosiers, C.; Kristian, T.; Murphy, R. C.; Fiskum, G.; Stanley, W. C. "Dietary omega-3 fatty acids alter cardiac mitochondrial phospholipid composition and delay Ca2+-induced permeability transition"; *Journal of molecular and cellular cardiology* **2009**, *47*, 819-827.

(336) Stanley, W. C.; Khairallah, R. J.; Dabkowski, E. R. "Update on lipids and mitochondrial function: impact of dietary n-3 polyunsaturated fatty acids"; *Current Opinion in Clinical Nutrition & Metabolic Care* **2012**, *15*, 122–126.

(337) Khairallah, R. J.; Sparagna, G. C.; Khanna, N.; O'Shea, K. M.; Hecker, P. A.; Kristian, T.; Fiskum, G.; Des Rosiers, C.; Polster, B. M.; Stanley, W. C. "Dietary supplementation with docosahexaenoic acid, but not eicosapentaenoic acid, dramatically alters cardiac mitochondrial phospholipid fatty acid

composition and prevents permeability transition"; *Biochimica et Biophysica Acta* **2010**, *1797*, 1555-1562.

(338) Tijburg, L. B.; Geelen, M. J.; Van Golde, L. M. "Biosynthesis of phosphatidylethanolamine via the CDP-ethanolamine route is an important pathway in isolated rat hepatocytes"; *Biochemical and Biophysical Research Communications* **1989**, *160*, 1275-1280.

(339) Zelinski, T. A.; Choy, P. C. "Phosphatidylethanolamine biosynthesis in isolated hamster heart"; *Canadian Journal of Biochemistry and Physiology* **1982**, *60*, 817-823.

(340) Bleijerveld, O. B.; Brouwers, J. F. H. M.; Vaandrager, A. B.; Helms, J. B.; Houweling, M. "The CDP-ethanolamine Pathway and Phosphatidylserine Decarboxylation Generate Different Phosphatidylethanolamine Molecular Species"; *Journal of Biological Chemistry* **2007**, *282*, 28362-28372.

(341) De Feyter, H. M.; van den Broek, N. M.; Praet, S. F.; Nicolay, K.; van Loon, L. J.; Prompers, J. J. "Early or advanced stage type 2 diabetes is not accompanied by in vivo skeletal muscle mitochondrial dysfunction"; *European journal of endocrinology* **2008**, *158*, 643-653.

(342) Trenell, M. I.; Hollingsworth, K. G.; Lim, E. L.; Taylor, R. "Increased daily walking improves lipid oxidation without changes in mitochondrial function in type 2 diabetes"; *Diabetes care* **2008**, *31*, 1644-1649.

(343) Fisher-Wellman, K. H.; Weber, T. M.; Cathey, B. L.; Brophy, P. M.; Gilliam, L. A.; Kane, C. L.; Maples, J. M.; Gavin, T. P.; Houmard, J. A.; Neufer, P. D. "Mitochondrial respiratory capacity and content are normal in young insulin-resistant obese humans"; *Diabetes* **2014**, *63*, 132-141.

(344) van Tienen, F. H.; Praet, S. F.; de Feyter, H. M.; van den Broek, N. M.; Lindsey, P. J.; Schoonderwoerd, K. G.; de Coo, I. F.; Nicolay, K.; Prompers, J. J.; Smeets, H. J.; van Loon, L. J. "Physical activity is the key determinant of skeletal muscle mitochondrial function in type 2 diabetes"; *The Journal of Clinical Endocrinology & Metabolism* **2012**, *97*, 3261-3269.

(345) Lefort, N.; Glancy, B.; Bowen, B.; Willis, W. T.; Bailowitz, Z.; De Filippis, E. A.; Brophy, C.; Meyer, C.; Hojlund, K.; Yi, Z.; Mandarino, L. J. "Increased reactive oxygen species production and lower abundance of complex I subunits and carnitine palmitoyltransferase 1B protein despite normal mitochondrial respiration in insulin-resistant human skeletal muscle"; *Diabetes* **2010**, *59*, 2444-2452.

(346) Fritsch, M.; Koliaki, C.; Livingstone, R.; Phielix, E.; Bierwagen, A.; Meisinger, M.; Jelenik, T.; Strassburger, K.; Zimmermann, S.; Brockmann, K.; Wolff, C.; Hwang, J. H.; Szendroedi, J.; Roden, M. "Time course of postprandial hepatic phosphorus metabolites in lean, obese, and type 2 diabetes patients"; *The American Journal of Clinical Nutrition* **2015**, *102*, 1051-1058.

(347) Petersen, K. F.; Befroy, D. E.; Dufour, S.; Rothman, D. L.; Shulman, G. I. "Direct Assessment of Hepatic Mitochondrial Oxidation and Pyruvate Cycling in Non Alcoholic Fatty Liver Disease by (13)C Magnetic Resonance Spectroscopy"; *Cell metabolism* **2016**, *24*, 167-171.

(348) Takamura, T.; Misu, H.; Matsuzawa-Nagata, N.; Sakurai, M.; Ota, T.; Shimizu, A.; Kurita, S.; Takeshita, Y.; Ando, H.; Honda, M.; Kaneko, S. "Obesity upregulates genes involved in oxidative phosphorylation in livers of diabetic patients"; *Obesity (Silver Spring, Md.)* **2008**, *16*, 2601-2609.

(349) Chiappini, F.; Barrier, A.; Saffroy, R.; Domart, M. C.; Dagues, N.; Azoulay, D.; Sebagh, M.; Franc, B.; Chevalier, S.; Debuire, B.; Dudoit, S.; Lemoine, A. "Exploration of global gene expression in human liver steatosis by high-density oligonucleotide microarray"; *Laboratory Investigation* **2006**, *86*, 154-165.

(350) Misu, H.; Takamura, T.; Matsuzawa, N.; Shimizu, A.; Ota, T.; Sakurai, M.; Ando, H.; Arai, K.; Yamashita, T.; Honda, M.; Yamashita, T.; Kaneko, S. "Genes involved in oxidative phosphorylation are coordinately upregulated with fasting hyperglycaemia in livers of patients with type 2 diabetes"; *Diabetologia* **2007**, *50*, 268-277.

(351) Perez-Carreras, M.; Del Hoyo, P.; Martin, M. A.; Rubio, J. C.; Martin, A.; Castellano, G.; Colina, F.; Arenas, J.; Solis-Herruzo, J. A. "Defective hepatic mitochondrial respiratory chain in patients with nonalcoholic steatohepatitis"; *Hepatology (Baltimore, Md.)* **2003**, *38*, 999-1007.

(352) Larsen, S.; Nielsen, J.; Hansen, C. N.; Nielsen, L. B.; Wibrand, F.; Stride, N.; Schroder, H. D.; Boushel, R.; Helge, J. W.; Dela, F. "Biomarkers of mitochondrial content in skeletal muscle of healthy young human subjects"; *The Journal of Physiology* **2012**, *590*, 3349-3360.

(353) Holness, M. J.; Kraus, A.; Harris, R. A.; Sugden, M. C. "Targeted upregulation of pyruvate dehydrogenase kinase (PDK)-4 in slow-twitch skeletal muscle underlies the stable modification of the regulatory characteristics of PDK induced by high-fat feeding"; *Diabetes* **2000**, *49*, 775-781.

(354) Wibom, R.; Hultman, E.; Johansson, M.; Matherei, K.; Constantin, T.; Schantz, P. "Adaptation of mitochondrial ATP production in human skeletal muscle to endurance training and detraining"; *Journal of Applied Physiology* **1992**, *73*, 2004-2010.

(355) Dalmonte, M. E.; Forte, E.; Genova, M. L.; Giuffre, A.; Sarti, P.; Lenaz, G. "Control of respiration by cytochrome c oxidase in intact cells: role of the membrane potential"; *Journal of Biological Chemistry* **2009**, *284*, 32331-32335.

(356) Piccoli, C.; Scrima, R.; Boffoli, D.; Capitanio, N. "Control by cytochrome c oxidase of the cellular oxidative phosphorylation system depends on the mitochondrial energy state"; *Biochemical Journal* **2006**, *396*, 573-583.

(357) Baldwin, K. M.; Klinkerfuss, G. H.; Terjung, R. L.; Mole, P. A.; Holloszy, J. O. "Respiratory capacity of white, red, and intermediate muscle: adaptative response to exercise"; *American Journal of Physiology* **1972**, *222*, 373-378.

(358) Hey-Mogensen, M.; Hojlund, K.; Vind, B. F.; Wang, L.; Dela, F.; Beck-Nielsen, H.; Fernstrom, M.; Sahlin, K. "Effect of physical training on mitochondrial respiration and reactive oxygen species release in skeletal muscle in patients with obesity and type 2 diabetes"; *Diabetologia* **2010**, *53*, 1976-1985.

(359) Leek, B. T.; Mudaliar, S. R.; Henry, R.; Mathieu-Costello, O.; Richardson, R. S. "Effect of acute exercise on citrate synthase activity in untrained and trained human skeletal muscle"; *American Journal of Physiology-Regulatory, Integrative and Comparative Physiology* **2001**, *280*, R441-R447.

(360) Tonkonogi, M.; Harris, B.; Sahlin, K. "Increased activity of citrate synthase in human skeletal muscle after a single bout of prolonged exercise"; *Acta physiologica Scandinavica* **1997**, *161*, 435-436.

(361) Buchner, D. A.; Yazbek, S. N.; Solinas, P.; Burrage, L. C.; Morgan, M. G.; Hoppel, C. L.; Nadeau, J. H. "Increased mitochondrial oxidative phosphorylation in the liver is associated with obesity and insulin resistance"; *Obesity (Silver Spring, Md.)* **2011**, *19*, 917-924.

(362) Brady, L. J.; Brady, P. S.; Romsos, D. R.; Hoppel, C. L. "Elevated hepatic mitochondrial and peroxisomal oxidative capacities in fed and starved adult obese (ob/ob) mice"; *Biochemical Journal* **1985**, *231*, 439-444.

(363) Chavin, K. D.; Yang, S.; Lin, H. Z.; Chatham, J.; Chacko, V. P.; Hoek, J. B.; Walajtys-Rode, E.; Rashid, A.; Chen, C. H.; Huang, C. C.; Wu, T. C.; Lane, M. D.; Diehl, A. M. "Obesity induces expression of uncoupling protein-2 in hepatocytes and promotes liver ATP depletion"; *Journal of Biological Chemistry* **1999**, *274*, 5692-5700.

(364) Rashid, A.; Wu, T. C.; Huang, C. C.; Chen, C. H.; Lin, H. Z.; Yang, S. Q.; Lee, F. Y.; Diehl, A. M. "Mitochondrial proteins that regulate apoptosis and necrosis are induced in mouse fatty liver"; *Hepatology (Baltimore, Md.)* **1999**, *29*, 1131-1138.

(365) Goldstein, B. J.; Mahadev, K.; Wu, X. "Redox paradox: insulin action is facilitated by insulin-stimulated reactive oxygen species with multiple potential signaling targets"; *Diabetes* **2005**, *54*, 311-321.

(366) Han, X.; Yang, J.; Cheng, H.; Yang, K.; Abendschein, D. R.; Gross, R. W. "Shotgun lipidomics identifies cardiolipin depletion in diabetic myocardium linking altered substrate utilization with mitochondrial dysfunction"; *Biochemistry* **2005**, *44*, 16684-16694.

(367) Watkins, S. M.; Reifsnyder, P. R.; Pan, H. J.; German, J. B.; Leiter, E. H. "Lipid metabolome-wide effects of the PPARgamma agonist rosiglitazone"; *The Journal of Lipid Research* **2002**, *43*, 1809-1817.

(368) He, Q.; Han, X. "Cardiolipin remodeling in diabetic heart"; *Chemistry and Physics of Lipids* **2014**, *179*, 75-81.

(369) Pan, D. A.; Lillioja, S.; Milner, M. R.; Kriketos, A. D.; Baur, L. A.; Bogardus, C.; Storlien, L. H. "Skeletal muscle membrane lipid composition is related to adiposity and insulin action"; *Journal of Clinical Investigation* **1995**, *96*, 2802-2808.

(370) Jiang, F.; Ryan, M. T.; Schlame, M.; Zhao, M.; Gu, Z.; Klingenberg, M.; Pfanner, N.; Greenberg, M. L. "Absence of cardiolipin in the crd1 null mutant results in decreased mitochondrial membrane potential and reduced mitochondrial function"; *Journal of Biological Chemistry* **2000**, *275*, 22387-22394.

(371) Paton, C. M.; Ntambi, J. M. "Biochemical and physiological function of stearoyl-CoA desaturase"; *American Journal of Physiology - Endocrinology And Metabolism* **2009**, *297*, E28-37.

(372) Voss, M. D.; Beha, A.; Tennagels, N.; Tschank, G.; Herling, A. W.; Quint, M.; Gerl, M.; Metz-Weidmann, C.; Haun, G.; Korn, M. "Gene expression profiling in skeletal muscle of Zucker diabetic fatty rats: implications for a role of stearoyl-CoA desaturase 1 in insulin resistance"; *Diabetologia* **2005**, *48*, 2622-2630.

(373) Yechoor, V. K.; Patti, M.-E.; Ueki, K.; Laustsen, P. G.; Saccone, R.; Rauniyar, R.; Kahn, C. R. "Distinct pathways of insulin-regulated versus diabetes-regulated gene expression: an in vivo analysis in MIRKO mice"; *Proceedings of the National Academy of Sciences of the United States of America* **2004**, *101*, 16525-16530.

(374) Higuchi, M.; Cartier, L. J.; Chen, M.; Holloszy, J. O. "Superoxide dismutase and catalase in skeletal muscle: adaptive response to exercise"; *The Journals of Gerontology* **1985**, *40*, 281-286.

(375) Turner, N.; Lee, J. S.; Bruce, C. R.; Mitchell, T. W.; Else, P. L.; Hulbert, A. J.; Hawley, J. A. "Greater effect of diet than exercise training on the fatty acid profile of rat skeletal muscle"; *Journal of Applied Physiology* **2004**, *96*, 974-980.

9 Abbreviations

ACN	acetonitrile
ADP	adenosine diphosphate
ATP	adenosine triphosphate
BCA	bicinchoninic acid
BCAA	branched-chain amino acids
BHT	butylated hydroxytoluene
C1	complex 1: NADH dehydrogenase
C2	complex 2: succinate dehydrogenase
C2C12	skeletal muscle cell line
C3	complex 3: cytochrome c reductase
C4	complex 4: cytochrome c oxidase
C5	complex 5: ATP synthase
Calx	calnexin
CE	cholesteryl ester
CER	ceramide
CL	cardiolipin
CON	control group
COX	cytochrome c oxidase
CoQ	ubiquinone
CS	citrate synthase
DAG	diacylglycerol
DC	differential centrifugation
DCM	dichlormethane
DOX	doxorubicin
DTNB	5,5’-dithiobis-(2-nitrobenzoic acid)
ER	endoplasmic reticulum
ESI	electrospray ionisation

ETC	electron transport chain
ETF	electron transferring flavoprotein
ETS	electron transfer system
FAD	flavine adenine dinucleotide
FAO	fatty acid oxidation (ß-oxidation)
FCCP	carbonyl cyanide-p-trifluoromethoxyphenylhydrazone
FCS	fetal calf serum
FDR	false discovery rate
FFA	free fatty acids
FT-MS	Fourier transform-based mass spectrometers
Gluc	glucose
HADHA	hydroxyacyl-CoA dehydrogenase/3-ketoacyl-CoA thiolase/enoyl-CoA hydratase (trifunctional prot ein), alpha subunit
HED	high energy diet
HEK	human embryonic kidney cells
HEPG2	human hepatocellular carcinoma cells
HexCER	hexosyl-ceramide
HRR	high-resolution respirometry
IPA	isopropyl alcohol
IR	insulin resistant
IRS	insulin receptor substrate
$J(O_2)$	oxygen flux
L	LEAK respiration
LC	liquid chromatography
LPC	lyso-phosphatidylcholine
LPE	lyso-phosphatidylethanolamine
LPI	lyso-phosphatidylinositol
MACS	magnetic cell isolation and separation, here: magnetic-bead assisted mitochondria isolation

MCAD	medium-chain acyl-CoA dehydrogenase
MeOH	methanol
MPC	mitochondrial pyruvate carrier
MS	mass spectrometry
MTBE	methyl tert-butyl ether
MUFA	mono-unsaturated fatty acids
NAD(H)	nicotinamide adenine dinucleotide
NAFL	non-alcoholic fatty liver
NASH	non-alcoholic steatohepatitis
OCR	oxygen consumption rate
OctM	octanoylcarnitine and malate
Ol	oleate
OMM	outer mitochondrial membrane
OXPHOS	oxidative phosphorylation
P	OXPHOS capacity
Pa	palmitate
PaCa	palmitoylcarnitine
PBS	phosphate buffered saline
PC	phosphatidylcholine
PCA	principal component analysis
PDH	pyruvate dehydrogenase
PDK	pyruvate dehydrogenase kinase
PDP	pyruvate dehydrogenase phosphatase
PE	phosphatidylethanolamine
PE-P	phosphatidylethanolamine plasmalogen
PG	phosphatidylglycerol
PI	phosphatidylinositol
PKC	protein kinase C
PS	phosphatidylserine
PUFA	polyunsaturated fatty acids

PyC	pyruvate carboxylase
R	ROUTINE respiration
RC	respiratory chain
ROX	residual oxygen consumption
ROS	reactive oxygen species
RP	reverse phase
RT	room temperature
run	training
SD	standard deviation
SDS-PAGE	sodium dodecyl sulfate polyacrylamide gel electrophoresis
sed	sedentary
SOD	superoxide dismutase
SM	sphingomyelin
SUIT	substrate-uncoupler-inhibitor titration
T2Dm	diabetes mellitus type 2
TAG	triacylglycerol
TCA	tricarboxylic acid
TCE	2,2,2-trichloroethanol
TMPD	N,N,N’,N’-tetramethyl-p-phenylenediamine
TNB	2-nitro-5-thiobenzoate
tP	total protein
UC	ultracentrifugation
UCP	uncoupling protein
U(H)PLC	ultra high performance liquid chromatography
ultra-pure water	water prepared with Milli Q system
VDAC	voltage-dependent anion channel
vs.	versus
WHO	World Health Organization

10 List of Figures and Tables

11 Declaration

I herewith declare that I myself wrote the PhD thesis submitted here under the title “Method development for valid high-resolution profiling of mitochondria and Omics investigation of mitochondrial adaptions to excess energy intake and physical exercise”. I made use of only the sources and auxiliary means in word or context mentioned as such, and which I listed up completely and marked as such. I declare that I adhered to the guidelines of securing good scientific practical experience of the University of Tübingen (conclusion of the Academic Senate of 25 May 2000). I hereby affirm in lieu of an oath (Eidesstattliche Versicherung) that all these declarations are true and that I did not conceal anything. I am well aware that false declarations made under oath will be punished by a prison sentence up to three years or by a monetary penalty.

At the moment I am not accepted or registered at another university as doctoral student. There were no former interrupted or terminated PhD procedures or corresponding examinations, which I have taken. This work has not been submitted for any other degree or professional qualification except as specified. I did not take part in any commercially arranged opportunities to take up the current PhD procedure. I especially did not contact any organisations which engage in the active search for supervisors for the PhD thesis and receive money for this service. I also do clearly exclude that I used such organisations, which adopt the applicant’s obligations and take care of the academic records partially or entirely. Furthermore, I confirm to be aware of the legal consequences of using a commercial thesis writing agency (exclusion from acceptance as a doctoral student and exclusion from admission to the doctoral qualification process, an end to the doctoral qualification process and annulment of the degree. I have no penal convictions, disciplinary measures and pending criminal- and disciplinary proceedings to declare.

Part of this work has been published:

Kappler, L., J. Li, H.-U. Häring, C. Weigert, R. Lehmann, G. Xu and M. Hoene (2016). "Purity matters: A workflow for the valid high-resolution lipid profiling of mitochondria from cell culture samples." Scientific Reports **6**: 21107.

(Lisa Kappler)

Tübingen, 3 April 2018

12 Share in experiments done in team work

Declaration according to § 5 Abs. 2 No. 8 of the PromO of the Faculty of Science

List of shared projects and contributions (unless not otherwise stated experiments and projects were performed by the candidate)

1. Method establishment

- Systematic comparison of optimized mitochondria isolation strategies in HEPG2 cells (4.1.1.2)

Methods and experiments were established and performed by candidate. Lipidomics analyses were performed by Jia Li, DICP Dalian. Paper writing was performed by candidate (80%) and Miriam Hoene and Rainer Lehmann (20%). Candidate is at position 1 of 7 authors. Candidate performed experiments, analysed data and wrote the manuscript. Jia Li performed lipidomics experiments, analysed data and edited the manuscript. Hans-Ulrich Häring interpreted the results. Cora Weigert interpreted the results and edited the manuscript. Rainer Lehmann interpreted the results and wrote and edited the manuscript. Guowang Xu conceived the experiments, interpreted the results and edited the manuscript. Miriam Hoene conceived the experiments, interpreted the results and wrote and edited the manuscript. Publication: Kappler, L., J. Li, H.-U. Häring, C. Weigert, R. Lehmann, G. Xu and M. Hoene (2016). "Purity matters: A workflow for the valid high-resolution lipid profiling of mitochondria from cell culture samples." Scientific Reports **6**: 21107.

- Respiratory measurements

Mouse fibre comparison of gastrocnemius and soleus were performed by bachelor student Daniel Bleher under candidate´s supervision (4.1.2.2.1). Human muscle biopsies used for respiratory measurements were taken by Dr. Anja Böhm.

- Establishment and optimization of a valid mitochondrial oxysterol profiling strategy in liver tissue and hepatic mitochondria (4.1.3.1)

Oxysterol extraction from liver tissue and mitochondria was planned, established and performed by candidate. Oxysterol analysis was established and performed by Ping Luo, DICP Dalian. Oxysterol analysis was modified and performed by Ping Luo and Qingqing Wang, DICP Dalian. Mouse handling and treatment (Doxorubicin) was performed by Bernhard N Bohnert, Internal Medicine 4, University Hospital Tuebingen.

2. Application: Mitochondrial function and insulin resistance

- Cell culture (4.2.1)

Respiratory measurements (solely Oxygraph measurements) and CS activity assays were performed by bachelor student Daniel Bleher under candidate´s supervision.

- Animal studies (4.2.2)

Mouse handling was designed and performed by Miriam Hoene, a member of our group. Sample preparation was performed by candidate. Lipid extraction of samples was performed by candidate. Lipidomics analyses were performed by Chunxiu Hu and Xiaoli Hou, DICP, Dalian. Respiratory measurements and CS activity assays of murine samples were performed by bachelor student Daniel Bleher under candidate´s supervision. Respiratory measurements of human samples were performed by the candidate for human liver and and by the candidate and Christoph Hoffmann for human skeletal muscle fibers.

This thesis was written by the candidate, and proof-read by R. Lehmann and C. Huhn.

I certify that the above statement is correct.

_____

Date, Signature of the candidate

I/We certify that the above statement is correct.

_____

Date, Signature of the doctoral committee or at least of one of the supervisors

13 Acknowledgements/Danksagung

An erster Stelle gilt mein größter Dank meinem Doktorvater Herr Prof. Dr. Rainer Lehmann für seine wissenschaftliche und methodische Unterstützung während der gesamten Dissertation und sein Vertrauen, das er mir stets entgegen gebracht hat. Ich bin auf das Äußerste dankbar für die ständige Förderung jeglicher Art, aber auch für das stete Bemühen um mein 100%iges wissenschaftliches und persönliches Wohlbefinden. Pu-Erh wirkt manchmal Wunder.

Außerdem gilt mein herzlichster Dank meiner Doktormutter Prof. Dr. Carolin Huhn, die sich bereit erklärt hat, mich bei meiner Dissertation zu begleiten, die mich stets durch zielführende Diskussionen und anhaltende überaus freundliche Hilfestellung unterstützt hat. Vielen Dank auch für die netten Erfahrungen über die Arbeit hinaus.

Ein besonderer Dank gilt Dr. Miriam Hoene für ihre tadellose Betreuung, enorme Unterstützung, ihre geteilte Begeisterung für Mitochondrien und ihre ständige Rettungsbereitschaft aus so mancher wissenschaftlicher Not. Auch dem lieben Rest unseres tollen Büros, Dr. Sabine Eckstein und Dr. Christoph Hoffmann, einen schokoladenschnäutzigen kaffeeduftenden herzlichen Dank, ihr wart so unfassbar wertvoll. Sei es für wissenschaftliche Fragen, Hilfestellungen aller Art oder einfach nur ein Lächeln.

Einen riesen Dank auch an Prof. Dr. Cora Weigert für jedwede konstruktive Diskussion und die unermüdlichen Ratschläge, die immer wieder neue Aspekte und Ansätze im Projekt eröffnet haben.

Herzlichen Dank auch an Prof. Dr. Andreas Peter für die Ermöglichung, meine Experimente mit humanem Gewebe aufzupeppen.

Additionally, I would like to express my sincere gratitude to our precious collaboration partner Prof. Dr. Guowang Xu and his lab members from the DICP in Dalian, China, for their continuous support of my PhD study and related research, for their motivation, effort and immense knowledge. I will always think back with huge gratitude to the research visits in Dalian. I learned so much about analytics, but also about an amazing culture and awesome people and best of all new friends.

Vielen Dank auch an mein ganzes Labor, ihr habt die Laborarbeit für mich noch süßer gemacht: Heike, Ann Kathrin, Nadine, Andras, Sebastian und Magnus, ihr seid super. Zu guter Letzt auch an mein Herzstück im Labor, Chrisi, danke ich für alles.

Daniel-San danke ich für seine unermüdliche Begeisterung und seinen Eifer dem Mito-Gott seine nötigen Opfer zu bringen. Du warst spitze.

Besonders möchte ich an dieser Stelle auch meiner Familie im Speziellen den Muppels, Pullers und den kleinen Kapplers mit meinem Lieblingsneffen Anton danken für ihre unermüdliche Stärkung, riesengroße Wärme und vorbehaltlose Unterstützung bei allem, was ich anpacke. Auf euch ist immer Verlass, dafür danke ich euch von ganzem Herzen. Außerdem danke ich meiner Oma Lotte für ihr ständiges Interesse an meiner Arbeit und unsere Gespräche über Diabetes. Du bist mit deiner Stärke und positiven Lebenseinstellung für mich ein immerwährendes Vorbild.

Mein außerordentlicher Dank geht an Rainer fürs unermüdliche Korrekturlesen, seine Hilfe, die immer gute Laune, den Glauben an mich, die Motivationsgabe und so vieles mehr. Du warst unerlässlich.

Zu guter Letzt danke ich meinen Mitochondrien für die Energiebereitstellung.

14 Curriculum vitae

Lisa Kappler
Hegelstr. 11
72072 Tübingen

Scientific interests:

Insulin resistance/diabetes, OMICS analyses/mass spectrometry, mitochondrial (dys)function, biological sample preparation methodology

Work experiences/Work abroad:

Since 6/2017	Regular research visits at Leibniz-Institut für Analytische Wissenschaften (isas), Dortmund (Prof. Dr. Albert Sickmann)
4/2017 – 6/2017 (China)	Second research visit at cooperating laboratory (Dalian Institute of Chemical Physics (DICP), Chinese Academy of Sciences (CAS), China, Prof. Dr. Guowang Xu) → Broaden experiences in chemical analytics (mass spectrometry, metabolomics/lipidomics and data processing)
4/2015 – 6/2015 (China)	Research visit at cooperating laboratory (Dalian Institute of Chemical Physics (DICP), Chinese Academy of Sciences (CAS), China, Prof. Dr. Guowang Xu) → Gaining experiences in chemical analytics and data processing
Since 12/2013	PhD student (Clinical Chemistry, Pathobiochemistry, Internal Medicine IV, University Hospital Tübingen, Prof. Dr. R. Lehmann) → OMICS investigation of metabolic (dys)regulation of mitochondria
11/2011 – 5/2013	Student research assistant (Chair of Molecular Nutritional Medicine, TUM, Prof. Dr. Klingenspor) → Investigating a XF96 Seahorse protocol for analysing mitochondria from white murine fat, characterization of white fat mitochondria by performing respiratory analysis comparing high fat fed mice and controls and X16ki-mouse models and controls
7/2012 – 9/2012 (Taiwan)	NSC/DAAD Scholarship in Taiwan (Department of Nutritional Science at the Fu Jen Catholic University, Taipei, PhD Hui-Chen Lo) → Supporting a study on a haemorrhagic rat model to investigate the effect of amino acids on reperfusion injury

Since 6/2017	Regular research visits at Leibniz-Institut für Analytische Wissenschaften (isas), Dortmund (Prof. Dr. Albert Sickmann)
3/2011 – 8/2011 (UK)	Internship at the MRC-HNR in the Biomineral Research Group in Cambridge, UK (PhD Jonathan Powell) Trace Elements Status and Speciation Analysis: - biological sample preparation (e.g. oocyte and tissue digestion) - dietary mineral analysis by ICP-OES: optimising methodology for Na, Ca, K, Sr, Si analysis of human skin/aorta biopsies - analysis of aluminium/contaminant metals in intravenous iron commercial preparations
10/2010 – 2/2011 (UK)	Internship at the University of Newcastle upon Tyne, UK (Vitamin A Research Group, Dr. Lietz)

Education:

4/2013-10/2013	Master thesis (Chair of Animal Hygiene, Prof. Dr. med. vet. Dr. med. vet. habil. Dr. h. c. Bauer) *"Identification of sources for tetM and strA-contamination in stored and processed meat"* – → Gaining experience in microbiology, Quantification of the changes in antibiotic resistance gene concentration by RT-PCR, SSCP-Gel-Analysis
10/2011-10/2013	Study Master of Nutritional Science at the Technical University Munich-Weihenstephan
4/2010 – 7/2010	Bachelor Thesis (Chair of Molecular Nutritional Medicine, Prof. Dr. Klingenspor) *„Functional characterization of brown fat and white fat mitochondria of obese and slim mice"* → Investigating a protocol to isolate white fat and brown fat mitochondria followed by respiratory measurements (Clark-electrode) and oxygen radical species analysis
10/2007 – 06/2010	Study Bachelor of Nutritional Science at the Technical University Munich-Weihenstephan
09/1998 – 07/2007	Gymnasium St. Johann Blönried- Aulendorf

14.1 List of publications in peer-reviewed journals

- *The effect of differentiation and TGF*β *on mitochondrial respiration and mitochondrial enzyme abundance in cultured primary human skeletal muscle cells*
  Christoph Hoffmann, Selina Höckele, Lisa Kappler, Martin Hrabě de Angelis, Hans-Ulrich Häring, and Cora Weigert; Nature Scientific Reports, Sci Rep. 2018 Jan 15;8,737

- *Purity matters: A workflow for the valid high-resolution lipid profiling of mitochondria from cell culture samples.*
  Lisa Kappler, Jia Li, Hans-Ulrich Häring, Cora Weigert, Rainer Lehmann, Guowang Xu, Miriam Hoene; Nature Scientific Reports, Sci Rep. 2016 Feb 19;6:21107 IF: 4.259 (2016)

- *Limited Mitochondrial Capacity of Visceral Versus Subcutaneous White Adipocytes in Male C57BL/6N Mice*
  Theresa Schöttl, Lisa Kappler, Katharina Braun, Tobias Fromme, Martin Klingenspor; Endocrinology, March 2015, 156(3):923–933. IF: 4.159 (2015)

- *Limited OXPHOS capacity in white adipocytes is a hallmark of obesity in laboratory mice irrespective of the glucose tolerance status*
  Theresa Schöttl, Lisa Kappler, Tobias Fromme, Martin Klingenspor; Molecular Metabolism 2015 Jul 15; 4(9):631-42. IF: 5.363 (2015)

14.2 Talks and Posters

- Talk at the HJ Staudinger Symposium June 2016 in Banz: *Lipid profiling of mitochondria: from workflow optimization to pathophysiological application*
  Lisa Kappler, Jia Li, Chunxiu Hu, Heike Runge, Guowang Xu, Hans-Ulrich Häring, Cora Weigert, Miriam Hoene, Andreas Peter, Rainer Lehmann

- Poster presentation at Deutscher Kongress der Laboratoriumsmedizin in Oldenburg October 2017: *Quantitative lipidomic comparison of mitochondria from mouse muscle and liver and integrated analysis of function and protein composition*
  Lisa Kappler, Jia Li, Chunxiu Hu, Christine von Törne, Stefanie Hauck, Guowang Xu, Hans-Ulrich Häring, Cora Weigert, Andreas Peter, Miriam Hoene, Rainer Lehmann

- Poster presentation at Deutscher Kongress der Laboratoriumsmedizin in Mannheim September 2016: *Robust and practical strategy for lipidomics of tissue-derived mitochondria*
  Lisa Kappler, Jia Li, Chunxiu Hu, Daniel Bleher, Heike Runge, Guowang Xu, Hans-Ulrich Häring, Cora Weigert, Andreas Peter, Miriam Hoene, Rainer Lehmann

- Poster presentation at 76th Scientific Sessions of the American Diabetes Association in New Orleans June 2016: *Lipid remodelling and decreased SOD activity in insulin resistant C2C12 myotubes*
  Lisa Kappler, Chunxiu Hu, Uli Ohmayer, Stefanie Hauck, Guowang Xu, Hans-Ulrich Häring, Cora Weigert, Miriam Hoene, Rainer Lehmann

Poster presentation at the Diabetes Kongress der deutschen Diabetesgesellschaft in Berlin May 2016: *Lipid remodelling and decreased SOD activity in insulin resistant C2C12 myotubes*
Kappler Lisa, Chunxiu Hu, Uli Ohmayer, Stefanie Hauck, Guowang Xu, Hans-Ulrich Häring, Cora Weigert, Miriam Hoene, Rainer Lehmann

- Poster presentation at Deutscher Kongress der Laboratoriumsmedizin in Leipzig in September 2015:
  Purity matters: A workflow for the valid high-resolution lipid profiling of mitochondria from cell culture samples.
  Kappler Lisa, Li Jia, Xu Guowang, Häring Hans-Ulrich, Weigert Cora, Hoene Miriam, Lehmann Rainer

- Poster presentation at the Mitochondria Physiology School in Copenhagen August 2015:
  Subcellular lipidomics: development of a robust, valid and sensitive strategy for mitochondrial lipid profiling.
  Kappler Lisa, Li Jia, Weigert Cora, Häring Hans-Ulrich, Lehmann Rainer, Xu Guowang, Hoene Miriam

14.3 Fellowships

- Travel Grant Deutsche Vereinte Gesellschaft für klinische Chemie und Laboratoriumsmedizin (DGKL) – Deutscher Kongress der Laboratoriumsmedizin Oldenburg October 2017
- Travel Grant Deutsche Vereinte Gesellschaft für klinische Chemie und Laboratoriumsmedizin (DGKL) – Deutscher Kongress der Laboratoriumsmedizin Mannheim September 2016
- DZD Fellowship – ADA New Orleans June 2016
- Travel Grant Deutsche Diabetes Gesellschaft (DDG) – Diabetes Kongress Berlin May 2016
- Travel Grant Oroboros Instruments – Oxygraph-2k Workshop Austria April 2016
- DZD fellowship – FELASA B Course Potsdam October 2015
- Boehringer Ingelheim Travel Grant - Mitochondria Physiology School Copenhagen August 2015

15 Supplement

Supplementary Table 1: Different conditions tested for mitochondria isolation with differential centrifugation and ultracentrifugation from cells; hMT= human myotubes, HEK=human embryonic kidney cells, C2C12= mouse skeletal muscle cells, HEPG2s= human liver hepatoma cells, FM= fusion medium. Conditions used in Section 4.1.1.2 are highlighted in grey.

Cell type	Dounce strokes	Nitrogen bomb pressure [bar]	Volume in douncer [ml]	Time under pressure in nitrogen bomb [min] and volume [ml]	Amount of 15 cm plates	Days on FM /donor numbers	Gradients (type/layers)	Centrifugation conditions
hMT	10, 20	20, 40	20			FM: 5, 6, 7, 9/ donors: 47, 11, 80, 52	Percoll	
HEK	7, 10	10, 20	20					
C2C12	13, 20, without second repeat	10, 30	10, 20	5 min, 15 min; 3 ml, 20 ml	1, 3, 6, 16		Sucrose/2+3; Percoll/ 3, continuous, trypsinated	8 000 vs 10 400 g
HEPG2	5, 10, 15, 20, without second repeat	10, 30	20	5 min, 2 ml, 20 ml	3, 6		Sucrose/2+3 layers, Percoll/(dis-), continuous	8 000 vs 10 400 g; 3x 10 400 g

Supplementary Table 2: Conditions tested during mitochondria isolation using MACS, hMT= human myotubes, HEK=human embryonic kidney cells, C2C12=mouse skeletal muscle cells, HEPG2s= human liver hepatoma cells. Conditions used in Section 4.1.1.2 are highlighted in grey.

Cell type	Dounce strokes	Syringe	Syringe strokes	Plate no	N_2 homogenisation	Gradient	Centrifugation	Other
hMT	5, 10, 20			2, 4, 6	20 bar, 40 bar (5 min, 20 ml)			Filtered before column, centrifuged before column
HEPG2	5, 10, 15, 20, 40	27,75 G, 30 G	15, 20	1.5 (~1x10^7 cells)		Sucrose	10 000 g after isolation	

Supplementary Table 3: Conditions tested during mitochondria isolation using tissue

	Dounce strokes	Gentle macs	Amount DC+UC [mg]	Amount MACS	Gradient	Enzymatic digestions	Digestion time
Muscle	various	following manufacturer's recommendations	700, 2 000	1 gastrocnemius	Percoll:2/ 3 layer, continuos	Collagenase, protease type 8	2.5, 3, 3.5 min
Liver	various	following manufacturer's recommendations	150, 300	100 mg	Percoll: 2/3 layer, continuos		
BAT	various		various				

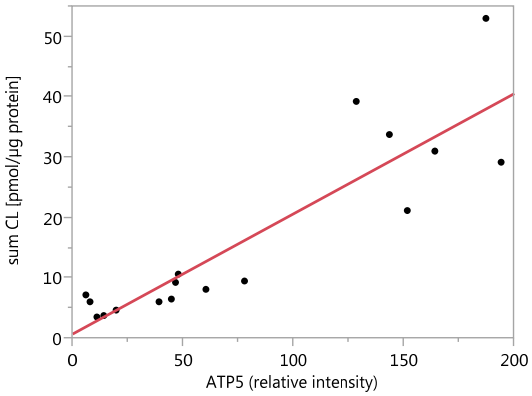

Supplementary Figure 1: Correlation of the sum of cardiolipins (CL) with the content of mitochondrial ATP synthase 5 (ATP5) protein as determined by western blot analysis (r= 0.79, p< 0.0001).

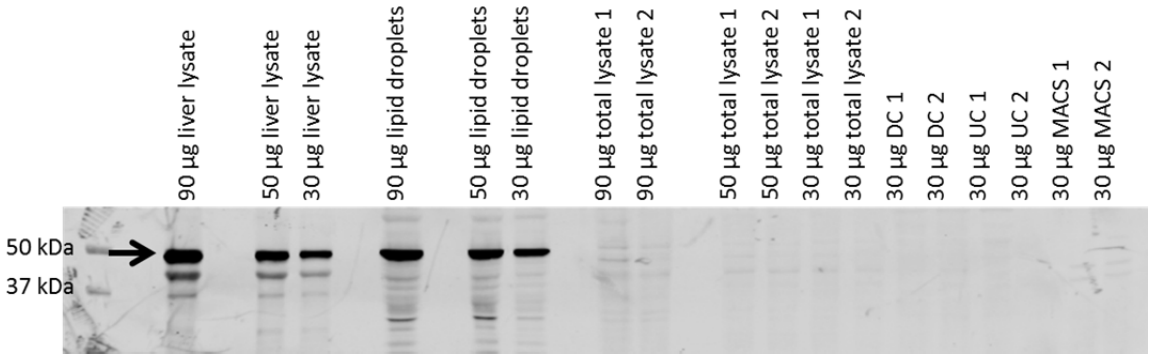

Supplementary Figure 2: PLIN 2 blot (predicted size 50 kDa), a strong PLIN2 band was clearly visible in liver lysate and purified lipid droplets. In 90 µg of total cell lysate, a faint PLIN2 band was visible that was not present in any of the mitochondrial fractions independent of the purification procedure. However, since this band was not visible for 30 µg of total lysate, this PLIN2 blot was not shown in Figure 12.

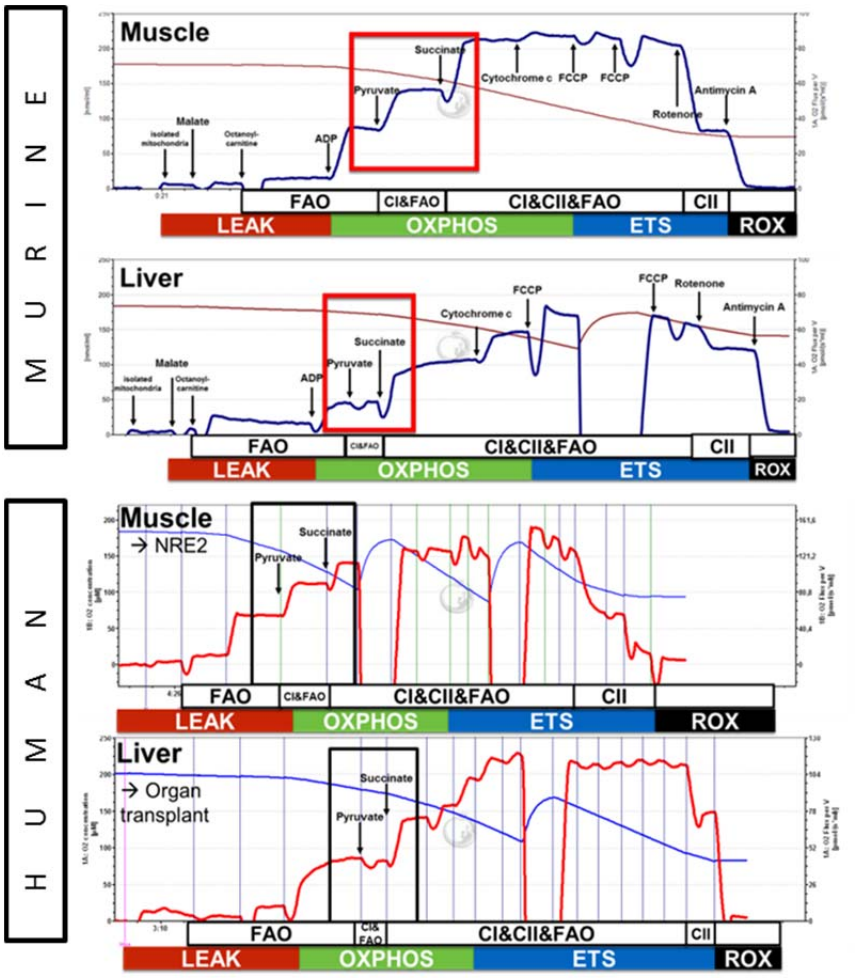

Supplementary Figure 3: Top two graphs: Mouse muscle and liver; Bottom two graphs: Human muscle and liver. Results of a representative Oxygraph-2k measurement with permeabilised muscle fibres and isolated liver mitochondria. Human liver derived from a healthy organ transplant. Dark red (murine)/blue line (human): O_2 concentration [nmol/ml]; blue line (murine)/red line(human): O_2 flux [pmol/(s*ml)]. Malate and octanoylcarnitine (M, Oct) were injected to induce fatty acid oxidation (FAO). LEAK respiration is the oxygen consumption under non-phosphorylating conditions due to the proton leak. ADP was added to induce oxidative phosphorylation (OXPHOS). Pyruvate was used as complex 1-associated substrate (C1/CI) and succinate as mainly complex 2-linked substrate (C2/CII). FCCP, a synthetic uncoupler, was titrated to uncouple the electron transport chain activity from ATP production and determine the maximal oxidative capacity of the electron transport chain (ETS= electron transfer system capacity). Complex 1 was inhibited by rotenone to solely investigate complex 2-associated respiration. The non-mitochondrial background respiration or residual oxygen consumption (ROX) were determined by addition of antimycin A to inhibit the cytochrome c reductase (C3/CIII).

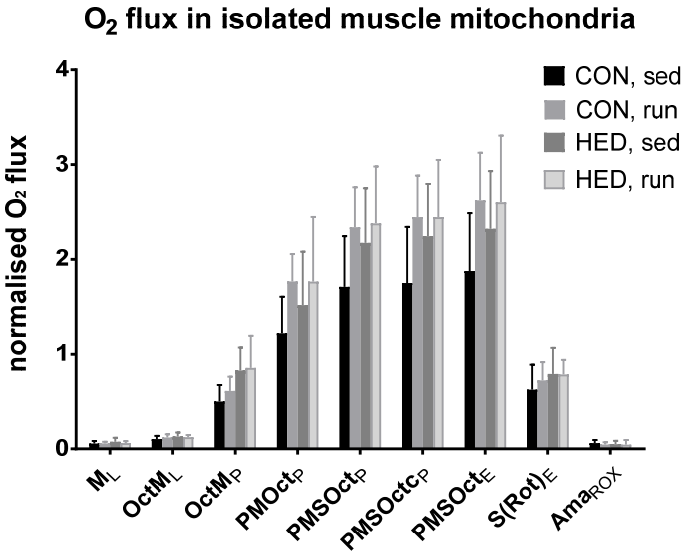

Supplementary Figure 4: Normalised oxygen flux (n= 7; mean + SD) in isolated mouse muscle mitochondria. Normalised for: mitochondrial amount (by protein), mitochondrial concentration changes, mean inter-day differences. CON= control diet; HED= high-energy diet; run= trained; sed= sedentary. States are explained in Table 5.

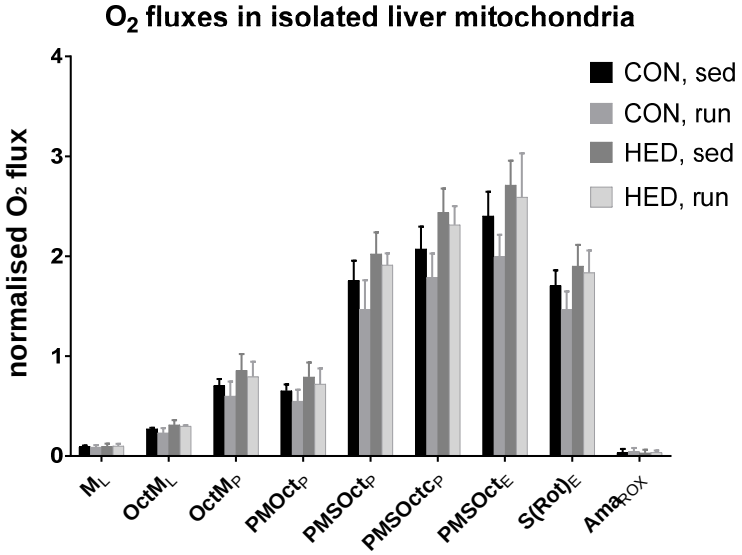

Supplementary Figure 5: Normalised oxygen flux (n= 5; mean + SD) in isolated mouse liver mitochondria. Normalised for: mitochondrial amount (by protein), mitochondrial concentration changes, mean inter-day differences. CON= control diet; HED= high-energy diet; run= trained; sed= sedentary. States are explained in Table 5.